National Library of Canada
Bibliothèque nationale du Canada

Canadian Theses Service
Service des thèses canadiennes

Ottawa, Canada
K1A 0N4

NOTICE

The quality of this microform is heavily dependent upon the quality of the original thesis submitted for microfilming. Every effort has been made to ensure the highest quality of reproduction possible.

If pages are missing, contact the university which granted the degree.

Some pages may have indistinct print especially if the original pages were typed with a poor typewriter ribbon or if the university sent us an inferior photocopy.

Previously copyrighted materials (journal articles, published tests, etc.) are not filmed.

Reproduction in full or in part of this microform is governed by the Canadian Copyright Act, R.S.C. 1970, c. C-30.

AVIS

La qualité de cette microforme dépend grandement de la qualité de la thèse soumise au microfilmage. Nous avons tout fait pour assurer une qualité supérieure de reproduction.

S'il manque des pages, veuillez communiquer avec l'université qui a conféré le grade.

La qualité d'impression de certaines pages peut laisser à désirer, surtout si les pages originales ont été dactylographiées à l'aide d'un ruban usé ou si l'université nous a fait parvenir une photocopie de qualité inférieure.

Les documents qui font déjà l'objet d'un droit d'auteur (articles de revue, tests publiés, etc.) ne sont pas microfilmés.

La reproduction, même partielle, de cette microforme est soumise à la Loi canadienne sur le droit d'auteur, SRC 1970, c. C-30.

Canada

THE OLIGOMERIZATION OF ACETYLENE

OVER FLUORIDATED ALUMINA CATALYSTS

-by-

VINCENZA M. ALLENGER

A Thesis

Submitted to the School of Graduate Studies

in Partial Fulfillment of the Requirements

for the Degree of

Doctor of Philosophy

University of Ottawa

August 1987

© Vicenza M. Allenger, Ottawa, Canada, 1988.

Permission has been granted to the National Library of Canada to microfilm this thesis and to lend or sell copies of the film.

The author (copyright owner) has reserved other publication rights, and neither the thesis nor extensive extracts from it may be printed or otherwise reproduced without his/her written permission.

L'autorisation a été accordée à la Bibliothèque nationale du Canada de microfilmer cette thèse et de prêter ou de vendre des exemplaires du film.

L'auteur (titulaire du droit d'auteur) se réserve les autres droits de publication; ni la thèse ni de longs extraits de celle-ci ne doivent être imprimés ou autrement reproduits sans son autorisation écrite.

ISBN 0-315-46699-5

UNIVERSITÉ D'OTTAWA
UNIVERSITY OF OTTAWA

SUMMARY

The performance of fluoridated alumina catalysts in the oligomerization of acetylene was investigated at atmospheric pressure in both a tubular fixed-bed flow reactor and a microbalance under various operating temperatures (300-400^{o}C), initial concentrations of acetylene (5-15 vol %) and weight-times (1-3 g.s.mL^{-1}). The catalysts exhibited high activity in this reaction and yielded a broad spectrum of gaseous, liquid and non-desorbable solid products. At low initial concentrations of acetylene, catalyst activity increased with catalyst acidity but at higher reactant concentrations, the activity decreased rapidly with increased fluoride content of the catalyst. Several reports in the literature have indicated that ion pair sites are necessary for acetylene adsorption and that fluoridation alters the number and acid strength of the ion-pair sites on the surface. The experimental observations in this study are consistent with these findings.

Catalyst deactivation was severe in this reaction. The loss in catalyst activity with time-on-stream was described adequately by an exponential decay model with two parameters, a_0, the initial activity and k_d, the specific rate of deactivation. The deactivation process was caused primarily by the deposition of carbonaceous species on the catalyst surface through a reaction associated with the same active sites (ion-pair sites) which were responsible for acetylene adsorption. Conditions which were found to minimize deactivation (loss in activity), namely 400^{o}C, 3 g.s.mL^{-1}, 5 vol. % C_2H_2, also minimized catalyst carbon content. Carbon deposition on the external surface of the catalyst increased with catalyst acidity, however, this process was not accompanied by severe losses in activity. On the other hand, small quantities of carbonaceous deposits throughout the bulk of the catalyst deactivated the catalyst readily. This suggested that more than one phenomenon was responsible for carbon deposition. The specific rate of deactivation, k_d, was found to increase with the ratio of the aliphatic to aromatic carbon

in the catalyst deposits implying that the aliphatic content of the deposits had a major influence in the deactivation. In addition, three peaks suggesting three types of carbonaceous species were detected through the temperature-programmed desorption studies of used catalysts. The specific rate of deactivation was also associated on a qualitative basis with the low temperature peak (corresponding to species which were removed from the catalyst surface at low temperature). Both of these findings could be interpreted in terms of polyenes (or molecules containing CH fragments) being responsible for the loss in activity.

A mechanism was proposed, based on cationic chain polymerization, to describe the catalytic reaction. The reaction mechanism consisted of generation of the initiator (e.g., vinyl cation), growth of the chain at the active centre (e.g., C_8 polyene), isomerization of the active centres followed by ring stabilization (e.g., aromatics) and desorption. Evidence from the activity, selectivity and deactivation data gathered in this study supported this mechanism. The low activation energy found for the deposition reaction, 8 kcal/mol for alumina and 7 kcal/mol for fluoridated alumina, was consistent with the proposed polymerization scheme. This hypothesis could also explain the increased relative yields of liquids with low molecular weights found at high conversions in terms of monomeric starvation of the growing chain. This condition probably favoured surface rearrangements (ring closing reactions) and other secondary reactions (dealkylation, condensation) which led to more desirable products. The mechanism also provided a good explanation for the enhanced catalyst activity and prolonged catalyst lifetimes found in the presence of infrared radiation. Presumably, the radiation provided sufficient vibrational energy to facilitate the transfer reaction between the radical cation (delocalised over 2 or more monomeric units of the conjugated polyene chain) and the active centre (at the end of the chain).

Alumina and fluoridated alumina were good initiators for acetylene oligomerization reactions. However, according to the postulated mechanism, high liquid

yields of desirable products (BTX) may only be obtained when the possibility for rearrangements of the hydrocarbon species adsorbed on the catalyst surface is high. Pure alumina satisfied this criterion to a larger extent than the fluoridated alumina catalysts and proved to be a more appropriate catalyst for this process.

ACKNOWLEDGEMENTS

I would like to express my gratitude to my research supervisors, Dr. Marten Ternan and Dr. David McLean for their extensive review of this manuscript and for their guidance, advice and constructive criticism throughout the course of this work.

I wish to extend my appreciation and thanks to my colleagues, Dr. C. Fairbridge, Dr. J. Brown, Dr. J. Galuszka and Dr. S. Ng and Dr. M. V. C. Sekhar for their valuable suggestions, their friendship and help during this work. I am also thankful for the technical assistance of E. McColgan in my experimental efforts.

The financial support of the Department of Energy, Mines and Resources, Canada is gratefully acknowledged.

Most of all, I would like to thank my family for their constant encouragement, understanding and infinite patience. I love you dearly.

CONTRIBUTIONS TO KNOWLEDGE

In the course of this research, the following contributions to existing knowledge were made:

1. New data were generated for the polymerization of acetylene to hydrocarbons using fluoridated alumina catalysts for which F/Al molar ratios varied between 0 and 3. Experimental measurements of catalyst activity, selectivity and deactivation as a function of processing conditions were obtained using a tubular, fixed bed and a microbalance.

2. Catalytic activity and selectivity in this reaction were correlated with the surface acidity of the catalyst (J. Catal., *105*, 5, 71-80; 1987).

3. A relationship was determined between catalyst deactivation and the quantity of linear polymer formed on the surface of the catalyst (App. Catal.- submitted).

4. A reaction mechanism, consistent with the data generated in this study, was proposed for the reaction of acetylene on alumina and fluoride-modified alumina catalysts.

5. Infrared radiation was found to have a major effect on the conversion of acetylene and on extending catalyst life (Fuel, *66*, 3, 1987).

6. Novel experimental techniques were developed to sample and analyze low concentrations of condensable vapors in process streams and to identify and quantify differences in solid catalyst residue in this process (J. Chrom. Sci., *24*, 3, 1986).

TABLE OF CONTENTS

TABLE OF CONTENTS CONT'D

TABLE OF CONTENTS CONT'D

TABLE OF CONTENTS CONT'D

TABLE OF CONTENTS CONT'D

APPENDICES CONT'D

LIST OF TABLES

LIST OF TABLES CONT'D

LIST OF FIGURES

LIST OF FIGURES CONT'D

LIST OF FIGURES CONT'D

LIST OF FIGURES CONT'D

LIST OF FIGURES CONT'D

LIST OF FIGURES CONT'D

NOTATION

$a(t)$	catalyst activity as a function of time [% conversion C_2H_2]
a_0	initial activity parameter in Eq. 8.1 [% conversion C_2H_2]
C	catalyst carbon content [mg/m^2]
C_{in}	ammonia injected in each pulse [mmol]
C_{out}	ammonia remaining in each pulse [mmol]
C_{NH3}	quantity of ammonia adsorbed by catalyst [mmol/g]
C_o	initial concentration [mol/L]
C_f	gas phase concentration of acetylene [mol/L]
$E(C)$	expected value of an evaluation criterion, C, e.g., conversion
E_a	activation energy [kcal/mol]
F_o	feed flow rate [mol/min]
k_d	specific rate of deactivation, parameter in Eq. 8.1 [min^{-1}]
k	rate constant for deposition reaction
l_i	parameters in polynomial model, Eq. 4.2.
m	mass of catalyst [g]
M	monomer
M_x	mole fraction of x-mer, n_x/N
n	number of pulses
n_x	number of molecules containing x M groups, both reacted and unreacted
N	total number of molecules present in the reaction system
N_o	original number of molecules present in the system
N_u	number of molecules which are unreacted
p	probability factor in the Flory distribution, extent of reaction
R	gas constant

NOTATION CONT'D

R_f	rate of carbon deposition at the end of 1 h [mg/min]
R_{max}	maximum rate of coke deposition [mg/min]
R_m^s	maximum rate of deposition based on catalyst surface area [mg/m^2/min]
R_f^s	rate of deposition at 1 h based on catalyst surface area [mg/m^2/min]
S_L	selectivity to liquids
S_C	selectivity to carbonaceous deposits
T	temperature
w	instantaneous sample weight [mg]
w_o	weight of cat in microbalance at time when reactant is introduced [mg]
w_f	weight at the end of the reaction time [mg]
x	independent variables in polyhomial model
x	no. of monomer molecules in the polymeric chain
x_n	average number of monomer units per chain
X	per cent conversion [%]
x_j	mol fraction of gas phase component j
y_i	mol fraction of liquid vapor component i
Y	yield

I. INTRODUCTION

At present, transportation fuels are almost exclusively manufactured from petroleum crude oil. However, natural gas might be an alternative feedstock in those geographical locations having abundant natural gas reserves. Several routes exist for the synthesis of transportation fuels from natural gas. The two commercial routes involve the Fischer-Tropsch and the Mobil methanol-to-gasoline (MTG) synthesis technologies.

Both routes involve several stages beginning with the production of synthesis gas, a mixture of carbon monoxide and hydrogen, by steam-reforming of natural gas (900°C, 2 MPa). In the Fischer-Tropsch process the synthesis gas is then contacted with an iron catalyst in fixed- or fluidized-bed reactors (300°C, 2 MPa) (24). The reactor effluent is cooled and fractionated to recover the desired products. The product distribution is spread over a wide range (28). In the Mobil MTG process synthesis gas is converted to methanol over a $Cu/Zn/Al_2O_3$ or $Cu/Zn/Cr_2O_3$ catalyst (260°C, 5 MPa) using the Imperial Chemical Industries (ICI) process. Subsequent reaction of the methanol over a ZSM-5 catalyst (370°C, 0.1 MPa) yields the desired product, gasoline.

Both routes require high initial capital investments because of the multiplicity of processing steps involved (75). Furthermore, the various operating conditions required for the individual stages (shown in parentheses above) significantly reduce the thermal efficiency of the overall processes. For these reasons it is worthwhile investigating routes for more directly producing liquid fuels from natural gas. An alternative route which is theoretically and technically feasible involves converting the natural gas to acetylene and then polymerizing and hydrogenating the acetylene to the required fuels. Such an integrated direct process has never been carried out commercially although patents pertaining to this methodology are available (95, 96).

The first phase of an integrated route, i.e., the production of acetylene by the pyrolysis of methane, has the following three requirements:

i. large energy inputs

ii. rapid heating rate for the reactants

iii. rapid cooling rate for the products

These requirements are dictated by thermodynamic and kinetic considerations. Fig. 1.1 shows the free energy of formation per carbon atom for several hydrocarbons. Details of the derived values and corresponding calculation procedures are given in Appendix 1.1. Several points are noted in Fig. 1.1. At any given temperature the tendency of a reaction is from a higher curve to a lower curve ($\Delta G < 0$). Methane is very stable compared with other hydrocarbons at temperatures up to 1200°C. Requirement (i) above is a result of this condition. Acetylene is the only hydrocarbon whose stability is increased with temperature, however it never becomes stable with respect to its elements. The following series of reactions have been postulated for non-catalytic methane pyrolysis (11, 65):

$$2\,CH_4 \xrightarrow{k_1} C_2H_6 + H_2 \qquad 1.1$$

$$C_2H_6 \xrightarrow{k_2} C_2H_4 + H_2 \qquad 1.2$$

$$C_2H_4 \xrightarrow{k_3} C_2H_2 + H_2 \qquad 1.3$$

$$C_2H_2 \xrightarrow{k_4} 2\,C + H_2 \qquad 1.4$$

The temperature dependence of the reaction rate constants k_1 to k_4 is shown in Fig. 1.2 (65). At high temperatures, reactions 1.1 to 1.3 proceed more quickly than reaction 1.4 and it is theoretically possible, therefore to obtain high yields of acetylene from methane at high temperatures and short reaction times. The effect of temperature on the maximum conversion of methane to acetylene at various times of reaction is shown in Fig. 1.3. This figure shows that a reaction time in the order of a few milliseconds is necessary to attain high acetylene yields.

Acetylene has been produced commercially by pyrolysis for many years using several techniques, namely regenerative pyrolysis, electric arc, plasma arc, partial oxidation and cracking (9, 37, 54, 92). The partial oxidation processes have the lowest cost when natural gas is employed as a feed. Combined yields of acetylene and ethylene in

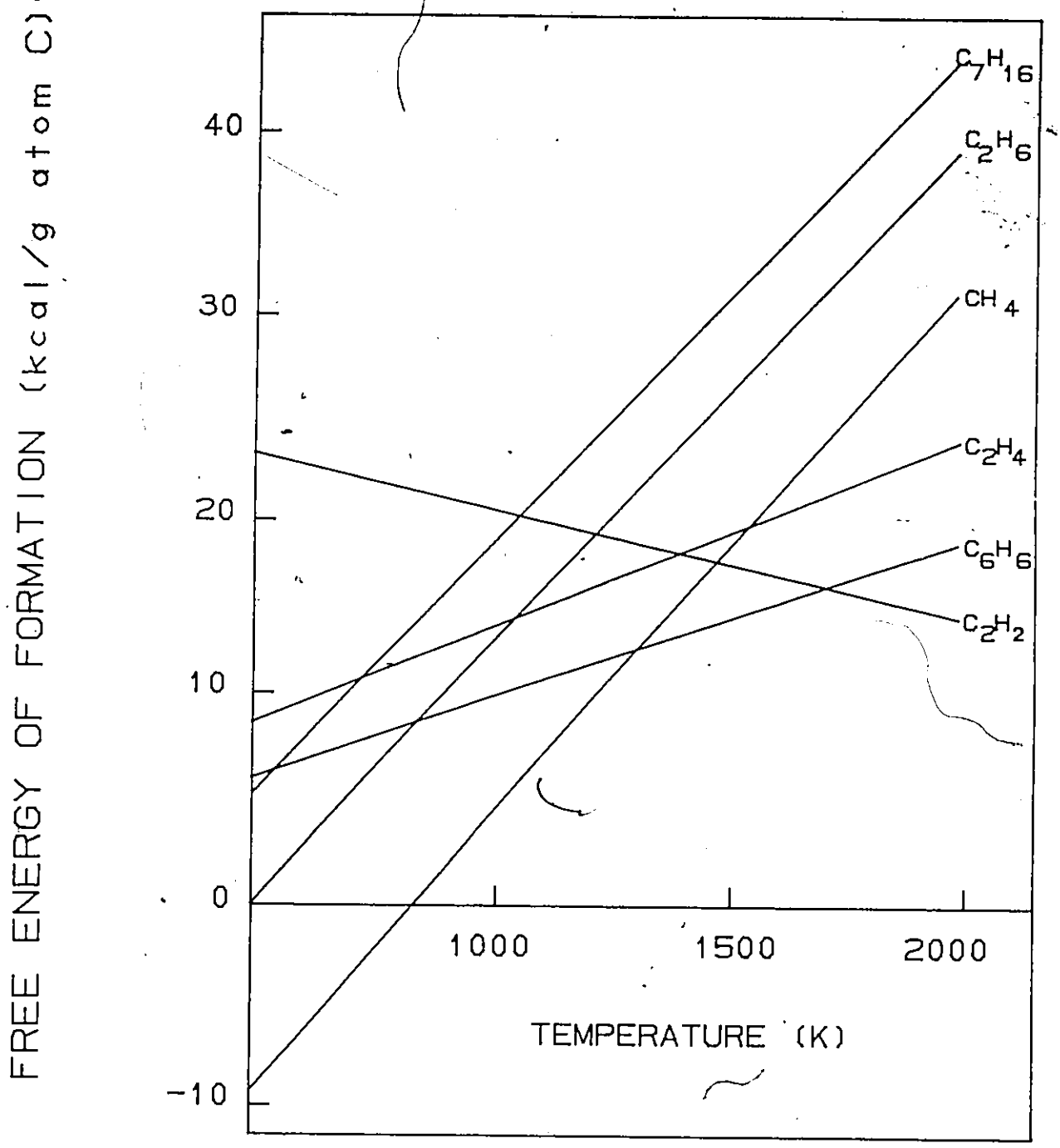

Fig. 1.1 Free energy of formation per carbon atom of some hydrocarbons.

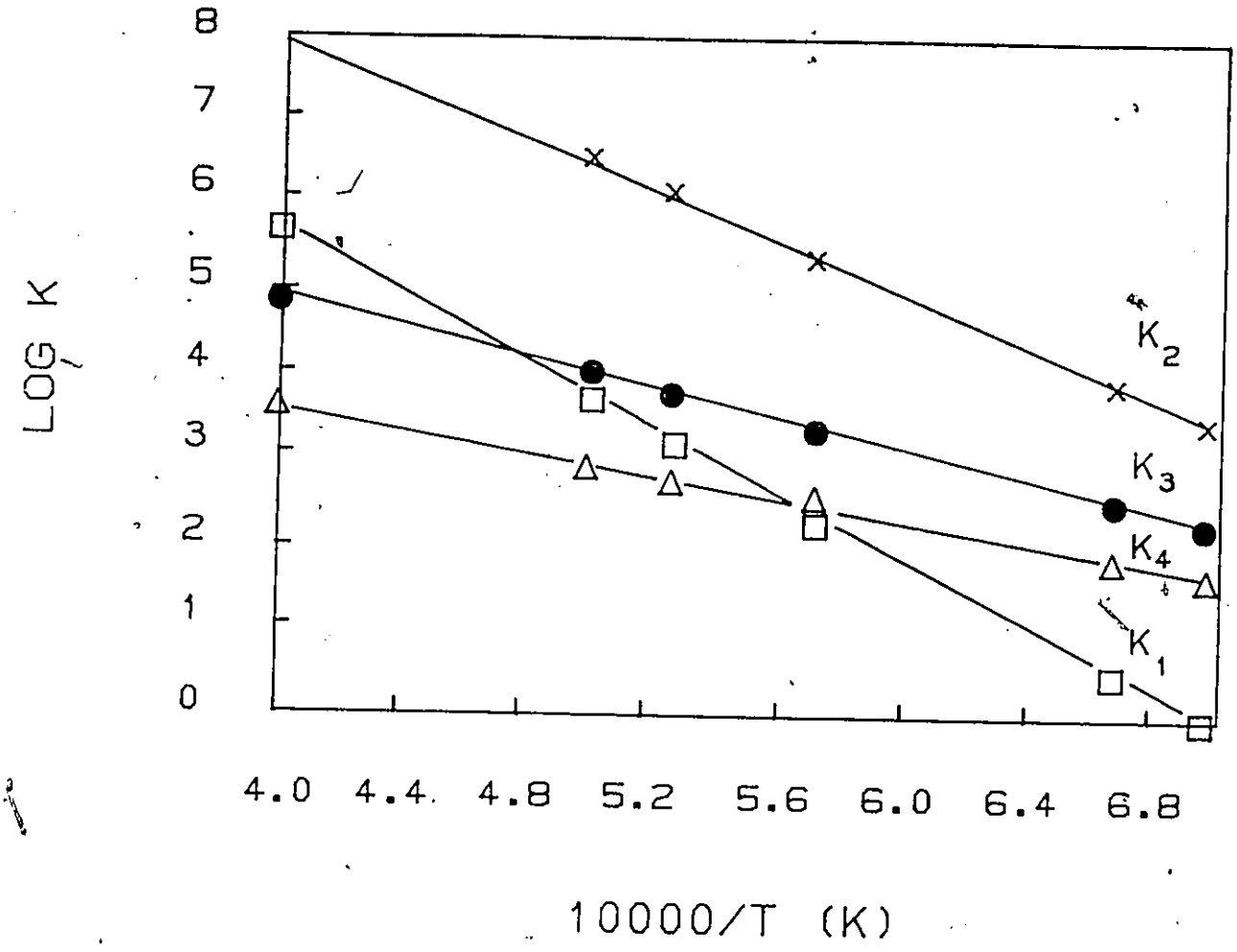

Fig. 1.2 Temperature dependence of reaction rate constants in the thermal decomposition of methane. (Ref. 65)

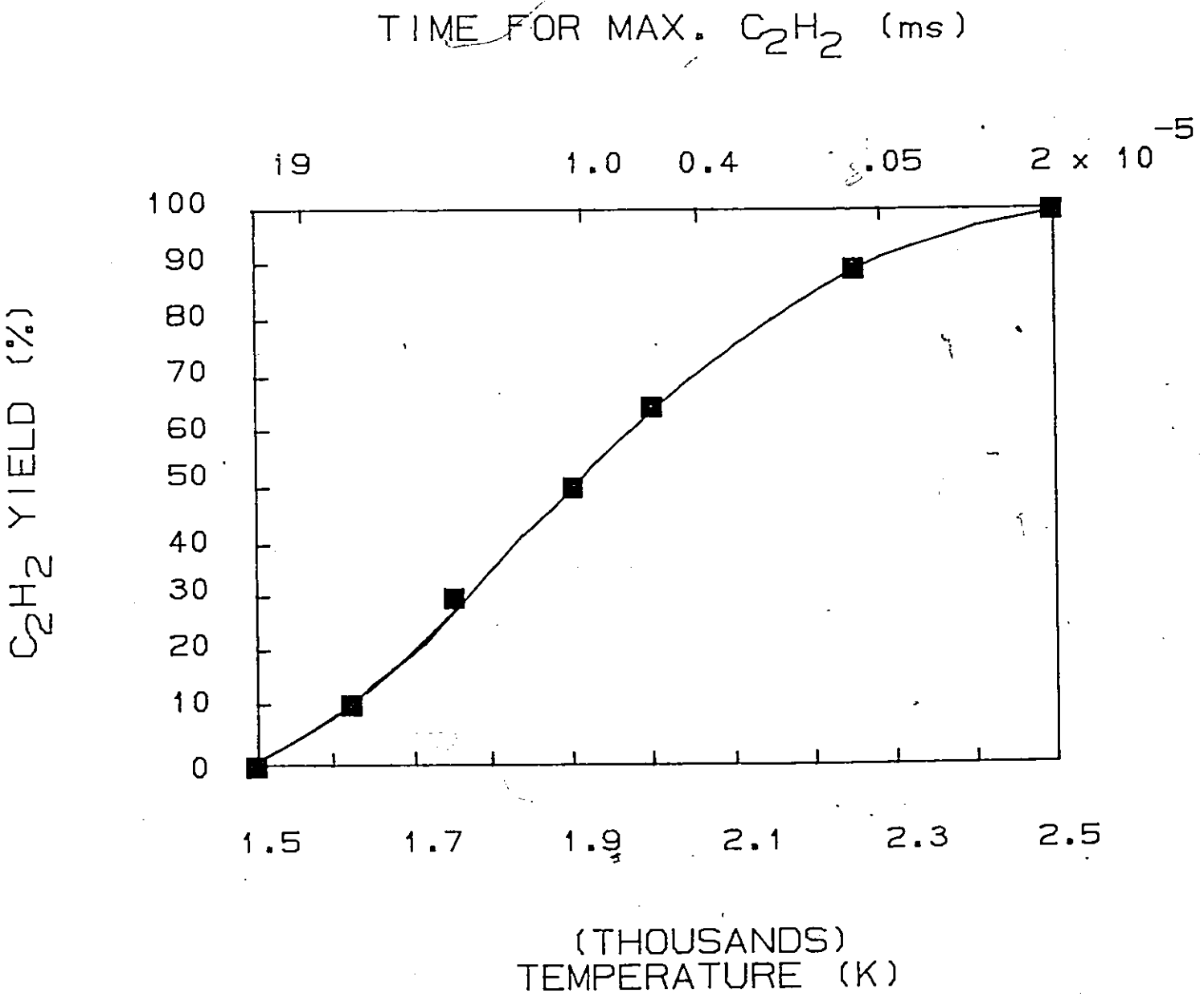

Fig. 1.3 Maximum conversion of methane to acetylene at various temperatures. (Ref. 65)

the partial combustion technique can reach 50 % and the ethylene to acetylene ratio can be varied from 0.1 to 3 (92). Some natural gas pyrolysis experiments were also performed as part of the current investigations (Appendix 1.2).

The second phase of this direct natural gas to liquids process involves the transformation of acetylene to the desired transportation fuel. It can be seen from Fig. 1.1 that low temperatures favor the conversion of acetylene to higher hydrocarbons. Equilibrium constants for some acetylene reactions are given as a function of temperature in Fig. 1.4. In the absence of hydrogen, two competing reactions are evident, i.e., trimerization and decomposition. Acetylene decomposition to its elements is extremely exothermic (54 kcal/mol). The trimerization of acetylene to benzene is similarly exothermic (49 kcal/mol). In the presence of hydrogen many other reactions can occur, e.g., hydrogenation and hydropolymerization.

It has long been recognized that significant yields of liquid products could be obtained by heating acetylene to below 800^{o}C (27). Although a simple molecule, acetylene yields a wide range of products when subjected to these temperatures. The effect of temperature on the reaction products is shown in Fig. 1.5 for a mixture of 22 % acetylene in helium at 101.1 kPa. The thermal polymerization of acetylene leads to complex mixtures made up largely of aromatic hydrocarbons. The production of aromatics is of particular importance because lighter aromatics which boil in the normal gasoline range, have very high octane numbers and are therefore excellent gasoline blending stocks. Major quantities of benzene are found in these liquid products. Meyer (63) identified many more components of the liquid product, e.g. toluene, xylene, styrene, indene, naphthalene, chrysene and fluoranthene. In general however, the thermal polymerization has not been used for synthesis mostly because many different products, including high molecular weight products, are also obtained. This disadvantage is minimized when acetylene is reacted in the presence of catalysts. Catalytic conversion of acetylene can produce quite narrow product distributions (86) and occurs at much lower temperatures.

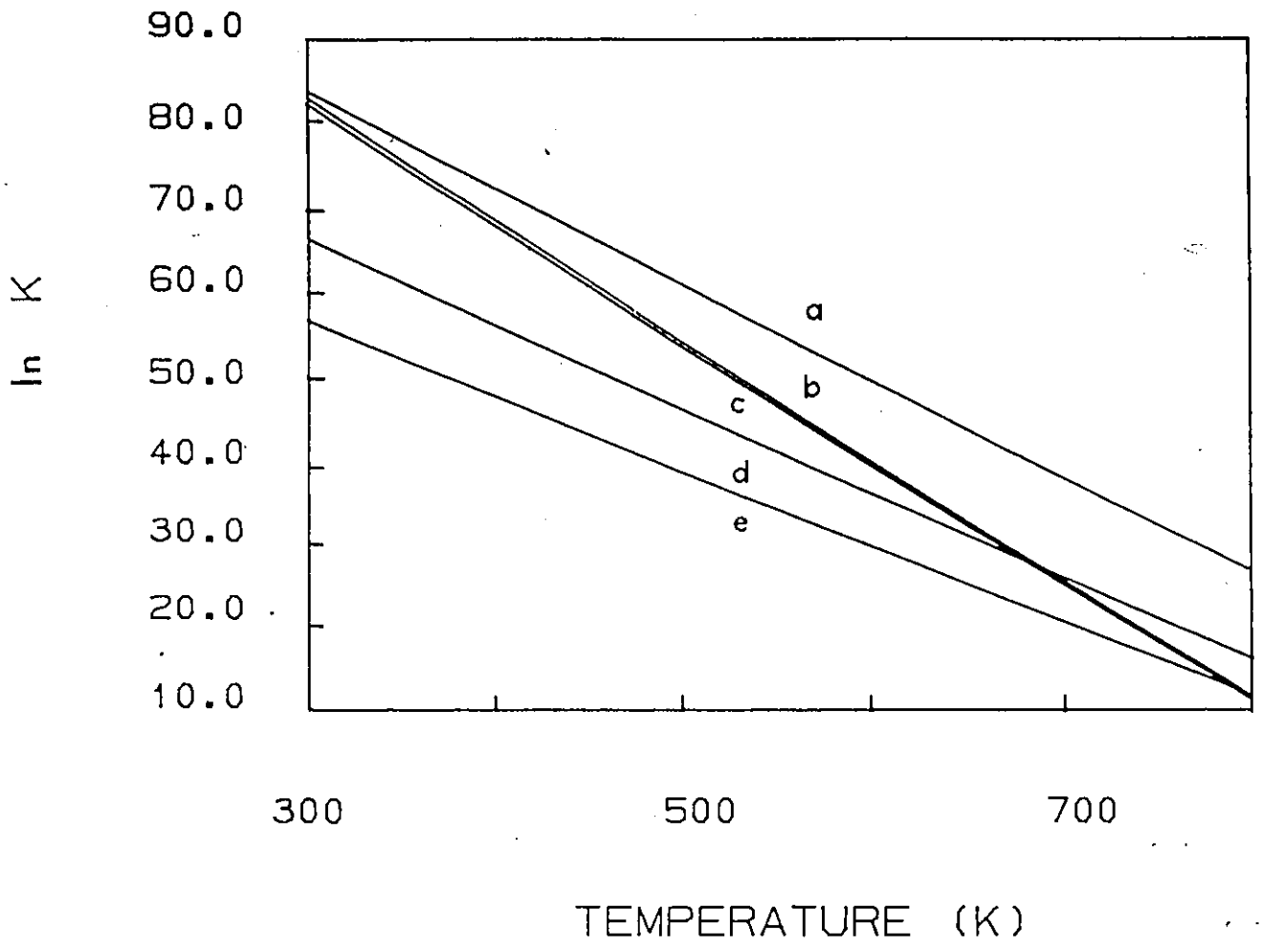

Fig. 1.4 Equilibrium constants as a function of temperature for some specific reactions:

a: C_2H_2	→	$2C + H_2$	decomposition
b: $C_2H_2 + 4/3\ H_2$	→	$1/3\ C_6H_{14}$	polymerization
c: $C_2H_2 + 6/7\ H_2$	→	$2/7\ C_7H_{16}$	
d: C_2H_2	→	$1/3\ C_6H_6$	trimerization
e: $C_2H_2 + H_2$	→	C_2H_4	hydrogenation

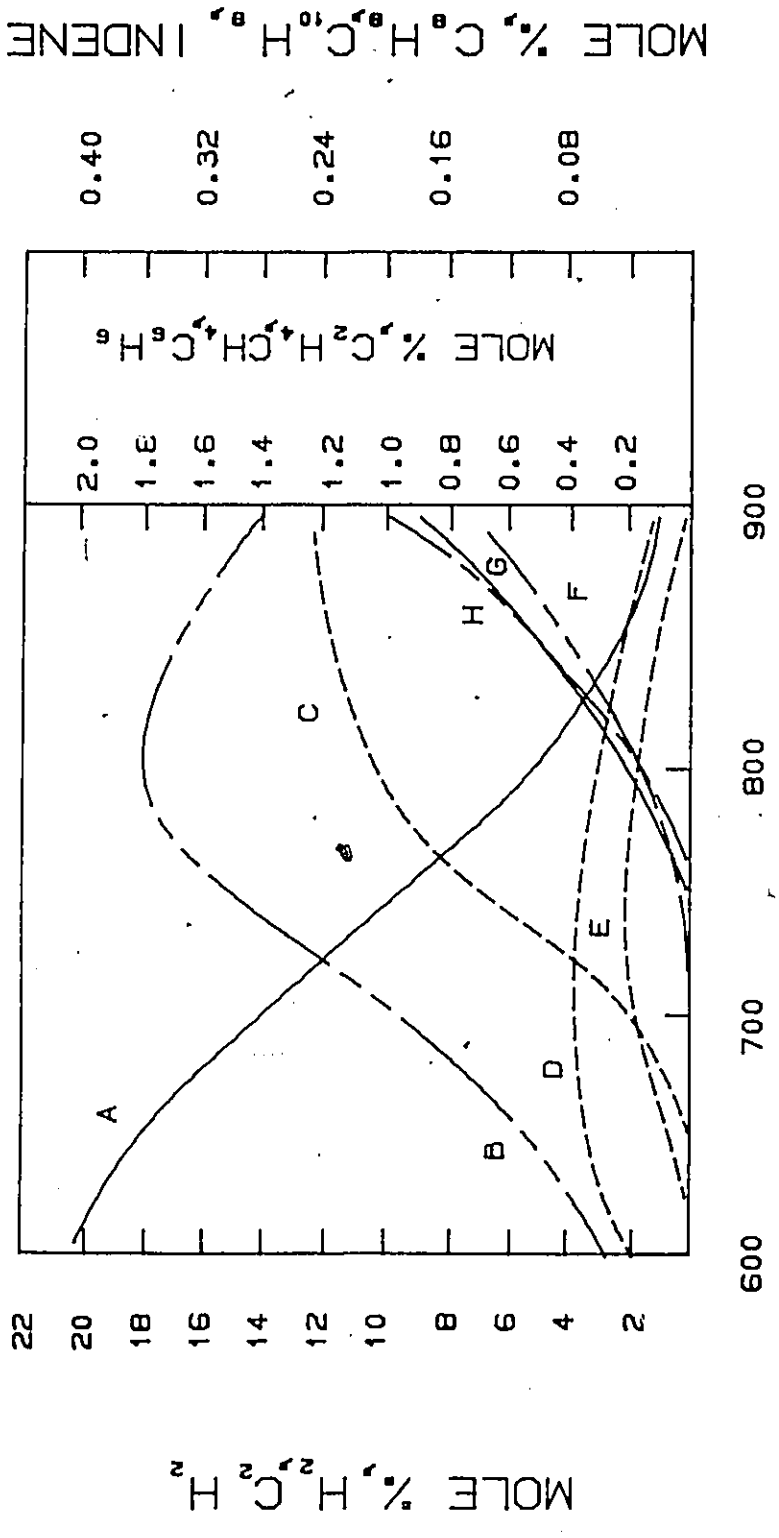

Fig. 1.5 Effect of temperature on the production of various hydrocarbons from C_2H_2.

A. acetylene B. benzene C. naphthalene D. styrene E. indene F. methane G. hydrogen H. ethylene (Ref. 65)

The reactions of acetylene have been studied extensively for the manufacture of specialty chemicals in the presence of a broad range of catalysts (92). These include transition metals, nickel carbonyls, carbonyls of other metals, organometallic catalysts, alumino-silicates and Ziegler-Natta catalysts (92). Many of these syntheses occur under very miid conditions. For example, cyclooctatetraene is synthesized using nickel carbonyl at 100°C and 1.5 MPa (86). Benzene has been reported to have been synthesized in a full-scale plant by the trimerization of acetylene over a chromium catalyst with 90 % yield (8). There are in comparison very few catalytic studies on polymerization of acetylene for liquid fuel production. There is motivation for carrying out a systematic investigation of the catalytic reactions which convert acetylene to liquid fuel.

The design and development of a catalyst is a difficult problem whether one is selecting among known catalysts or searching for new catalysts for carrying out the desired conversion. One strategy is to explore the merits of catalysts used in known catalytic reactions which are believed to be analogous to the reaction in question (84). This approach was adopted in this study. The transformation of acetylene to liquid fuels must involve polymerization. Since polymerization reactions of unsaturated hydrocarbons are believed to be acid-catalyzed (84) it was of interest to examine the role of catalyst acidity in the reactions of acetylene. Alumina (Al_2O_3) has been used extensively as a catalyst and catalyst support for acid-catalyzed reactions such as isomerization, alkylation and polymerization. Furthermore, fluoridation of alumina has been shown to be an effective means to alter the acidic properties and to enhance the polymerization of olefins and conjugated dienes (88). The objectives of this research were:

1. to investigate the effect of acidity on the activity, selectivity and deactivation of fluoridated alumina in the polymerization reaction.
2. to determine the operating conditions for such a process and
3. to develop a mechanistic interpretation of the data in terms of the fundamental processes involved.

2. LITERATURE REVIEW

The literature on acetylene and the reactions of acetylene is voluminous. The two volumes by Miller (65) and the recent book by Tedeschi (92) are noteworthy in their treatments of the reactions of acetylene. Much of the early work on acetylene polymerization has been summarized in a review by Egloff (27). The two reactions of acetylene of interest in this study are catalytic hydrogenation and polymerization (which includes cyclization). The literature in these areas is discussed in subsequent sections.

2.1 HYDROGENATION

The catalysts which have been used in hydrogenation reactions are essentially those in group VIII of the periodic table, e.g., Fe, Co, Ni, Pd, and Pt (15). Metals and/or supported metals catalyze this process by virtue of their ability to adsorb hydrogen (15). Other transition elements or their oxides (Cr, Mo, W, Cu, Zn) have also been found useful, however they effect hydrogenation at moderate temperatures only when high pressures are used (16).

Like the simple carbon-carbon double bond, the triple bond in acetylene can be hydrogenated in the presence of a wide variety of metals. A unique feature of the hydrogenation of acetylene is that hydrocarbons containing more than two carbon atoms are found in the products and that they sometimes constitute a major part of the products (15). This tendency of acetylene towards hydrogenative polymerization is called hydropolymerization. In the presence of hydrogen, hydrocarbon polymers are formed at temperatures substantially less than that at which acetylene polymerizes by itself, even in the presence of a catalyst. Evidence for this comes from infrared studies of acetylene adsorption on various supported metals in the presence of hydrogen and from thermal desorption studies following acetylene hydrogenation on Pt/Al_2O_3, Pt/SiO_2, Rh/SiO_2 and evaporated Pd films (16).

Bond (16) has shown that the same catalyst can be used for hydrogenation and hydropolymerization and that reaction conditions determine which reaction predominates. An increase in temperature favors hydropolymerization because the activation energy is believed to be higher than for hydrogenation. The nature and distribution of the polymers in the products of acetylene hydrogenation have been investigated using nickel on zinc chloride, nickel-pumice and nickel-alumina as catalysts (16). The approximate distribution in terms of the carbon atoms in the polymer molecules formed over nickel-pumice in a flow system between 200 and 250°C is given in Table 2.1. Approximately two-thirds of the products are low boiling hydrocarbons ($C_n < 14$). The C_4 fraction represents a sizeable yield. Since the processes for the conversion of butenes to gasoline have been used in petroleum refineries, this fraction will be explored further. The C_4 fraction of the polymers formed in the hydrogenation of acetylene over some alumina-supported Group VIII metals has been analyzed and is shown in Table 2.2. The temperatures used are low, 15 to 130°C, in order to avoid thermal reactions. The major products appear to be butenes. The distribution of the C_4 oligomers is altered substantially depending on the metal component and the temperature. Iridium leads to a significant proportion of saturated product, butane. Polymerization in the presence of hydrogen seems chiefly associated with metals of smaller atomic radii (91). At comparable temperatures and gas pressures, hydropolymerization increases in the order shown:

Ir	≈	Pt	<	Pd	≈	Rh	<	Cu	<	Ni	<	Co	<	Fe
0.126		0.129		0.128		0.125		0.117		0.115		0.116		0.117

Atomic radii (nm)

with iron being the most effective. This ranking provides a useful guide for selecting transition elements for bifunctional catalysts.

Some of the more recent studies on the C_4^+ oligomers formed during acetylene hydrogenation have been carried out in connection with the removal of acetylene from

Table 2.1

Distribution of polymers formed in the hydrogenation of acetylene over Ni-pumice (Ref. 91)

Number of carbon atoms C_n	Approximate yield (%)	Products identified in fraction
4	25	butadiene
5	2	n-pentane, 2-methylbutane
6	25	n-hexane, 3-methylpentane, C_6H_6
7	2	3-methylhexane
8	5	2-, 3-, 4-methylheptane
9-14	7	n.d.[a]
15-30	17	n.d.
31^+	17	n.d.

[a] not determined

Table 2.2

Composition of the C_4 products (%) from acetylene hydrogenation over alumina-supported group VIII metals (16)

(initial H_2/C_2H_2 = 1)

Metal	T [°C]	Butadiene	1-butene	2-butene cis	2-butene trans	butane
Pd	17.6	tr	59.3	13.5	23.3	3.9
Rh[a]	13.0	0.0	42.5	34.3	7.3	7.2
Pt	135	8.3	46.5	20.3	22.1	2.8
Ir	130	0.0	35.4	17.9	1.5	45.2

[a] isobutene detected in product 8.7 %

ethylene streams, therefore, the concentration of acetylene used in these experiments is very low (51, 60, 66, 82, 83). Much of the research effort has been directed at minimizing the amount of "green oil" or oligomeric products formed in acetylene hydrogenation. Nevertheless, under some conditions, approximately 20 % of the acetylene in these streams has been converted to C_4^+ oligomers. The C_4^+ oligomers consist of volatile products (butenes, butane, butadiene) and non-volatile products (surface polymer) at the reaction temperature. Table 2.3 shows the selectivity to the volatile oligomers (mostly butenes) for a variety of supported palladium catalysts (83). The zeolites with very high Si/Al ratios, e.g., silicalite and ZSM-5 exhibit the highest selectivity. The amount of surface polymer formed as a function of time on stream for several alumina supported Pd catalysts is given in Table 2.4. The amount of polymer formed shows significant variation with the support used. This suggests that the support may play a major role in the hydropolymerization process.

Bond has proposed the following mechanism to explain polymer formation from acetylene reacting over oxide-supported Group VIII metals (15).

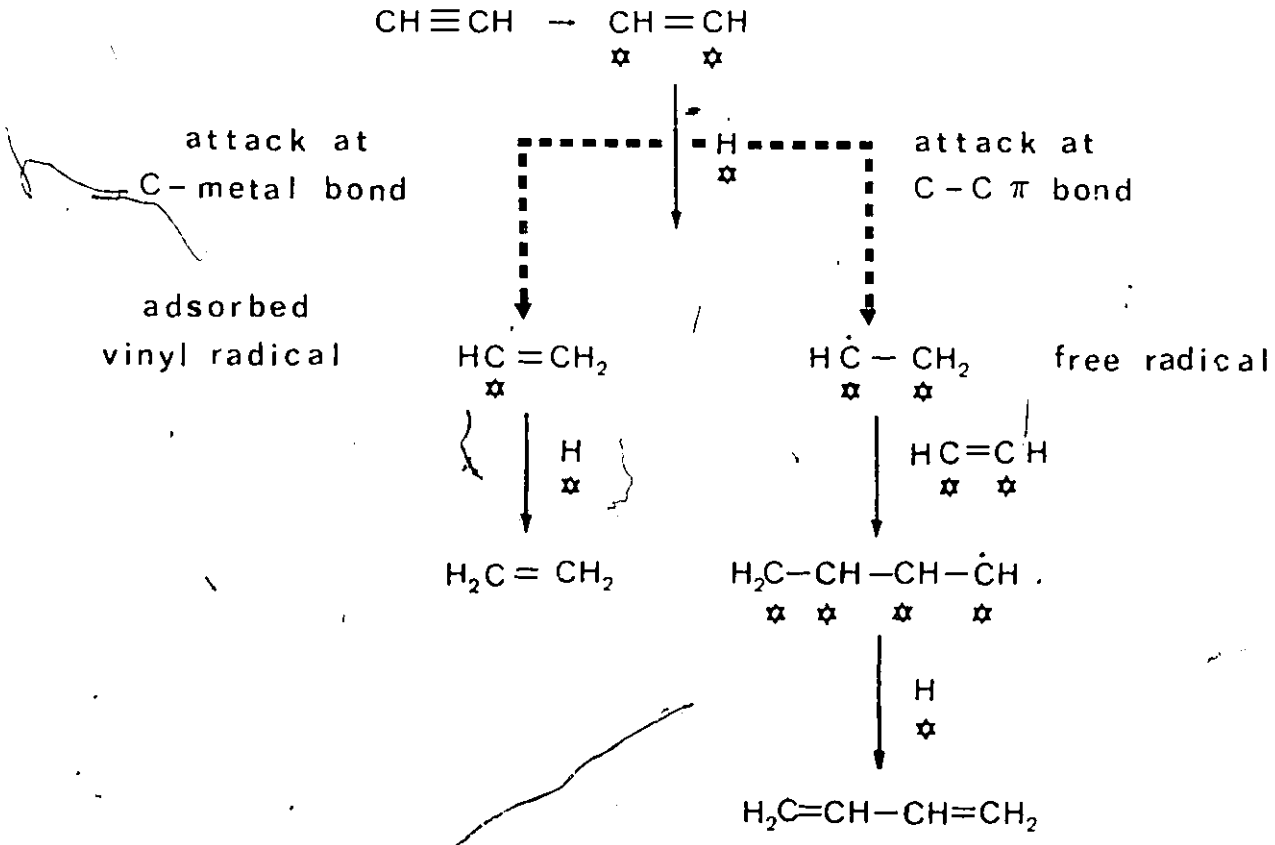

Table 2.3

Average selectivities to oligomer on various catalysts at 80°C for low hydrogen feed gas (83)

Catalyst	S (oligomers)
0.031% Pd on silicalite	0.31
0.057% Pd on ZSM-5	0.23
0.033% Pd incorporated into ZSM-5	0.29
0.024% Pd on Na-Mordenite	0.13
0.040% Pd on γ-alumina	0.24

Table 2.4

Amount of surface polymer formed in the hydrogenation of acetylene over various catalysts (60)

Catalyst	Time-on-Stream [h]	Polymeric Product Amount [mg/g cat]	Rate of formation [mg/g/h]
$Pd/\gamma\text{-}Al_2O_3$	12	3.68	0.30
	47	10.2	0.21
	227	36.3	0.16
ICI 38-1[a]	140	17.13	0.12
$Pd/\gamma\text{-}Al_2O_3$[b]	150	6.17	0.04
Cu/ICI 38-1[c]	77	12.76	0.16

[a] ICI 38-1 contained 0.04 % Pd on γ-alumina
[b] 0.017 % Pd on γ-alumina
[c] 95 % Cu on ICI 38-1

The first step in this mechanism is the adsorption of the acetylene molecule. Adsorption of acetylene on hydrogenation catalysts is so strong (stronger than alkanes, alkenes) that associatively adsorbed acetylene is assumed to be irreversibly adsorbed. Subsequent attack by adsorbed hydrogen leads to an adsorbed vinyl radical when a carbon-metal bond is broken and a free-radical when a π bond between two carbons is eliminated. The free-radical form of the adsorbed vinyl radical is believed to initiate a vinyl polymerization process in which adsorbed acetylene molecules act as the monomeric units. Although free-radical mechanisms have been useful in describing the thermal reactions of acetylene (10), there is little, if any, experimental evidence that free radicals exist under catalytic conditions, therefore some uncertainty exists in their suitability in describing the catalytic reaction of acetylene. Nevertheless, the adsorption of acetylene and hydrogen on the catalyst surface appears to play a major role in the reaction scheme and warrants further comment.

Several workers (1, 47) have proposed the existence of two other adsorbed acetylene states, the ethylidyne complex and a C_2H_x species ($x < 2$).

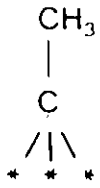

-a-

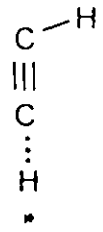

-b-

Kesmodel et al. (47) have detected the ethylidyne complex on the Pt(111) surface using LEEDS (Low Energy Electron Diffraction Spectroscopy) and have speculated that this complex is responsible for the hydrogenation of acetylene to ethane directly. Two criteria must be met for the ethylidyne species to exist, the presence of hydrogen atoms on the surface and the presence of three surface sites in a given geometrical arrangement. The third acetylene state, i.e., the C_2H_x species, is believed to be responsible for the

formation of C_4 oligomers and the polymeric deposits on the catalyst surface (1). Al-Ammar et al. (1) have found that the value of x varies with the metal component, e.g., x=1.4 for Pd (0.128), 1.6 for Ir (0.126) and 1.8 for Rh (0.125) (1). The atomic radii for these elements is given in parentheses. The fact that x varies inversely with the atomic radii of the metal may be significant. Unfortunately, no determination of the value of x has been made for transition metals with lower atomic radii, e.g., Fe and Ni, which as discussed previously have higher hydropolymerization activity. The exact nature of this C_2H_x species is not known.

2.2 POLYMERIZATION

Polymerization of acetylene has been studied using both homogeneous and heterogenous catalysts. The homogeneous catalysts, which are used in the liquid phase, include catalysts based on metal carbonyls (99), e.g., $Ni((CO)PPh_3)_2$, organometallics (41, 77), e.g., $Al(C_2H_5)_3$ and mineral acids (67), e.g., H_2SO_4, H_3PO_4. Carbonyls and carbonyl complexes of iron and nickel have been used as cyclization catalysts mostly for laboratory-scale purposes and have not in general been considered for industrial use (41). The long list of heterogeneous catalysts includes clays and related oxide systems, e.g., activated clay, alumina, activated carbon, silica gel and zeolites, e.g., Y zeolite, ZSM-5. With the exception of the organometallics, the unifying thread in most of these catalysts is the belief that the polymerization reactions in general are acid-catalyzed (74). Homogeneous organometallic-catalyzed and heterogeneous acid-catalyzed polymerization are discussed below.

2.2.1 Homogeneous catalysts

Homogeneous catalysts were first used for acetylene reactions as early as 1910 for the synthesis of ethanol (41). Research peaked in the 1940's when wartime restrictions on raw materials forced the Germans to investigate both CO and C_2H_2 based

processes for the production of fuels. Ziegler-Natta organometallic catalysts, which consist of titanium chlorides with aluminum and magnesium alkyls, have been widely used in the polymerization of alkenes and alkynes (77). The polymerization of acetylene in the presence of $Al(C_2H_5)_3$ + $TiCl_4$ at 25°C, yields 50 % benzene and 24 % linear polymer (77). Replacement of $TiCl_4$ by $TiCl_3$ leads to the formation of extremely unsaturated linear polyacetylenes. Similarly, if $Al(C_2H_5)_3$ is replaced by $Cr(C_2H_5)_4$, $Ti(C_2H_5)_4$, the sole reaction product is linear polyacetylene. Replacement of the titanium halide by VCl_4 however leads to the exclusive formation of benzene. Some workers have reported obtaining benzene from acetylene in up to 72 % yield (77). The general feature of all these catalysts is the formation of a coordination complex bond between the π-orbitals of the acetylene and the d-orbitals of the transition metal (Ti, V) together with redistribution of the electrons and the formation of new C-C bonds.

The disadvantage of these homogeneous transition metal complexes as catalysts is the difficulty of handling them and separating them from the reactants. The success of two commercial homogenous processes, the Wacker process for oxidation of ethylene to acetaldehyde and the Monsanto process for carbonylation depends partly on the relatively low boiling points of the products (acetaldehyde 20.8°C and acetic acid 117.9°C) (41). This will in general not be the case for motor fuels production. These catalysts, therefore, will not be considered further.

2.2.2 Heterogeneous Catalysts

Much of the work on the polymerization of acetylene over solid catalysts has been carried out in the period 1900-1970. A large number of these are summarized in Tables 2.5 and 2.6. The catalysts used include sand, alumina, charcoal, silica gel, acid clay, silicon carbide and many others. Of note are the high liquid yields obtained and the significant low boiling aromatic fraction (useful fuel range hydrocarbons) of the liquid product. These studies carried out at high temperatures are not conclusive and are

Table 2.5

Maximum liquid yields reported from acetylene pyrolysis (1900-1935)

Reference	Description	Temp [°C]	Liquid Yield [wt %]	Benzene Content [wt %]
Meyer(63)	Series flow tube H_2 as coreactant	650	60	20
Zelinski(101)	Glass flow tube Activated charcoal	650	70	35
Kovache and Tricot(50)	Porcelain flow tube, various packings	650	70	35
Ika and Ogura(44)	U-shaped flow tube	650	70	60
Fujio(32)	Glass, porcelain flow tube, acid clay	650	82	-
Fisher et al. (30)	Porcelain flow tube, silica gel	650	70	38
Hague and Wheeler(39)	Quartz flow tube	650	61	26
Berl and Hofmann(14)	Glass flow tube, H_2O as coreactant various packings, $CaO, SnO_2, NaSiO_3$	740	-	30

Table 2.6

Maximum liquid yields reported from acetylene pyrolysis (1935-1970)

Reference	Description	Temp [°C]	Liquid Yield [wt %]	Benzene Content [wt %]
Schwarz and Bessel(87)	Flow tube, V_2O_5 on pumice, CO as co-reactant	650	22 44	66 40
Cadariu(19)	Flow tube, Al_2O_3, AlF_3, SiC, graphite C_2Ca	650	80	45
Cullis and Nettleton(23)	Static, IR cell Al, Fe, Zn, Ni carbon, clays	400	98	10
Massimilla et al.(58)	Fluidized bed, silica sand, silica gel, graphite, carbon	650	85	60
Chang-Li(20)	Flow tube, glass wool	650	44.5	64

far from systematic. The advantage, if any, of the various packing materials used is unclear in most of this early work because of three factors. First the thermal reaction is significant in the temperature range investigated ($400^{o}C$-$750^{o}C$). At these high temperatures, secondary reactions play a major role in determining the product distribution. Second, the liquid analysis is simply based on boiling point cuts and definition of these cuts is ambiguous. Third, the exothermicity of these acetylene reactions is high and consideration of isothermality is questionable. Massimilla et al. (58) were able to minimize the heat transfer problem in the polymerization of acetylene by using a fluidized bed reactor. They also obtained much higher liquid yields with the fluidized bed than with the fixed bed. Nevertheless, they found no significant improvement with the various packing materials used. The temperature in this investigation was $650^{o}C$ and the catalytic effect may very well have been masked by the thermal reactions. The factors highlighted here were considered carefully in the present investigation.

Many more recent studies on polymerization of acetylene have been of a fundamental nature including infrared and Raman studies on alumina and zeolites and have concentrated on the formation of polyacetylene chains, i.e., linear polymers (12, 42, 90, 93, 100). Spectral evidence indicates that on both γ-alumina and zeolite KX, monomeric acetylene is physisorbed via its π-electron system in "side-on" orientation. Heaviside et al. (42) have shown that the length of polyene chain varies with the activation temperature of the γ-alumina used (temperature of calcination), longer chains being observed at higher activation temperatures. Gravimetric results show that very little polyene (0.5 mg/g) was formed on these alumina surfaces at room temperature. Acetylene polymerizes, nevertheless, at very low temperatures over these oxides which makes these catalysts worth investigating.

Mardaleishvili and Rapoport (57) have studied the kinetics of the cyclotrimerization of acetylene over niobium oxide (NbO_2) at $0^{o}C$. The catalyst

deactivation was severe even at this low temperature and occurred in two stages. During the course of the first stage (fast deactivation) 70 to 90 % of the catalyst surface was rapidly covered with a layer of carbonaceous deposits with the composition H/C = 1. During the course of the second stage (slow deactivation) the H/C ratio of the deposit decreased while the quantity of carbon remained essentially constant.

The conversion of acetylene to benzene over Pd supported on alumina has been studied as part of an extensive investigation of the pressure dependence of this reaction using AES (Auger Electron Spectroscopy) and LEEDS (81, 56). Acetylene cyclotrimerization to benzene was examined on palladium single crystals, films and supported on alumina in ultrahigh vacuum (10^{-12} atm) where the reaction is stoichiometric and at atmospheric pressure where the reaction is catalytic. Appreciable amounts of benzene were observed with palladium on alumina only at temperatures exceeding 150°C. Benzene, ethylene and ethane were the only products observed. At temperatures above 200°C, the relative amount of benzene increased.

Several important findings emerged from these studies. First, at atmospheric pressure, the cyclotrimerization reaction was found to have a low activation energy, 2 kcal/mol. This activation energy appeared to be independent of the palladium surface (whether film, single crystal or supported). Rucker et al. (56, 81) suggest that perhaps the benzene is formed on an overlayer of ethylidyne or other carbonaceous fragments onto which it would be loosely bound. They also suggest that the low activation energy can also be explained by incorporating an adsorption equilibrium constant into the rate law. The effect of additives (K, Si, P, S, and Cl) on the high-pressure catalytic reaction (1 atm) was studied only on palladium single crystals. On the most active surface, potassium and silicon enhanced the rate of cyclotrimerization, phosphorous, sulfur and chlorine, decreased the rate. Sulfur, chlorine and potassium decreased the rate of benzene formation. The activation energy and pressure dependence for benzene formation on additive covered surfaces did not change from the values obtained on the clean surface.

Sulfur and chlorine, the electron-withdrawing additives also increased the amount of carbon present on the surface after the reaction. It was postulated that the difference in the rate of benzene formation for the different modified surfaces was related to the amount of open Pd surface area. During the reaction, carbon deposited on the surface and blocked reaction sites. This surface carbon could be in the form of amorphous carbon or polymer with CH or C_2H stoichiometry. Electron-withdrawing additives enhanced the polymerization process by acidifying the metal surface. The increased surface carbon coverage decreased the rate of benzene formation. Electron-withdrawing additives kept the surface cleaner by slowing the surface polymerization reaction. At high pressures the additives shifted the product distribution of the acetylene reaction between benzene and surface polyacetylene or decomposition.

Homogeneous nickel catalysts (organonickel compounds) (99), nickel supported on silica gel (Ni^{2+}/SiO_2) (29) and nickel ions in NiY zeolites (73) have been shown to be active in the cyclotrimerization of acetylene at room temperature. The conversion of acetylene to benzene occurs with close to 100 % selectivity over thermally reduced Ni/SiO_2 (73). Acetylene cyclotrimerization proceeds 30 to 40 times more slowly on the unreduced catalyst than on the reduced catalyst. Catalyst preparation and pretreatment are important in supported metal catalysts and warrant careful consideration.

The cyclotrimerization of acetylene on NiY zeolites containing 10, 14 and 19 Ni cations per unit cell after treatment in oxygen at 200 and 600°C was investigated by X-ray diffraction analysis (XRD), IR and EPR spectroscopies (73). The acetylene was added at room temperature. The trimerization of acetylene is much slower on the zeolites containing lesser amounts of nickel. The samples calcined at 200°C contained 0, 1.2, and 5.8 Ni^{2+} ions in the supercages (XRD) and were far less active than those treated at 600°C. These studies showed that catalyst activity depends on the number of dehydrated or partly dehydrated Ni_2^+ ions inside the supercages. In fact, only traces of benzene are formed on Ni-10 after 24 h of contact. Two reasons were given for this. First, C_2H_2

molecules cannot reach and complex the Ni^{2+} ions inside the hexagonal prisms. Second, the Ni_2^+ ions in the sodalite cages are inactive in the production of significant amounts of benzene since a benzene molecule cannot escape through the 2.3 Å sodalite cage aperture. The Ni^{2+} population in the Y zeolite cage is roughly constant for the samples treated at 600°C whereas the amount of C_6H_6 formed varies from traces (Ni-10) up to the filling of the supercages (Ni-14 and Ni-19). Furthermore, the benzene formed could be completely removed from the zeolite by evacuation at 100°C.

Pichat et al. (73) also showed that cyclotrimerization is not the only reaction which occurs. Other species are found in small amounts, Ni^0 and Ni^+ were detected by electron spin resonance studies. By comparison with studies of nickel supported silica, $-CH_2$ groups found were attributed to linear polymerization of acetylene on nickel metal. The amounts of Ni^0 and $-CH_2$ species increase with contact time and nickel content (73). Careful characterization of these catalyst surfaces has been shown to be very important in determining the role of the metal and of the support in these reactions.

The cyclotrimerization reaction has also been studied over Cr-exchanged Y zeolite in a quartz microbalance (52, 53). At a reaction temperature of 160°C, the acetylene reaction using CrY zeolite yields only benzene. Cr(VI) has been shown to be a more active catalyst than CR(III). At higher temperatures the reaction is less selective, with benzene, aliphatic (C_4-C_6) and alkylaromatic hydrocarbons being obtained. Acetylene adsorption on CrY is much higher than on NaY zeolite. NaY zeolite does not show any significant activity between 70 and 350°C and 4 kPa. NiY zeolite (Ni-8) was tested under the same conditions at 200°C and showed similar conversions and selectivity to CrY (Cr-8). There is evidence here of some disagreement with Pichat et al. (73) who report virtually no reaction with NiY for Ni^{2+} concentration under 10 ions/unit cell. Léglise et al. (52) suggest that, at the higher temperatures, cyclotrimerization is limited by the zeolite structure, i.e., pore blockage by high molecular weight residue. Below 200°C, activity increases with Cr content. Above 200°C the activity becomes independent of chromium

content.

In a static pyrex reactor, Léglise et al. (53) studied the formation of alkylaromatics by acetylene reaction over CrY zeolites. These workers found that benzene was the major product at 350 ^{o}C but toluene, ethylbenzene, xylene and higher alkylbenzenes (and traces of naphthalene) altogether exceed benzene. In the aromatic C_8 fraction, styrene is abundant over NaY but almost absent over CrY. In addition to aromatic hydrocarbons, some aliphatics are formed over both zeolites. Vinyl acetylene is the main aliphatic in the reaction over NaY but the distribution is more diversified in the case of CrY, e.g., C_6 (C_6H_{14} to hexadienyne), C_4 (butane to vinylacetylene), C_5 (C_5H_{12} to C_5H_8) and C_3 (propane to propyne). The role of sodium in these reactions is not clear. Moreover, in these high conversion batch experiments secondary reactions, e.g., isomerization and alkylation, are prominent and this limits the usefulness of the information obtained.

The effect of temperature on the products and residue formed over CrY (Cr-12.9) after two hours is illustrated in Fig. 2.1. The acetylene conversion first increases up to 150^{o}C and then decreases from 150^{o}C to 300^{o}C but rises again at higher temperatures. Studies undertaken in a vacuum microbalance showed that the composition of the irreversibly adsorbed residue was temperature dependent (53). At 70^{o}C, the residue came off as benzene upon heating at 360 ^{o}C. At 200 ^{o}C, only 80% of the residue desorbed upon heating to 360^{o}C and the products were C_3 to C_6 aliphatics (36%), toluene (16%), C_8 (15%), C_9 (14%), benzene (10%) and acetylene (8%). For higher reaction temperatures (300 and 360^{o}C) no change in mass was noted after prolonged heating but some hydrogen was evolved. This would imply that at reaction temperatures above 300^{o}C significant secondary reactions are occurring which lead to tar formation.

Recently, investigations of acetylene reactions over ZSM-5 type catalysts have been reported (94, 97). The reactions of acetylene over these zeolites were studied by Tsai and Anderson (94) in a quartz flow microreactor containing 0.1 g of catalyst at a

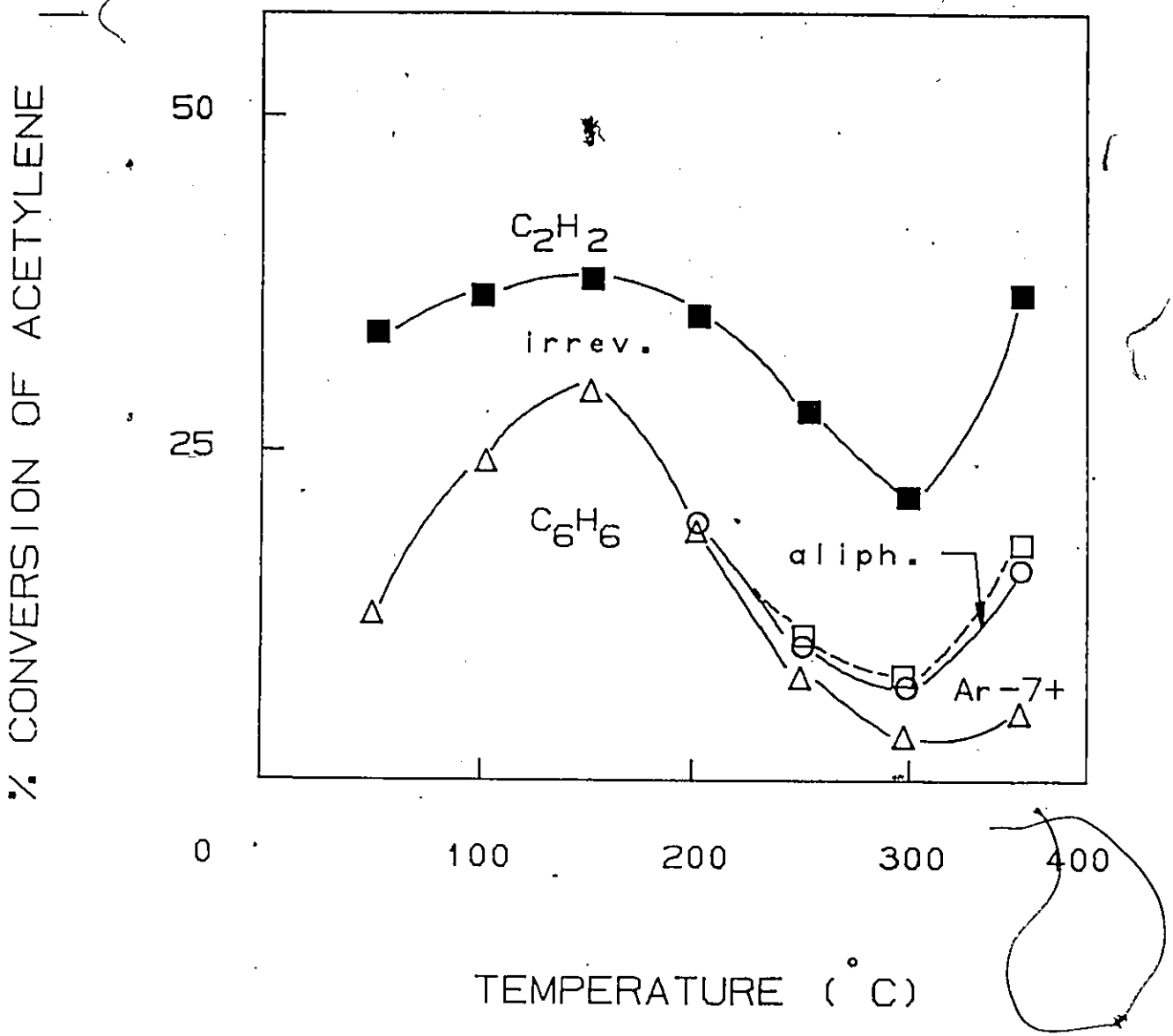

Fig. 2.1 Effect of temperature on the products formed over CrY zeolite. (Ref. 53)

△ C_6H_6

○ Ar 7^+

□ aliphatic

■ C_2H_2

total pressure of 101.1 kPa and temperatures between 250 and 500°C. Three important results emerge from their work. First, in the absence of hydrogen in the feed, acetylene was converted with very high selectivity to aromatics (99%) in the C_6 to C_{13} range. The aromatic products in this range were always a mixture but the following main components in each class were identified: C_6 - C_8 (benzene, toluene, xylene), C_9 (methylethylbenzene, trimethylbenzene), C_{10} (naphthalene, tetralin, alkylbenzenes), C_{11} (2-methyl-naphthalene), C_{12} (dimethylnaphthalene, 2 ethyl-naphthalene) and C_{13} (alkyl-naphthalenes). Second, when hydrogen was used as a coreactant, the product distribution was altered significantly in that it resulted in the conversion of a substantial fraction of acetylene to ethylene. Third, catalyst deactivation was severe in all cases and most of the activity data are given for 15 min on stream. Although acetylene conversion at 350°C was noted to decrease from 30 % to 7 %, as the SiO_2/Al_2O_3 ratio in ZSM-5 was varied from 25 to 436, it was not pointed out that the decrease was linear for Si/Al ratios below 240. Recently it was shown that varying the SiO_2/Al_2O_3 ratio in ZSM-5 alters the acidity of the catalyst surface (13). Higher ratios were shown to correspond to a lesser number of Bronsted acid sites. Although the conversion decreases by only 2 % from a Si/Al ratio of 243 to 436, the liquid product distribution changes somewhat as seen in Figs. 2.2 and 2.3. A shift to lower molecular weight products is evidenced as the Si/Al ratio is increased. Acetylene conversion increased with temperature (250-500°C) from 4.3% to 38.2%, however, space velocity increased simultaneously with reaction temperature in these experiments. At higher space velocities the conversion decreases therefore the effect of temperature on conversion is likely to be greater than reported. Furthermore, at 400 and 500°C, thermal conversion of acetylene is expected, yet no thermal reactions were reported. Catalyst deactivation increased with increasing time-on-stream. The product distribution shifted to larger quantities of C_{10} - C_{13} aromatics with longer times-on-stream.

The use of Fe replacing Al in the ZSM-5 framework has recently been disclosed in the patent literature (97). Table 2.7 summarizes some examples of acetylene conversion

Table 2.7

Acetylene conversion to liquids over ZSM-5 (97)

Conditions		Experiment 14	19	23
Feed C_2H_2	[cm^3/min]	0.5	0.5	0.4
H_2		-	1.0	2.2
He/N_2		2.9	6.0	3.0
Catalyst		H-ZSM-5	H-ZSM-5	Fe-ZSM-5
SiO_2/Al_2O_3		120	120	140
Temperature	[°C]	400	400	400
WHSV C_2H_2	[h^{-1}]	0.4	0.4	0.3
Results				
Conversion	[%]	45.1	35.5	86.9
Products	[wt %]			
	Non-aromatics	11.3	13.1	4.1
	BTX	60.4	55.5	30.6
	C_9	10.5	25.2	10.7
	C_{10}^+	17.9	6.1	54.3

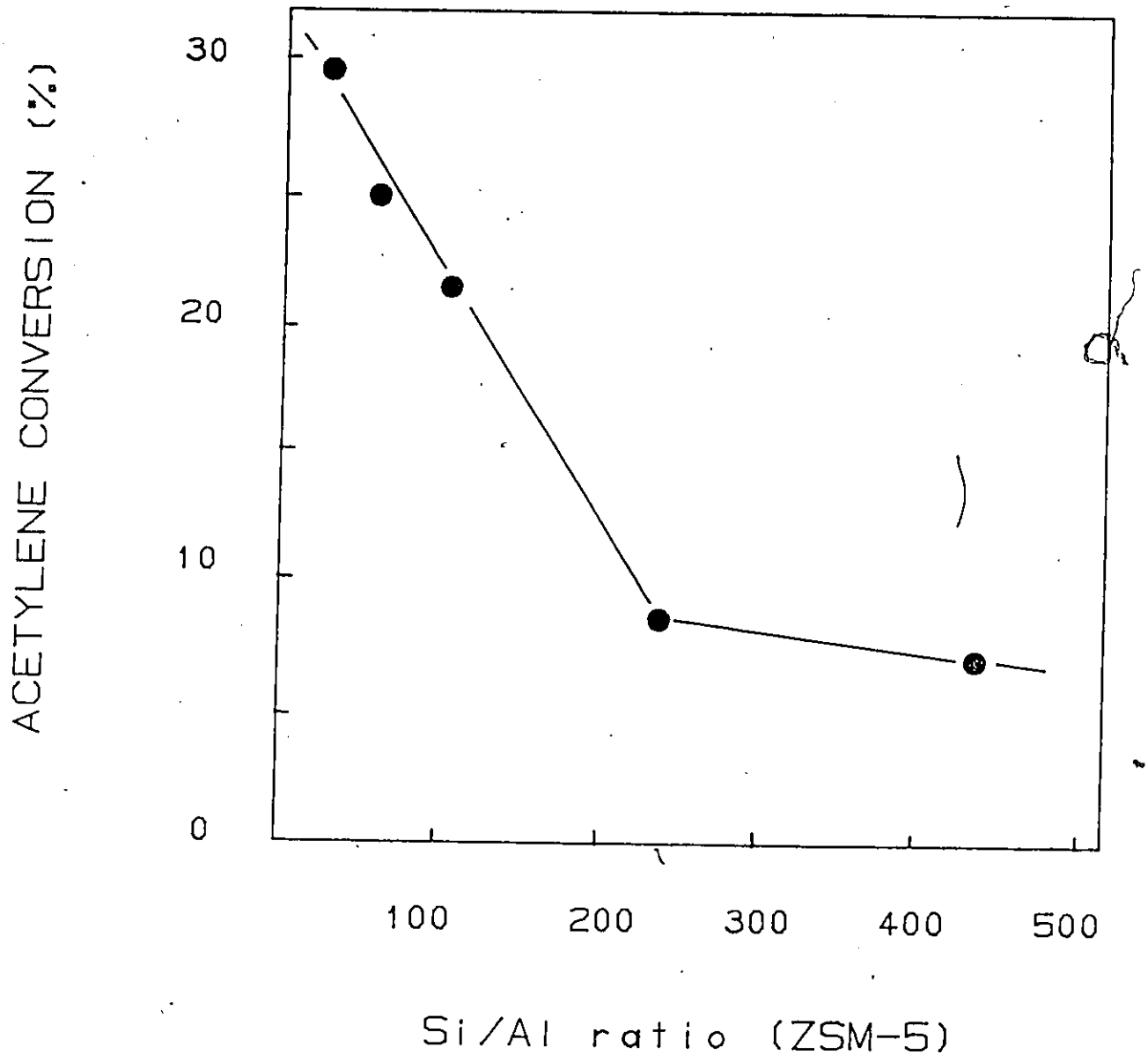

Fig. 2.2 Acetylene conversion as a function of Si/Al ratio in ZSM-5 (94).

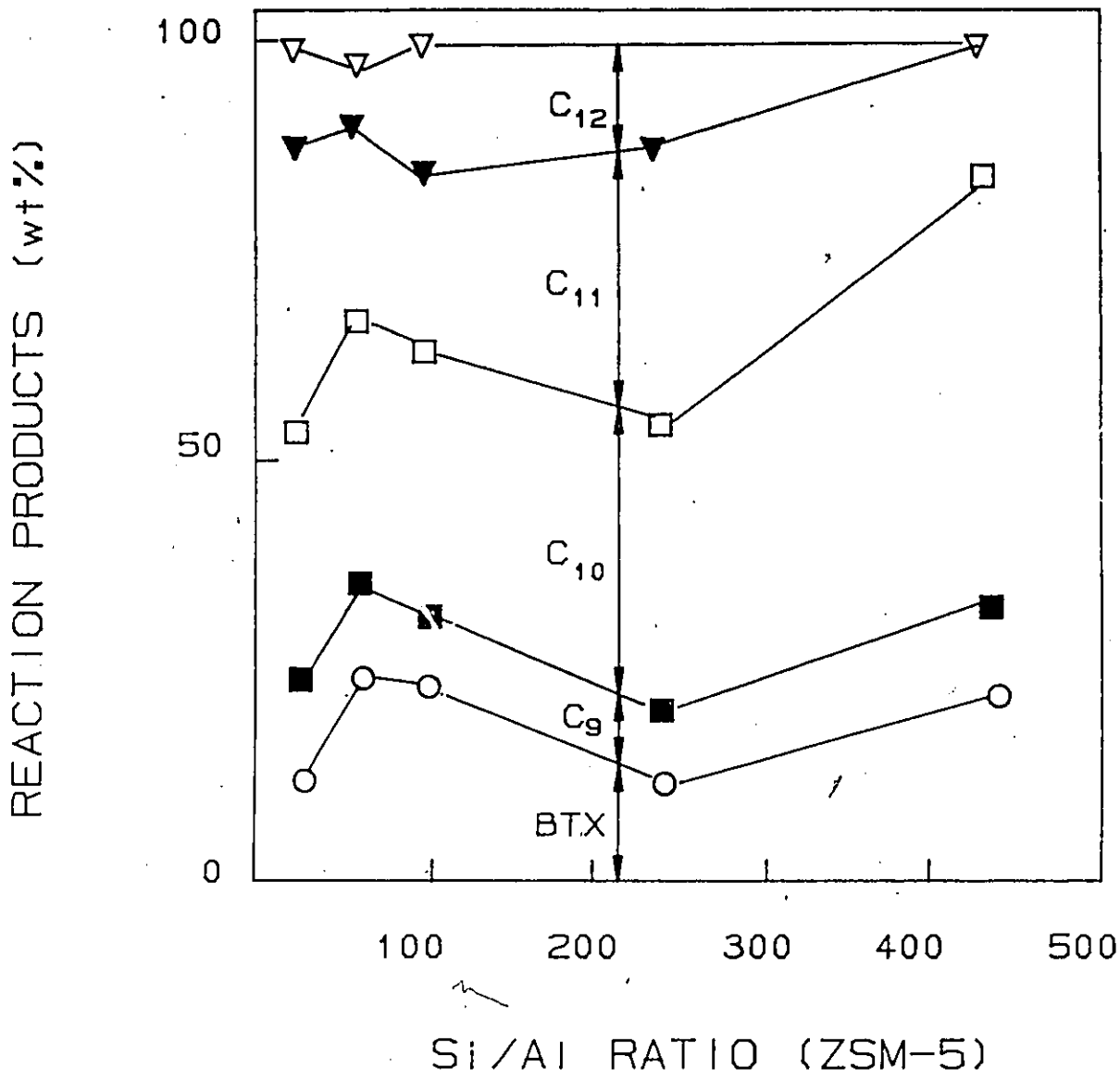

Fig. 2.3 Product distribution in the conversion of acetylene to liquids over ZSM-5. (94)

from the patent. If it is assumed that all the conversions and product distributions are reported for 15 min on stream, then it appears that the presence of iron drastically alters the activity and the product distribution of the ZSM-5 catalyst. A discussion would be speculative because of the scanty description given in the patent.

2.2.3 Reaction mechanism

Polymerization reactions of unsaturated hydrocarbons are believed to be acid-catalyzed (74). Tsai and Anderson (94) have proposed the following mechanism for the reaction of acetylene over ZSM-5:

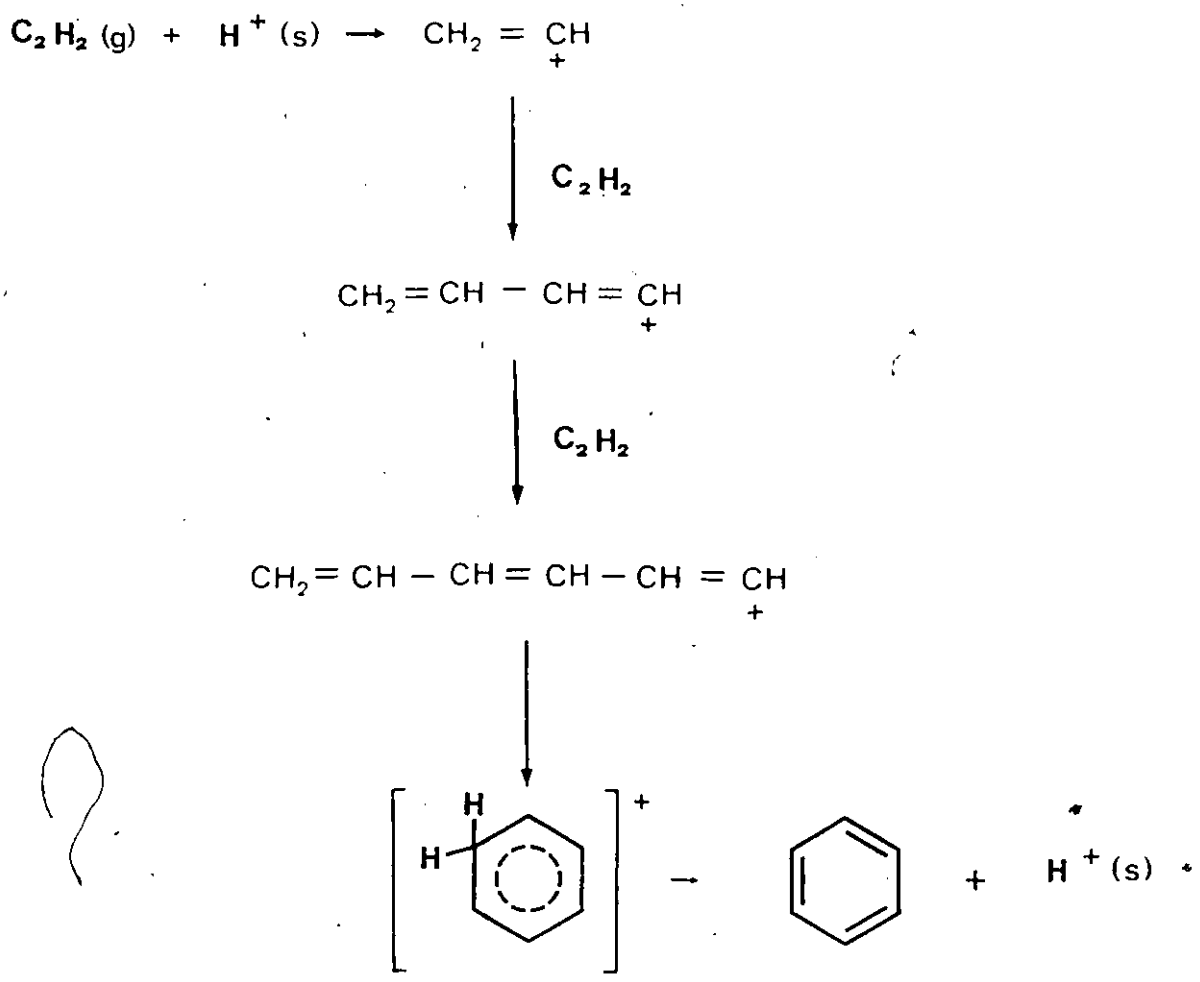

The polymerization is proposed to proceed via a vinyl cation intermediate. The concept of the vinyl cation appears to explain the aromatic products found and is consistent with the carbonium ion theory of acid-catalyzed reactions. However, reactions between the vinyl cation and H_2 (g) suggested by these workers to explain the non-aromatic products found is extremely speculative. Furthermore rearrangement of the carbonium ions in steps 2 and 3 to more stable intermediates (3^0 ions) is highly probable. A significant amount of butenes and branched C_4's would result which have not been observed. This mechanism is therefore not consistent with their experimental findings.

The amount of acidity and acid-strength distribution have been shown to vary with the nature of the cation present, the degree of exchange and the heat treatment (18, 76). Partial poisoning of the acid sites in ZSM-5 by Na exchange (54 % exchange) was shown to cause a 50 % reduction in acetylene conversion (94). A significant shift to higher molecular weight products in the product distribution was also noticed for the polymerization reaction. This may imply that even weak acid sites are active in secondary tar-forming reactions.

The vinyl cation mechanism would imply considerable coke formation since once aromatics are present, they can react to give higher molecular weight hydrocarbons and coke, which are believed to be formed by condensations and combination of aromatics with other aromatics as coke. The formation of coke from benzene is illustrated by the following reaction sequences (33):

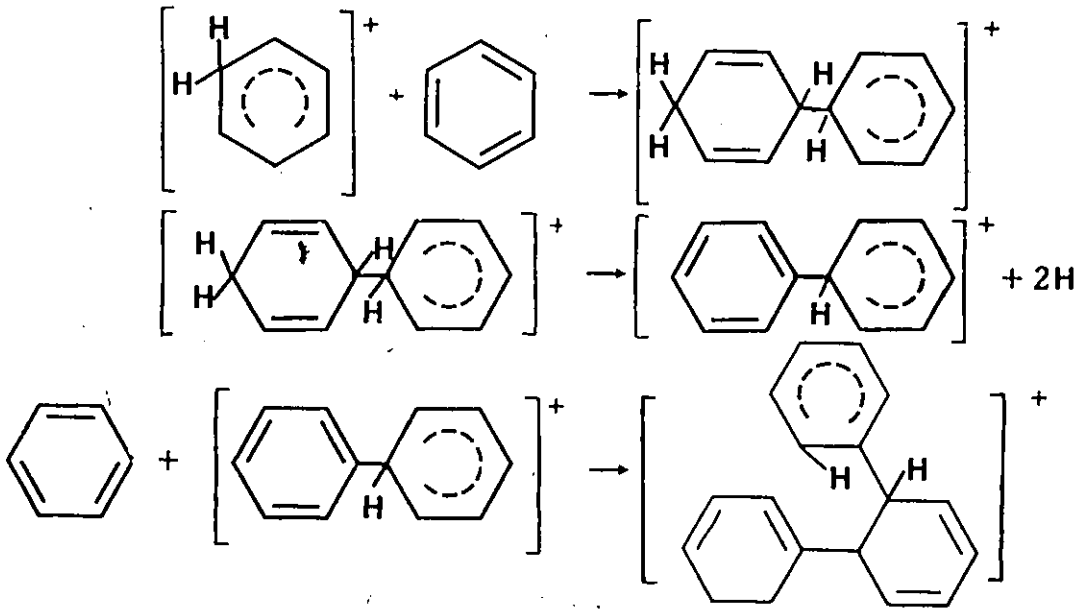

The interest that recent workers have shown in zeolites as catalysts for acetylene polymerization may stem from the following observations on acid-catalyzed reactions (25):

(1) the rate of formation of coke is lower in zeolites than in their amorphous counterparts,

(2) the coking tendency changes with variations in structural constraints.

It has been demonstrated with zeolite ZSM-5 that alkylaromatics once formed cannot react further (by cyclization, dehydrogenation or further alkylation) and lead to coke deposition because of the smaller dimensions of the zeolite channels (25). In Mobil's methanol to gasoline process (25) which uses the ZSM-5 zelite, the catalyst has low coking activity and the coke which is formed is believed to be deposited for the most part on the outer surface. The exterior area of the zeolite crystals is only about 1 % of the total, but if diffusion limitations are significant, it becomes necessary to poison or inactivate exterior sites so they do not contribute excessively to the reaction.

Tsai and Anderson (94) compared catalyst deactivation on ZSM-5 for two Si/Al ratios, 25 and 60 respectively. Less coking occurred with the zeolite having the higher Si/Al ratio and presumably the lower acidity. This appears to be consistent with cracking reactions where very high acid strengths, either zeolite x, zeolite Y or silica-alumina lead to excessive formation of coke. Unfortunately deactivation studies for a much higher Si/Al ratio were not reported thus no conclusion can be made as to the effect of the Si/Al ratio in ZSM-5 and other catalysts. Since catalyst deactivation is an important feature of these acetylene reactions, more work is warranted in this area.

It is evident from the studies cited that more experimental work is required in order to understand acetylene polymerization and the role of the catalyst in assisting polymerization. Some catalyst properties intimately related to this reaction which have emerged from this discussion include, acidity, crystallinity, nature of the cation and the degree of exchange. Catalysts with high acidity appear to be appropriate for acetylene

polymerization. The relationship between catalyst performance in this reaction and the catalyst acidity needs to be explored further.

3. RESEARCH OBJECTIVES

The transformation of acetylene to liquid fuels must involve polymerization. The brief discussion in the previous section summarizing the existing literature has identified a large number of catalyst properties which affect polymerization reactions. The scope of the present investigation is to elicit the relationships between some of these catalyst properties and catalyst performance in the polymerization of acetylene. The specific objectives of this research program and the approaches used to attain them are described in detail in sections 3.1 and 3.2.

3.1 EXPERIMENTAL CONSIDERATIONS

One of the major objectives of this study was to obtain quantitative information regarding activity and selectivity of various catalysts in acetylene polymerization. Two problems must be addressed in order to meet this objective. First, a suitable reactor must be designed and constructed and second provision must be made for analysis of the gaseous, liquid and solid products. A detailed description of the tubular flow reactor and the product analysis system which were used for activity and selectivity studies is provided in Chapter 4.

As noted earlier, both hydrogenation and polymerization have large heats of reaction. With fast exothermic reactions, one must be concerned with the elimination of large temperature gradients between catalyst particles, in the gas film surrounding the catalyst and inside the catalyst particles. Axial temperature gradients were minimized through use of a multi-zoned temperature control system in which the tubular reactor was inserted in a metal block which was heated by a three-zone resistance furnace. The use of an inert diluent in the reacting mixture further assisted in attaining isothermality. Calculations based on a number of theoretical criteria were made to determine the extent of the temperature gradients across the gas film and within the catalyst particle

(Appendix 3.1). The results of these calculations, based on some preliminary experiments, were used in determining to some extent the acceptable catalyst particle size, the partial pressures and the total pressure used in the present study to ensure insignificant deviations from isothermality.

Significant emphasis was also placed on the analytical techniques required for the analysis of the reaction products, as detailed in Chapter 4. These techniques included gas chromatography using packed and capillary columns, flame ionization and thermal conductivity detectors, mass spectrometry and numerous surface spectroscopic techniques. In order to make the analysis of the liquid products quantitative a tracer was added to the product stream from the reactor. For the gaseous products, the nitrogen, used as an inert carrier, permitted quantitative analysis. Elemental analysis and solid-state ^{13}C NMR of the carbonaceous catalyst residue was also carried out. With these techniques, the gas, liquid and solid products were quantified and described.

The process variables in the study included the reaction temperature (300-400^{o}C), the weight-time (1-3 g.s.mL^{-1}), and the concentration of acetylene (5-15 vol % C_2H_2). Because of equipment limitations, the absolute pressure range was narrow (130-200 kPa) and was not considered to be an operating variable.

3.2 CATALYTIC CONSIDERATIONS

3.2.1 Surface Acidity

Polymerization reactions of unsaturated hydrocarbons are believed to be acid-catalyzed (74). The polymerization of olefins, e.g., ethylene, propylene and butylene to hydrocarbons boiling in the gasoline range has been carried out commercially using both sulphuric and phosphoric acid (67). To facilitate handling of these viscous mineral acids, they have been supported on inert substances such as diatomaceous earth or silica gel. Supported phosphoric acid has been used since the 1930's to catalyze the

polymerization of refinery streams (C_3 and C_4 olefins) to gasoline-range iso-olefins (C_6-C_{10}). Reactions catalyzed by solid acids, e.g., polymerization, cracking, and isomerization, exhibit features similar to reactions catalyzed by mineral acids and supported mineral acids. By analogy to solution chemistry, the primary requirement for catalytic activity by solids is that the solid be acidic. Alumina, silica-alumina and zeolites have been used as solid acid catalysts in polymerization reactions (84). Since solid acids promote polymerization reactions, a second major objective of this study was to investigate the role of surface acidity in acetylene polymerization.

Pure alumina (Al_2O_3), which has been used extensively as a catalyst and catalyst support may exhibit acidic properties depending on the nature of the heat treatments and resulting changes in structure (84). The acid strength of alumina may be deliberately increased by incorporation of halogen ions such as chloride and fluoride (72). Fluoridation has been shown to enhance the polymerization of olefins and of conjugated dienes (21). Fluoride has also been used as a promoter in co-polymerization (21). Increases in activity occur at low fluoride contents, typically 1 to 6 wt% F (21). In order to investigate the role of surface acidity, a series of catalysts were prepared with various fluoride loadings (F/Al atomic ratios between 0 and 3) and various surface acidities. The performance (activity, selectivity and decay) of these catalysts was then determined for the polymerization of acetylene.

Solid acids are more complex than mineral acids. The acidity of strong mineral acids, such as H_2SO_4 and HNO_3 is completely characterized by measuring the concentration of hydronium ions (pH). On a solid surface the heterogeneity of the sites gives rise to a distribution of acid strengths. In addition, acid sites in solid catalysts may be of the Bronsted type in which the site donates a proton to an unsaturated hydrocarbon or of the Lewis type in which the site acts as an electron pair acceptor from a hydrocarbon. Studying the acidity of a surface consists in measuring the acid strength of the various sites (not all methods distinguish between types of sites i.e., Bronsted or Lewis) and in

determining how many sites are present (38). The techniques used to measure acidity vary and include non-aqueous titrations using Hammett indicators, infrared spectroscopy of hydroxyl groups, adsorption of a gaseous-base (NH_3, pyridine, etc.) (38). The catalysts prepared in this study were characterized by the latter technique because of its versatility. The adsorption temperature was chosen so that the measurements would be representative of the catalyst in its working environment. These studies of ammonia adsorption are described in detail in a subsequent section.

3.2.2 Catalyst Decay

The catalysts discussed in the previous section exhibit severe deactivation under the conditions used for the polymerization of acetylene. This catalyst deactivation is not uncommon to other hydrocarbon systems or to other catalysts. Although catalyst deactivation has been attributed to a large number of factors, one of the major contributors is the buildup of carbonaceous species (residues) on the catalyst surface. Despite its importance, limited information is available on the quantity and type of residues formed over various catalysts in the polymerization of acetylene. One of the objectives of this investigation was to study the behaviour of these fluoridated catalysts as a function of time-on-stream. The tubular flow reactor is not amenable to studies on catalyst deactivation by carbon deposition without significant experimental effort. For this reason the rate of deactivation was studied using the microbalance described in Chapter 4.

The microbalance was used to determine the influence of surface acidity and the influence of the operating variables on catalyst deactivation. The process variables in the microbalance study were within the boundaries of the process variables used in the study with the tubular reactor. They included the reaction temperature (300-400^{o}C), the linear velocity defined as the ratio of the total gas flowrate at reaction conditions to the cross-sectional area of the reaction tube (5-15 cm/min), and the concentration of

acetylene in the gas phase (2.5 - 6.4 vol %). These studies with the fluoridated alumina catalysts were chosen to complement the studies carried out in the tubular reactor; therefore the selected operating conditions were very similar.

4. EXPERIMENTAL PROGRAM

4.1 CATALYST PREPARATION

The materials used in this study were α-alumina monohydrate (Catapal SB, Conoco, Peterboro, New Jersey), ammonium fluoride (Aldrich Chemical Co.) and aluminum fluoride trihydrate (Aldrich Chemical Co.). The fluoridated alumina catalysts were prepared by mixing the α-alumina monohydrate powder with an aqueous solution of NH_4F of the appropriate concentration at room temperature. Approximately 1-2 wt % stearic acid was added as a binder to this solution. Additional distilled water was added to obtain an alumina gel suitable for extrusion. The alumina and fluoridated alumina extrudates were dried in air at 105°C for 8 h and calcined in air at 450°C for 8 h. Following calcination, these extrudates were crushed and separated into three fractions. A catalyst particle size of 0.25 to 1 mm was used throughout this work. The aluminum fluoride trihydrate was highly corrosive and could not be pelletized. It was dried overnight at 110°C and used in a powder form. After preparation, each catalyst was analyzed by selective ion electrode methods to determine the bulk fluoride content and by X-ray photoelectron spectroscopy (XPS) to determine the surface fluoride content. The nominal composition of the catalysts, i.e. the fluoride content of the catalysts calculated from the preparation procedure (a sample calculation is given in Appendix 4.1), ranged from 0 to 68 wt % F.

4.2 CATALYST CHARACTERIZATION

Emphasis was placed on correlating catalyst behaviour (performance) with the physico-chemical properties of the catalyst. Physical and chemical catalyst characterization therefore constituted an integral part of this research program.

4.2.1 Physical Characterization

In order to compare the different catalysts it was necessary to know the extent to which a change in activity was caused by a change in the surface area of a catalyst, in contrast to a change in the intrinsic reactivity caused by a change in the chemical composition. For this reason, measurements were made of the internal pore surface area using a Carlo Erba Sorptomatic Model 1800 instrument and of the pore size distribution using a Micromeritics Autopore 9200 instrument.

To supplement these analyses, surface analytical methods, e.g., XPS, X-ray photoelectron spectroscopy and infrared spectroscopy were used to improve our understanding of the effect of various catalyst modifications on the catalyst performance. XPS is a powerful technique which can analyze semi-quantitatively all the elements except hydrogen and helium (61). This technique was used to determine the surface fluoride loading in the fluoridated alumina catalysts and to identify the presence of AlF_3 in both fresh and spent catalysts. XPS was also used to determine the surface carbon content of catalysts after being exposed to the reaction. XPS observations were made using a Physical Electronics Model 548E X-ray photoelectron spectrometer with a dual Al/Mg anode X-ray gun operating at 300 W in the MgK_α mode (1253.6 eV). The samples were prepared by pressing the powdered catalysts into KBr type discs (14 mm x 2 mm) using an infrared die and hydraulic press.

The structure of the fresh and spent catalyst can also be determined by nuclear magnetic resonance spectrometry (62, 69). In studying ^{19}F NMR of fluoridated aluminas, Schlup and Vaughan (85) concluded that the fluoride occupies the surface phase up to the order of 5 wt % F, and forms a bulk phase of AlF_3 at higher concentrations of fluoride. In this study, solid state magic angle-spinning cross-polarization ^{13}C NMR was used to explore the nature of the coke deposits on the spent catalysts. Measurements were carried out on a Varian XL-300 NMR spectrometer and recorded using a 10 MHz sweep width, an acquisition time of 0.128 s, a pulse width of 8 ms and a contact time of 1 ms.

4.2.2 Chemical Characterization

Surface acidity has been shown to be a catalyst property which is very important in hydrocarbon conversions especially polymerization, alkylation, and isomerization. Therefore, measurement of the relative acidity of the solid catalysts is important. Solid acids are more complex than mineral acids. The acidity of strong mineral acids, such as H_2SO_4 and HNO_3, is completely characterized by measuring the concentration of hydronium ions (pH). Water has a "leveling effect" since hydronium ions, all of equal strength, are the only acidic centres present in aqueous solution. On a solid surface, the heterogeneity of the sites gives rise to a distribution of acid strengths. In addition, both Bronsted and Lewis sites may exist. Thus to characterize a surface completely. it is necessary to measure the number, strength and type of acid sites.

The relative acidity of the catalysts used in this study was determined by adsorption of ammonia at high-temperature. Ammonia will adsorb on both Lewis and Bronsted sites thereby establishing the total acidity of each sample. The adsorption capacity of the catalysts for ammonia was measured using a pulse-chromatographic technique (36) at conditions similar to those in the reactor. The catalyst samples were dried in air at 105°C for 1 h. Subsequently, 40 mg of catalyst was loaded into a 4 mm ID Pyrex tube and this was installed in a gas chromatograph oven (Varian Vista 6000). A schematic of the experimental set-up is shown in Fig. 4.1. The column oven temperature was raised from 300°C to 350°C at 10°C/min and maintained at that temperature for 1 h prior to adsorption studies at 350°C. Moisture- and oxygen-free argon flowed through the sample throughout this period. The exit stream was continuously monitored by means of a thermal-conductivity detector. Pulses of anhydrous ammonia (normally 15 pulses of 10 u mol) were injected into the argon stream via a temperature-controlled, automatic gas-sampling valve. Automation of the chromatograph, injection of the sample and integration of the signal were accomplished with a Varian Vista 402 data station. The

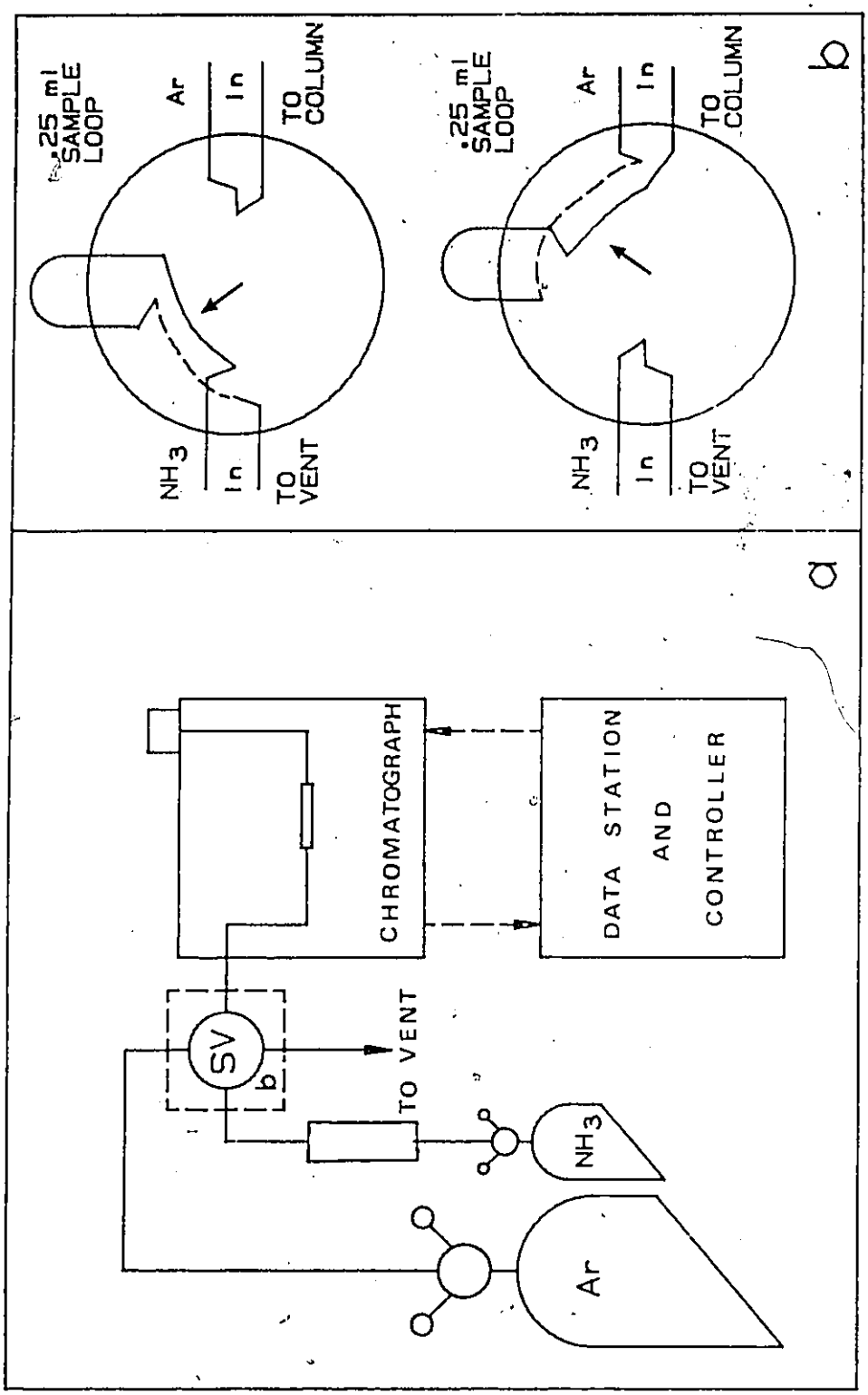

Fig. 4.1 a)Schematic of the experimental set-up for ammonia adsorption studies. b) valving configuration.

adsorption capacity of the catalyst for ammonia, C_{NH3}, was calculated as:

$$C_{NH3} = \left(\sum_{i=0}^{n} (C_{in} - C_{out}) \right)/m \qquad (4.1)$$

where n = number of pulses

C_{in} = ammonia injected in each pulse [mmol]

C_{out} = ammonia remaining in each pulse after adsorption [mmol]

m = mass of catalyst [g]

Sample calculations are given in Appendix 4.2.

4.3 CATALYST TESTING

4.3.1 Fixed Bed Reactor

An experimental system was constructed and assembled for testing these catalysts for the conversion of acetylene. The experimental testing facility consisted of an inlet gas purification and delivery manifold, a fixed-bed tubular reactor and analytical equipment as shown in Fig. 4.2. Each of these is described below:

Inlet Gas Manifold

Nitrogen (99.99%) supplied by Air Products was fed via a two-stage pressure regulator through a low pressure gas purifier (Linde) and an oxygen-trap to a mass flowmeter (Matheson Gas Co.). Atomic absorption grade acetylene (99.5% stated purity) was dissolved in acetone in the gas cylinder supplied by Canadian Liquid Air. Purification was carried out in three stages. The acetylene gas was passed through a cold trap ($-60^{o}C$) where most of the acetone vapor was condensed, bubbled through a concentrated sulphuric acid bath (98%) for further acetone removal and finally passed over an activated charcoal

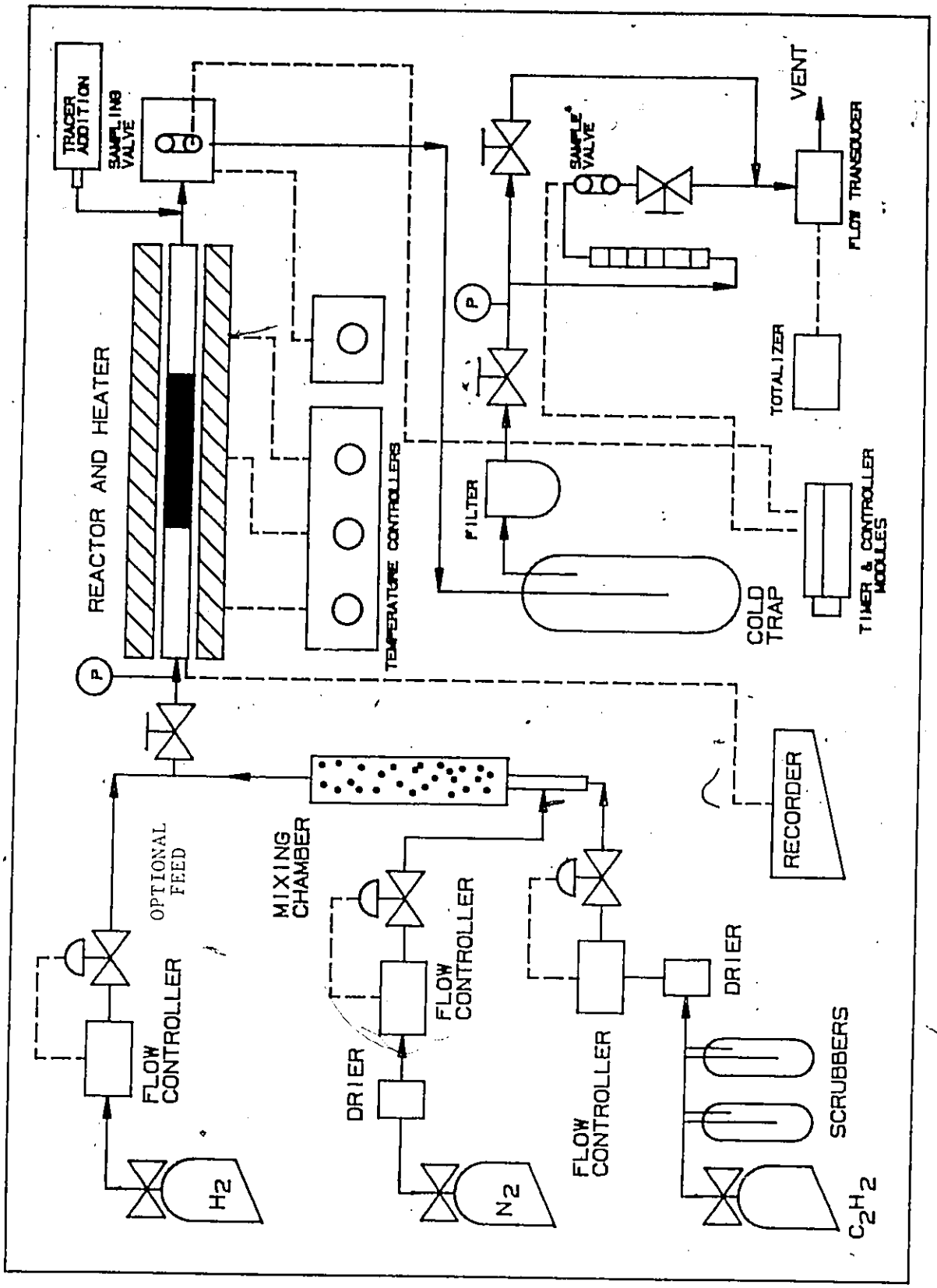

Fig. 4.2 Schematic of fixed bed tubular flow reactor experimental set-up.

trap for trace acetone removal. The purified acetylene stream was metered with a mass flowmeter. Mixtures of acetylene in nitrogen were prepared by having both gases flow at the required rate into a mixing chamber filled with Berl saddles. From the exit of the mixing chamber, the gas mixture was sent to the reactor.

Reactor and Heater

The experiments were carried out in a quartz tubular-flow reactor at a total pressure of 101 kPa and between 300-400^{o}C. The catalyst charge of 5 g was loaded in a 10-mL annular volume (1 cm internal diameter x 15 cm in length) containing a centred stainless steel thermowell (.375 cm OD). Heating was supplied by a three-zone resistance furnace made by wrapping heating coils around a 5 cm OD stainless steel block 1 cm thick. The control thermocouples for the three zones were located on the exterior surface of the stainless steel block. Seven thermocouples along the coaxial thermowell permitted the measurement of axial temperature profiles during an experiment. A maximum temperature variation of +/- 5 K was observed over the 15 cm catalyst section during reaction. Quartz chips and quartz wool were used to separate the inert quartz packing from the catalyst. The pressure drop in the reactor bed was calculated to be approximately 14 kPa (See Appendix 4.3 for calculations).

Product Analysis

The effluent gas was mixed with a stream of nitrogen, which had been saturated with n-heptane, as it exited the reactor. n-Heptane was introduced as a tracer in order to obtain quantitative analysis of the products. Saturation of the nitrogen stream was achieved by flowing nitrogen through a bubbler filled with liquid n-heptane which was maintained at a desired temperature, -15^{o}C. The reaction products exited the reactor via heated lines and flowed through a heated 16-port sampling valve (Valco Model No. AH4-CST-16-HTA) where at regular intervals, the valve position was switched and a product gas sample was stored for later analysis. At the exit of the gas sampling valve the product stream was immediately cooled in a dry ice-acetone bath to condense the liquid

products, e.g., n-heptane, benzene, toluene, naphthalene, etc. The uncondensed components including unreacted acetylene, nitrogen and uncondensed reaction products, e.g., C_2H_4, CH_4, n-butane were sent to a second sixteen-port gas sampling valve where again at regular intervals, the valve position was switched and a gas sample was stored for subsequent gas analysis. This exit gas was monitored with a mass flow meter and a totalizer (Matheson Gas Co.) and later vented. Pressure was monitored using a pressure transducer (Viatron Corp.).

Analysis of the gas samples stored in the multiloop valves was carried out using a Carle AGC 111 Series S gas chromatograph equipped with a thermal conductivity detector. This chromatograph was specially configured (columns and micro valve switching) for natural gas analysis, e.g., alkanes (C_1-C_5), alkenes (C_2H_4, C_3H_6), and alkynes (C_2H_2). A Spectra-Physics 4270 integrator was used to measure peak areas and retention times. Details may be found in Fig. 4.3 and Appendix 4.4. A typical gas chromotogram is provided in Fig. 4.4.

Vapour analysis, i.e., condensible products kept in the gas phase by heating the first 16-port valve was carried out using a gas chromatograph (Varian Vista 6000) equipped with two FID detectors and with capillary and packed column options. A Spectra Physics 4270 integrator was used to measure peak areas and retention times. A 0.25 mm ID, 0.25 µm film DB-5 capillary column 30 m in length was used for trace analysis. Automation of this analysis system is shown in Fig. 4.5 and described in detail by Allenger et al. (6) (see Appendix 4.5).

When possible, the liquid product from the cold trap was recovered and a simulated distillation on a Hewlett Packard 5880A Series Gas Chromatograph with a 0.5 m stainless steel column filled with 10% WC-W982 on Chromosorb PAW was carried out.

4.3.2 Experimental Design and Analysis

A fair comparison of the performance of several catalysts requires examination

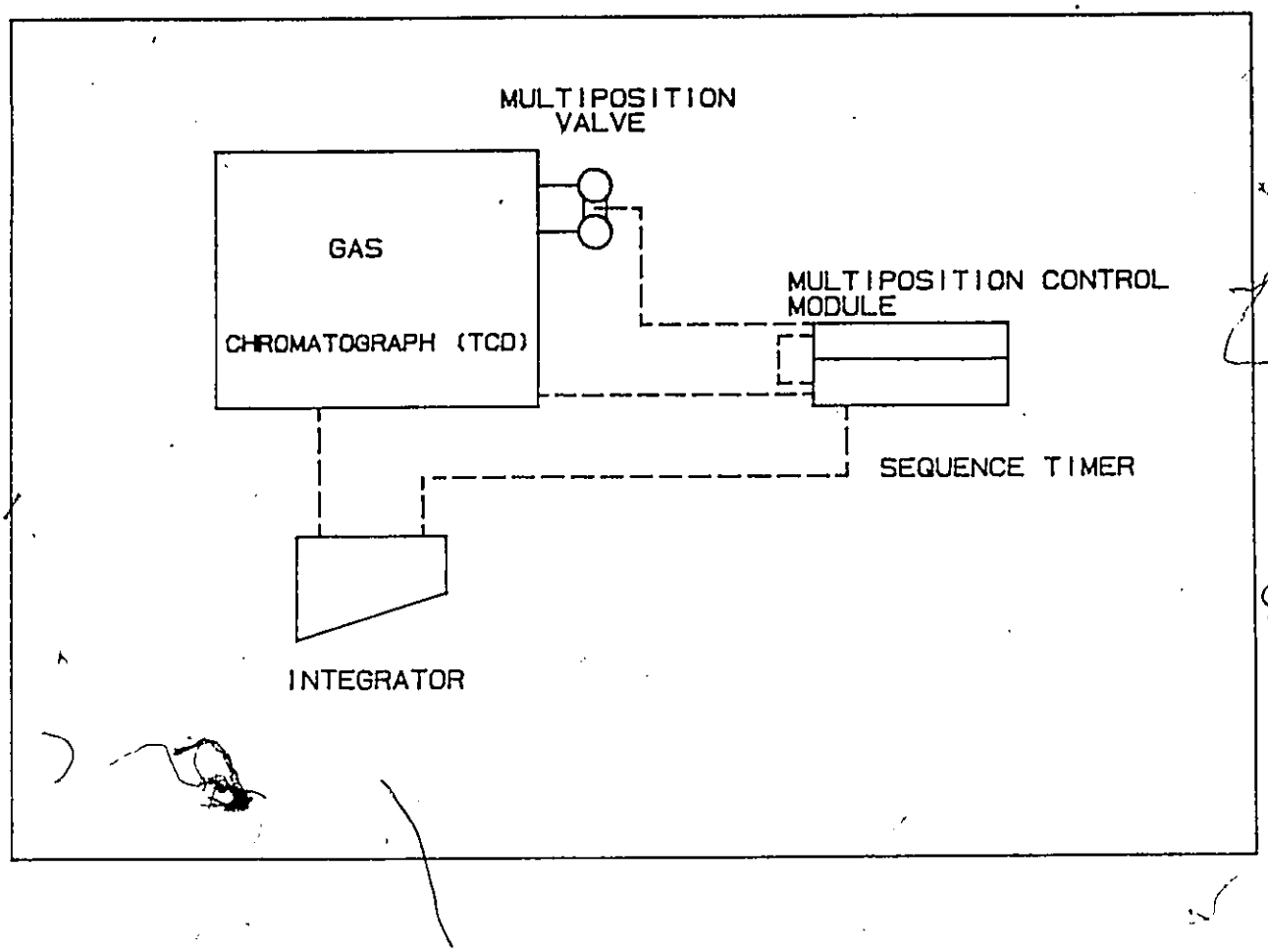

Fig. 4.3 Gas chromatographic configuration for gas analysis with the thermal conductivity detector.

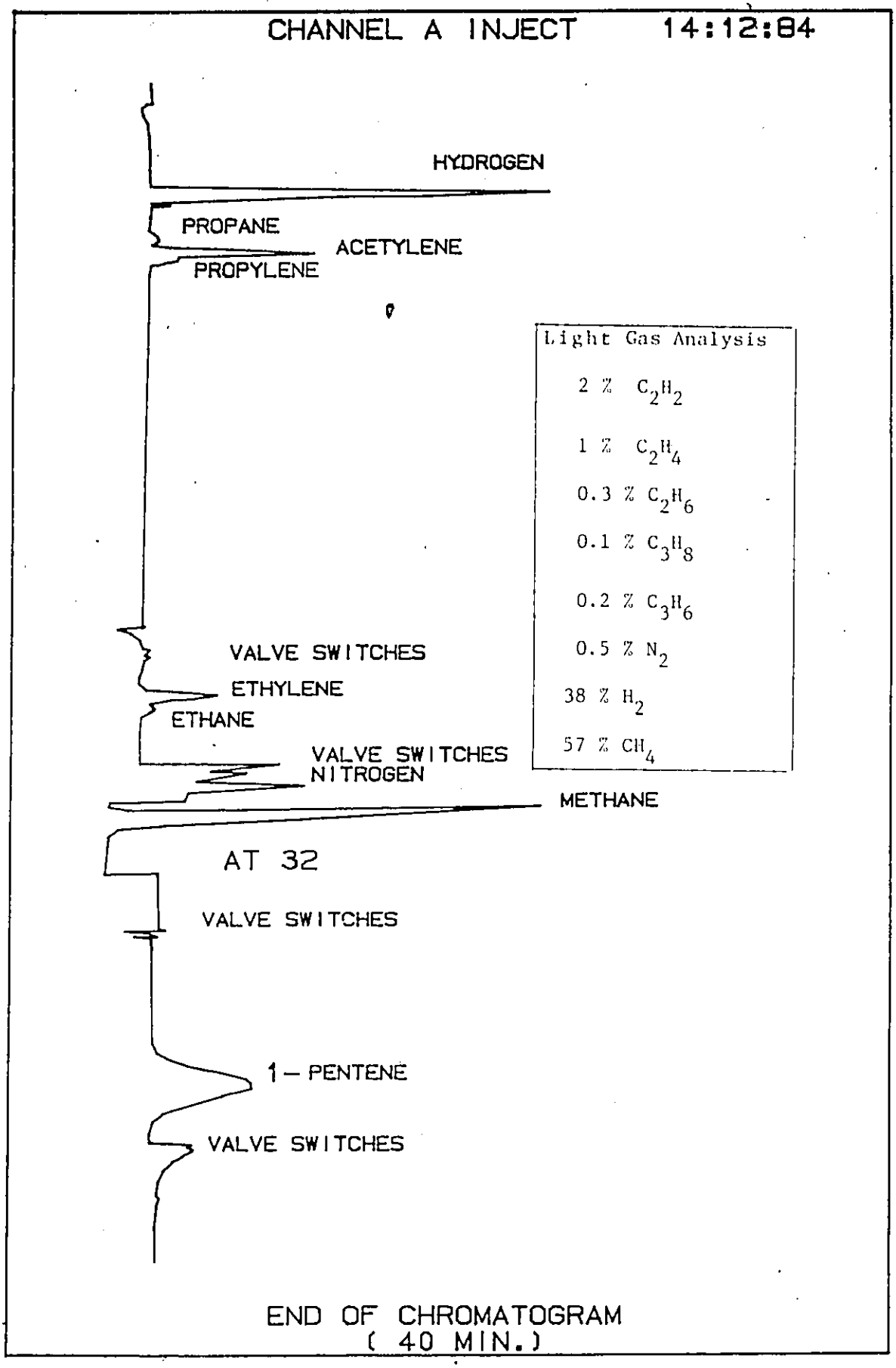

Fig. 4.4 A typical chromatogram of gaseous reaction products.

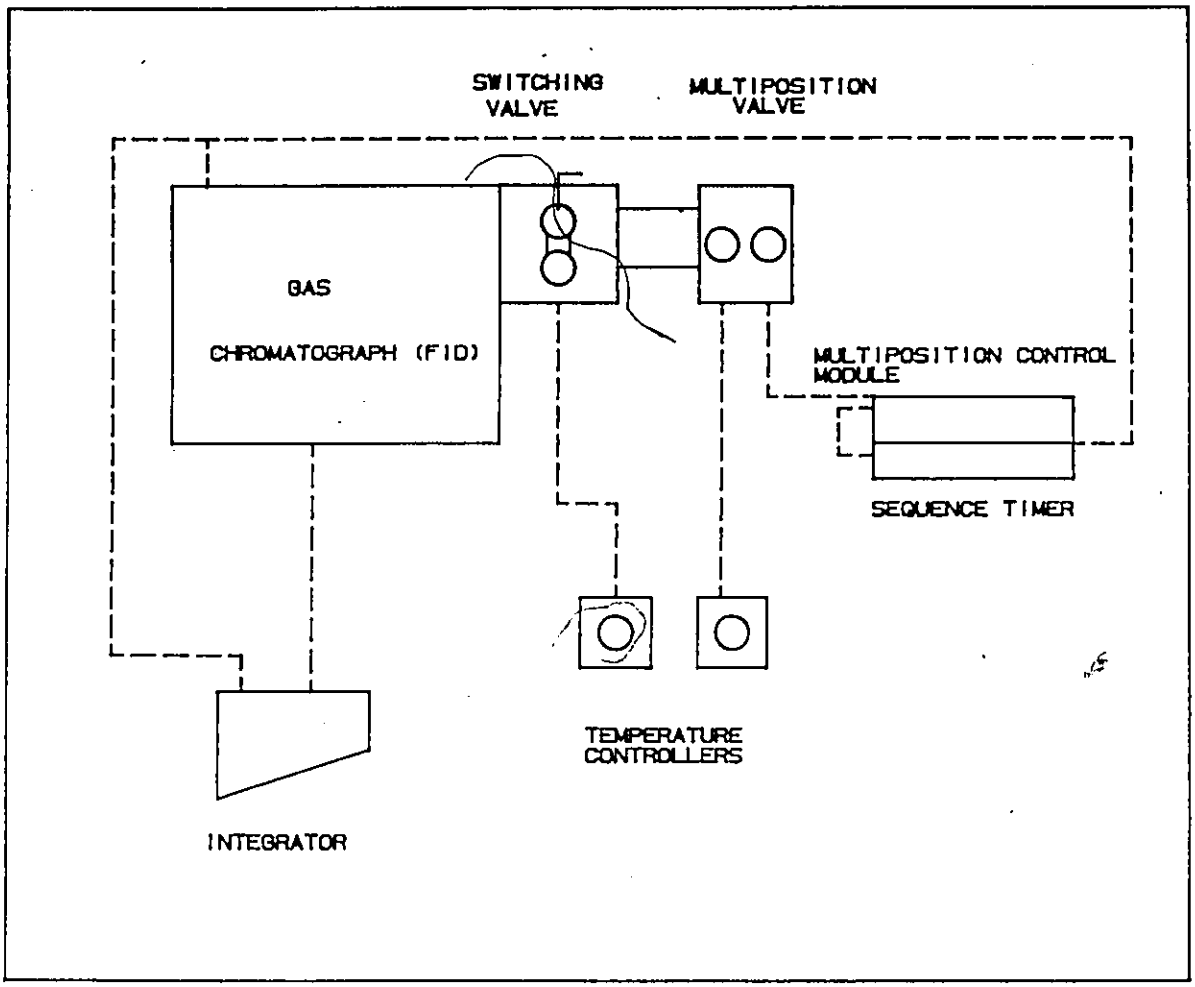

Fig. 4.5 Gas chromatographic configuration for vapor analysis with the flame ionization detector.

of the catalytic reaction under a variety of operating conditions. However, a complete investigation of each catalyst at various levels of temperature, weight-time (defined as the ratio of the weight of catalyst to the total volumetric feed rate at reaction conditions) and feed concentration of acetylene would require a large number of experiments. To achieve efficiency of experimentation a central composite experimental design (43) was used. Five catalysts were examined at five levels of the operating variables.

To study the effects of the operating variables and the catalyst type on the acetylene reaction in the tubular-flow reactor the central composite design consisted of a 2^{4-1} fractional factorial design, star points, and replicates (43). The experimental design and coding for these variables are given in Table 4.1. The order of execution of the experiments was randomized. Not all replicated experiments were carried out at the centre point of the design. The operating region for this work is defined by the following limits: temperature (300-400^{o}C), weight-time (1-3 g.s.mL^{-1}), initial concentration of acetylene (5-15 vol%) and the catalyst composition (0-68 wt % F).

Empirical models were developed to describe the performance as a function of temperature, weight-time, initial concentration of acetylene and degree of fluoridation. The following second degree polynomial was used to describe the performance criterion (e.g., conversion of acetylene, deactivation):

$$E(C) = l_0 + l_1 x_1 + l_2 x_2 + l_3 x_3 + l_4 x_4 + l_5 x_5 + l_6 x_6 + l_7 x_7 + l_8 x_1^2 + l_9 x_2^2 + l_{10} x_3^2 + l_{11} x_4^2 \qquad (4.2)$$

E(C) is the expected value of the performance criterion and x_1, x_2 , x_3 and x_4 are the coded variables corresponding to temperature, type of catalyst, weight-time and initial

Table 4.1

Experimental operating conditions and design

Experiment No.	Coded Variable x_1	x_2	x_3	x_4
1	1	1	1	1
2	1	1	-1	-1
3	1	-1	1	-1
4	1	-1	-1	1
5	-1	1	1	-1
6	-1	1	-1	1
7	-1	-1	1	1
8	-1	-1	-1	-1
9	2	0	0	0
10	-2	0	0	0
11	0	2	0	0
12	0	-2	0	0
13	0	0	2	0
14	0	0	-2	0
15	0	0	0	2
16	0	0	0	-2
17	0	0	0	0

x_1 -(Temperature [^{o}C] - 350)/ 25
x_2 - refer to Table 5.1
x_3 - (Weight-time [g.s.mL^{-1}] - 2)/ 0.5
x_4 - (Conc of C_2H_2 [vol. %] - 10)/ 2.5

concentration of acetylene, respectively. The variables x_5 , x_6 and x_7 represent the combination of interaction terms x_1x_2 , x_1x_3 and x_1x_4. The values of the parameters (l_i's in Eq. 4.2) were estimated by least squares fitting of the model to the data using the statistical package SPSS (68). Since the central composite experimental design was based on a 2^{4-1} fractional factorial design some confounding of the interaction effects occurred. The defining relation for the design was $I = x_1x_2x_3x_4$ which led to the following aliases:

l_5 estimates the combined effects of the interactions x_1x_2 and x_3x_4

l_6 estimates the combined effects of the interactions x_1x_3 and x_2x_4

l_7 estimates the combined effects of the interactions x_1x_4 and x_2x_3

Throughout the analysis the effects of the third and higher order interactions were assumed to be negligible.

4.3.3 Microbalance

All the catalysts discussed in the literature review were reported to exhibit severe deactivation under conditions of hydrogenation and/or polymerization of acetylene. Although catalyst deactivation has been attributed to a large number of factors, one of the major contributors is the buildup of carbonaceous species (residues) on the catalyst surface. In this study, the rate of coking of the fluoridated catalysts was determined with a microbalance (Perkin Elmer TGA7). In addition, a temperature-programmed pyrolysis (in inert gas) of the carbonaceous residues and an analysis of the gas phase products by mass spectrometry (Spectrum Scientific Spectramass GA100) was carried out whenever appropriate.

A schematic of the experimental system for studying deactivation is shown in Fig. 4.6. The balance internals were purged with a flow of 32 mL/min of nitrogen

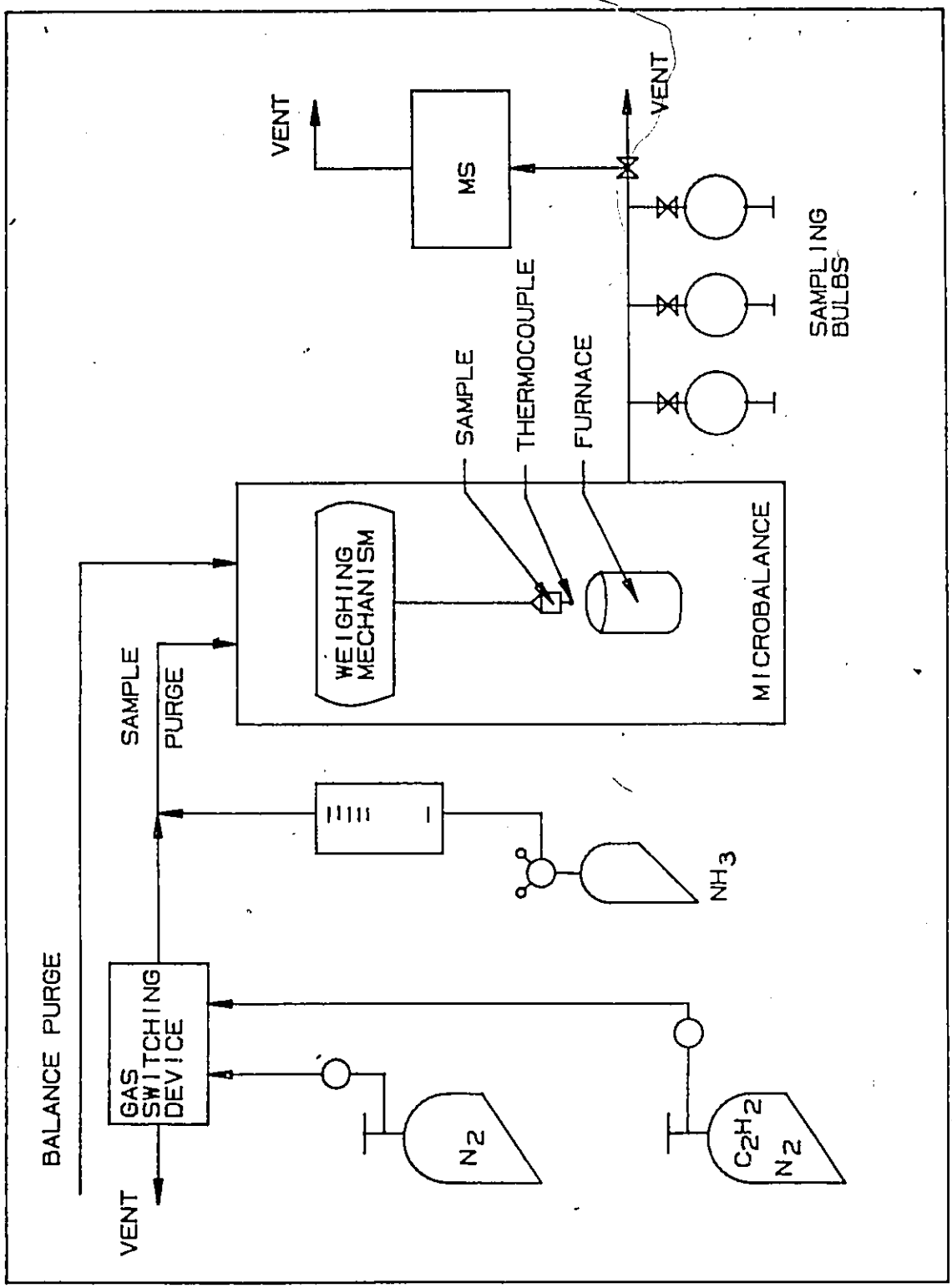

Fig. 4.6 Schematic of microbalance experimental set-up.

throughout these experiments. Approximately 20 mg of fresh catalyst was loaded into a platinum sample boat. The sample was held at 40°C for 5 min. and then heated to the reaction temperature at a rate of 10°C/min under flowing nitrogen. At this point, the purge gas was automatically switched from nitrogen to the reactant gas mixture (Matheson Gas Co. - certified standard C_2H_2/ N_2 mixtures) through the side arm of a two-arm furnace by using a gas-switching accessory controlled by the microcomputer. The catalyst was maintained at a constant temperature for 1 hour while the reactant gas mixture flowed over it. The moisture lost by the catalyst during this time was negligible (Appendix 4.6). Gas samples of the balance effluent were taken using evacuated gas sample bottles at 15, 30 and 55 minutes time-on-stream. The isothermal step was followed by a) automatic switching to nitrogen as the sample purge and b) dynamic heating of the catalyst at 10°C/min to 600°C, held at this temperature for 5 minutes (until there was no weight loss) and heated at 10° C/min to 900°C. The system was automatically cooled on completion of the heating program. The measurement thermocouple was close to but not in contact with the catalyst during analysis. Therefore, the temperature of the gas near the catalyst was measured. At temperatures between 300 and 400°C the radiation effect is limited. To minimize any difference between the temperature measured by the thermocouple and that in the solid sample, the particle sizes and the sample used were small, the concentration of C_2H_2 was low and the flow rate of the gases high.

The experiments in the microbalance were carried out at 101 kPa, the reaction temperature was between 300 and 400°C, the gas flow rate between 30 and 80 mL/min, and the initial acetylene concentration between 2.5 and 6.3 vol %. A typical weight-time history and the corresponding temperature-time history is shown in Fig. 4.7. The solid line corresponds to the rate of weight loss curve. The isothermal reaction step is the region between the points labelled A, corresponding to a starting weight, w_o and B, corresponding to a final weight w_f. The apparent rapid changes in weight observed at points labelled S correspond to the gas sampling times and arise from sudden changes in system pressure.

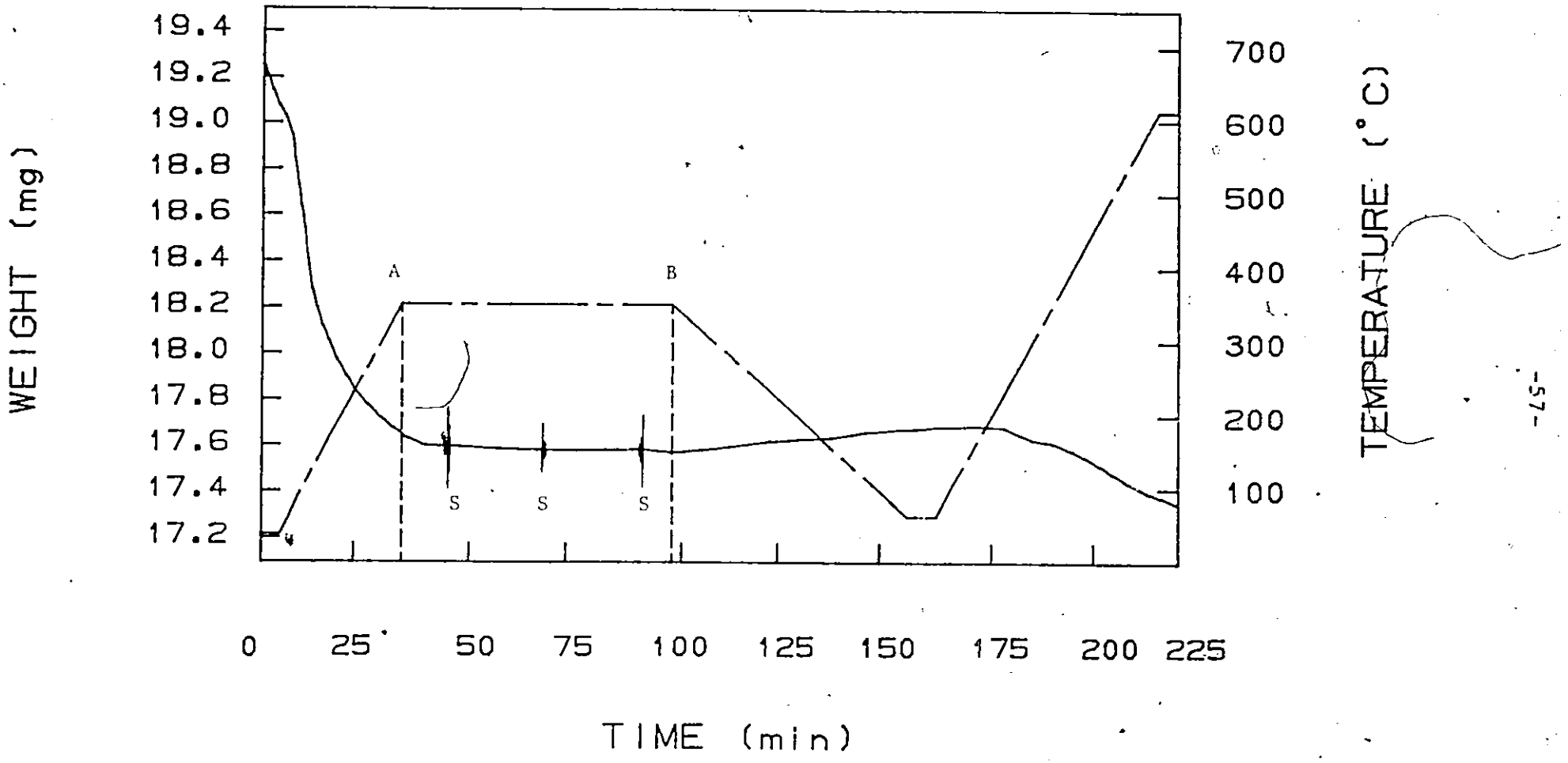

Fig. 4.7 A typical microbalance experiment weight-time and temperature-time curve. — — — Temperature _____ Weight

The system appears to return quickly to normal after these perturbations.

Pyrolysis, in inert gas, of the coke residue on the catalysts begins at point B and continues until the end of the run. Characteristic of all these curves are a) a maximum rate of moisture loss of the fresh catalyst, b) a maximum rate of weight gain upon introduction of the reactant gas (R_m) and c) an asymptotic final rate of weight gain R_f at the end of 1 h reaction time and d) less than 100 % removal of coke deposit at the final pyrolysis temperature of 900°C. The spent catalysts removed from the sample pan were black at the end of this heat treatment.

4.4 CATALYST EVALUATION

Characterization of catalytic activity, selectivity and decay for the reactions being studied requires useful and representative measures for these performance criteria. Activity, in this study is expressed in terms of the total conversion of acetylene, i.e., conversion of acetylene to all products:

$$X = 100 \times (C_o - C)/C_o \qquad (4.3)$$

where C_o is the concentration of acetylene at the reactor inlet (mol/L), C is the concentration of acetylene (mol/L) at the reactor outlet and X is the percent conversion.

When more than one product is obtained as is the case here, then the selectivity of the catalyst, which refers to the ratio of the yield of one product to the yield of a second becomes important. The selectivity can be determined, therefore, by measuring the yields of the components of interest as shown in Eq. 4.4.

$$Y(i) = \frac{y_i F}{(x_o F_o)} \quad ; \quad X(j) = \frac{x_j F}{(x_o F_o)} \qquad (4.4)$$

where Y, X = yield of vapor component i or of gaseous component j

y_i = mole fraction of condensable component i maintained in the vapour phase in product stream

x_j = mole fraction of component j in product stream

F = flow rate of product stream (mL/min)

F_o = flow rate of feed stream (mL/min)

x_o = mole fraction acetylene in feed stream

The data analysis procedure used to obtain these yields is described in detail in Appendix 4.7. The selectivity to liquids (S_L) can be calculated as shown below:

$$S_L = \frac{\sum_{i=1}^{m} y_i F}{\sum_{j=1}^{n} x_j F} = \frac{\text{Total liquid product}}{\text{Total gas product}} \qquad (4.5)$$

where m is the total number of vapor components and n is the total number of gaseous components. A number of other selectivity ratios can also be defined, e.g.,

$$S_C = \frac{\text{Total residue}}{\text{Total liquid product}}$$

In this study the selectivity to C_n oligomers (liquids) where n > 6 were of interest.

Catalyst aging has been described by decay models. Most models use empirical power laws because the coking rate is a complex function of temperature, space velocity and the time the catalyst has been exposed to the reacting mixture. In the microbalance studies, the coking rate was determined as follows:

$$R_c = 1/w_o \, (dw/dt) \qquad (4.6)$$

where w_o = initial catalyst weight (mg).

w = instantaneous weight of catalyst (mg)

t = time catalyst has been exposed to reactant (min)

R_c = rate of coke deposition (mg C/mg cat/min)

The influence of the operating variables was examined for both the maximum rate of deposition and for the rate of deposition at 1 h on stream.

These simple definitions proved very useful in unveiling relationships between catalyst properties and catalyst performance in the polymerization of acetylene.

5. CATALYST PROPERTIES

5.1 PHYSICAL PROPERTIES

A summary of the properties of the five catalysts examined in this investigation is given in Table 5.1. Generally, good agreement was found between the amount of fluoride in the catalyst calculated from the preparation procedure (nominal composition) and that found in the bulk, indicating that little fluoride was lost during calcination. A notable exception was the $AlF_3.3H_2O$ (catalyst designation: 2), for which the bulk fluoride content was considerably lower than expected. This was attributed to a non-linearity in electrode calibration at high concentrations of fluoride ions. A comparison of the bulk F/Al atomic ratio and the XPS-determined surface atomic ratio showed some evidence of surface enrichment of fluoride as a result of the impregnation technique. Small differences in surface area measured by N_2 adsorption were observed in catalysts containing between 0 and 5 wt % F. The surface area of the aluminum fluoride trihydrate was less than 20 m^2/g and could not be determined accurately with our apparatus. Other studies (85) have shown that a bulk phase of aluminum fluoride does not form until concentration of fluoride exceeds 5 wt %. This finding supports the negligible change in surface area reported in Table 5.1 since the presence of a bulk aluminum fluoride phase would have significantly reduced the surface area of the catalysts. The pore volume of these catalysts as determined by mercury porosimetry varied between 0.4 and 0.6 (mL/g). The mean pore diameter was 60 Å.

5.2 ACIDITY

The influence of fluoride on total acidity (Lewis and Bronsted) of the catalysts was determined by measuring their adsorption capacity for ammonia at conditions similar to those in the reactor. The reader is referred to Fig. 4.1 and Chapter 4 for a description of the equipment. Ammonia may react with Bronsted and Lewis sites and therefore the acidity determined by ammonia adsorption is the sum of both Lewis and Bronsted acidity.

Table 5.1

Properties of fluorided alumina catalysts

Catalyst Designation	Surface Area[a] [m^2/g]	Composition			
		Nominal[b]	Bulk[c] [wt %]	Surface[d]	Bulk [μmol F/m^2]
[-2]	189	0	0	0	0
[-1]	222	1.8	1.5	3.6	3.4
[0]	199	3.6	2.6	3.2	6.8
[1]	156	6.9	4.4	8.3	14.7
[2]	<20	68	18	68	-

[a] Surface area quoted +/- 20 m^2/g

[b] Fluoride content of catalyst based on preparation procedure

[c] Analysis accuracy +/- 2 % of quoted value

[d] Analyses were performed at 10^{-9} torr. The spectrometer's energy scale was calibrated using Au (Au $4f_{7/2}$ - 838 eV) and Cu^o (Cu $2p_{3/2}$ -932.8) Photolines were referenced to the hydrocarbon (C 1s) line at 284.6 eV. A charge neutralizer system (electron flood gun) was used to control specimen charging. The elemental composition of each catalyst's surface was determined using XPS elemental sensitivity factors and the measured photoline intensity. These were calculated according to theoretical photoelectr n cross-sections, the kinetic energy dependence of the cylindrical minor analyser (CMA) and an average value for the dependence of the electron escape depth on kinetic energy.

Results for the chemisorption of ammonia at 350°C are given in Fig. 5.1. Pure and fluoride-promoted alumina show significant differences in adsorptive capacity for ammonia. A maximum in ammonia chemisorption was observed between 1.5 and 3 wt % fluoride. This result is in good agreement with Gerberich et al. (35) who studied ammonia adsorption at 500°C and found a maximum between 1.2 and 2.7 wt % fluoride. It thus appears that the fluoride content of the catalyst has a complex influence on surface acidity.

Studies on the acidic properties of fluoride-modified alumina by infrared adsorption of pyridine have shown that fluoridation produces a small concentration of Bronsted acid sites (17). Furthermore, these studies have shown that the addition of fluoride ions increases the Lewis acidity of alumina, although it remains unclear whether more sites are generated or existing sites are strengthened. It can nevertheless be concluded that fluoridation resulted in a redistribution of the acid sites on the alumina surface.

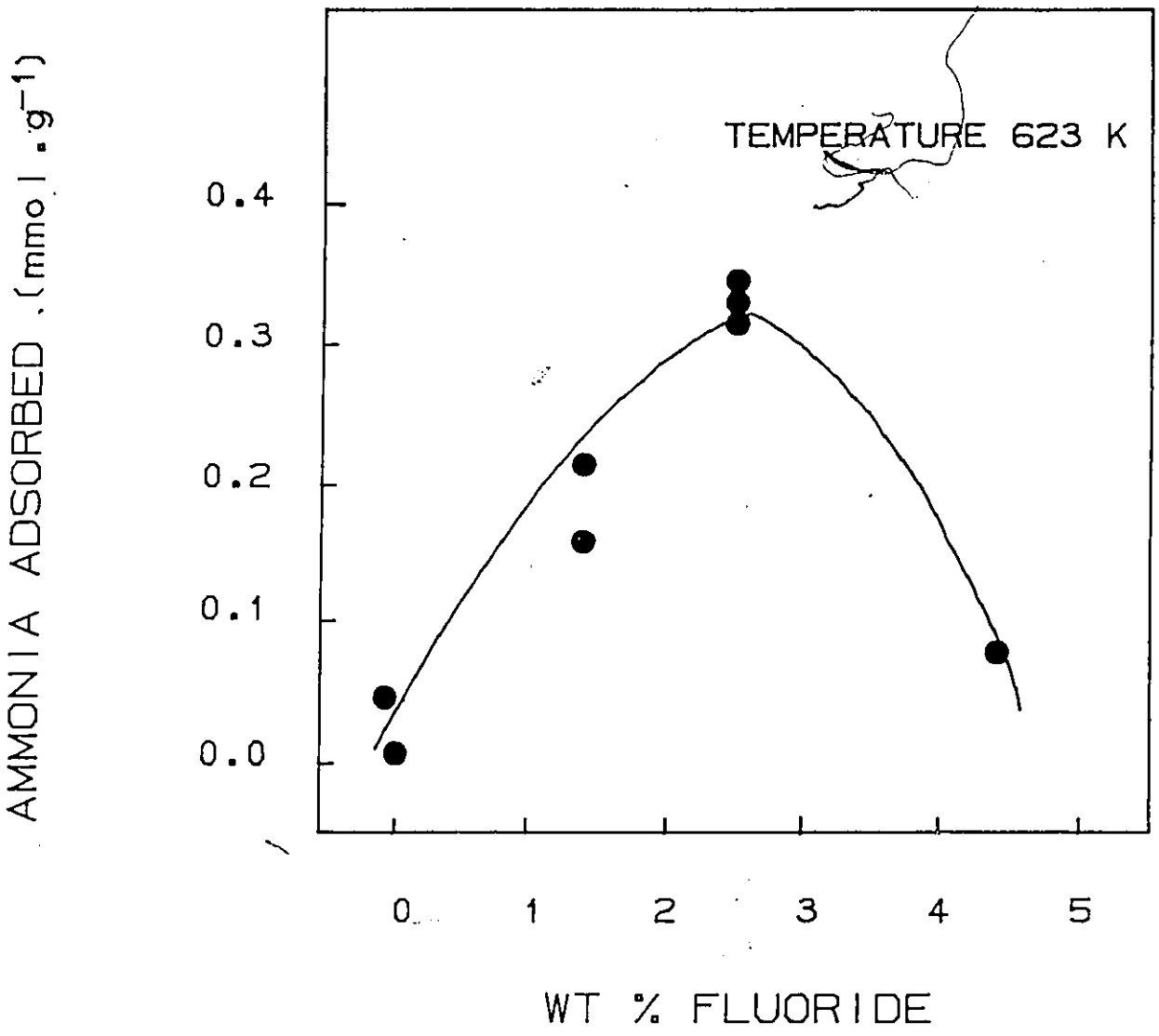

Fig. 5.1 Chemisorption of ammonia on fluorinated alumina at 350°C as a function of fluoride content.

6. CATALYST ACTIVITY

Experiments performed using a feed gas consisting of 10% acetylene and 90% nitrogen by volume showed that the thermal reaction of acetylene was negligible below 400°C. However, acetylene was highly reactive over fluoridated alumina catalysts at temperatures as low as 200°C. The reaction products consisted mainly of aromatic hydrocarbons although small amounts of hydrogen, methane, ethylene and higher olefinic hydrocarbons were also produced. A typical product distribution at a time-on-stream of 15 min was 59% liquid, 3% gas, 38% solid deposits. The nature of the reaction products changed with increasing time-on-stream. For example, the generation of high boiling aromatics (B.P.> 200°C) increased considerably over the first hour of operation. Therefore, the experimental runs were limited to 1 h to avoid condensation of the reaction products in the heated lines and sampling valve. Appreciable deactivation was observed at certain operating conditions. For this reason, the effects of temperature, weight-time, initial concentration of acetylene and degree of fluoridation on the conversion of acetylene were examined at the earliest reliable sample times which correspond to those taken at a time-on-stream of 15 min. The results of 24 runs in the tubular flow reactor are listed in Table 6.1.

6.1 MODEL OF CATALYST ACTIVITY

Using the modelling techniques described earlier, a model was determined for the conversion of acetylene over these catalysts at a time-on-stream of 15 min. Examination of the residuals revealed that the activity of AlF_3 (experiment 11) was inconsistent with that found for the fluoridated aluminas. This may have been due in part to the incomplete dehydration of the catalyst in the drying process (10% of the H_2O remained). Consequently, this experiment was deleted from the analysis. The estimates for the parameters in Eq. 4.2 which had a significant effect on the predictive ability of the

Table 6.1

Acetylene conversion at 15 min on stream for experiments in the tubular flow reactor

Experiment No.	Conversion (%)[a]
1, 1R[b]	51.5, 57.8
2, 2R	41.0, 48.1
3, 3R	99.5, 99.3
4, 4R	98.9, 96.3
5	48.0
6	0
7, 7R	97.6, 99.3
8, 8R	59.0, 50.0
9	98.1
10	28.8
11 [c]	85.9
12	99.3
13	87.2
14	29.2
15	99.6
16	90.3
17, 17R	73.9, 64.5

[a] $\left[\frac{\text{moles of } C_2H_2 \text{ in feed - moles of } C_2H_2 \text{ in product at 15 min on stream}}{\text{moles of } C_2H_2 \text{ in feed}}\right]$

[b] repeated experiment

[c] experiment subsequently deleted from the analysis

model together with their marginal 95% confidence intervals are listed in Table 6.2. The model is summarized below:

$$X = 60.63 + 13.82\,x_1 - 26.26\,x_2 + 13.36\,x_3 - 4.97\,x_2^2 + 7.83\,x_4^2 - 9.81\,x_2x_4 \qquad (6.1)$$

where X is the predicted value of the total per cent conversion and x_1 through x_4 are the coded operating variables described in Table 4.1. The significance of the global regression (Eq 6.1) is expressed by the ratio of the mean regression sum of squares to the mean residual sum of squares and, in this case, was calculated to have the value 70 (Appendix 6.1). When this value is compared with the appropriate value of the F-distribution, i.e., 6 degrees of freedom associated with mean regression sum of squares, 14 degrees of freedom associated with the residual sum of squares and a 95 % confidence level, F (6,14,0.05) = 2.85, it was concluded that the model is a useful predictive tool. This is further demonstrated by a comparison of the experimental and predicted conversions for all reaction conditions in Fig. 6.1. An excellent fit is indicated with $R^2 = 0.96$. Neither lack of fit test ratios (26) nor analysis of residual plots revealed any significant lack of fit of the model. Having confirmed the adequacy of the model, it was then used to describe and predict the effects of the operating variables and the role of the fluoride on the catalyst activity throughout the operating region.

6.2 MODEL INTERPRETATIONS

Based on the fitted model the three operating variables and the catalyst type were all found to have a significant effect on the conversion of acetylene either singly or jointly. However, as a result of the confounding discussed earlier and the large values of l_1 to l_3, l_6, l_9 and l_{11}, some ambiguity in the interpretation of the results arises. As stated previously, l_6 estimates the combined effects of the interactions x_1x_3 and x_2x_4. This implies that either the temperature and weight-time interaction or the catalyst and acetylene concentration interaction or both are significant. An interaction

Table 6.2

Parameter estimates for Equation 6.1

Parameter	Estimate
l_0	60.63 +/- 5.58 [a]
l_1	13.82 +/- 3.24
l_2	-26.26 +/- 4.16
l_3	13.36 +/- 3.17
l_6	-9.81 +/- 4.05
l_9	-4.97 +/- 4.18
l_{11}	7.83 +/- 2.95

[a] 95 % confidence interval

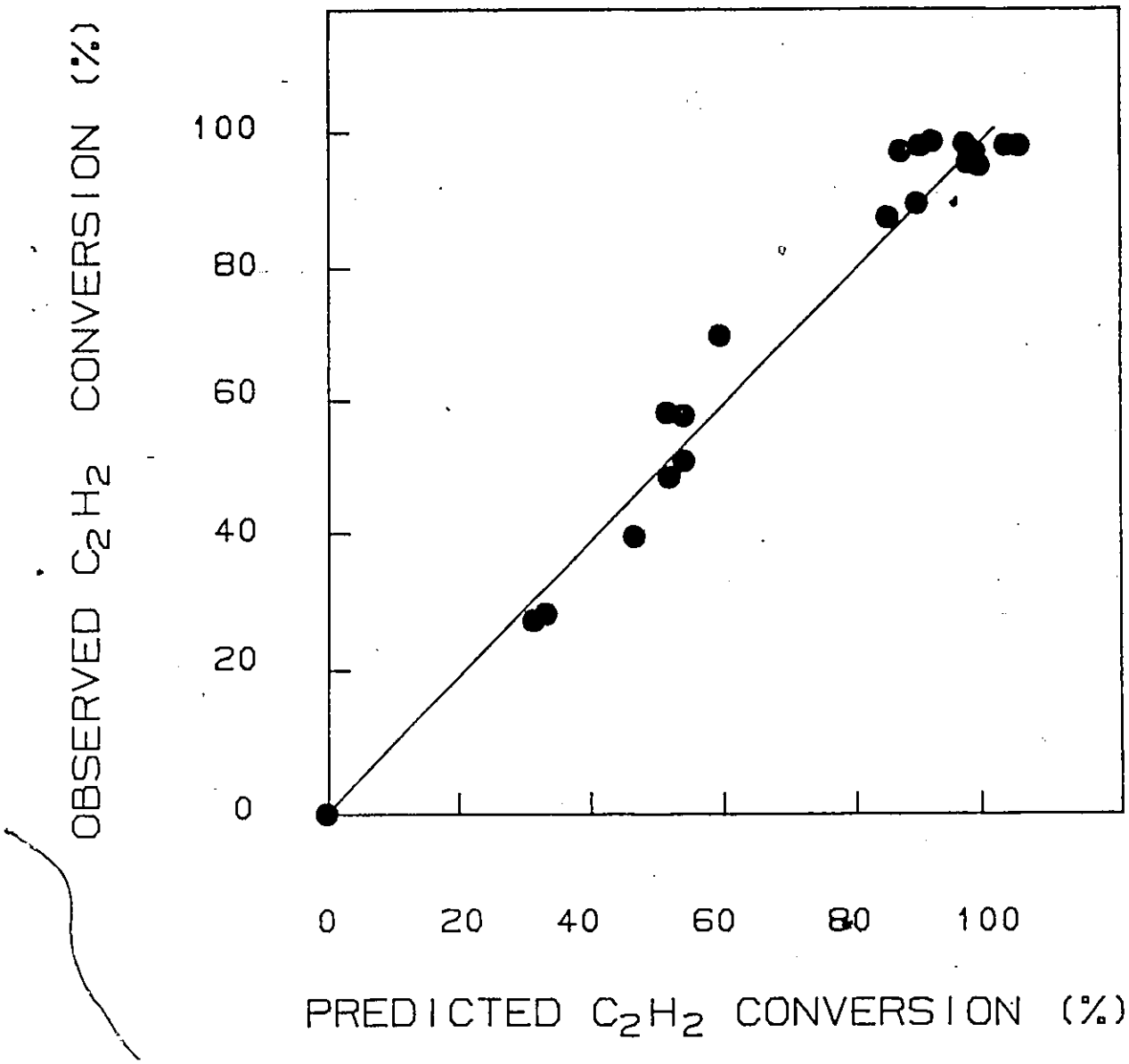

Fig. 6.1 Observed acetylene conversion (%) versus the predicted acetylene conversion (Eq. 6.1).

between the reaction temperature and the weight-time means that the effect of temperature on conversion depends upon the value of the weight-time and vice versa. If the entire effect is attributed to the interaction x_1x_3, then the fitted model predicts a maximum conversion at 385°C, and a weight-time of 2.7 g.s.mL^{-1} , both values being less than their upper operating limits. This situation is highly unlikely. On the other hand, if the l_6-effect is attributed to the interaction x_2x_4, the model predicts a maximum conversion of acetylene at a boundary of the operating region corresponding to maximal levels of both temperature and weight-time. This is a more probable situation and is the interpretation taken here.

The effects of the reaction temperature and the weight-time on the conversion of acetylene are shown in Figs. 6.2 and 6.3. The solid lines represent the predicted response for 1.5, 2.6 and 4.3 wt % F on alumina catalysts. It can be seen in Figs. 6.2 and 6.3 that the conversion of acetylene increases with temperature and weight-time for any type of catalyst. This implies that the maximum conversion for any catalyst is obtained at an operating boundary defined by a temperature of 400°C and a weight-time of 3 g.s.mL^{-1}. Therefore, these would be appropriate conditions for comparing acetylene conversions for catalysts of this family.

Because of the significant interaction, x_2x_4, the effects of catalyst type, x_2, and initial concentration of acetylene, x_4, must be considered jointly. To do this contours of acetylene conversion were plotted in the x_2-x_4 plane for the midpoint values of x_1 and x_3 (temperature 350°C, weight-time 2 g.s.mL^{-1}) and are given in Fig. 6.4. The operating region used in this study (the region where the experiments were performed and where the model is valid) is contained within the dashed lines shown in Fig. 6.4. The contour surface shown in Fig. 6.4 has a saddlepoint, indicated by a plus sign, at a 0.5 wt % fluoride content (x_2= -1.632) and a 7.5 vol. % initial concentration of acetylene (x_4 = -1.023). This point represents a minimum in the conversion as the acetylene concentration is varied from 5 to 15% (at 0.5% F) and a maximum in the conversion as the fluoride

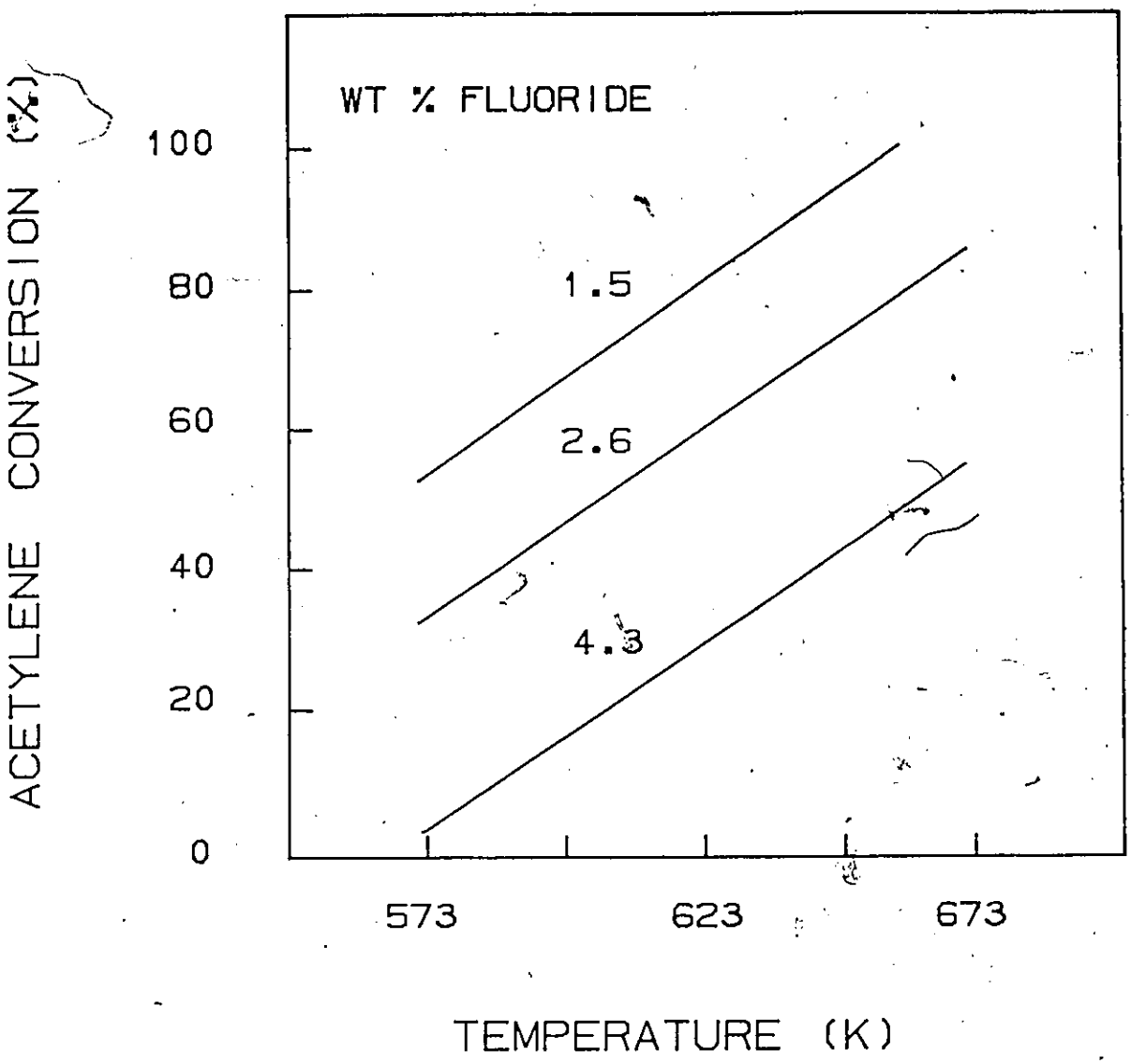

Fig. 6.2 The effect of temperature on acetylene conversion over fluorinated alumina for various fluoride loadings. (weight-time 2 g.s.mL^{-1}, C_2H_2 10 vol %)

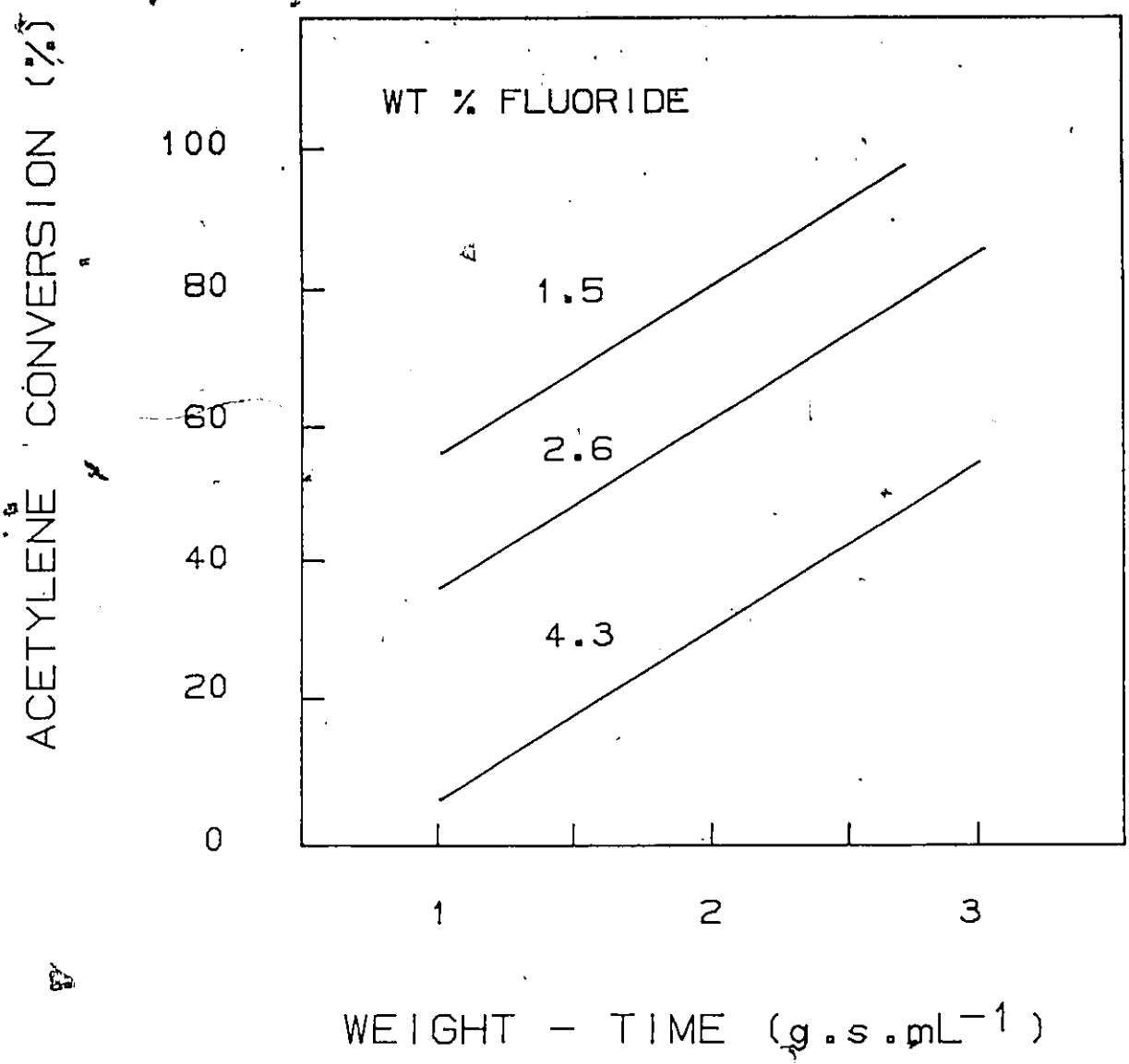

Fig. 6.3 The effect of weight-time on acetylene conversion over fluorinated alumina for various fluoride loadings. (Temp 350°C, 10 vol % C_2H_2)

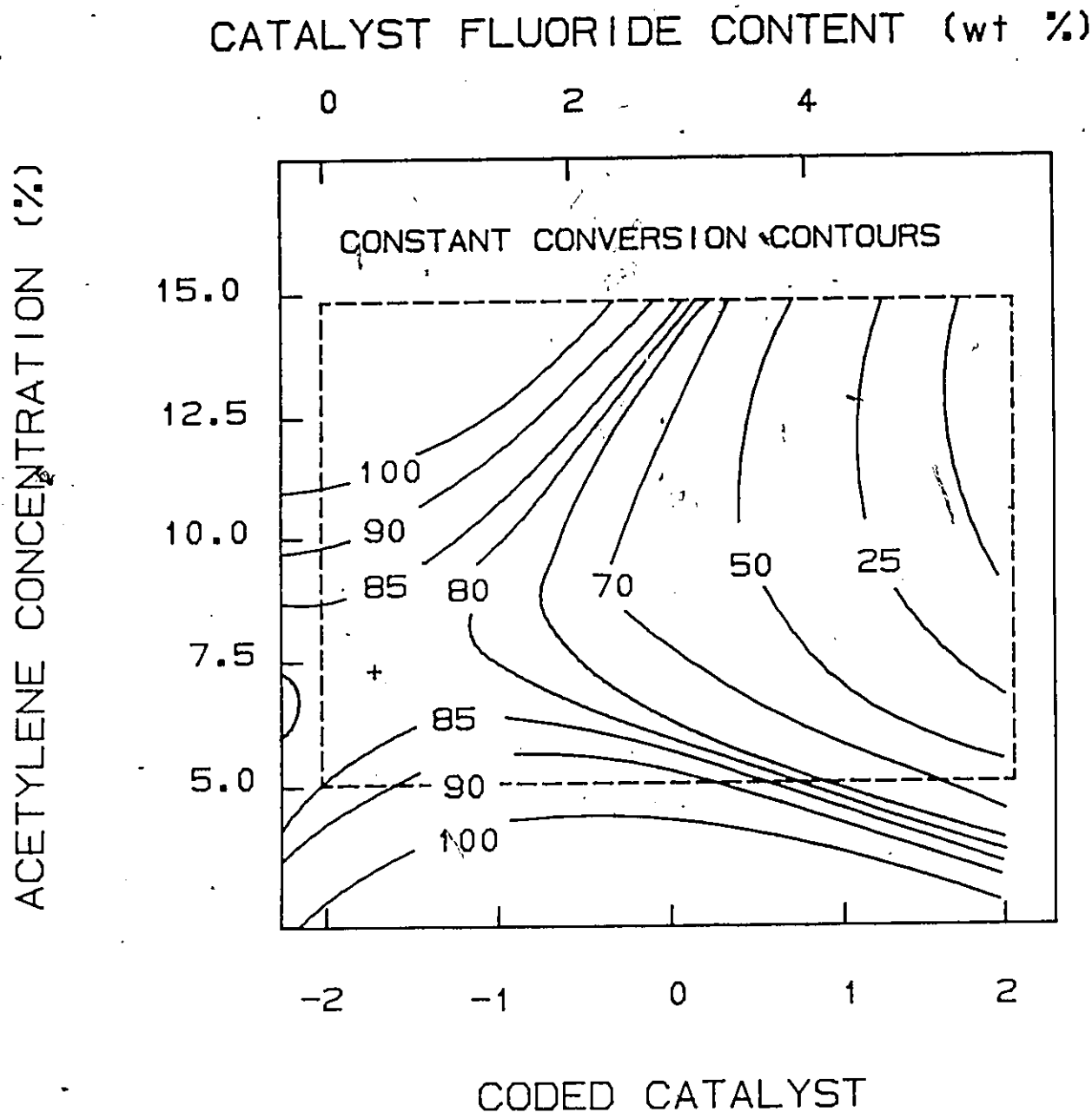

Fig. 6.4 A constant conversion contour plot of the concentration of acetylene and the catalyst fluoride content. (Weight-time 2 g.s.mL^{-1}, temp 350°C)

content of the catalyst is varied from 0 to 5% (at 7.5 vol. % acetylene). For any given type of catalyst (vertical line in Fig. 6.4), the conversion of acetylene passes through a minimum with respect to the initial concentration of acetylene. This minimum is clearly evident in the family of curves shown in Fig. 6.5. At any level of initial concentration (horizontal line in Fig. 6.4), the conversion passes through an optimum with respect to the type of catalyst. At low initial concentrations of acetylene, this optimum lies within the operating region and is fairly broad, as depicted in Fig. 6.6. As the initial concentration of acetylene is increased, however, this optimum shifts to lower fluoride contents, moves rapidly out of the experimental region and narrows considerably. Only the declining portion of the curve can be represented within the operating region and need be discussed further. For example, at an initial concentration of 12.5 vol % acetylene any degree of fluoridation results in a loss of activity for polymerization of acetylene.

The outer dashed lines in Fig. 6.6 define the upper and lower limits of the 95% confidence interval calculated for the expected value of conversion at an initial concentration of 7.5 vol % acetylene. For this model it can be seen that the variance of the predicted conversion increases as the operating conditions at which the prediction is made move away from the centre of the design. Although the existence of a family of maxima is indicated, some caution was exercised in drawing conclusions solely from these results because of the large variances.

6.3 MICROBALANCE STUDIES

Experiments conducted in the microbalance were very useful in confirming the trends observed in the tubular reactor and predicted by the model at low initial concentrations of acetylene. The total conversion was computed from the feed and effluent gas analyses. The acetylene conversion results, at 15 min time-on-stream, of the experiments carried out in the microbalance, are listed in Table 6.3. The effects of temperature, gas flow rate, initial concentration of acetylene and degree of fluoridation

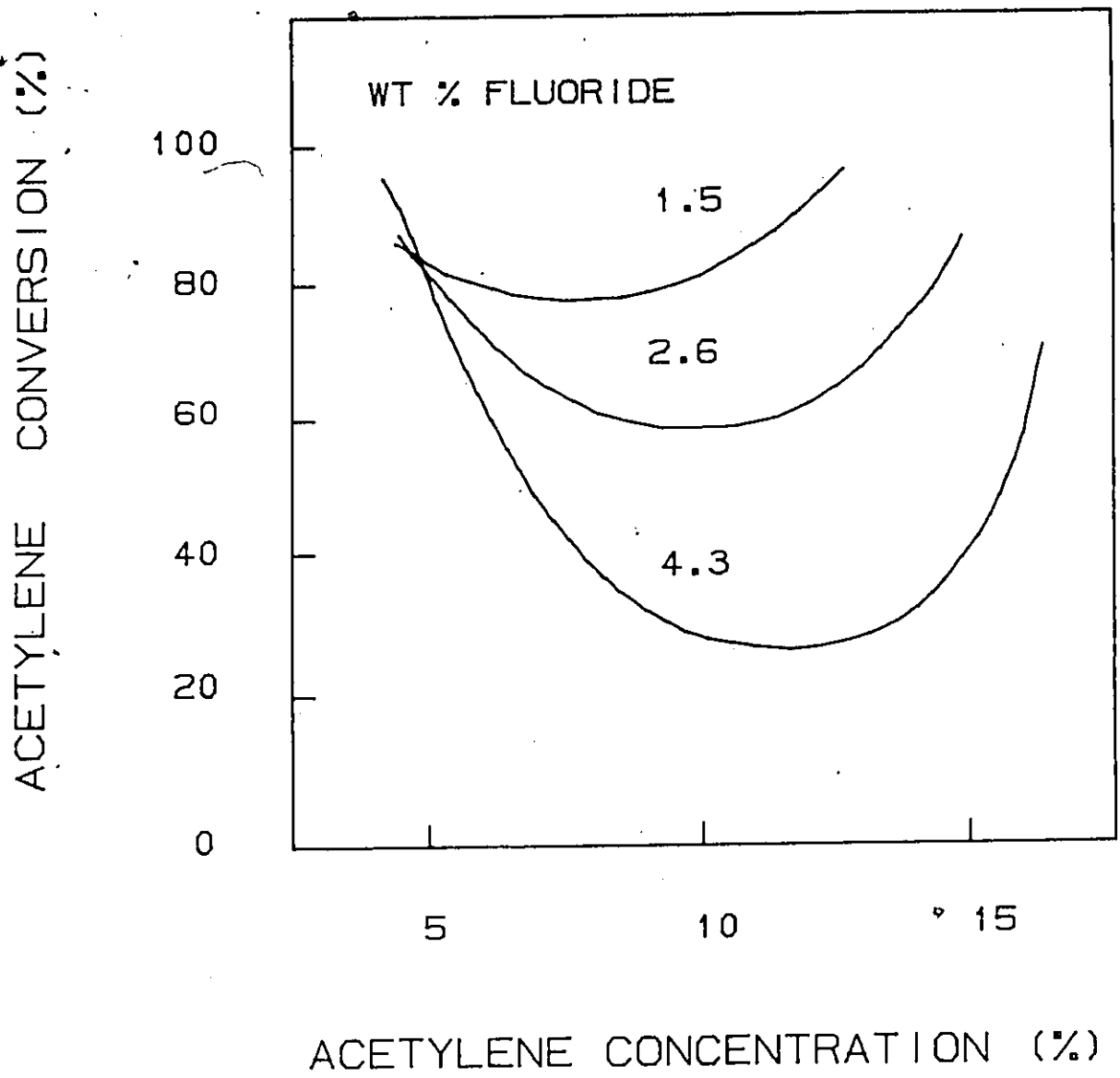

Fig. 6.5 The effect of acetylene concentration on acetylene conversion over fluorinated alumina catalysts at various fluoride loadings. (Weight-time 2.g.s.mL^{-1} , temp 350°C)

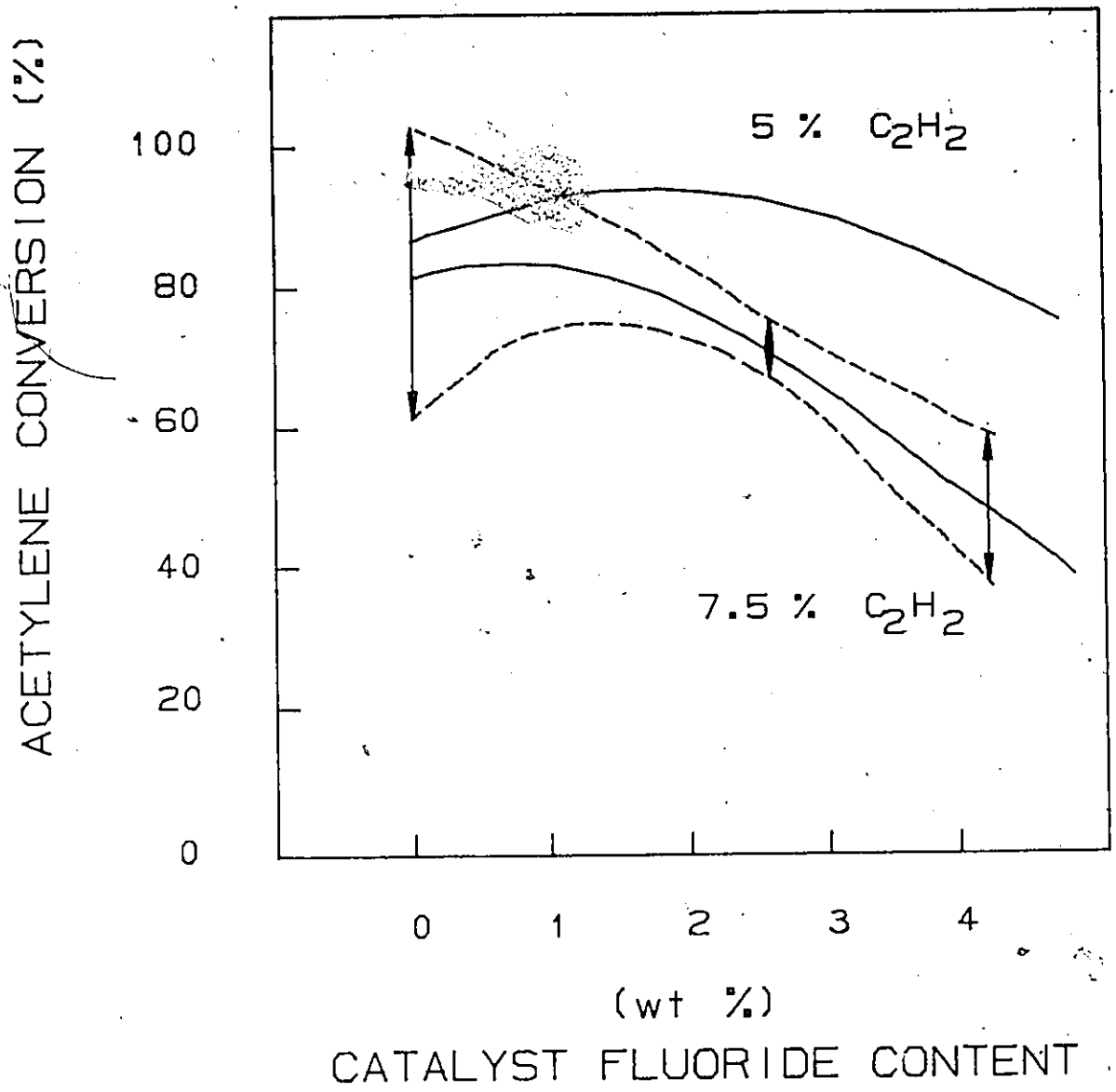

Fig. 6.6 The effect of fluorination on acetylene conversion at various concentrations of acetylene. Dashed lines represent 95 % confidence region. (Weight-time 2 g.s.mL^{-1}, temp 350°C)

Table 6.3

Acetylene conversion at 15 min on stream for experiments in the microbalance

Expt No	Temp [°C]	Gas velocity [cm/s]	Conc of C_2H_2 [vol %]	Catalyst[a]	Conversion [%]
1	400	0.48	5.2	none	< 5
2	400	0.48	5.2	[-2]	20.5
3	350	0.45	5.2	[-2]	19.0
4	300	0.41	5.2	[-2]	15.3
5	400	0.48	5.2	[0]	32.3
6	350	0.45	5.2	[0]	31.1
7	300	0.41	5.2	[0]	30.0
8	350	0.22	5.2	[-2]	21.6
9	350	0.56	5.2	[-2]	4.8
10	350	0.45	6.3	[-2]	38.6
11	350	0.45	2.4	[-2]	34.6
12	350	0.45	6.3	[0]	43.4
13	350	0.45	2.4	[0]	37.4
14	350	0.45	2.4	[-1]	37.2
15	350	0.45	2.4	[1]	35.8
16	350	0.45	2.4	[0]	34.4

[a] coded as in Table 5.1

are shown in Figs. 6.7 to 6.10 respectively. The conversion of acetylene increases as the temperature is increased which is consistent with the model predictions (Eq 6.1). As the flow rate of the reactant gas is increased in the microbalance, the contact time between the gas and the catalyst diminishes. Lower conversions were observed at low contact times which is again consistent with the model predictions. As in the case of the tubular reactor, the effect of the initial concentration of acetylene is complex, the conversion appears to go through a minimum at some intermediate value of concentration which implies some competing phenomena are important.

Experiments in the microbalance provided further evidence for the existence of a maximum with respect to the degree of fluoridation . It can be seen in Fig. 6.7 that at all temperature levels, the fluoridated alumina catalyst showed higher catalytic activity than its unfluoridated counterpart. Furthermore it can be seen in Fig. 6.10 that a maximum in acetylene conversion is observed between 1.5 and 3 wt % F for an initial concentration of 2.5 vol. % acetylene.

The minimum in the conversion of acetylene with respect to the initial concentration observed in both the tubular reactor and in the microbalance experiments can be explained, at least qualitatively, as the result of two competing effects. First, the initial rate of the reaction of acetylene will increase with increasing initial concentrations of acetylene. Second, the rate of deactivation of these catalysts was observed to be a function of the initial concentration of acetylene (therefore a function of catalyst activity). For example, the activity of a 2.6 wt % F on alumina catalyst in the tubular reactor, as a function of the time-on-stream is shown in Fig. 6.11 at three levels of initial concentrations. At small times-on-stream, the conversion of acetylene is the greatest when the initial concentration of acetylene is the highest, but, at large times-on-stream, the conversion is the least at the highest initial concentration of acetylene. A larger decrease in activity is evident at the highest initial concentration of acetylene in the feed. The results at a time-on-stream of 15 min clearly show the

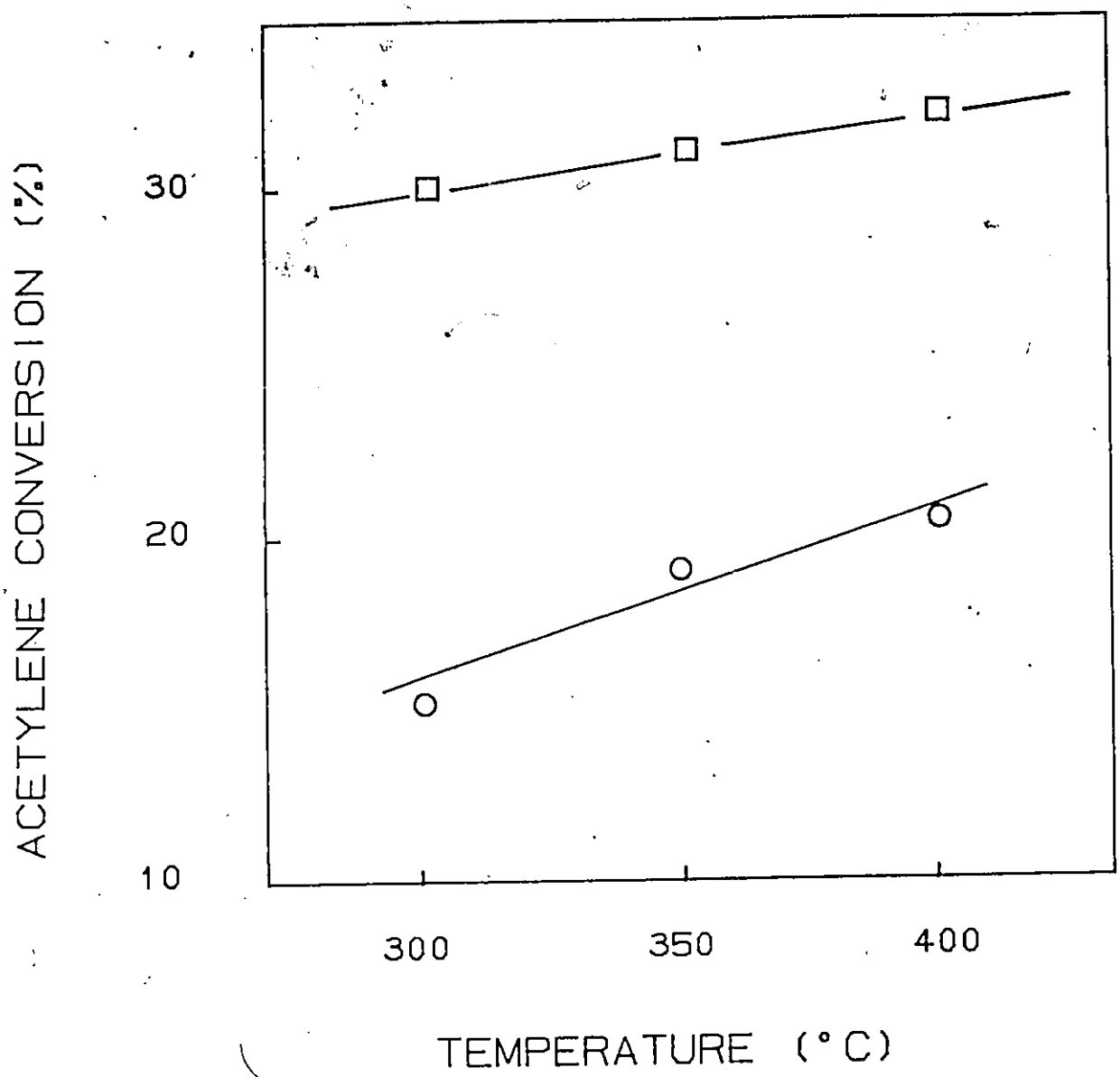

Fig. 6.7 The effect of temperature on acetylene conversion over alumina and fluorinated alumina in the microbalance. (5.3 vol % C_2H_2, 64 mL/min) ○ alumina

□ 2.6 wt % F on alumina

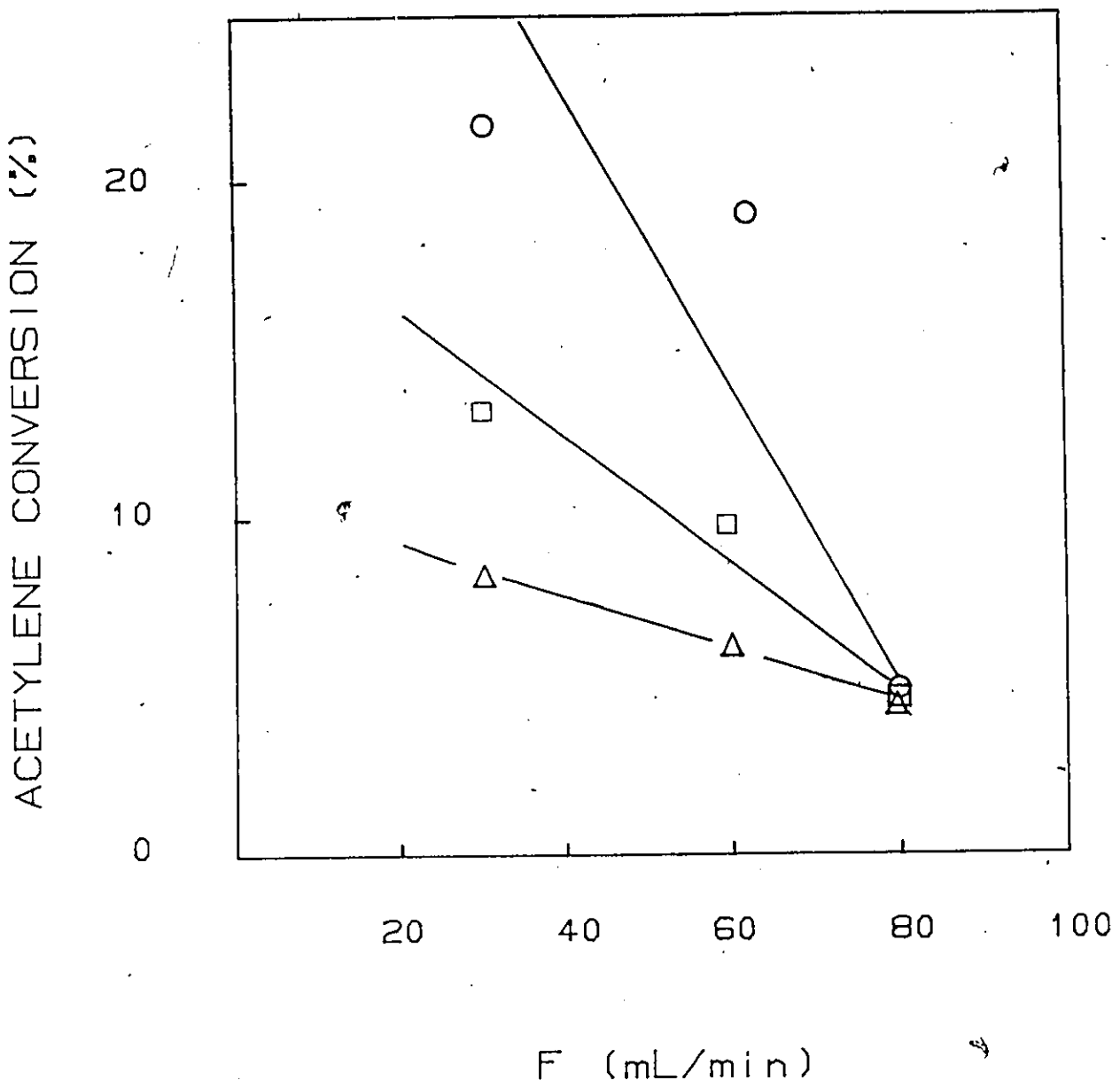

Fig. 6.8 The effect of flowrate (contact-time) on the acetylene conversion in the microbalance at various times-on-stream.(5.2 % C_2H_2, 350°C)

○ 15 min time-on-stream

□ 30 min time-on-stream

△ 55 min time-on-stream

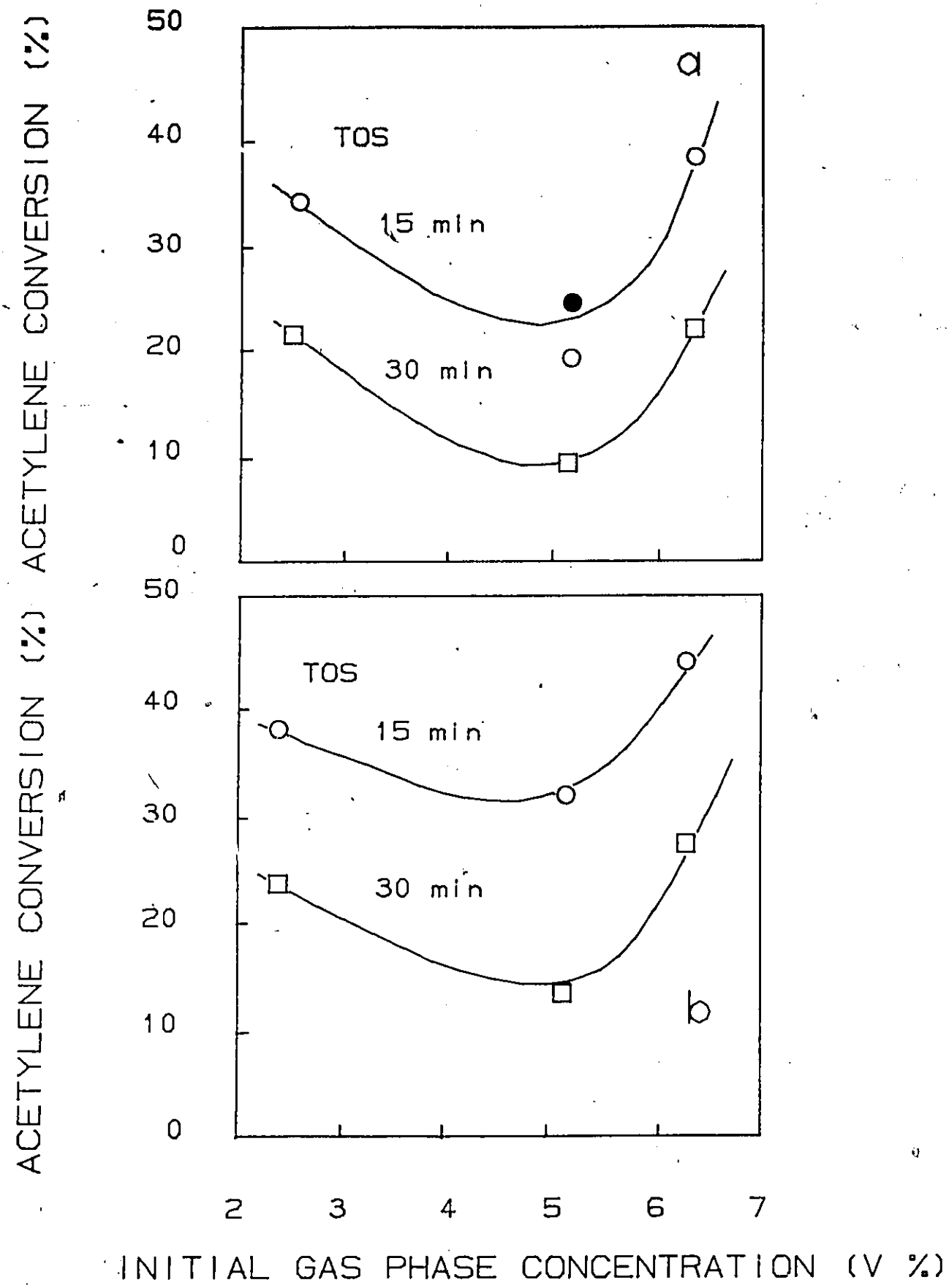

Fig. 6.9 The effect of concentration on acetylene conversion in the micro-balance. a) alumina catalyst b) 2.6 wt % F on alumina (350°C, 64 mL/min)

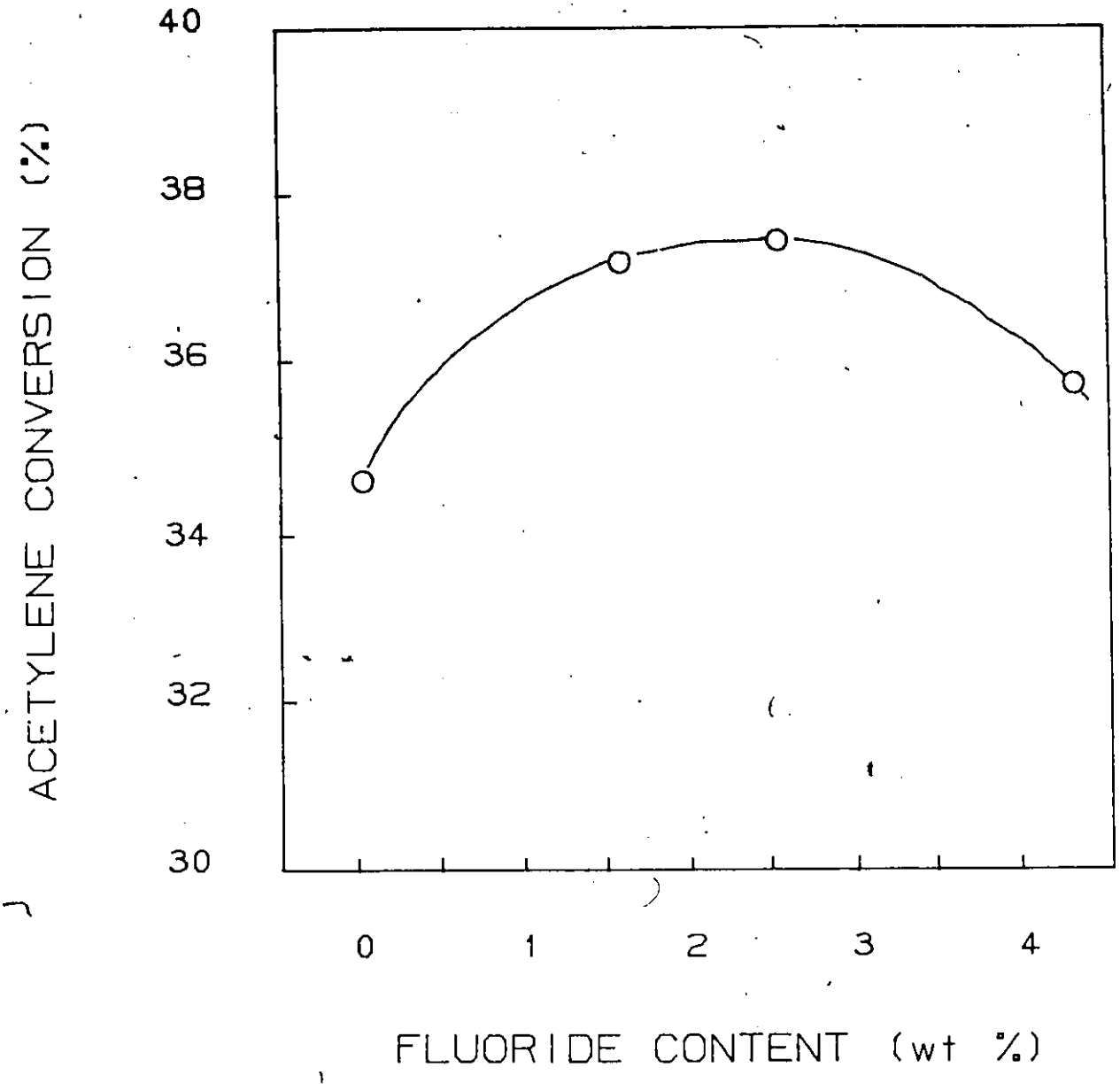

Fig. 6.10 The influence of fluoride content on the conversion of acetylene in the microbalance (350°C, 64 mL/min, 2.5 vol %).

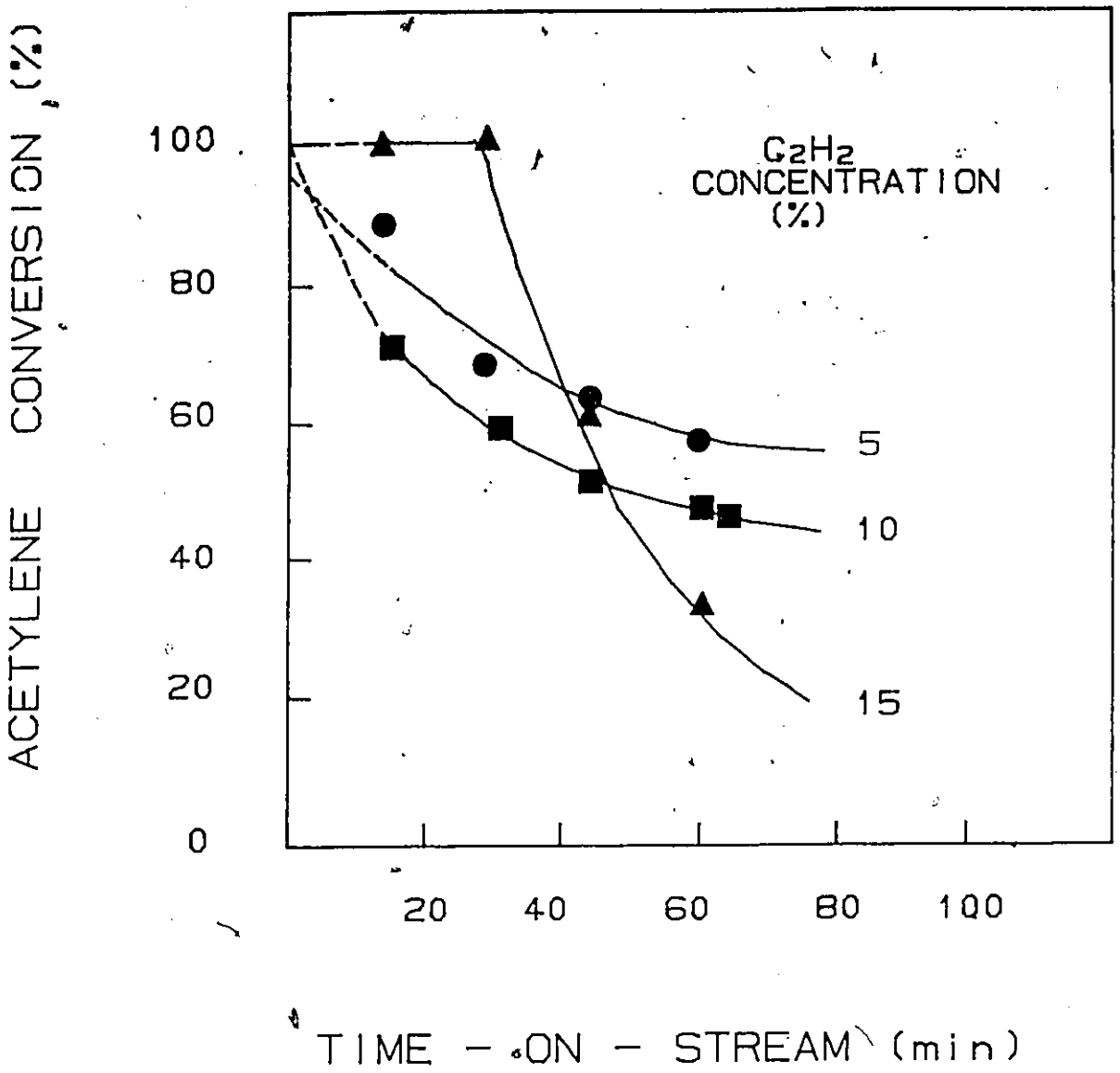

Fig. 6.11 Decrease in catalyst activity with time-on-stream for a 2.6 wt % F on alumina catalyst. (350°C, 2 g.s.mL^{-1})

existence of a minimum at an intermediate initial concentration of acetylene.

Experiments, conducted on the microbalance, in which the gas-phase conversion and the coke deposition rate were measured simultaneously provided further evidence to support this hypothesis. It can be seen in Fig. 6.12 that the changes in activity brought about by altering the gas-phase concentration of acetylene are accompanied by similar although opposite changes in the rates of coke deposition and in the absolute amounts of coke deposited. As the initial concentration is increased from 2.5 to 4 vol % the rate of coke deposition increases drastically resulting in a loss of activity. On the other hand, as the initial concentration is increased from 4 to 6.5 vol. % the rate of coke deposition decreases moderately indicating less severe deactivation under these conditions. The interaction of these two phenomena explains the minima in the curves in Figs. 6.5 and 6.9.

6.4 EFFECT OF FLUORIDATION

The effect of the fluoride content of the catalyst on the conversion of acetylene, observed in Fig. 6.6, can be understood in terms of the chemical interactions of fluoride with alumina. The modifications of the catalyst surface induced by the addition of fluoride include changes in the surface acidity (71) and in the number of sites available for adsorption of acetylene (35). Infrared and Raman studies of the adsorption of acetylene on alumina (12, 42, 90) have demonstrated that variations in the number of exposed aluminum ions (Al^{+3}) and hydroxyl groups (OH) on the catalyst surface strongly influence the mode of adsorption of acetylene at room temperature. As a result, Bhasin et al. (12) have postulated that the chemisorption of acetylene on alumina occurs at ion-pair sites consisting of exposed aluminum ions (Lewis acid sites) and neighbouring oxide ions or OH groups (Bronsted sites). Other studies (35, 72) have shown that replacement of surface hydroxyl and oxide ions with fluoride serves to decrease the number of such ion-pairs. The decrease in the catalyst activity with increased fluoride loadings is consistent with these findings. It is generally accepted that polymerization reactions

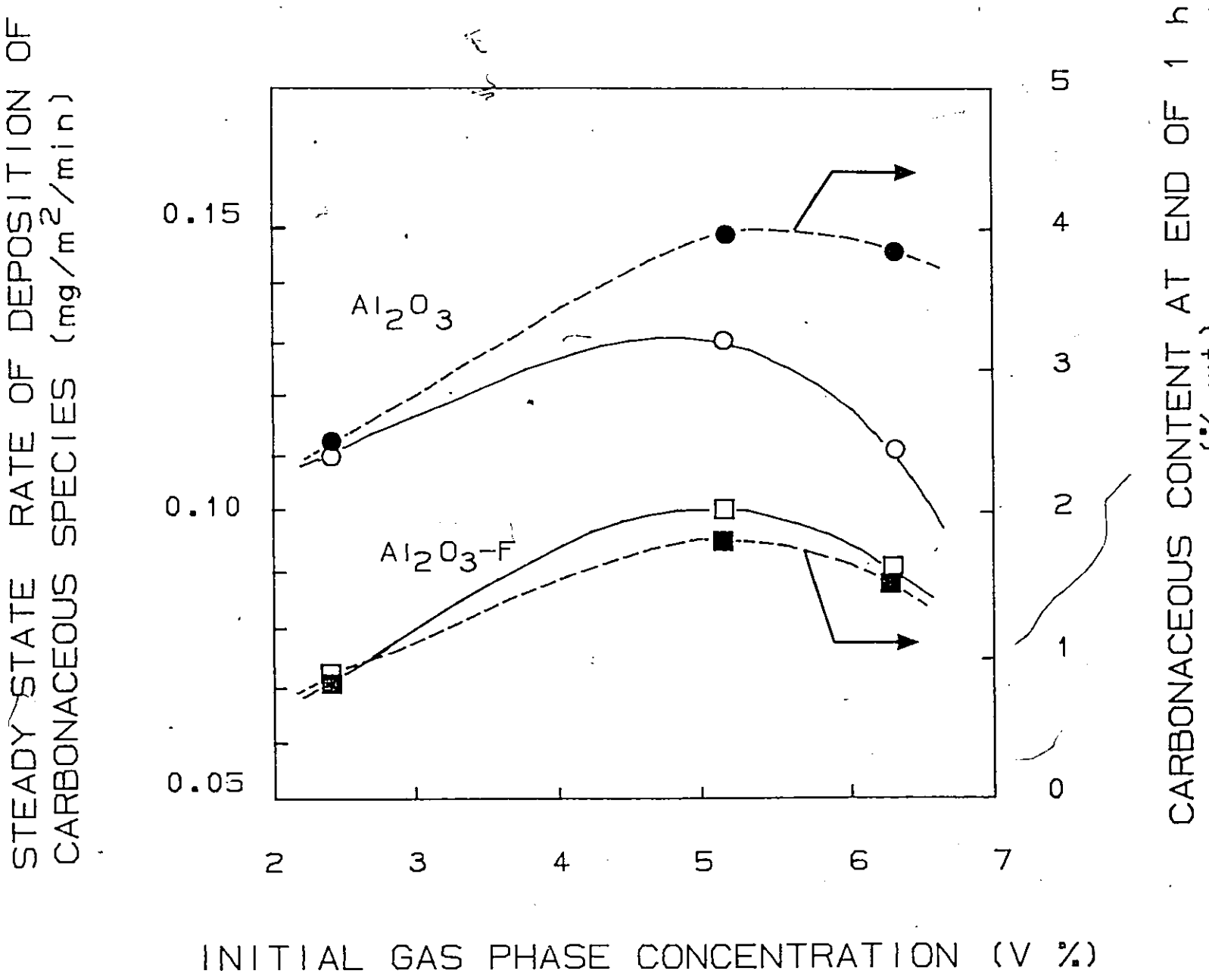

Fig. 6.12 The effect of gas-phase concentration on both the carbonaceous content and its

are acid catalyzed. More specifically, Tsai and Anderson (94) proposed that acetylene polymerized to form aromatic products via a vinyl cation intermediate when a ZSM-5 zeolite catalyst was used. The concept of the vinyl cation is consistent with the carbonium ion theory of acid-catalyzed reactions. It was shown in Fig. 5.1 that fluoridation altered the acidity of alumina. In addition, Paukshtis et al. (71) have shown that the introduction of fluoride generates a different distribution of acid sites on the alumina surface. Fluoride-modified alumina possessed a greater portion of medium and strong acidic centres. It would appear, therefore, that the reaction may have been influenced by the acid site distribution at low gas phase concentrations of acetylene. This would be consistent with the correspondence between the maximum in the acidity (Fig. 5.1) and the maximum in conversion (Figs. 6.6 and 6.10). In contrast, the reaction may have been influenced by the number of reaction sites at large gas phase concentrations of acetylene. This would be consistent with the continuous decrease in conversion as the catalyst fluoride concentration increased. The influence of fluoride on conversion could be a result of a combination of these two factors, the strong acid sites which are generated and the ion-pair (adsorption) sites which are lost in the fluoridation process.

On the basis of the above discussion, the high activity of alumina and fluoride-modified alumina could result from the presence of a significant number of ion-pair sites available for adsorption and from the particular acid strength distribution of these sites. At comparable operating conditions, the fluoridated alumina catalysts used in this study were more active than the ZSM-5 zeolite used by Tsai and Anderson. Tsai and Anderson concluded in their work that acetylene conversion was a Bronsted acid-catalyzed reaction. Alumina is at best a very reluctant Bronsted acid, yet high conversions were observed with pure alumina in this study. This would imply that Lewis acid sites are perhaps as or more important than the Bronsted sites. As discussed earlier, fluoridation produces a small number of Bronsted acid sites and increases the Lewis acidity of the starting alumina (17). The correlation obtained between the total

acidity of the fluoride-modified alumina (as measured by adsorption) and the acetylene conversion at low initial concentrations discussed earlier implies that this surface redistribution of sites affects the acetylene reaction. It cannot be concluded from this work however which sites are the active sites for the polymerization reaction. Nevertheless one can postulate based on the concept of the ion-pair sites necessary for acetylene adsorption that the presence of both Bronsted sites and stronger Lewis acid sites would enhance the reaction as demonstrated here.

6.5 CONCLUSION

The conversion of acetylene to aromatic products was shown to proceed relatively easily over fluoridated alumina catalysts. This activity is believed to be the result of acid-base properties of the fluoride modified alumina. The following empirical model was obtained to describe the total percent conversion of acetylene (X) over fluoridated alumina within the operating region used in this study:

$$X = 60.63 + 13.82\, x_1 - 26.26\, x_2 + 13.36\, x_3 - 4.97\, x_2^2 + 7.83\, x_4^2 - 9.81\, x_2 x_4$$

where x_1 is the coded reaction temperature (300-400^{o}C), x_2 is the coded catalyst (0 to 4.5 wt % F), x_3 is the coded weight-time (1 to 3 g.s.mL^{-1}) and x_4 is the coded initial concentration of acetylene (5 to 15 vol %). Examination of the model revealed that the maximum conversion was achieved at the upper boundaries of the operating region in temperature and weight-time. A complex interaction between the initial concentration of acetylene (x_4) and the type of catalyst (x_2) suggested that testing of other catalysts at a minimum of 3 levels of initial concentration may be warranted. A correlation between catalyst activity and catalyst acidity at low initial concentrations of acetylene was revealed by the model and corroborated by studies in the microbalance.

7. PRODUCT DISTRIBUTION

In the previous chapter, the conversion of acetylene was found to vary with acidity of the catalyst. It was clear, however, that attention had to be given to decreasing the rate of deactivation of the catalyst and to optimizing the reaction products. In this chapter, the focus will be on examining the product distribution as a function of the operating conditions and of the catalyst properties.

7.1 REACTION PRODUCTS

The products in this reaction are gases, liquids or solids at reaction temperature. The analysis procedures for the gas samples and for the condensable liquid samples were outlined in Chapter 4 and details may be found in Appendices 4.4 and 4.5. A complete discussion of the solid residue will be given in Chapter 8.

A typical chromatogram of the content of one of the sample loops on the gas sampling valve is shown in Fig. 7.1. The major components of the gas phase are unreacted acetylene, ethylene, methane, ethane, butenes and butadiene. A very broad shoulder toward the end of the chromatogram indicates the presence of C_6^+ hydrocarbons which were not retained in the dry ice trap. These compounds can be recognized as products from the hydropolymerization process discussed in Chapter 2. Very minor amounts of hydrogen (<1%) were detected in some experiments.

A typical chromatogram of the content of one of the sample loops on the heated sampling valve using flame ionization is shown in Fig. 7.2. A wide spectrum of products is visible. The large peak at the beginning of the chromatogram contains all the light gas components described above. Distinct peaks (compounds) may be distinguished in the first 25 minutes of the chromatogram. However, the fusing of peaks increases between 25 and 50 minutes or as the temperature is ramped from 150 to 250^{o}C. As described in Chapter 4 samples stored in the loops of the heated valve were also analyzed using mass

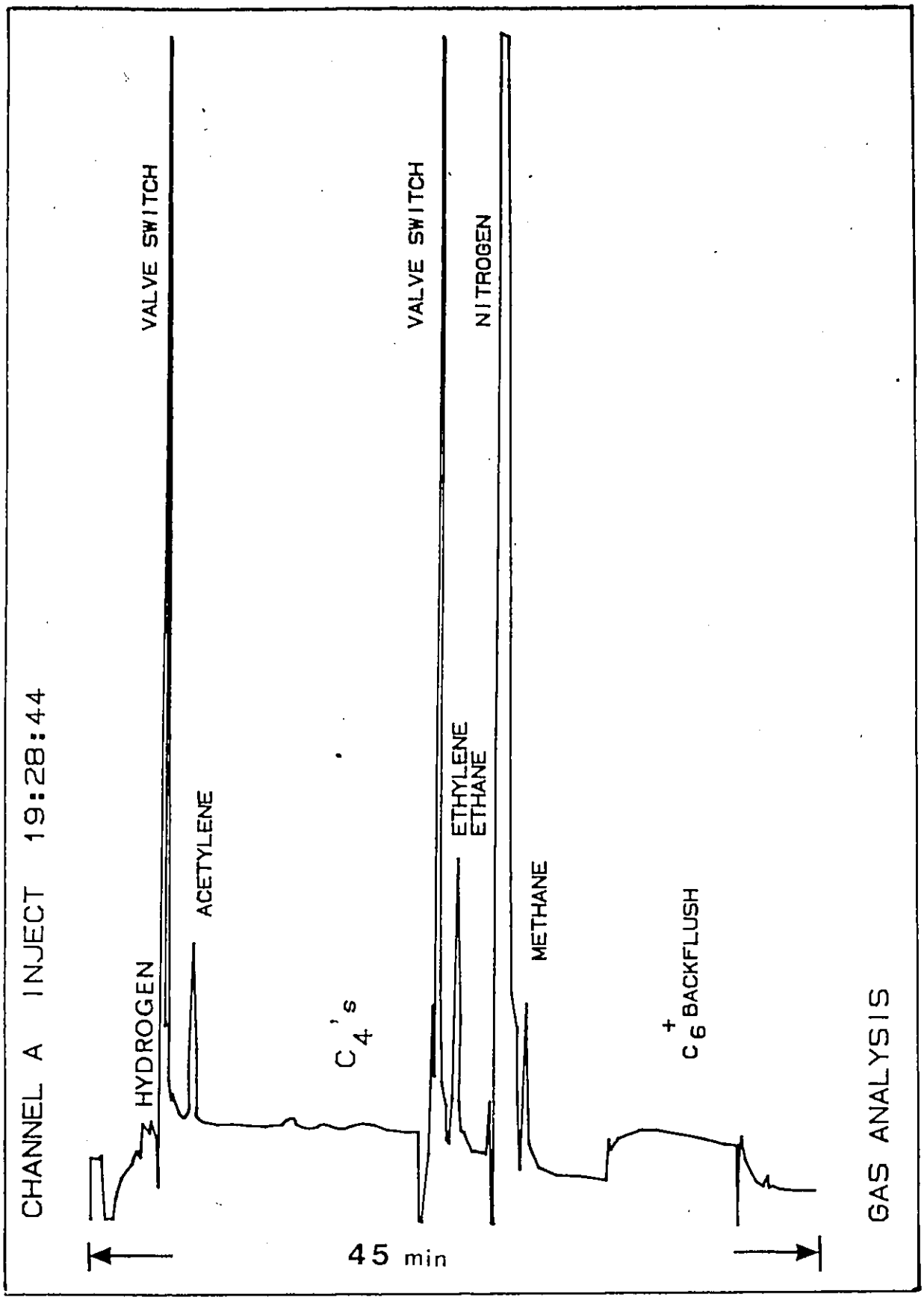

Fig. 7.1 A sample chromatogram of the response of the TCD to gas sample (Exp't 9)

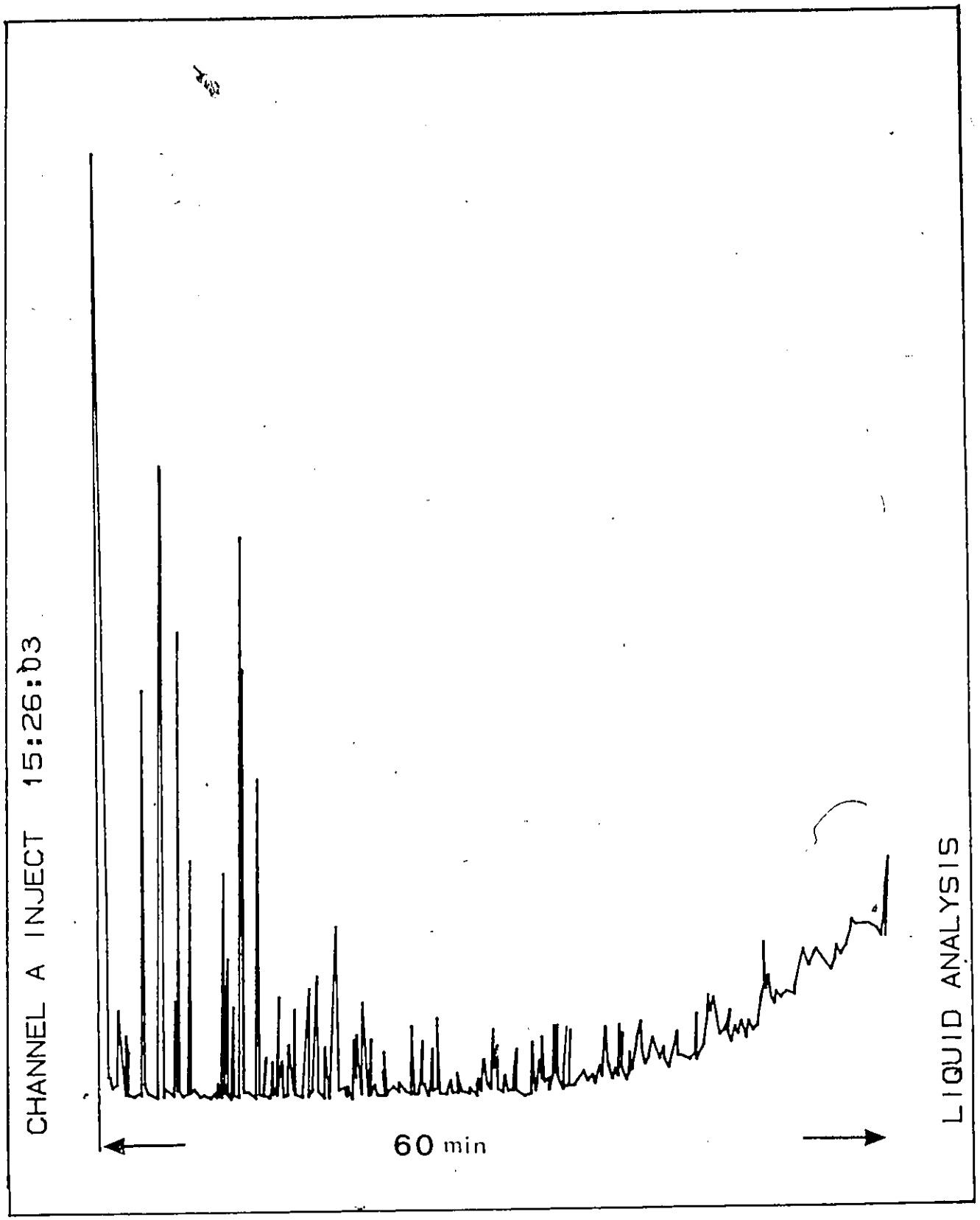

Fig. 7.2 A sample chromatogram of the response of the FID to a vapour sample (Exp't 1).

spectrometry. Analysis using the mass spectrometer of the sample which generated the chromatogram of Fig. 7.2 is shown in Fig. 7.3 for comparative purposes. Despite the expansion of the abscissa in Fig. 7.3 (cf Fig. 7.2), a peak by peak comparison reveals that the number of peaks is identical and the resolution in the two chromatograms are similar. Loss of resolution in the mass spectral data occurs somewhat later in the chromatogram (~ 30 min). Clues as to the possible identities of the components which made up the chromatographic peaks were obtained by searching the National Bureau of Standards Computer Library and comparing the mass intensity ratios of the unknown compounds with mass intensity ratios for standards. For the components of greater interest, a positive identification was made by matching the retention times of these components observed in the FID trace with retention times obtained with pure compounds.

A summary of the reaction products identified and confirmed by these techniques is given in Table 7.1. Several items should be noted in this table. First, n-heptane was not a reaction product, it was used as the external tracer which permitted quantitative analysis of the sample. Second, most of the products are aromatic in nature. Third, reaction products whose molecular weights exceed approximately 170 cannot be identified easily. After 1 h of analysis the compounds which are being eluted have a minimum molecular weight of 275 ($C_{22}H_{12}$). These values of the molecular weights were used to determine the liquid product distribution in terms of weight percentages.

Elemental analysis of the used catalysts from the tubular reactor provided a measure of the coke which was deposited on the catalyst surface during the experiment. Since this analysis could only be done at the end of an experiment, the yield of carbon at 15 min on stream was obtained by linear interpolation of the 1 h measurement for the purpose of determining the material balance closure at that time-on-stream. A more complete discussion of the solid reaction products is given in Chapter 8.

Analysis of these three categories of reaction products permitted the calculation of the material balance at a time-on-stream of 15 minutes. A sample

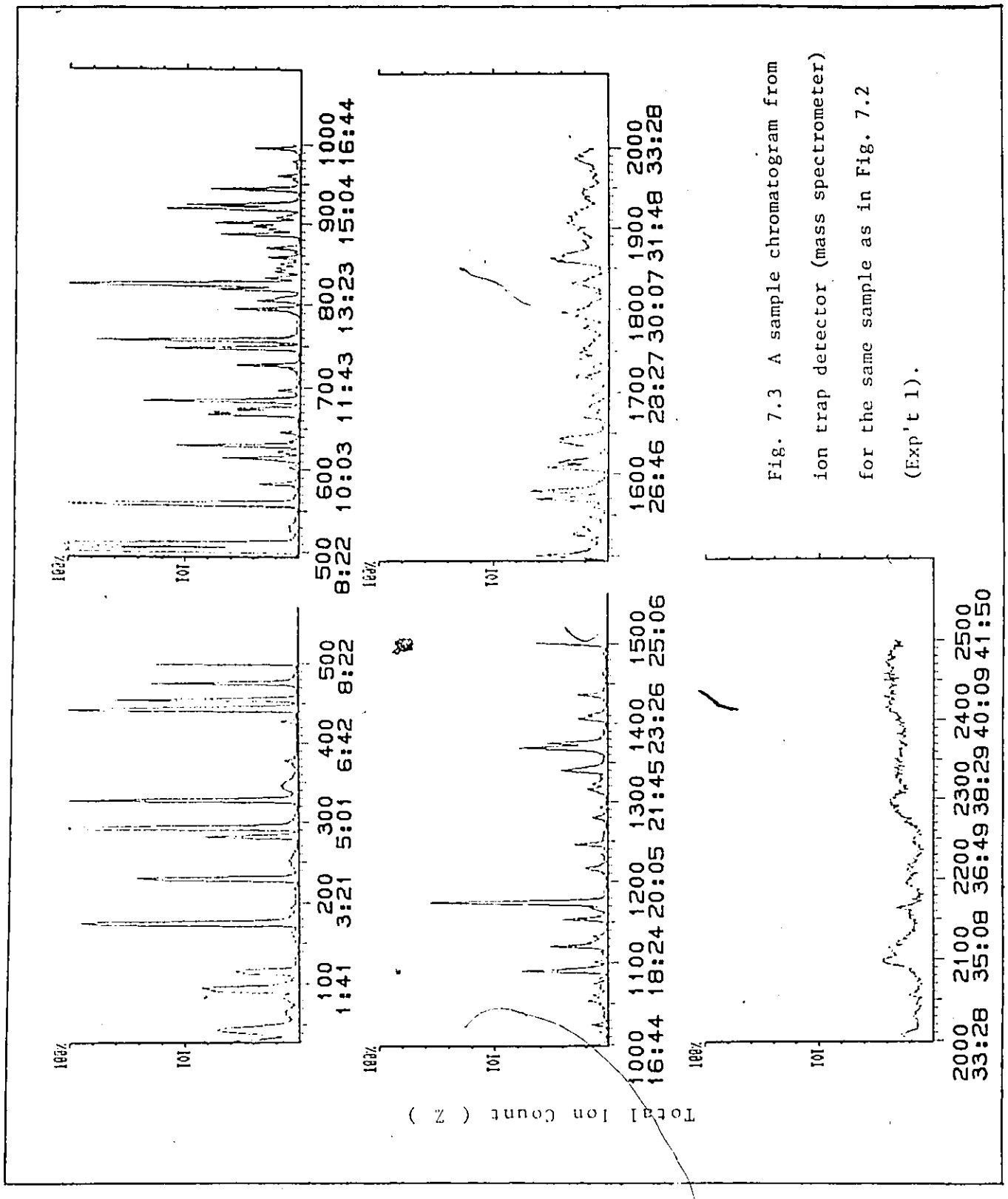

Fig. 7.3 A sample chromatogram from ion trap detector (mass spectrometer) for the same sample as in Fig. 7.2 (Exp't 1).

Table 7.1

Liquid product component identification*

Retention Time (min)	Compound	Formula	Method of Identification	Molecular Weight
2.89	Benzene	C_6H_6	FID, MS	78
3.20	n-Heptane	C_7H_{16}	FID, MS	100
4.22	Toluene	C_7H_8	FID, MS	92
5.15	Ethylbenzene	C_8H_{10}	FID, MS	106
6.08	p-xylene	C_8H_{10}	FID, MS	106
6.28	m-xylene	C_8H_{10}	FID, MS	106
6.87	*O*-xylene	C_8H_{10}	FID, MS	106
8.61	trimethylbenzene	C_9H_{12}	FID, MS	120
8.88	" isomer	C_9H_{12}	MS	120
9.08	" isomer	C_9H_{12}	MS	120
9.43	" isomer	C_9H_{12}	MS	120
9.94	" isomer	C_9H_{12}	MS	120
10.86	p-cymene		FID, MS	134
11.26	unknown			134
14.31	3,4-dimethylstyrene		MS	134
15.42	1,1 dimethylindan		MS	146
15.84	p-ethylcumene		MS	146
19.13	dimethyl tetrahydro-naphthalene		MS	160
26.08	trimethylnaphthalene		MS	170
49.50	anthanthrene	C_{12}-C_{24}	MS	276

* Retention times are those for FID. The retention times on the mass spectrometer are delayed because scanning was begun only after the light gas peak was eluted.

calculation is provided in Appendix 7.1. Over 75% of the experiments were within 100+/-35 % closure. This was deemed to be quite respectable considering the spectrum of products produced and the limited quantity of acetylene reacted (0.05-0.30 g).

7.2 THERMODYNAMIC CONSIDERATIONS

The thermodynamic equilibrium concentrations of the products (C_6 to C_{15}) arising from the transformation of acetylene have been calculated by Mikulec et al. (64) as a function of temperature and hydrocarbon partial pressure with and without the presence of methane. The equilibrium mixture composition based on these calculations at 350 ^{o}C and 1 atm. is given in Table 7.2. Equilibrium calculations show that paraffins are present in small amounts particularly if methane is not considered. If methane is present in the mixture, then naphthalene represents the major product. Otherwise, naphthalene, 2-methyl-naphthalene, benzene, toluene and xylenes are present in considerable amounts. Mikulec et al. (64) also found that at equilibrium the overall yields of aromatics decreased with temperature, while the yield of benzene increased. Furthermore, an increase in pressure led to an increase in the yield of aromatics at the expense of paraffins. A similar calculation, allowing for the presence of light olefins such as butenes, butadiene and ethylene would have been useful in determining the equilibrium yields of the latter.

The experimentally observed data on the liquid product distribution in the transformation of acetylene in the absence of catalysts (20), over fluoridated alumina and over the ZSM-5 zeolite (94) is shown in Table 7.3. A significant difference exists between the non-catalytic and catalytic product distributions. The thermal experiment was carried out at 600^{o}C and showed a large proportion of benzene and toluene. The catalytic experiments were carried out at substantially lower temperature (350^{o}C) and showed much higher proportion of the heavier aromatics (C_9^+). The transformation over ZSM-5 revealed that increasing the space velocity had little effect on the product distribution observed

Table 7.2

Equilibrium composition of selected hydrocarbons [wt %] from acetylene (621 K and 1 atm)

Component	Concentration [mol %] Methane included	Methane excluded
Methane	7.517	-
Paraffins	0.002	4.115
Benzene	1.170	17.52
Toluene	0.419	14.73
Xylenes	0.0005	4.13
C_9 aromatics[a]	tr	0.5066
C_{10} aromatics[b]	89.18	36.8
C_{11} aromatics[c]	2.081	20.15
C_{12} aromatics[d]	0.0069	1.582
C_{13} aromatics[e]	0.0018	0.399
C_{14} aromatics[f]	tr	0.012
C_{15} aromatics[g]	tr	0.061

[a] includes ethylbenzene and styrene
[b] consists of ethyltoluene, trimethylbenzene
[c] consists of diethylbenzene, tetramethylbenzene, naphthlene
[d] 2-methylnaphthlene
[e] 1,7-dimethylnáphthalene
[f] 2-ethylnaphthalene
[g] 2-propylnaphthalene
[h] 2-ethyl-6-methylnaphthalene

Table 7.3

Comparison of liquid product distributions (mol %) for the transformation of acetylene

Catalyst	none[a]	ZSM-5[b]	ZSM-5[b]	Al_2O_3-F[c]	Al_2O_3-F[d]
Time-on-stream [min]	na	15	15	15	15
Space Velocity [h^{-1}]	–	3900	15000	1000	1000
Conversion [% C_2H_2]	44	11	4	5	26
Composition (mol %)					
Benzene	64.1	4.2	3.2	6.0	6.5
Toluene	17.5	6.7	5.3	2.4	2.1
Xylenes	4.3	11.8	8.3	5.8	20.7
C_9-Ar	3.5	1.2	7.3	9.0	11.2
C_{10}-Ar	4.4	39.2	36.4		8.2
C_{11}-Ar	1.9	36.9	36.4		15.1
C_{12}-Ar	0.5	tr	3.1		15.6
C_{13}-Ar(+)	0.6	tr	tr	76.8	20.6

[a] 873K, 4-7 L/h

[b] Si/Al in ZSM-5 -60, 573 K, C_2H_2/He = 0.133

[c] F^- in Al_2O_3 = 4.3 wt %, 598 K, C_2H_2/N_2 = 0.125

[d] F^- in Al_2O_3 = 2.6 wt %, 573 K, C_2H_2/N_2 = 0.10

at 15 min time-on-stream. The experimentally observed yields of C_{10} and C_{11} over ZSM-5 are very close to their predicted values at equilibrium. This feature was not observed over fluoridated alumina. The approach to equilibrium in the case of the zeolite is perhaps due to steric constraints imposed by the zeolite cage structure which are not present in amorphous catalysts, e.g., fluoridated alumina. Significantly lower relative yields of low carbon number aromatics when compared with the thermodynamic values (no methane) are observed over both catalysts. It follows from this comparison that the data available are nonequilibrium and that kinetic factors participate in the transformations described.

7.3 PRODUCT YIELD AND DISTRIBUTION

A summary of the absolute and relative yields measured in the tubular flow reactor at a time-on-stream of 15 min is given in Table 7.4. The absolute yield is defined as the ratio of the weight of product to the weight of acetylene fed to the reactor. The relative yield is defined as the ratio of the weight of product to the weight of reactant which is converted. Because of the nature of the experiments the absolute yield of the solid product was measured only at 60 min on stream; its relative yield at 15 min on stream was calculated by difference. In order to simplify the discussion which follows, results from the star point experiments in the experimental design of Table 4.1 are grouped together in Table 7.4 followed by the experiments which complete the fractional factorial. Details of the gas and liquid product distribution also at 15 min on stream, are given in Tables 7.5 and 7.6 respectively.

7.3.1 General Observations

Absolute Yields

For all the experiments carried out in the tubular flow reactor, the yield of gaseous products (C_1-C_5) at 15 min on stream was very low (under 10 wt %). A large

Table 7.4

Product yields for experiments in tubular flow reactor

Experiment No.	X [%]	Product Yields(%) Liquid		Gaseous		Solid	
		Abs[a]	Rel[b]	Abs	Rel	Abs[c]	Rel[d]
1	55	19.2	34.7	7.56	13.7	9.5	51.6
2	44.5	53.6		3.63	8.2	22.1	-
3	99.4	12.6	13.0	1.9	2.0	29.2	85.
4	97.5	92.1	94.5	5.9	6.0	35.6	0
5	50.3	49.5	98.4	1.6	3.2	5.0	0
6	<5	32.9	-	0.3	-	3.0	0
7	98.5	3.8	3.8	0.4	0.4	11.1	96.
8	55.	2.2	4.0	14.4	26.3	9.3	70.
9	98.1	90.1	91.0	8.8	9.0	28.5	0
10	28.8	7.5	26.2	0.83	2.9	8.75	71
12	99.3	59.2	59.6	2.0	2.0	49.7	38
13	87.2	66.4	76.2	3.0	3.5	33.5	20
14	29.2	17.65	61.3	1.4	4.9	11.6	34
15	99.3	1.8	1.8	0.7	0.7	10.1	98
16	90.3	13.4	14.9	3.7	4.1	17.8	81
17	72.0	8.4	11.7	2.6	3.7	25.9	85

[a] Abs yields : yield of product expressed as ratio of g product to g C_2H_2 fed to the reactor at a time-on-stream of 15 min *100.

[b] Rel yields : yield of product expressed as ratio of g product to g C_2H_2 reacted at a time-on-stream of 15 min * 100.

[c] Yield of solid product: expressed as the ratio of g of carbon to g of C_2H_2 fed to reactor at a time-on-stream of 60 min.

[d] by difference

Table 7.5

Composition of gas-phase products [vol. %] at 15 min on stream from the transformation of acetylene

Component	Retention Time[min]		Experiment 1	2	3	4	5	6	7
Unknown	3.13	E-02	1.22	1.02					
Hydrogen		E-01	2.82		2.16	1.17			
Unknown	3.70	E-01			2.67				
Propylene		E-02							
Acetylene		E+00	5.06	3.85	0.04	0.30	3.47	10.81	0.18
isobutane		E-02	1.37						
n-butane		E-02				2.32			
t-2-butene		E-03	8.60			1.37			
butadiene		E-03	7.7			10.5			
isopentane		E-04				1.9			
Unknown	15.92	E-02							
Pentane		E-04							
Ethylene		E-02	19.61	17.19	8.88	2.67	8.75	3.21	3.74
Ethane		E-02				3.52			
Unknown	23.3	E-01	2.74						
Methane		E-02	30.4	0.97	0.82	16.24			0.65
Unknown	24.11	E-02		3.62		7.96			
Unknown	24.70	E-02				18.49			
Unknown	25.00	E-02	13.0	6.17			3.19		
C_6+		E-04	8.0		4.0				
Nitrogen		E+00	93.72	95.86	99.37	98.80	96.41	89.15	99.77

Table 7.5 cont'd

Composition of gas-phase products [vol. %] at 15 min on stream from the transformation of acetylene

Component	Retention Time [min]		Experiment 8	9	10	11	12	13	14
Unknown	3.13	E-02	1.46	2.53					2.76
Hydrogen		E-01	1.70	1.58		1.19			
Unknown	3.70	E-01							
Propylene		E-02					1.69		
Acetylene		E+00	3.13	0.18	6.45	0.07	1.35	1.27	6.41
isobutane		E-02		1.37					
n-butane		E-02							
t-2-butene		E-03		7.5		7.9		7.4	
butadiene		E-03						9.2	
isopentane		E-04						1.3	84.0
Unknown	15.92	E-02			1.4			1.1	
Pentane		E-04	3.5						
Ethylene		E-02	8.23	52.93	3.25	13.82	5.36	20.25	7.00
Ethane		E-02							
Unknown	23.3	E-01	7.57						
Methane		E-02							
Unknown	24.11	E-02							
Unknown	24.70	E-02							
Unknown	25.00	E-02	2.98	33.05		2.49		2.23	4.24
C_6^+		E-04		2.0	4.0	5.0	4.0	4.0	
Nitrogen		E+00	95.82	98.75	93.50	99.64	98.57	98.48	93.44

Table 7.5 cont'd

Composition of gas-phase products [vol. %] at 15 min on stream from the transformation of acetylene

Component	Retention Time(min)		Experiment 15	16	17
Unknown	3.13	E-02	0.82		
Hydrogen		E-01			
Unknown	3.70	E-01			
Propylene		E-02			
Acetylene		E+00	0.06	0.48	2.74
isobutane		E-02			
n-butane		E-02		1.70	
t-2-butene		E-03			7.30
butadiene		E-03			
isopentane		E-04			8.60
Unknown	15.92	E-02			1.67
Pentane		E-04			
Ethylene		E-02	8.50	11.51	13.80
Ethane		E-02			
Unknown	23.3	E-01			
Methane		E-02			
Unknown	24.11	E-02			
Unknown	24.70	E-02			
Unknown	25.00	E-02	1.51	2.27	3.53
C_6^+		E-04			
Nitrogen		E+00	99.83	99.36	97.05

Table 7.6

Liquid product composition [wt %] at 15 min on stream from the transformation of acetylene

Component	Retention Time[min]	Experiment 1	2	3	4	5	6	7
Benzene	2.89	2.18	2.17	0	11.7	0.70	2.95	6.93
Toluene	4.22	8.57	6.64	0	8.89	1.26	1.36	10.96
Ethylbenzene	5.15	33.4	0.73	0	0.43	0.34	1.31	6.64
p-xylene	6.08	0.84	2.25	0	8.69	0.25	0.43	8.03
m-xylene	6.28	5.15	10.6	58.4	8.72	0.79	1.25	0
-xylene	6.87	1.79	5.38	41.6	1.64	0.40	0.80	0
trimethyl	8.61[a]	0	0	0	0.87	0.49	0	4.49
benzene	8.88	1.46	8.32	0	6.31	0.21	0.87	0
isomers	9.08	0.87	1.08	0	0	1.18	0.25	0
"	9.43	0.42	2.37	0	0	0.18	0.25	0
"	9.94	26.7	19.97	0	3.26	0.48	1.81	4.85
p-cymene	10.86	0.42	9.26	0	0	0	0.84	0
	11.32	0	0	0	0	0	0	0
	11.84	0	0	0	0	0	0.36	0
	12.09	0	3.57	0	0	0	0.31	0
	12.75	0	0	0	0	0	0	0
	12.82	0	0	0	0	0	0	0
	12.88	0	0	0	0	0	0.20	0
	13.05	0	7.48	0	0	0	0.25	12.2
	13.83	0	0	0	0	0	0.19	0
	14.15	0	0	0	0	0	0	0
	14.31	0.350	0	0	0	0	0	0
	15.04	0	0	0	0	0	0	0
	15.42	0	0	0	0	0	0	0
	15.49	0	0	0	0	0	0	11.08
	15.84	8.4	5.73	0	0	0	0	0
	16.61[b]	0	0	0	0	0	0	0
	>16	0	0	0	2.85	0	1.84	0
	<18	0	0	0	4.23	0	0	0
	<20	0	0	0	12.1	0	0	0
	>20 [c]	8.4	14.4	0	30.2	93.7	84.7	34.8

[a] peaks eluting between 8.5 and 18 min are referred to as C_9^+
[b] peaks eluting between 16.75 and 20 min are referred to as C_{18}^+
[c] peaks eluting after 20 min are referred to as C_{20}^+

Table 7.6 cont'd

Liquid product composition (wt %) at 15 min on stream from the transformation of acetylene

Component	Retention Time(min)	Experiment 8	9	10	11	12	13	14
Benzene	2.89	0	1.27	3.7	20.2	5.81	1.91	4.21
Toluene	4.22	54.57	4.36	1.35	4.24	1.78	4.91	7.47
Ethylbenzene	5.15	17.20	0.45	8.4	1.00	53.2	2.20	2.89
p-xylene	6.08	20.11	1.50	3.78	3.58	0	1.95	1.62
m-xylene	6.28	0	5.10	2.12	2.42	0	4.01	3.18
-xylene	6.87	0	2.75	1.76	7.28	0	3.17	3.53
trimethyl	8.61	0	0.27	3.12	0.48	0	0.49	1.81
benzene	8.88	0	3.46	1.87	1.39	0	3.85	0.64
isomers	9.08	0	1.39	0.97	0	0	0	0.87
	9.43	0	1.10	3.84	0.64	25.8	2.42	3.37
	9.94	0	6.78	0	2.48	0	4.81	1.67
p-cymene	10.86	0	3.16	1.29	0.38	0	0	0.40
	11.32	0	0.42	1.06	0	0	1.53	0
	11.84	0	0	0	1.07	0	0	1.99
	12.09	0	1.05	1.87	1.49	0	0	0
	12.75	0	0	3.29	0	0	0	0
	12.82	8.12	2.02	0	0.23	0	0	0
	12.88	0	0	0	0	0	0	1.83
	13.05	0	0	0	0	0	0	0.752
	13.83	0	5.86	0	0	0	0	0
	14.15	0	0	0	0.54	8.49	0	7.44
	14.31	0	7.64	1.11	0	0	3.50	12.5
	15.04	0	0	0	0	0	0	0
	15.42	0	0	4.28	12.87	0	0	9.57
	15.49	0	8.18	0	0	4.94	0	0
	15.84	0	0	11.22	0	0	0	0
	16.61	0	0	0	4.49	0	0	0
	>16	0	4.90	14.4	0	0	0	6.47
	<18	0	25.49	4.03	0	0	0	4.55
	<20	0	11.15	26.4	0	0	0	19.2
	>20	0	1.69	0	35.2	0	65.2	3.91

Table 7.6 cont'd

Liquid product composition (wt %) at 15 min on stream from the transformation of acetylene

Component	Retention Time(min)	Experiment 15	16	17
Benzene	2.89	1.89	11.7	15.58
Toluene	4.22	77.9	15.16	32.95
Ethylbenzene	5.15	0	4.32	2.01
p-xylene	6.08	0	3.89	9.21
m-xylene	6.28	0	11.12	16.04
-xylene	6.87	0	4.58	2.20
trimethyl	8.61	0	5.38	22.00
benzene	8.88	0	2.46	0
isomers	9.08	0	2.74	0
	9.43	0	0	0
	9.94	20.2	11.9	0
p-cymene	10.86	0	5.02	0
	11.32	0	0	0
	11.84	0	0	0
	12.09	0	1.75	0
	12.75	0	0	0
	12.82	0	0	0
	12.88	0	0	0
	13.05	0	1.28	0
	13.83	0	0	0
	14.15	0	0	0
	14.31	0	1.64	0
	15.04	0	0	0
	15.42	0	0	0
	15.49	0	1.89	0
	15.84	0	0	0
	16.61	0	0	0
	>16	0	0	0
	<18	0	5.54	0
	<20	0	6.27	0
	>20	0	3.32	0

variation was observed in the liquid yield (2 to 92 wt%) based on the total amount of acetylene fed to the reactor at 15 min on stream. The absolute yield of solid product or catalyst residue at the end of the experiment (i.e., 1 h) varied between 0 and 50 wt %.

Examination of Table 7.4 reveals the influence of the operating variables on the individual absolute yields of the products. The individual absolute yields of all the products increased as the reaction temperature and conversion increased. The yields of liquid and gas increased as the reactant feed concentration was decreased, despite the conversion level. However, the solid yield reflects the change in conversion very closely. Similarly, the yields of gas and solid increase as the weight-time and conversion increase. The yield of liquid product appears to go through a minimum at an intermediate level of weight-time. From the trends observed in Table 7.4, it can be concluded that the maximum liquid yields are obtained by operating at high temperature ($400^{o}C$), low reactant concentration (5 vol % C_2H_2) and high weight-time (3 $g.s.mL^{-1}$), conditions which for the most part also lead to high conversion levels.

Relative Yields

The yields of the gaseous and liquid products were also expressed on the basis of the fraction of acetylene which was converted in the reactor. These yields are included since the conversions varied considerably in these experiments. The relative yield of the solid residue could be calculated by difference at 15 min on stream and is provided in the last column of Table 7.4. Relative yields of solid product varied from 0 to 98 %.

The effects of the reaction temperature, weight-time, and initial concentration of acetylene on these relative yields are depicted in Fig. 7.4. It is apparent in Fig. 7.4 that the undesirable solid reaction product sometimes represents the largest fraction of the product spectrum. In general, gas and liquid yields increased with increased reaction temperature at the expense of the catalyst solid residue. The single largest effect on the gas yields was observed with variations in the reaction temperature (Fig.

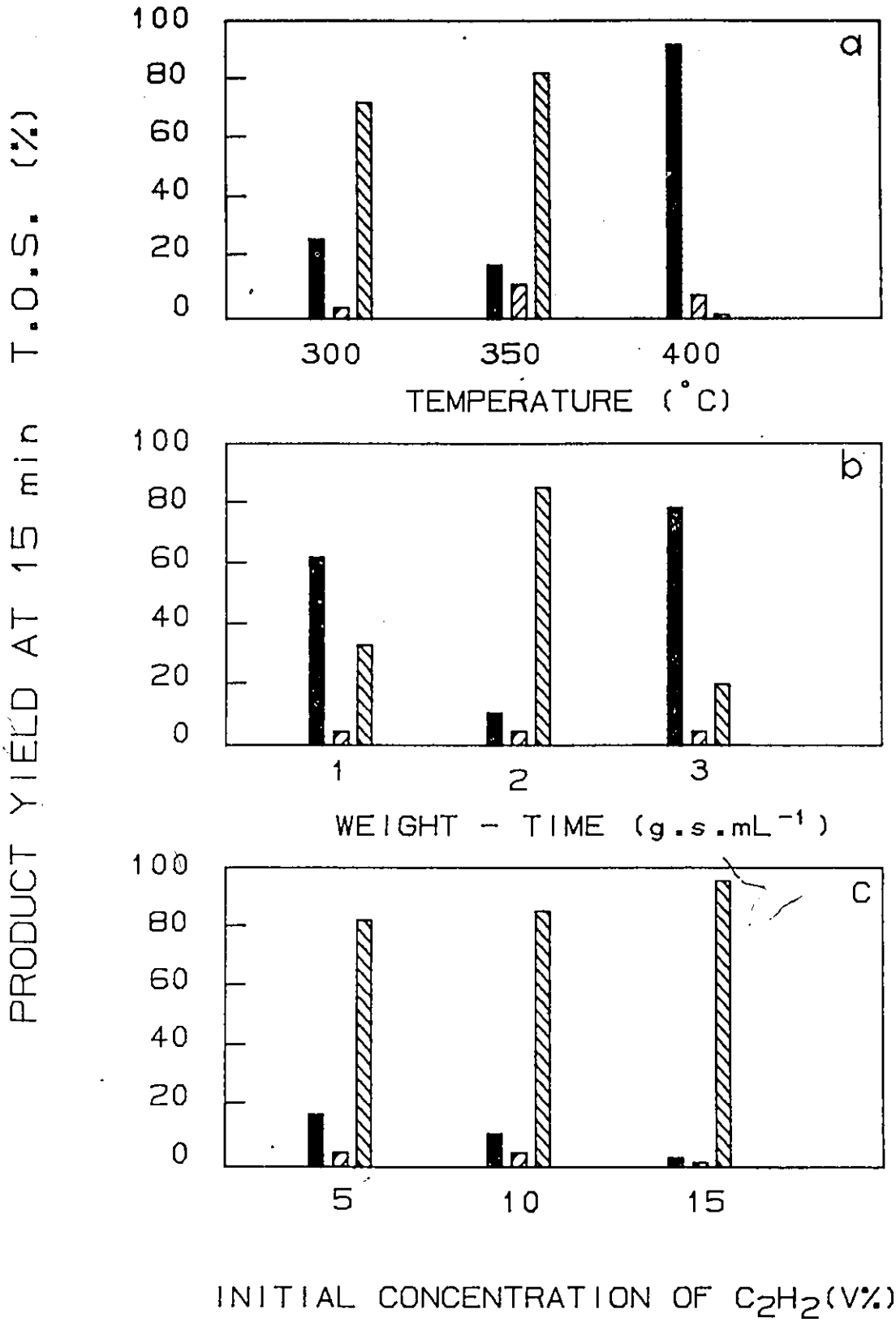

Fig. 7.4 Effect of operating variables on product yield at 15 min on stream in the tubular flow reactor for a 2.6 wt % F on alumina catalyst. ▣ Liquid ▨ Gas ▧ Solid

7.4). The increase in gaseous products was attributed largely to a single component of the gas phase, ethylene. The most marked increase occurs in the liquid yield as the temperature is raised from 350 to 400^{o}C. The production of liquids appears to be favored by high temperatures and low concentrations of reactant. However the dependence on weight-time is more complex. A minimum in the liquid yield is observed at intermediate weight-times. As will be shown subsequently, the character of the liquid produced at various weight-times is quite different.

7.3.2 Effect of Operating Variables on Liquid Product Distribution

The liquid product distribution, as a function of reaction temperature, weight-time and concentration of acetylene is shown in Fig. 7.5. Increasing temperature resulted in dramatic changes to the distribution of the various liquid species. Relative amounts of BTX increased, at the expense of the C_9 and higher components, as the temperature was increased to 350^{o}C probably as a result of dealkylation.

High liquid yields were obtained at both high and low weight-times (Fig. 7.4). However, it was also observed that a significantly higher proportion of liquids of high molecular weight (MW >250) were present at high weight-times (low space velocity). A corresponding reduction in the C_6-C_{18} fractions was also visible compared with that obtained at both low and intermediate weight-times. Consequently, the high liquid yields obtained at high weight-times were accompanied by a shift in the distribution of liquids which was undesirable. At low weight-times, a large C_9^+ fraction is visible. Increasing the weight-time from 1 to 2 g.s.mL^{-1}, results in a substantial increase in the BTX fraction at the expense of the C_9^+ and C_{18}^+ fractions. Unfortunately, the highest selectivity to BTX products coincides with the lowest liquid yields obtained (cf. Fig. 7.4 and 7.5).

At low initial concentration of the reactant, the liquid produced covers a wide spectrum of molecular weights, a significant portion of which is BTX. As the initial

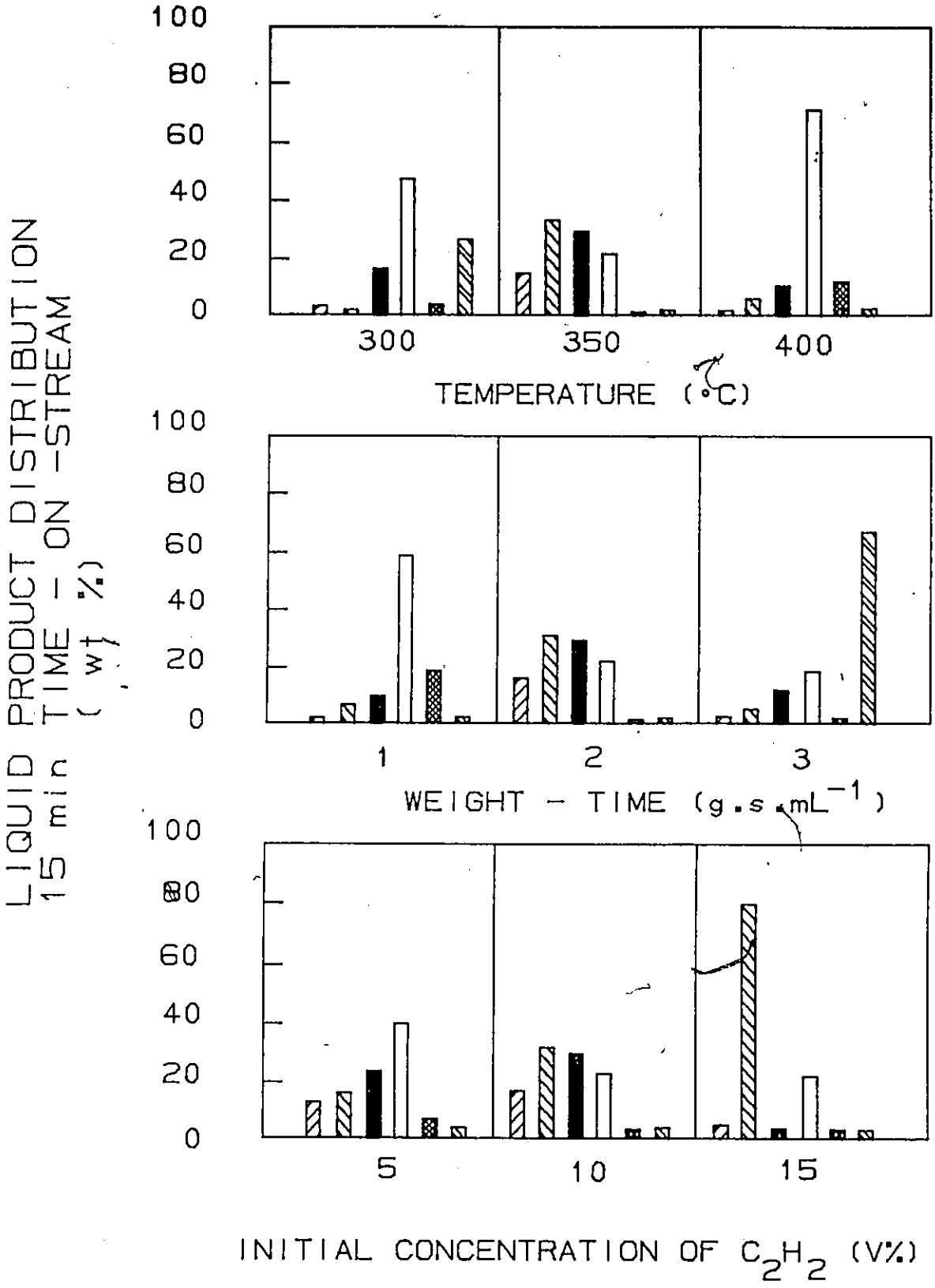

Fig. 7.5 Effect of operating variables on liquid product distribution at 15 min on stream in the tubular flow reactor for a 2.6 wt % F on alumina cat st. C_6, C_7, C_8, C_9^+, C_{18}^+, C_{20}^+,

concentration is increased the spectrum narrows, i.e. light ends, C_6 and heavy ends, C_{20}^+ are absent from the distribution. An increase in the proportion of the C_7 fraction appears to take place at the expense of the benzene and C_8 components. Unfortunately, this narrow distribution occurs simultaneously with the lowest liquid yield observed.

Two desirable characteristics of the liquid product are narrow product spectrum and a large proportion of BTX. For the liquids produced at 15 min on stream, these characteristics were obtained at an intermediate value of weight-time (2 $g.s.mL^{-1}$) and at intermediate to high values of feed gas concentration (10-15 vol%) and temperature (350-400^{o}C). It can be concluded that the conditions under which high liquid yields and moderate to high conversions are obtained also give liquid products which possess these desirable characteristics.

7.4 CHANGES IN PRODUCT YIELD AND DISTRIBUTION WITH TIME-ON-STREAM

Liquid Product

A comparison of the liquid product yields at various times-on-stream for a single experiment is given in Table 7.7. Trends observed in this experiment were typical of other experiments. The absolute yield of liquid product which is based on the total weight of acetylene fed decreases with longer times-on-stream. This however also reflects the fact that the conversion to all reaction products decreases with time-on-stream as discussed in Chapter 6. Examination of the relative yields of liquid product, which is based on the amount of acetylene which is converted, reveals very little change in the liquid yield with time-on-stream. Consequently, the liquid fraction is not being sacrificed at the larger times-on-stream. In fact, if we consider the incremental yield, defined as the ratio of the weight of liquid produced in a fixed increment of time and the weight of acetylene converted in the same increment of time, we find that there is perhaps between 30 and 60 min on stream a gradual increase in incremental yield. The implication would be that more liquids are being formed per unit of acetylene converted. Rather, in

Table 7.7

Comparison of liquid yields with time-on-stream[a]

Time-on-Stream [min]	Liquid Yields		
	Absolute	Relative	Incremental
5	0.292	0.422	0.423
15	0.225	0.378	0.350
20	0.236	0.414	0.56
25	0.236	0.434	0.53
30	0.216	0.420	0.30
35	0.195	0.396	0.19
40	0.183	0.389	0.32
45	0.173	0.389	0.34
50	0.166	0.389	0.43
55	0.165	0.395	0.51

[a] Experiment 1

Table 7.8

Liquid product composition [wt %] as a function of time-on-stream

Retention Time [min]	Component	Molecular Weight	Time-on-Stream [min] 15	30	45	60
2.89	Benzene	78	2.18	2.26	2.69	1.30
4.22	Toluene	92	8.57	8.10	6.03	7.70
5.15	Ethylbenzene	106	33.44	45.48	19.45	16.59
6.08	p-xylene	106	0.84	-	1.01	1.58
6.28	m-xylene	106	5.16	0.60	5.02	6.75
6.87	-xylene	106	1.79	3.80	-	2.70
8.88	tri	120	1.46	-	-	-
9.08	methyl	120	0.87	-	-	-
9.43	benzene	120	0.42	-	-	2.19
9.94	isomers	120	26.7	30.35	-	7.15
10.86	-cymene	134	1.41	-	8.84	-
14.31			0.35	-	-	-
15.42		146	-	1.27	-	4.08
15.84			8.40	8.15	-	-
<20	tetranaphthalene	160	-	-	56.95	49.97
>20	trimethyl-naphthalene	170	8.41	-	-	-

fact, the nature of the liquid product is changing as shown in Table 7.8. Between 30 and 60 min on stream the liquid product distribution shifts considerably to higher molecular weights. After 60 min on stream, over 50 %, by weight, of the liquid has a molecular weight above 160. The combined effects of the liquid product becoming heavier and the conversion lower contribute to the possible rise in the incremental yield.

A comparison of the PONA (paraffin, olefin, naphthene, aromatic) analysis of the cumulative liquid product collected for all the experiments of 1 h and 5 h duration respectively is given in Table 7.9. The average molecular weight of the liquid product recovered in the cold trap after 1 h on stream is significantly lower than the average molecular weight of the liquid product obtained after 5 h on stream. Furthermore, the liquids contain a higher portion of aromatic hydrocarbons at the expense of both paraffinic and naphthenic hydrocarbons. The increase in aromaticity must correspond to the increase in the high molecular weight components which are formed in increasing proportions at large times-on-stream (Table 7.8). Formation of condensed ring structures or polynuclear aromatics must account for the steady increase in incremental liquid product yield.

Gas Product

The total yield of gaseous products was low (<9 %) in all the experiments therefore only the molar yield of the major component, ethylene is tabulated for three experiments as a function of time-on-stream (Table 7.10). For the most part, a steady decrease in the absolute yield of ethylene with time-on-stream was observed. On the other hand, the relative yields of ethylene in the experiments increased with time-on-stream. This increase in the production of ethylene is probably tied to the changing character of the liquid product at long times-on-stream. The presence of H_2 as indicated in Table 7.5 is probably a result of the dehydrogenation of naphthenes to aromatics. The presence of CH_4 and C_2H_4 is probably the result of dealkylation of ring compounds.

Table 7.9

Composition of cumulative liquid product[a]

Reaction Time [h]	Paraffins [wt%]	Naphthenes [wt%]		Aromatics [wt%]		Molecular Weight
1	8.7	49.4	8.4	41.9	3	175
			1.6		35	
			8.0		1	
			5.1		36	
5	2	23.1	37.6	74.9	24.2	238
			10.2		7.4	
			0.0		4.5	
			1.6		5.8	

[a] PONA analysis

Table 7.10

Yield of ethylene [mol%] as a function of time-on-stream

Time	Absolute Yields			Relative yields		
[min]	1[a]	9	16	1	9	16
15	1.77	5.59	2.49	3.44	5.70	2.77
30	1.51	6.43	1.87	3.34	6.78	2.69
45	1.24	5.38	1.46	5.06	6.34	2.27
60	1.15	3.80	1.25	5.75	8.02	1.99

[a] Experiment No.

7.5 PRODUCT DISTRIBUTION AS A FUNCTION OF CONVERSION

A link was established in the previous discussion between the conditions which maximize liquid yields and those which maximize conversion. Furthermore, these conditions for the most part gave desirable liquid product distributions at 15 min on stream. One avenue which was not explored in the previous analysis was the possibility of interactive effects of the operating variables on the product distribution. The distribution of benzene, toluene, C_8 (xylenes and ethylbenzene) and higher hydrocarbons (denoted as > C_9) at 15 min on stream for all the experiments was plotted as a function of conversion and is shown in Fig. 7.6. A smooth curve is drawn through the data. It is apparent from the overall distribution of the liquid components that significant quantities of the desirable liquid components (BTX) are attained only at high conversions. A fairly high molecular weight product and minor amounts of BTX are observed at low conversions. This pattern which is observed is typical of consecutive reactions in series.

7.6 EFFECT OF FLUORIDATION

The liquid product distributions over alumina and 2.6 wt % F on alumina at 15 min on stream (350^{o}C, 2 g.s.mL^{-1}, and 10 vol % C_2H_2) are compared in Fig. 7.7. The most noticeable difference is the remarkable lack of C_{18}^{+} compounds in the fluoridated alumina spectrum. The large relative solid yield at 15 min on stream with fluoridated alumina (Exp't 17 in Table 7.4, 85 %) compared with alumina (Exp't 12 , 38 %) implies that a non-desorbable carbonaceous layer forms very readily in the former case at early times-on-stream. Although high molecular weight species are formed over both catalysts, they do so at different rates. The narrower liquid product distribution obtained with the more acidic catalyst (2.6 wt% F) is obtained at the expense of a reduction in liquid yield (Table 7.4). This observation has been made earlier in discussing the effects of the

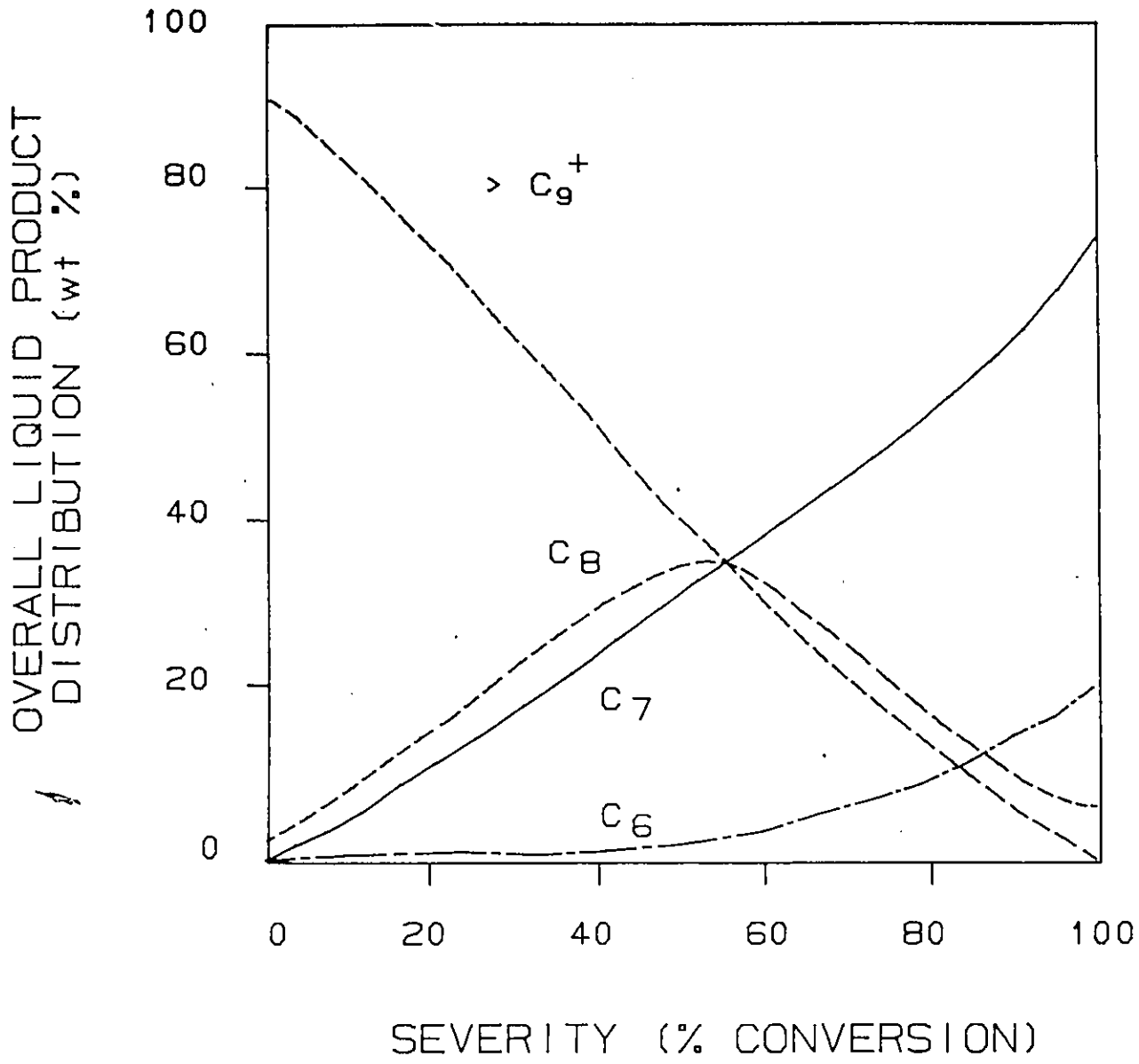

Fig. 7.6 Liquid product distribution as a function of severity in tubular flow reactor.

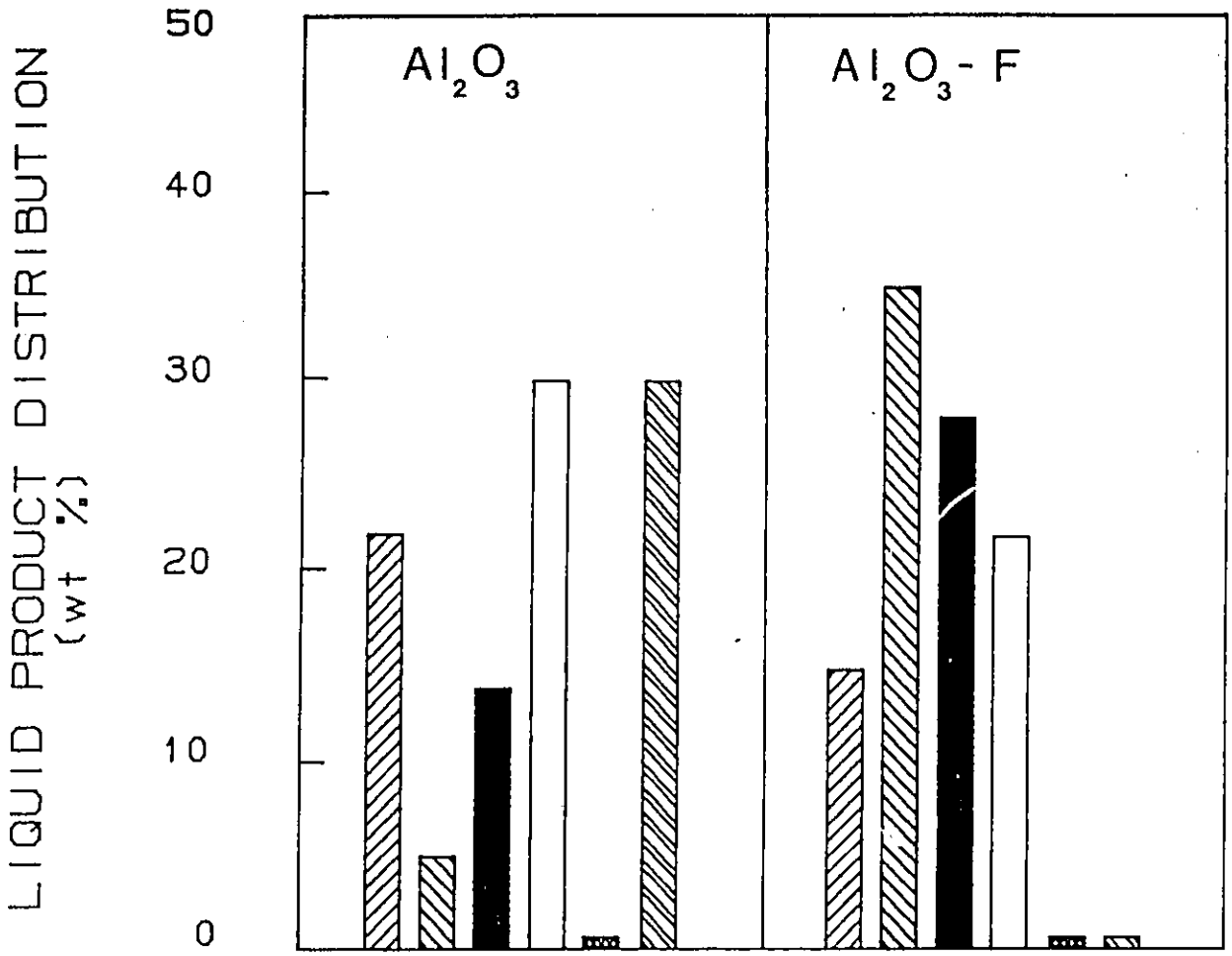

Fig. 7.7 A comparison of the liquid product distribution with and without fluoride in the catalyst.

C_6 C_9- C_{18}

C_7 C_{18}- C_{20}

C_8 C_{20}

operating variables and remains consistent for this reaction.

The overall liquid product distribution has been shown to vary with the conversion at 15 min on stream (Fig. 7.6). In Fig. 7.8, a comparison is made of the changes in conversion and changes in the profiles of two components of the liquid product, benzene and C_8 isomers, with time-on-stream for catalysts with different fluoride contents. In all cases, the decrease in acetylene conversion is noticeable at 1 h on stream. An optimum in the amount of C_8 isomers is evident with the time-on-stream. The time at which this optimum is reached is a function of the fluoride content, 30 min (0 wt % F), 15 min (1.5 wt % F), 4 min (2.6 wt % F), 20 min (4.3 wt % F). More striking however is the fact that this time value decreases linearly as catalyst acidity increases (cf. Fig. 5.1 also Fig. 9.17). From this relationship, it can be speculated that these C_8 isomers play a key role in this reaction.

Three trends are observed in the benzene content of the liquid product, an increase (0 and 1.5 wt % F), no change (2.6 wt % F) and a decrease (4.3 wt % F) with time-on-stream. No change or an increase in benzene levels would indicate that although the catalyst is deactivating, the active sites for benzene formation are not being lost or alternatively, that the deactivation process might actually be assisting in destroying very active sites for other unfavorable reactions. In the case of high fluoride contents, benzene levels cannot be maintained probably because of the presence of only a small number of active sites of the appropriate type.

7.7 CONCLUSIONS

The products in this reaction were gases, liquids or solids at reaction temperature. Gas yields were under 15 wt % for all operating conditions, the major component of the gas phase being ethylene. The liquid yields varied between 2 and 93 wt %. The maximum absolute yield of liquids was achieved under the following conditions, 400°C, 3 $g.s.mL^{-1}$ and 5 vol % C_2H_2 at 15 min onstream. The liquid product .

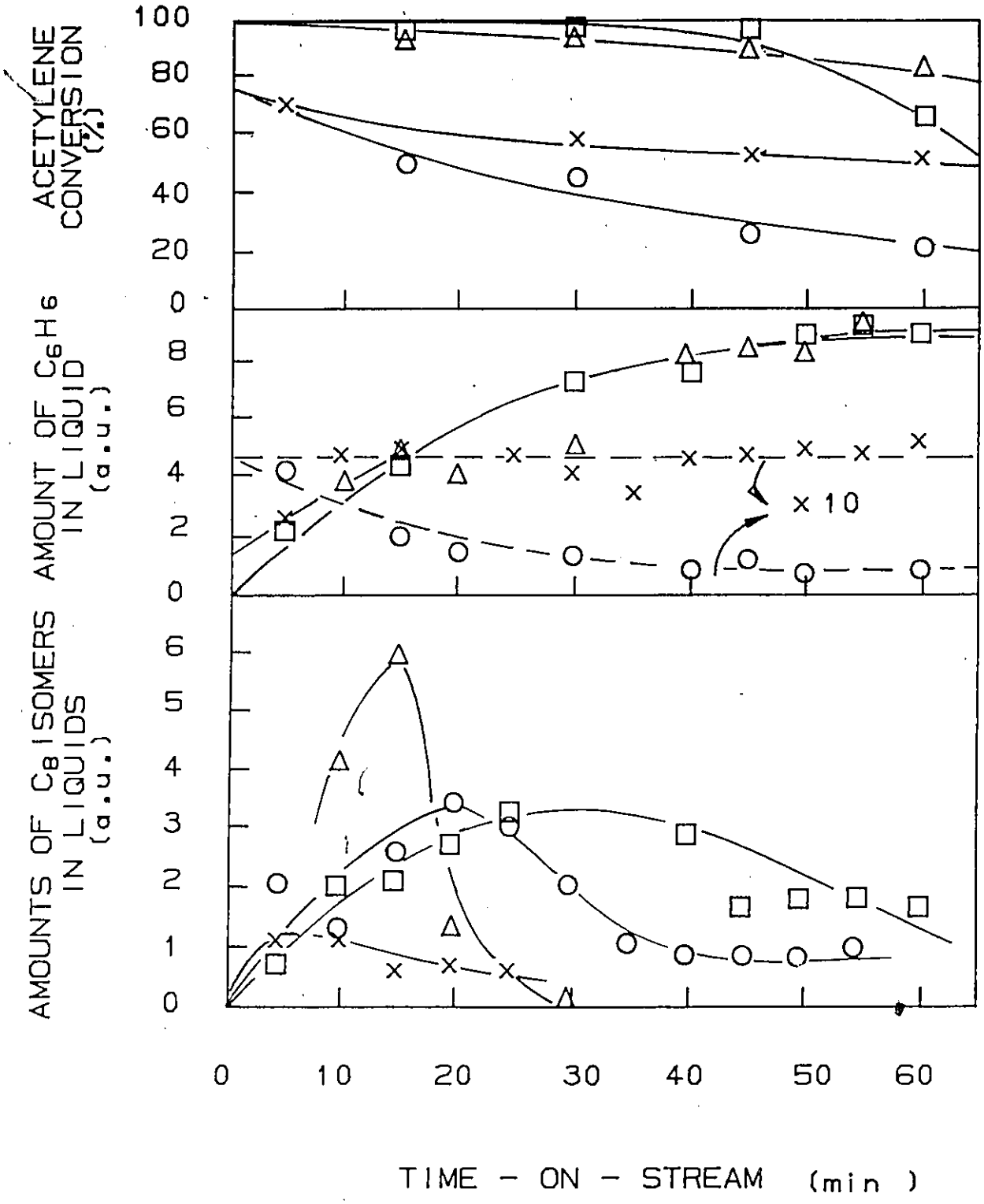

Fig. 7.8 A comparison of conversion, benzene and C_8 levels as a function of time-on-stream and catalyst fluoride content.

□ alumina △ 1.5 wt %F on alumina

X 2.6 wt % F ○ 4.3 wt % F

spectrum ranged in general from C_6 to C_{20}^+. The highest proportion of BTX in the liquid product distribution was obtained under the following conditions 350°C, 2 g.s.mL^{-1}, and 15 vol % C_2H_2. In general, operating conditions which led to favorable liquid distributions gave low liquid yields. Significant quantities of these components were attained only at high conversions.

The liquid product obtained with the fluoridated catalysts contained considerably less heavy ends than the unfluoridated alumina, however according to Table 7.4 this unavoidably lowers the yields. The time at which the maximum in the yield of C_8 isomers in the liquid products is reached decreases with catalyst acidity. These isomers may be key compounds in establishing a reaction mechanism.

8. CATALYST DEACTIVATION

The conversion of acetylene at a time-on-stream of 15 minutes over fluoridated alumina was discussed in Chapter 6. Appreciable deactivation, or decline in activity with time, was observed in experiments carried out with these catalysts in both the tubular reactor and in the microbalance . The conversions of acetylene as a function of catalyst time-on-stream for experiments conducted in both reactor systems are reported in Table 8.1 and 8.2 respectively. It was mentionned earlier that catalyst deactivation in this study was always accompanied by the accumulation of carbonaceous compounds on the catalyst surface. For this reason, experiments at some run conditions were carried out in the tubular reactor for both 1 h and 4 h and the catalysts analyzed for carbon. Two examples of the decrease in conversion occurring simultaneously with the increase in carbon content of the catalyst are shown in Fig. 8.1 (Appendix 8.1). Similar observations, an example of which is given in Fig. 8.2, were made in the microbalance where an instantaneous measure of the deposited coke was obtained as a function of time. This finding is not uncommon and has been reported for other catalyst systems used in carrying out this reaction (57). Despite its importance, limited information is available on the cause of the deactivation or on the quantity and the type of residues formed over various catalysts in the conversion of acetylene. The aim of this chapter is to explain the deactivation phenomenon and to describe the coke produced over alumina and fluoridated alumina.

8.1 GENERAL OBSERVATIONS

In many experiments, for example those shown in Fig. 8.1, the catalyst deactivation proceeded in two stages which differed sharply in rates - a fast stage followed by a slow stage. In the course of the fast stage, the catalyst activity dropped by an order of magnitude in 1 h. Although the slow stage lead to further deactivation, some reaction was still observed up to 5 h on stream.

Table 8.1

Acetylene conversion as a function of time-on-stream for experiments carried out in the tubular reactor

EXPERIMENT	TIME-ON-STREAM [min] 15	30	45	60	65
1	51.5	45.4	24.5	20.0	-
1R	57.8	36.1	24.2	23.2	-
2	41.0	38.1	36.5	33.2	
2R	48.1	50.5	44.2	46.1	
3	99.5	98.2	91.6	82.4	80.3
3R	99.3	98.9	98.7	96.9	89.4
4	98.9	93.8	84.0	74.0	
4R1	-	98.4	95.9	-	
4R2	96.3	97.8	95.3	84.1	
5	53.6[1]	30.8	30.1	18.2	14.3
6	0	0	0	0	
7	97.6	53.9	52.4	42.8	
7R	99.3	52.0	50.6	-	41.9
8	59.0	41.5	33.7	30.9	-
8R	50.0	48.6	33.0	25.7	23.6
9	98.1	94.8	84.9	77.4	
10	28.8	19.3	16.6	17.8	16.0
11	99.3	99.2	98.8	65.1	55.3
12	85.9	-	36.1	32.5	
13	87.2	72.2	66.1	57.9	
14	29.2	25.9	24.0	20.9	
15	99.6	99.5	62.2	37.7	
16	90.3	69.4	64.3	62.7	
Blank	5.0	5.0	5.0	5.0	
17	91.4[2]	54.6[3]	42.3[4]	-	40.9
17R	71.9	59.1	52.4	50.0	48.0

[1] 10 min on stream [2] 5 min on stream [3] 20 min onstream [4] 43 min onstream

Table 8.2

Acetylene conversion as a function of time-on-stream for experiments carried out in the microbalance

EXPERIMENT No.	CONDITIONS TEMP [°C]	CAT [wt%F]	FLOW [mL/min]	CONC [v %]	TIME-ON-STREAM [min] 15	30	55
01	350	0	62	5.15	n.d.	n.d.	n.d.
02	350	0	62	5.15	n.d.	n.d.	n.d.
03	350	0	62	5.15	n.d.	n.d.	n.d.
04	350	0	62	5.15	14.8	n.d.	n.d.
05	350	0	62	5.15	19.0	n.d.	n.d.
06	400	0	62	5.15	20.5	16.1	n.d.
07	300	0	62	5.15	15.3	0	n.d.
08	400	-	62	5.15	5.0	n.d.	n.d.
09	350	2.6	62	5.15	31.1	n.d.	n.d.
10	300	2.6	62	5.15	30.0	9.0	5.0
11	400	2.6	62	5.15	32.3	12.4	10.0
12	350	0	32	4.81	21.6	13.0	8.3
13	350	0	80	5.22	4.8	4.7	4.4
14	350	0	80	5.15	n.d.	n.d.	n.d.
15	350	0	62	5.15	38.1	20.9	n.d.
16	350	0	62	5.15	24.8	9.7	6.2
17	350	0	62	5.15	32.1	10.0	10.5
18	-	-	-	5.15	n.d.	n.d.	n.d.
19	350	2.6	62	5.15	26.3	-	3.2
20	350	0	62	6.29	38.6	22.3	20.6
21	350	2.6	62	6.29	43.4	26.8	31.6
22	350	0	62	2.42	34.6	21.8	16.7
23	350	2.6	62	2.42	37.4	23.3	n.d.
24	350	1.5	62	2.42	37.2	n.d.	n.d.
25	350	4.3	62	2.42	35.8	n.d.	n.d.
26	350	0	65	2.42	n.d.	n.d.	n.d.

n.d. - not determined

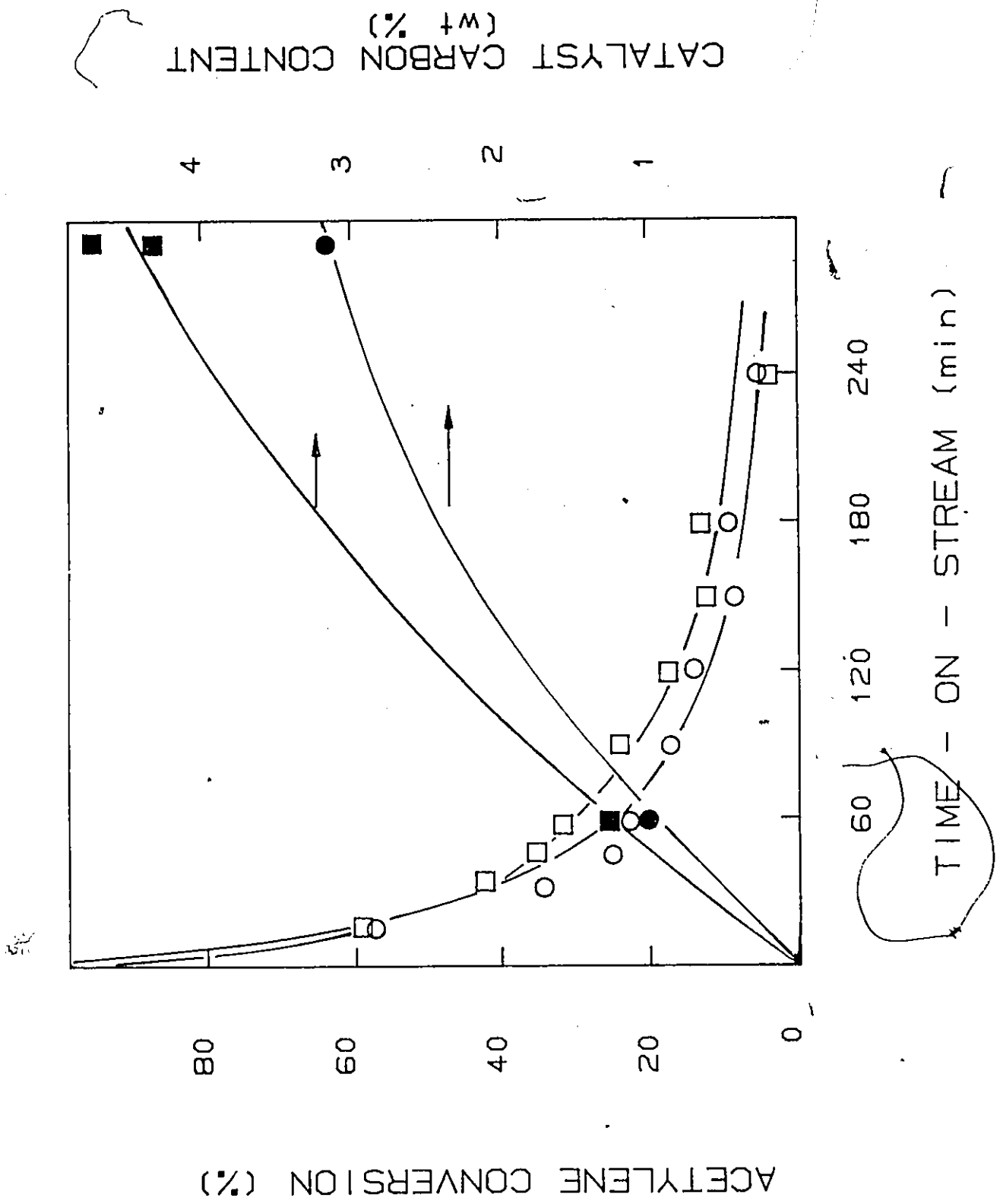

Fig. 8.1 Acetylene conversion in the tubular flow reactor and catalyst carbon content as a function of time-on-stream. ● ○ Exp't 1 ■ □ Exp't 8

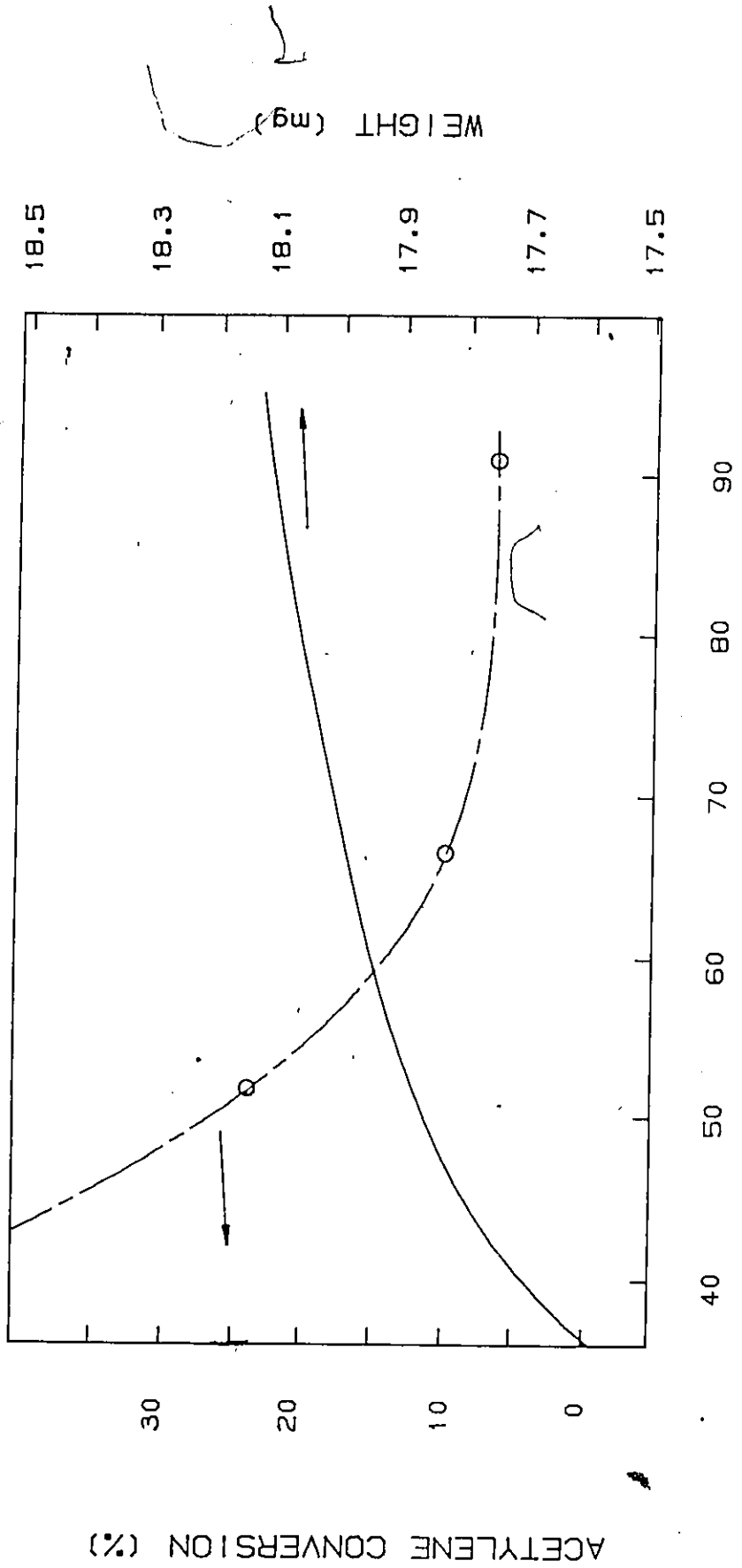

Fig. 8.2 Acetylene conversion in microbalance and catalyst coke content as a function of time-on-stream.

A two-stage deactivation has also been observed by other researchers with similar reactions. For example, Mardeleishvili and Rapoport (57), who studied the kinetics of the trimerization of acetylene to benzene over niobium oxide (NbO_2), observed an initial period of rapid deactivation during which 70 to 90 percent of the catalyst surface was quickly covered by a layer of carbonaceous material having a H/C ratio of approximately 1. This was followed by a period of slow deactivation during which the H/C ratio of the deposit decreased while the quantity of deposited carbon remained essentially constant. Data from the microbalance experiments (e.g. Fig. 8.2) confirm a two-stage rate of coke deposition accompanying the deactivation. Results on the nature of the coke deposits, to be discussed subsequently, also corroborated this change in the character of the deposits.

Having determined qualitatively that catalyst deactivation and coke deposition were related in this reaction it was of interest to determine quantitatively the effects of catalyst composition and the operating variables on deactivation and deposition. This analysis suggested optimal operating conditions and provided insight into the role of fluoridation in the deactivation and deposition processes. The models developed from the data obtained in the tubular flow reactor for this purpose follow.

8.2 MODELING CATALYST DEACTIVATION AND COKE DEPOSITION

8.2.1 Model for Deactivation

The decline in catalyst activity with time-on-stream for each run (Table 8.1) was described empirically using the following exponential decay model,

$$a(t) = a_0 \exp(-k_d t) \qquad (8.1)$$

where a(t) is the conversion of acetylene, t is the catalyst time-on-stream (min) and a_0 and k_d are model parameters. The parameter a_0 can be thought of as a measure of the conversion of acetylene on a fresh catalyst (i.e. at t=0), the parameter k_d as a measure

of the specific rate of deactivation [min^{-1}]. In the subsequent discussion these will be referred to as the initial activity and deactivation parameter respectively.

Estimates of a_0 and k_d along with approximate marginal 95 % confidence intervals obtained via nonlinear regression are listed in Table 8.3 for each run. Comparisons of observed and predicted conversions for some of the runs are shown in Figs. 8.3 through 8.5 for catalysts having 1.5, 2.6, and 4.3 wt % F respectively and demonstrate the adequacy of Eq. 8.1 in describing catalyst decay.

Models for a_0 and k_d.

The estimated values of a_0 and k_d were fitted by second order polynomials in the coded independent variables x_1 through x_4 defined in Table 4.1. The resulting fitted models are

$$\hat{a}_0 = 70.2 + 7.9\ x_1 - 23.0\ x_2 + 14.7\ x_3 + 11.3\ x_4 + 13.4\ x_4^2 \qquad (8.2)$$

$$\hat{k}_d = 10^{-4}(10.2 - 5.3x_1 + 4.3x_2 + 2.4x_3 + 3.6\ x_4 + 2.8\ x_2^2 + 1.8\ x_4^2) \qquad (8.3)$$

where $\hat{a}_0$ and $\hat{k}_d$ are the predicted values of the initial activity and deactivation parameter respectively. Comparisons of "observed" and predicted (by Eq. 8.2 and 8.3) values are shown in Fig. 8.6; marginal 95 % confidence intervals for the parameters are given in Table 8.4. Examination of the residuals (observed minus predicted values of a_0 and k_d) revealed no significant lack of fit (Appendices 8.2 and 8.3); R^2 values of 0.86 and 0.73 respectively were obtained. In Eq. 8.3, the terms involving x_3, x_2^2 and x_4^2 were only marginally significant and as a result the interpretation of this model was somewhat ambiguous.

8.2.2 Model for Coke Deposition

The carbon contents of the catalysts after a time-on-stream of 1 h are given in Table 8.3 (Appendix 8.4). A second order polynomial in the coded independent variables was fitted to the data and after deleting any terms not having a significant effect on the

Table 8.3

Estimates and 95 % confidence intervals for deactivation parameters, a_0 and k_d and measured catalyst carbon contents

Experiment No.	a_0	10^3 k_d [min^{-1}]	Carbon content[a] [$\mu g/m^2$]
1	74.4 +/- 23.2	2.15 +/- 1.03	67 [b]
1R	80.9 +/- 20.0	2.45 +/- 0.86	- [c]
2	43.8 +/- 1.4	0.44 +/- 0.08	162
2R	50.4 +/- 2.5	0.17 +/- 0.01	148
3	109 +/- 7.0	0.44 +/- 0.14	91
3R	103 +/- 7.6	0.15 +/- 0.26	90
4	111 +/- 6.9	0.63 +/- 0.16	293
4R	103 +/- 12.2	0.27 +/- 0.01	351
5	77.1 +/- 21.1	2.93 +/- 1.83	24
6	- [d]	-	38
7	124 +/- 47.1	2.02 +/- 1.23	59
7R	144 +/- 58.4	2.74 +/- 1.64	-
8	72.3 +/- 13.6	1.6 +/- 0.57 [f]	52
8R	66.8 +/- 14.2	1.51 +/- 0.56	-
9	108 +/- 6.7	0.53 +/- 0.16	154
10	31.5 +/- 8.5	1.15 +/- 0.69	56
11	125 +/- 40	0.97 +/- 0.79	308
12	123 +/- 29.3	2.47 +/- 0.84	-
13	98.2 +/- 7	0.90 +/- 0.20	135
14	33.0 +/- 2.2	0.79 +/- 0.18	135
15	156 +/- 96.2	2.28 +/- 2.09	85
16	98.0 +/- 19.2	0.86 +/- 0.54	55
17	78.5 +/- 7.4	0.80 +/- 0.22	157
17R	81.3 +/- 30.7	1.29 +/- 1.16	150

[a] measured at end of 1 h on stream.
[b] +/- 2 % of quoted value.
[c] not available
[d] conversion < 5%

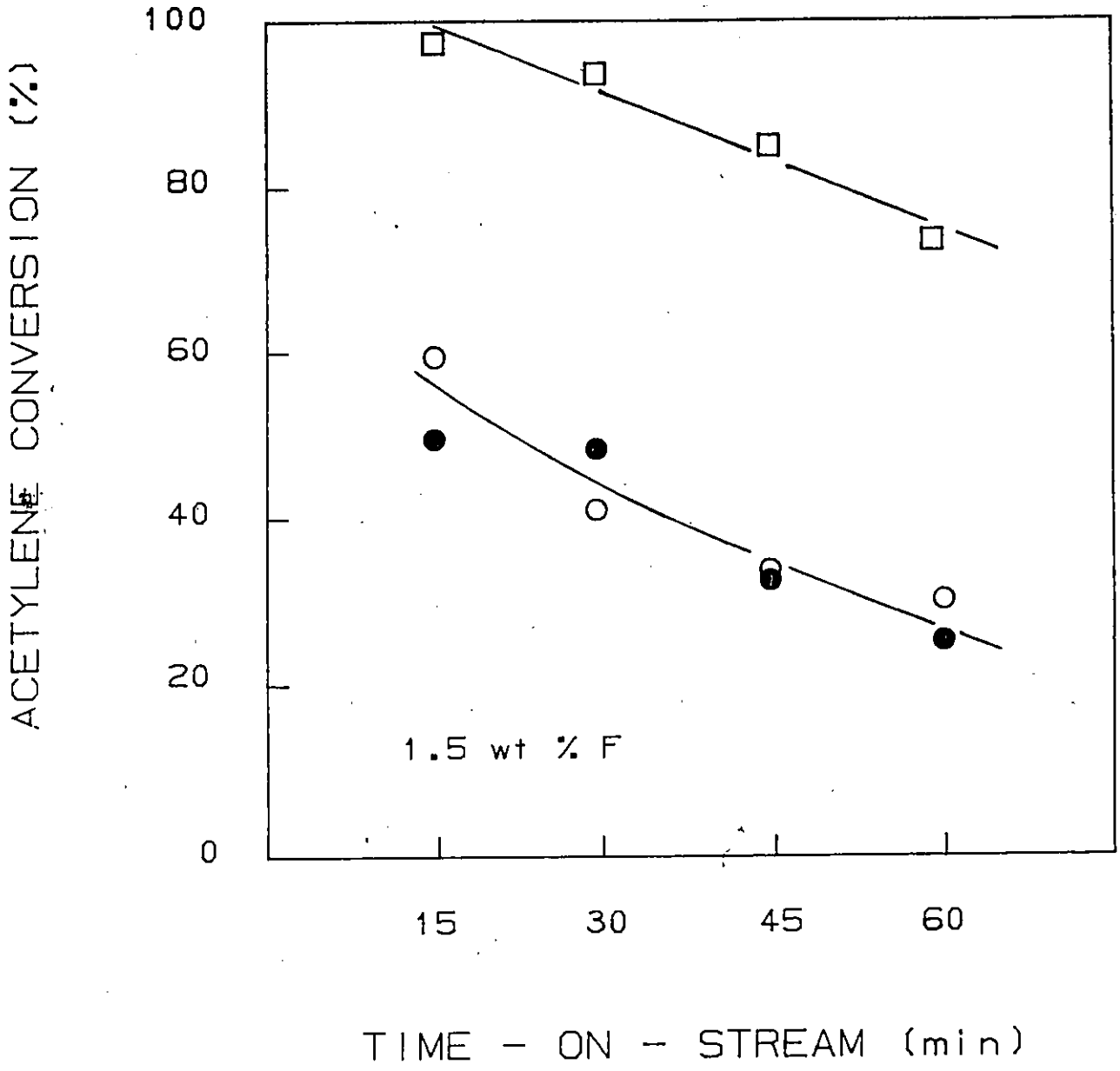

Fig. 8.3 Acetylene conversion over 1.5 wt % F on alumina as a function of time-on-stream. □ Exp't 4 , ○● Exp't 8

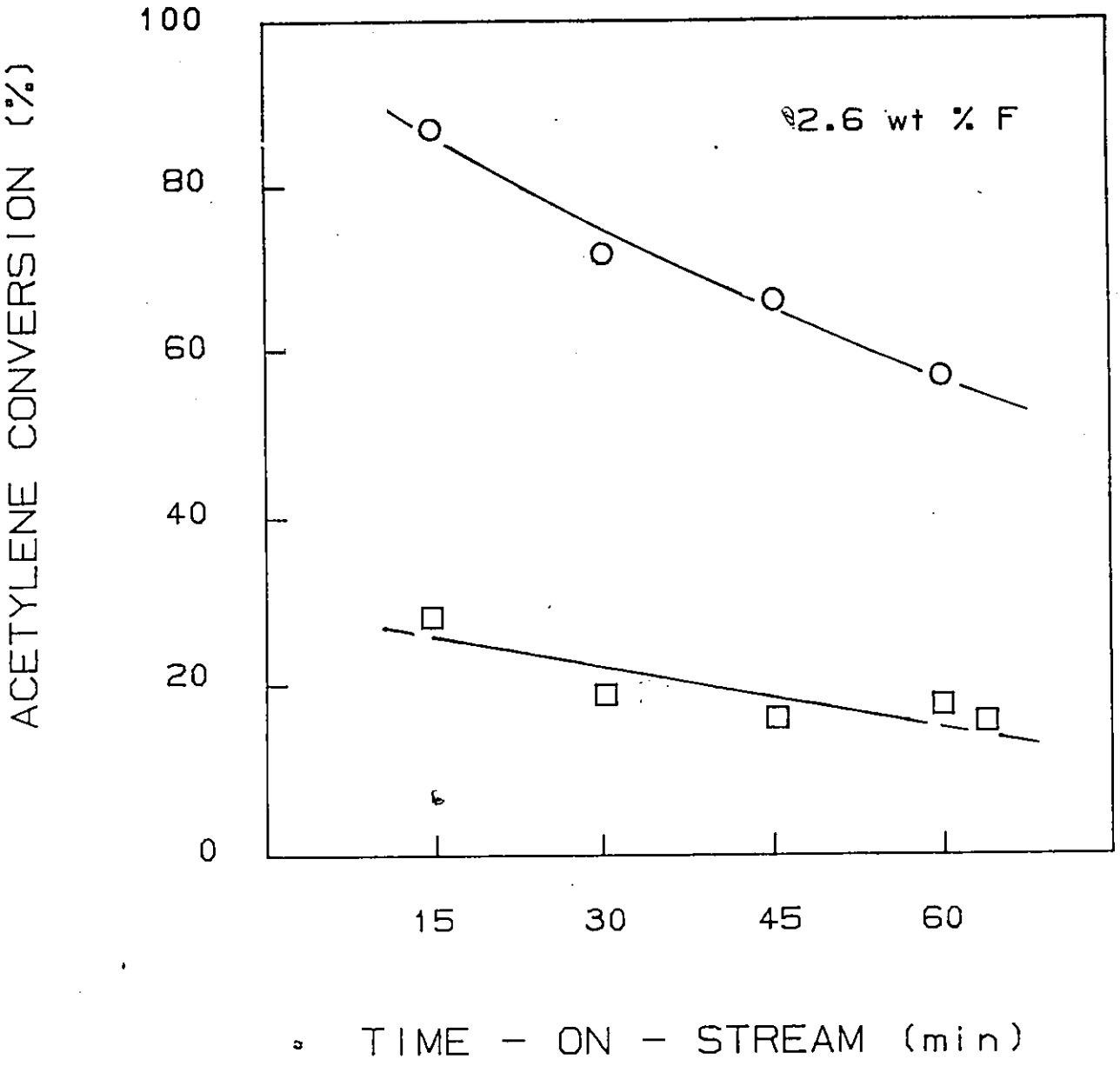

Fig. 8.4 Acetylene conversion over 2.6 wt % F on alumina as a function of time-on-stream. ○ Exp't 13 □ Exp't 14

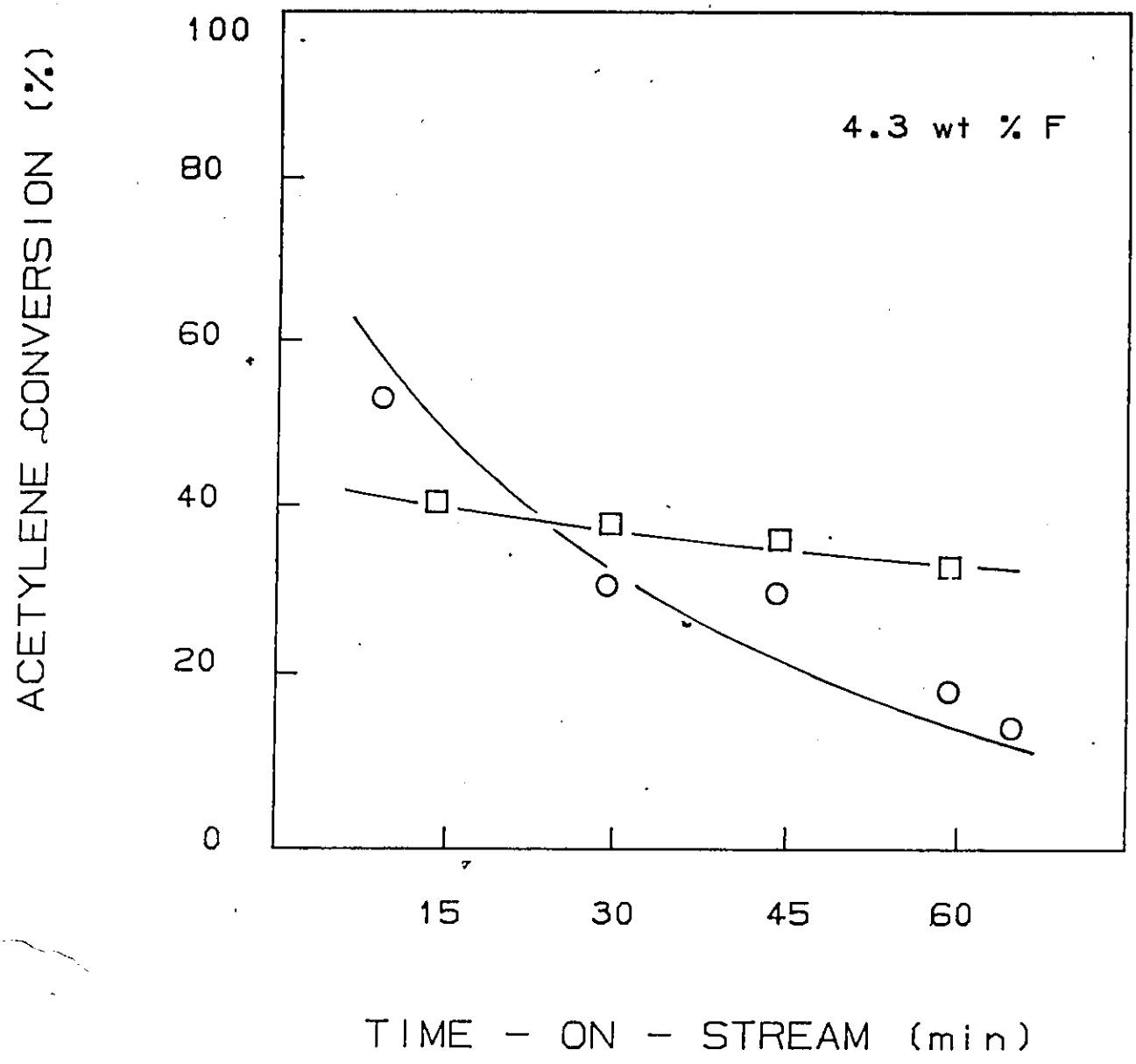

Fig. 8.5 Acetylene conversion over 4.3 wt % F on alumina as a function of time-on-stream. ○ Exp't 5 □ Exp't 2

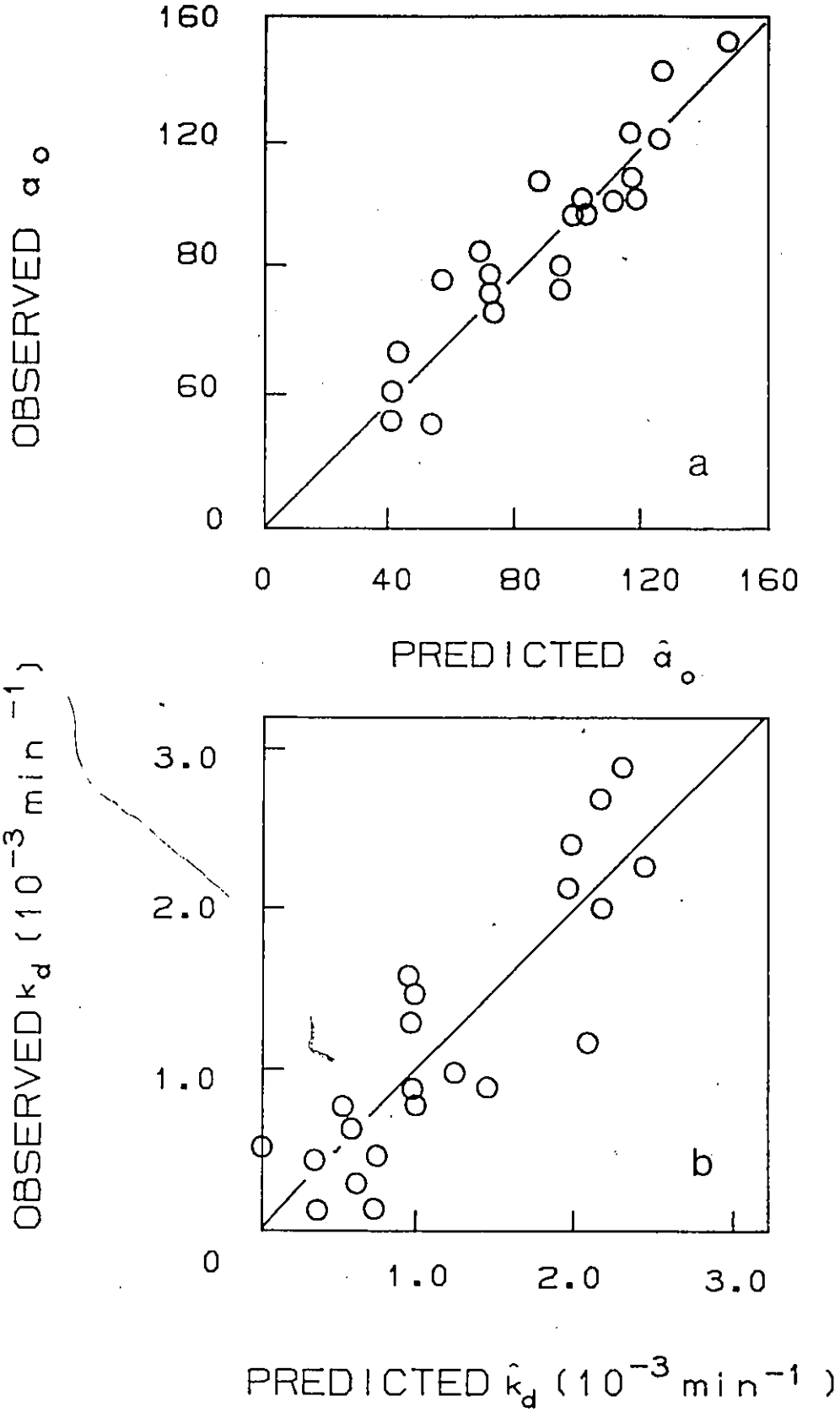

Fig. 8.6 The observed parameter values in the two-parameter time-on-stream model versus the predicted values.

Table 8.4

95 % confidence interval for coefficients in regression equations of responses $\hat{a}_0$, $\hat{k}_d$, and $\hat{C}$

Term	Least squares estimates of parameters		
	Equation [1] $\hat{C}$	Equation [3] a_0	Equation [4] k_d
Constant	13.1 +/- 3.3	70.2 +/- 9.1	10.2 +/- 4.1
x_1	4.1 +/- 2.5	7.9 +/- 6.9	-5.3 +/- 2.6
x_2	-23.0 +/- 7.9	4.3 +/- 3.3	-5.0 +/- 2.9
x_3	-2.4 +/- 2.6	14.7 +/- 6.8	2.4 +/- 2.6
x_4	1.8 +/- 2.5	11.3 +/- 6.8	3.6 +/- 2.5
$x_1x_2+x_3x_4$	-[a]	-	-
$x_1x_3+x_2x_4$	-4.6 +/- 3.4	-	-
$x_1x_4+x_2x_3$	-	-	-
x_1^2	-	-	-
x_2^2	-	-	2.8 +/- 3.2
x_3^2	-	-	-
x_4^2	-1.9 +/- 2.2	13.4 +/- 6.1	1.8 +/- 2.3

[a] indicates the term is insignificant

predicted value of the response (i.e. C, the carbon content in $\mu g/m^2$), the following model with an R^2 value of 0.8 was obtained (Appendix 8.5).

$$\hat{C} = 10^2 (1.32 + 0.41\ x_1 - 0.50\ x_2 - 0.24\ x_3 + 0.18\ x_4 - 0.46\ x_1x_3 - 0.18\ x_4^2) \quad (8.4)$$

Analysis of the residuals revealed no significant lack of fit. Observed and predicted values of the catalyst carbon content are compared in Fig. 8.7; marginal 95 % confidence intervals for the parameters are also given in Table 8.4. The interaction term x_1x_3 is confounded with the term x_2x_4. In Eq. 8.4, the temperature weight-time interaction term, x_1x_3, was chosen as being significant rather than the catalyst-concentration interaction term, x_2x_4, based on the strong evidence obtained in the microbalance studies that a negative dependence on x_2 is clearly the more appropriate behaviour. The terms in x_3, x_4 and x_4^2 were also retained in spite of the fact that the confidence interval included zero because the response with these terms more closely approximated the data obtained in the microbalance experiments.

8.3 INTERPRETATION OF FITTED MODELS

Based on Eq. 8.2 through 8.4 the operating variables and degree of fluoridation of the catalyst were found to have a significant effect on $\hat{C}$, $\hat{a}_0$, and $\hat{k}_d$ either singly or jointly. Pertinent features of each of these relationships are depicted graphically in Figs. 8.8 through 8.10 and will now be discussed.

8.3.1 Influence of Temperature and Weight-time

Because of the significant interaction observed in the coke deposition data between the temperature and the weight-time, the effects of temperature, x_1, and weight-time, x_3, on catalyst carbon content were considered jointly. Contours of constant carbon content are plotted in the x_1-x_3 plane shown in Fig. 8.8a for the mid-point values of x_2 (2.6 wt% F) and x_4 (10 vol% C_2H_2). The carbon content of the catalyst is seen to be quite sensitive to the levels of these operating variables. As well, this response

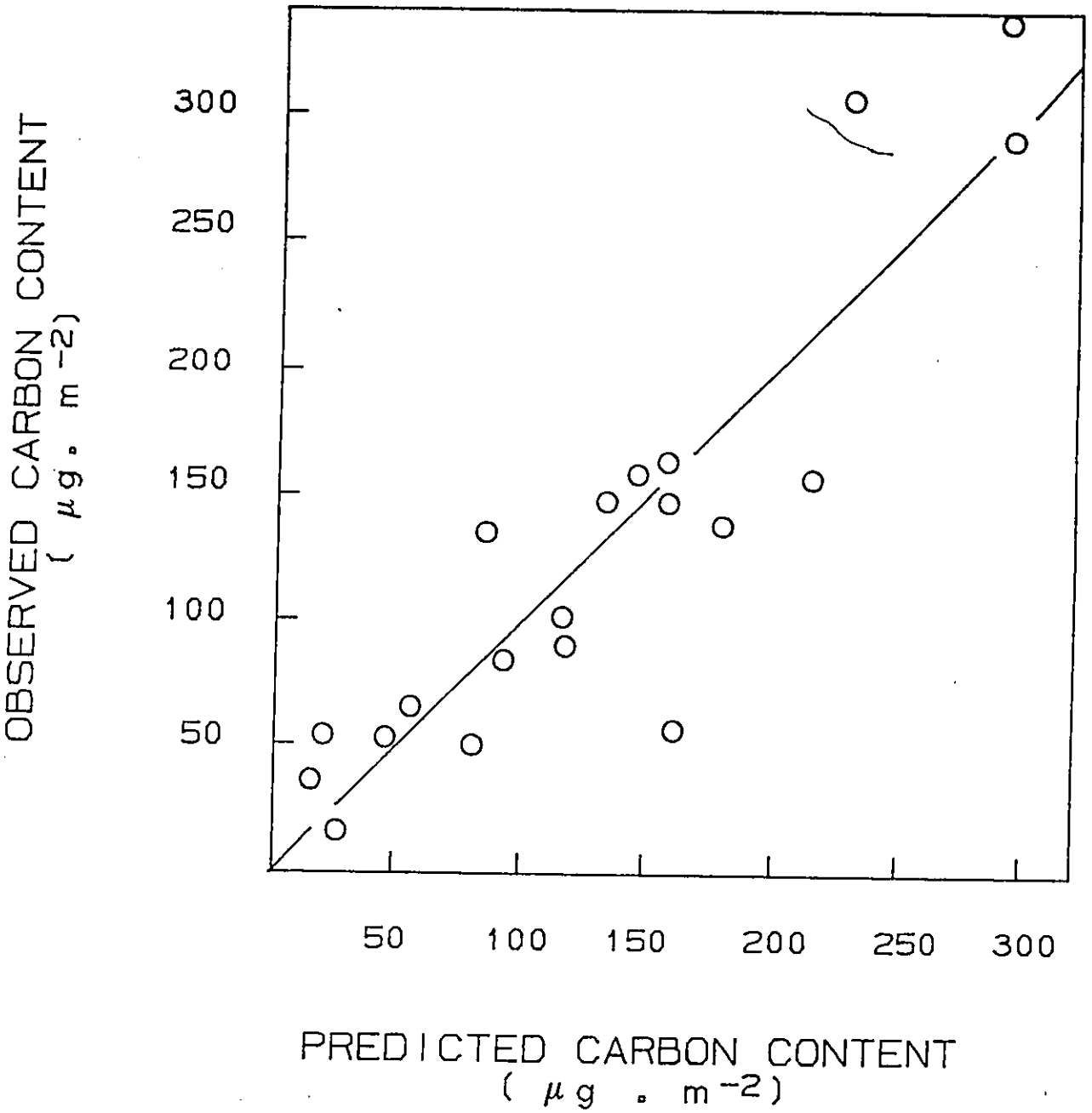

Fig. 8.7 The observed catalyst carbon content at 1 h time-on-stream versus the predicted catalyst carbon content.

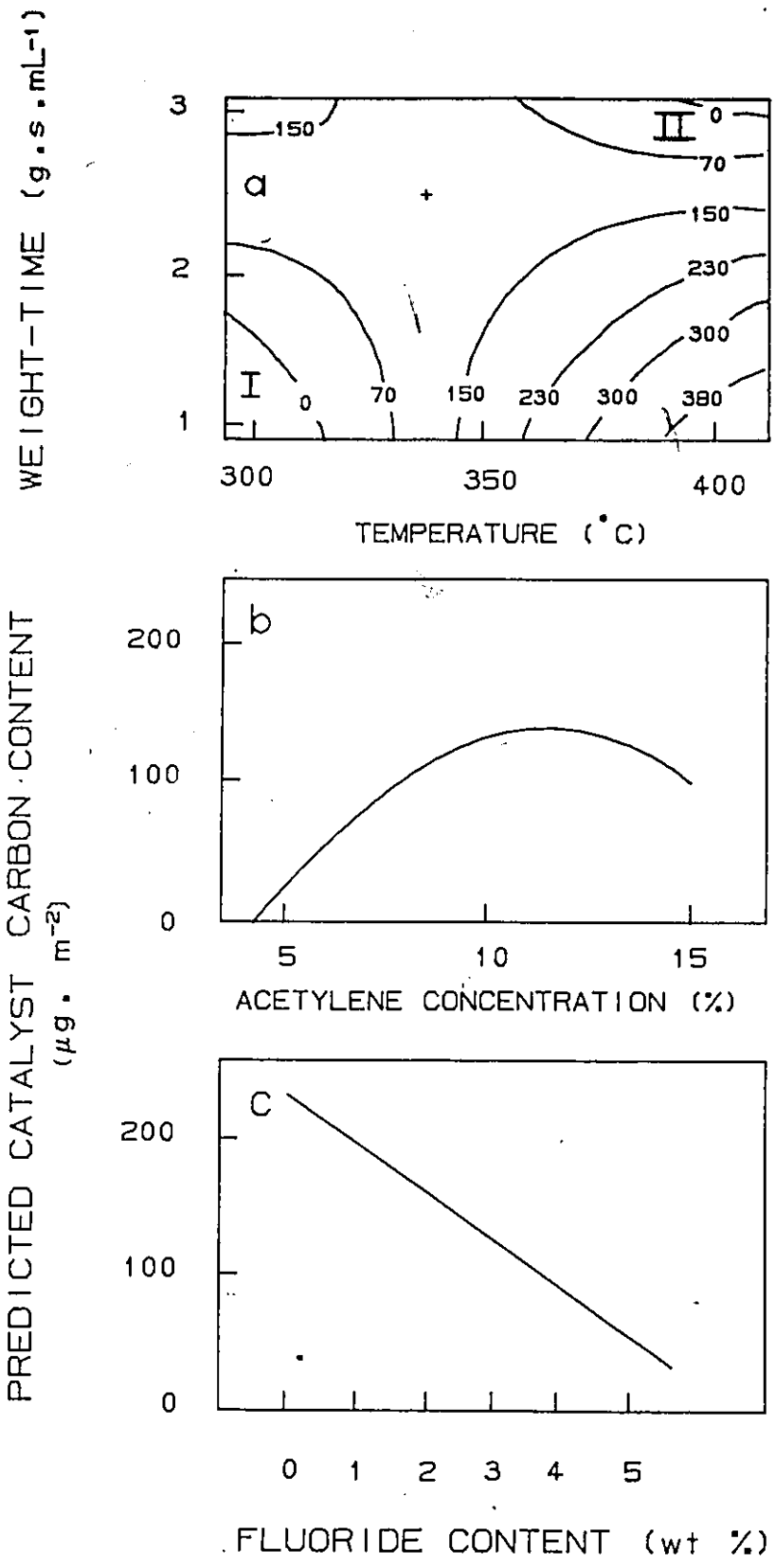

Fig. 8.8 Graphical representation of model Eq. 8.4 for the catalyst carbon content at 1 h on stream.

a) constant carbon content contours
carbon content vs acetylene concentration
carbon content vs fluoride content

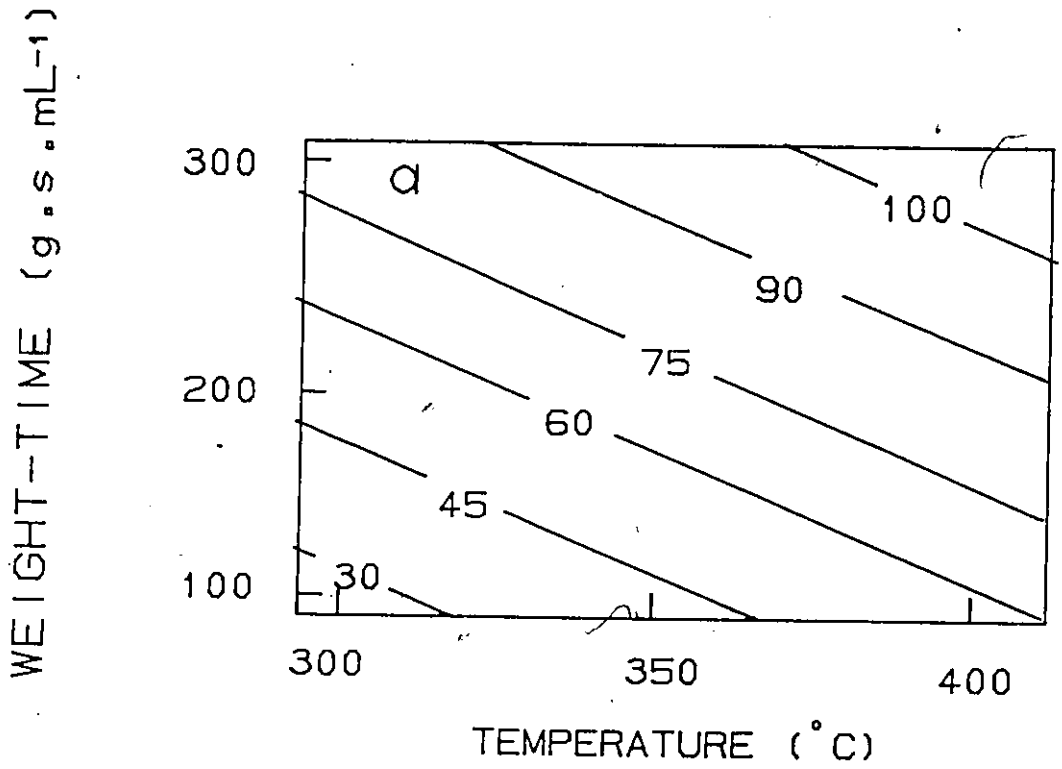

Fig. 8.9 Graphical representation of model equation 8.2 for the initial activity parameter, $\hat{a}_0$.

a) constant initial conversion contours (x_2=0, x_4=0)

b) initial activity versus acetylene concentration

c) initial activity versus fluoride content

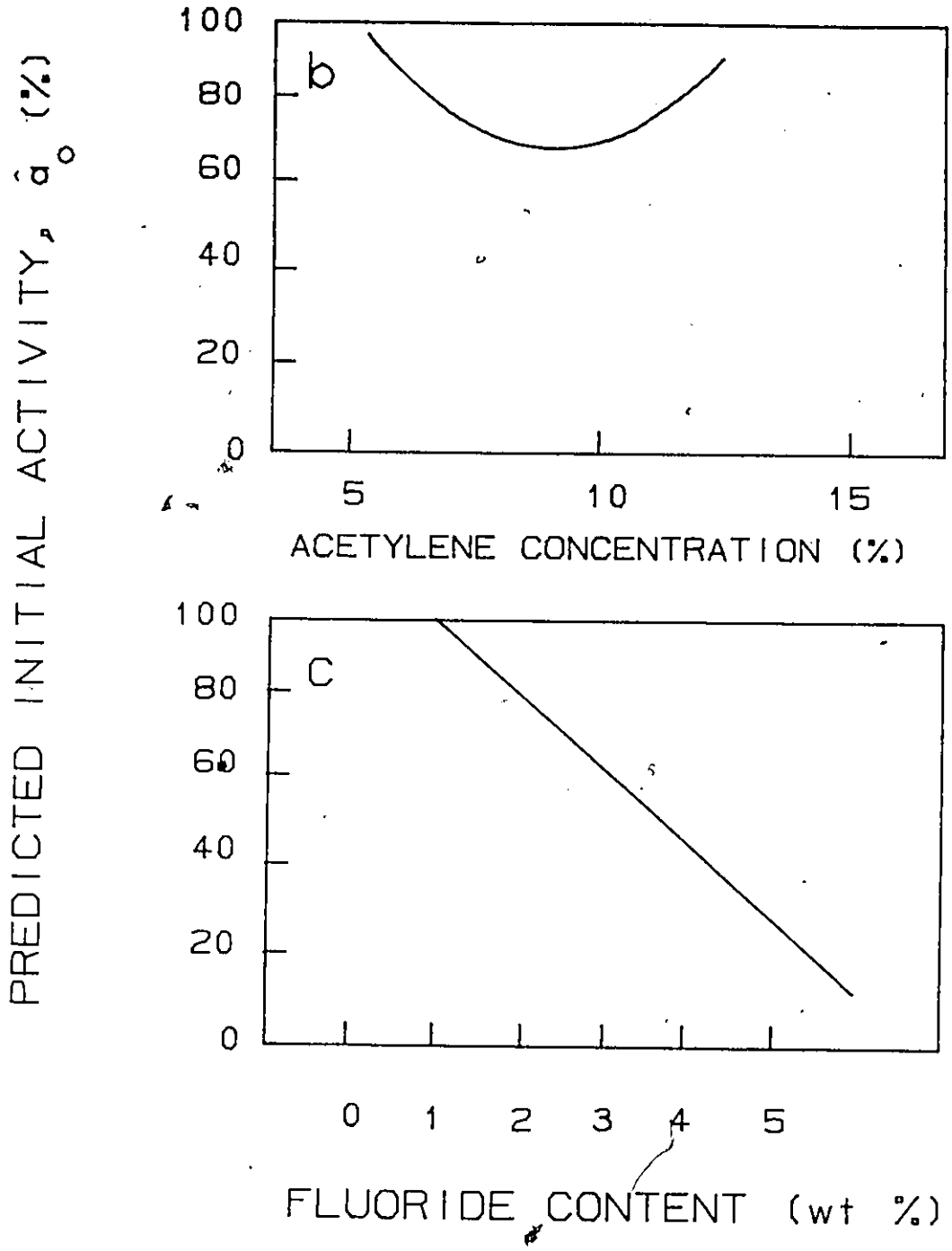
PREDICTED INITIAL ACTIVITY, $\hat{a}_o$ (%)
100
80
60
40
20
0
b
5
10
15
ACETYLENE CONCENTRATION (%)
100
80
60
40
20
0
C
0
1
2
3
4
5
FLUORIDE CONTENT (wt %)

Fig. 8.9 cont'd

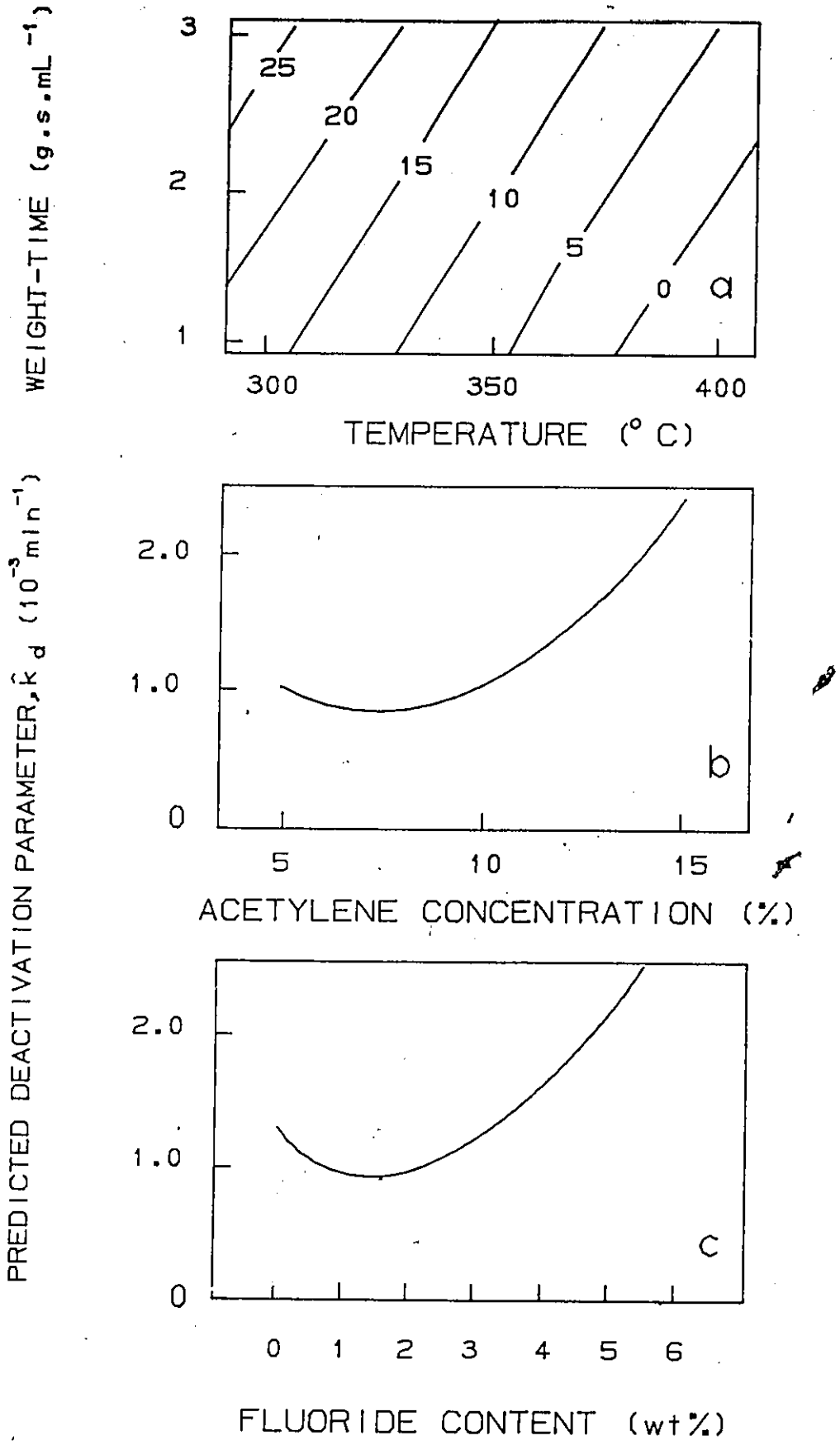

Fig. 8.10 Graphical representation of model Eq. 8.3 for the deactivation parameter, $\hat{k}_d$.

a) constant $\hat{k}_d$ contours, b) $\hat{k}_d$ vs concentration
$\hat{k}_d$ vs fluoride content

surface has a saddlepoint at a temperature of 338°C (x_1 = -0.52) and a weight-time of 2.25 g.s.mL^{-1} (x_3 = 0.90). The saddlepoint represents a maximum in the coke content as the temperature is varied from 300 to 400 °C (at 1.75 g.s.mL^{-1}) and a minimum in carbon content as the weight-time increases from 1 to 3 g.s.mL^{-1} (at 338 °C). There are two regions in Fig. 8.8a which lead to low levels of coke deposition, denoted as region I corresponding to low temperatures and low weight-times and region II corresponding to high temperatures and high weight-time. It is worthwhile examining these two regions in more detail.

Examination of Fig. 8.9a reveals that the initial activity is low in Region I, it is not surprising, therefore, that low catalyst carbon contents are observed. It must also be noted, however, that whatever coke does form on the catalyst under these conditions appears to deactivate the catalyst drastically as evidenced by the relatively large values of $\hat{k}_d$ obtained at low temperatures (Fig. 8.10a). This is consistent with observations made in Chapter 7 that at low conversions a great deal of high molecular weight material was observed in the liquid products (Fig. 7.6).

In region II, the initial catalyst activity is high (Fig. 8.9a) and the specific rate of deactivation is relatively low (Fig. 8.10a). Therefore region II would appear to be ideal for process operation. This is also consistent with the observations of Chapter 7 that under conditions of high conversion the amount of high molecular weight material decreased substantially.

Although similar amounts of coke were deposited, the coke which is formed under the conditions of region II does not appear to deactivate the catalyst as readily as that which forms in region I (evidenced by the lower values of $\hat{k}_d$ in Fig. 8.10a for region II). To account for this difference in the deactivation parameter one must assume that either the distribution or the nature of the coke is different.

In order to limit the disturbances introduced into the microbalance system a maximum of three effluent gas samples were taken at 15, 30 and 55 min time-on-stream. The

conversion was calculated from the feed and effluent gas analyses. The conversions as a function of temperature and time-on-stream are shown in Figs. 8.11 and 8.12 for an alumina and a fluoridated alumina catalyst respectively. The catalyst deactivation is more severe at low temperatures. This behaviour is similar to that observed in the fixed-bed reactor and predicted by the deactivation model of Eq. 8.3. A decline in activity with time-on-stream was also observed at low and medium flowrates, but not at high flowrates (Fig. 6.8). This may be due to the limitations of the analytical equipment for measuring conversions under 5 %. Nevertheless, it can be seen from Fig. 6.8 that the deactivation decreases as the gas flowrates increase and the corresponding contact-times are lowered, consistent with studies in the tubular reactor.

8.3.2 Influence of the Initial Concentration of Acetylene

The effects of the initial concentration of acetylene on the catalyst carbon content, initial activity and deactivation parameter are shown in Figs. 8.8b, 8.9b and 8.10b respectively. Although the effect on carbon content was imprecise, it would appear that as the initial concentraton of acetylene increased to approximately 10 percent, the carbon content of the catalyst also increased and then stabilized with further increases in acetylene concentration. An increase in carbon content with higher concentrations of acetylene in the feed is not surprising since the rate of conversion of acetylene is expected to increase with the concentration of acetylene in the gas phase. The gas phase concentration is a function of the initial concentration of acetylene and of the conversion level. Comparing Fig. 8.8b with 8.9b, one can see that as the initial activity decreases (for acetylene concentrations below 10 vol %) the catalyst carbon content increases. Rising gas-phase concentrations of acetylene, due to the decrease in the initial activity and to the increase in feed concentration lead to the steady increase in catalyst coke levels observed. However, at high enough feed concentrations, the initial activity increases rapidly and it follows that the gas-phase concentration is

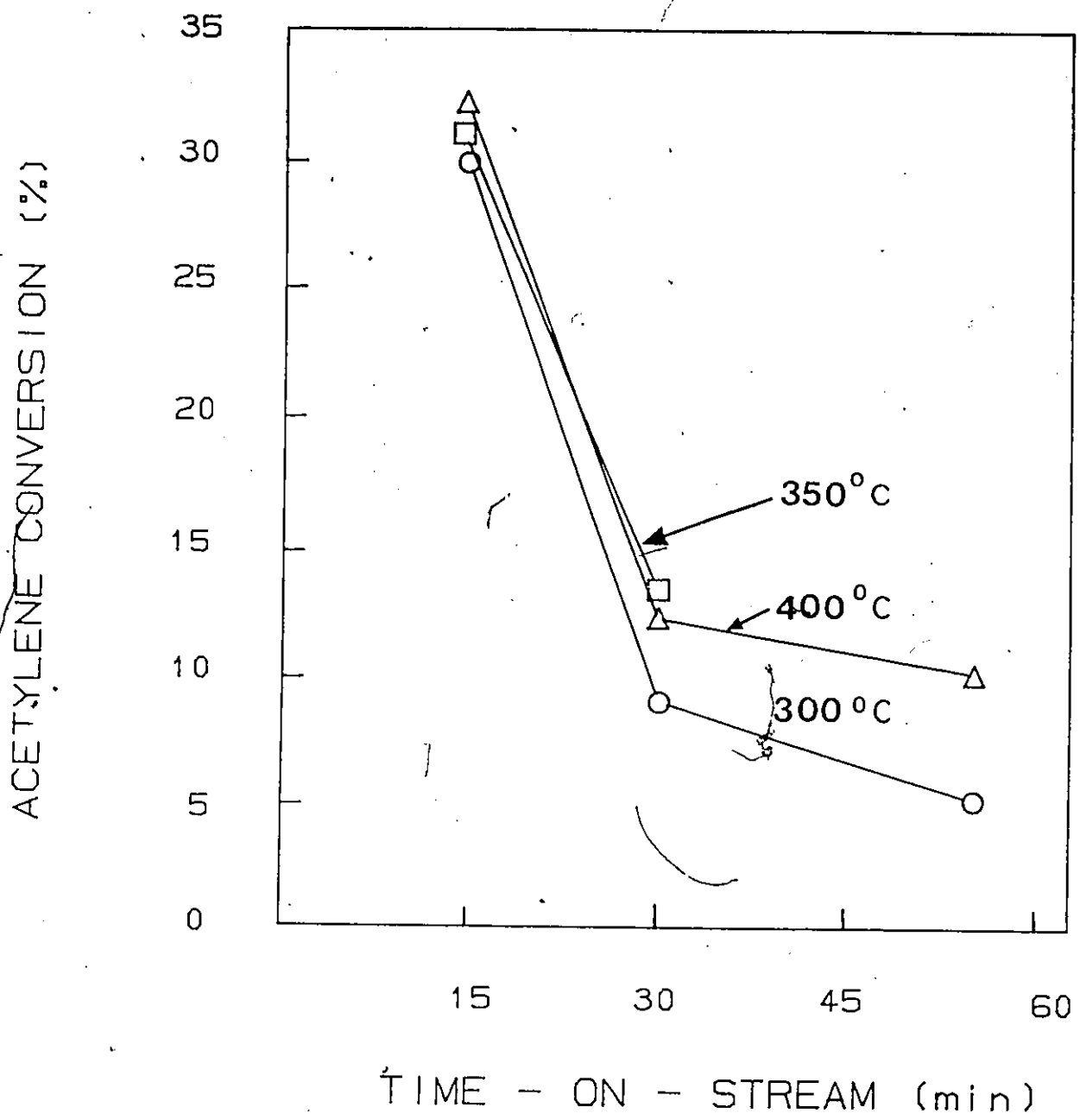

Fig. 8.11 Acetylene conversion over alumina in microbalance as a function of time-on-stream and temperature.

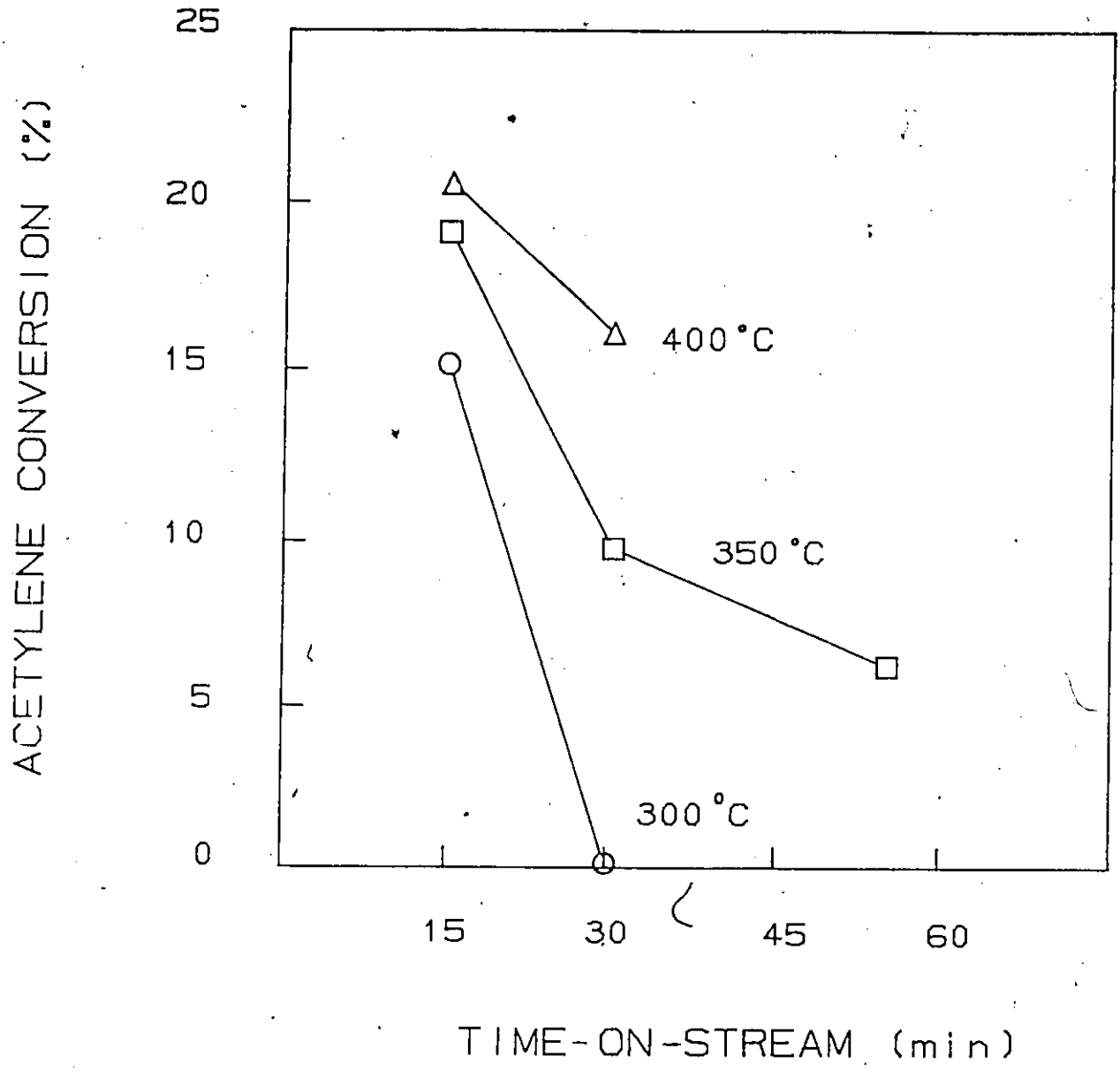

Fig. 8.12 Acetylene conversion over fluorided alumina in microbalance as a function of time-on-stream and temperature.

significantly lower than the feed gas concentration, resulting in the stabilization and subsequent decrease in carbon content observed.

The effect on initial activity was a decline in conversion up to about 10 percent acetylene in the feed followed by an increase in conversion as the feed concentration was further increased (Fig. 8.9b). At low feed concentrations of acetylene, although rates of conversion were low, the weight-time was sufficiently high that 100 percent conversion was achieved. As the feed concentration increased it appears that the rise in conversion rate was small, the weight-time no longer provided complete conversion and conversion levels fell. At higher feed concentrations the rate of conversion increased more rapidly and conversion levels rose. Rates of conversion which have a very low dependence on concentration at low concentrations but which increase rapidly at higher concentrations are typical of polymerization reactions requiring an initiation period (80) and thus the behaviour observed here is consistent with the postulated polymerization reactions of acetylene (Chapter 11).

Up to 10 percent acetylene in the feed, the deactivation parameter remained relatively constant and then increased with higher initial concentrations. This behaviour is consistent with the proposed initiation period or initial low concentration dependence of conversion rate followed by a high concentration dependence of conversion and suggests a direct connection between the reaction products and deactivation. This is further substantiated when one compares the activity versus initial concentration curves obtained in the microbalance at 15 and 30 min on stream (Fig. 6.9). Although there is a significant loss in activity at concentrations up to 6.3 vol. %, the curves remain parallel, so very little difference in deactivation is observed in this concentration range.

In summary, the process operating conditions which minimized coke formation and deactivation in the tubular reactor involved high temperatures, high weight-times and low feed concentrations of acetylene. The nature of the coke deposits also appeared to be

highly dependent on reaction conditions.

8.3.3 The Influence of Fluoridation

The catalyst carbon content at the end of 1 h on stream was found to decrease linearly with the degree of fluoridation (Fig. 8.8c). A decrease in initial activity of the catalyst parallelled the decrease in carbon content (Fig. 8.9c). This implies that the modifications of the alumina brought about by fluoridation succeeded in diminishing the total quantity of coke formed.

In previous studies, the addition of fluoride ions has been shown to alter the number of sites available for adsorption of acetylene (12, 90) and to alter the surface acidity (36, 71). Infrared and Raman studies of the adsorption of acetylene on alumina (90, 100) have demonstrated that variations in the number of exposed aluminum ions and hydroxyl groups on the catalyst surface strongly influence the mode of adsorption of acetylene. As a result, Bhasin et al. (12) postulated that the chemisorption of acetylene on alumina occurs at ion-pair sites consisting of exposed aluminum ions (Lewis acid sites) and neighbouring oxide ions or hydroxyl groups (Bronsted sites). Other studies (35, 72) have shown that replacement of surface hydroxyl and oxide ions with fluoride ions served to decrease the number of such ion-pairs. The observed decrease in the catalyst carbon content with increased fluoride loadings therefore suggests that the reaction leading to coke formation was also catalyzed by the same type of sites. This is consistent with the polymerization mechanism outlined in Chapter 11.

Fluoridation also altered the acidity of alumina catalysts used in this study as demonstrated in Table 5.1 and discussed in Chapter 5. Paukshtis et al. (71) have shown that introduction of fluoride generated a different distribution of acid sites on the alumina surface. It has been suggested that fluoridation produces a small number of Bronsted acid sites and increases the Lewis acidity of alumina (17). Although the acid-catalyzed production of coke has been postulated by a number of workers (40) no

evidence of this was observed with acetylene (vis. Fig. 8.8c). Although the amount of deposited coke decreased with the degree of fluoridation of the catalyst the possible minimum in the relationship between k_d and degree of fluoridation (Fig. 8.10c) suggested that the specific rate of deactivation was not solely related to the quantity of deposited coke but also related to the nature and distribution of the coke, i.e., not all the coke formed deactivated the catalyst at the same rate. These results imply that the nature and distribution of the coke varied with the degree of fluoridation and consequently with the acidity of the catalyst. A maximum in the total acidity of the catalysts was observed in the range 1.5 to 3.0 wt % F (Chapter 5) and corresponds to the minimum in k_d (Fig. 8.10c) at approximately 2 wt % F. Consequently, it appears that the specific rate of deactivation decreased with increasing total acidity. One possible explanation for this is that the coke built up on the strong acid sites generated in the fluoridation process before distributing itself throughout the bulk. This explains why the specific rate of deactivation was a function of the catalyst acidity while the total catalyst carbon content was not. However, at the high fluoride content, the total surface acidity, the number of adsorption sites and the total amount of carbon were reduced, yet the specific rate of deactivation increased. This suggests that, with the surface modifications induced by fluoridation, a greater proportion of the coke consituents responsible for deactivating the catalyst were formed.

A significant decay in catalyst activity has also been reported in the case of C_2H_2 polymerization over ZSM-5 in the range 250-500^{o}C (94). The deactivation was most severe at lower Si/Al ratios (Si/Al = 25, a/a_0 = 0.15; Si/Al = 60, a/a_0 = 0.55). Berak et al. (13) have found a positive linear correlation between the integral absorbance value of the Bronsted band and the weight percent aluminum in ZSM-5. This implies that an increase in aluminum content produced a simultaneous increase in the catalyst acidity. It follows therefore, that the catalyst with the lower Si/Al ratio (3.5 wt % Al) exhibited higher Bronsted acidity than the catalyst with the higher ratio (1.5 wt % Al).

Consequently, it seems that deactivation increased as the Bronsted acidity increased. These results corroborate those of the present study.

The surface fluoride and carbon contents of the fresh and used catalysts for selected runs were determined by X-ray photoelectron spectroscopy and are listed in Table 8.5. No loss of fluoride was observed in the catalysts used in these investigations. The deactivation observed with time on stream cannot be attributed therefore to leaching of the fluoride ion or to changes in chemical composition. XPS spectra for a fresh and spent catalyst (1.5 wt % F) are compared in Fig. 8.13. In comparing the two scans, it is clear that the ratio of C to Al in the used catalyst was significantly greater than in the fresh catalyst, therefore considerable carbon covers the catalyst surface. The nature of the carbon layer and its deposition are the subject of the next section.

8.4 NATURE OF THE COKE AND ITS DEPOSITION

In the previous discussion deactivation was linked to the nature and distribution of the deposited coke. A number of additional tests and analyses were performed to provide a better understanding of coke formation in acetylene polymerization.

Under conditions giving high conversions, the gas-phase concentration of acetylene decreases significantly along the catalyst bed suggesting that a profile in the carbon content of the catalyst should also exist. Three layers of spent catalyst from the entrance, mid-section and exit of the bed, for a high conversion run were examined for carbon content. These results, summarized in Table 8.6, show that the carbon content decreased along the bed in parallel with the decrease in gas-phase concentration of acetylene. This may imply that coke formation is a primary product of acetylene conversion and not the result of further interaction of other products in the gas phase with the catalyst.

The distribution of the coke deposit on the catalyst was also examined.

Table 8.5

X-ray photoelectron spectroscopic semi-quantitative surface analyses of fresh and spent catalysts

Experiment Number	Surface composition, at. % (+/- 10%) Al	O	C	F
11	35.6	59.7	4.7	-
	33.2	50.4	16.1	-
4	35.1	54.9	6.4	3.6(F)[a]
	25.9	41.1	28.9	2.7(S)[b]
14	34.8	55.3	4.9	5.0(F)
	32.6	50.5	12.0	4.6(S)
1	34.9	51.3	5.5	8.4(F)
	32.5	51.4	7	9.1(S)

[a] F- refers to fresh catalyst.
[b] S- refers to spent catalyst.

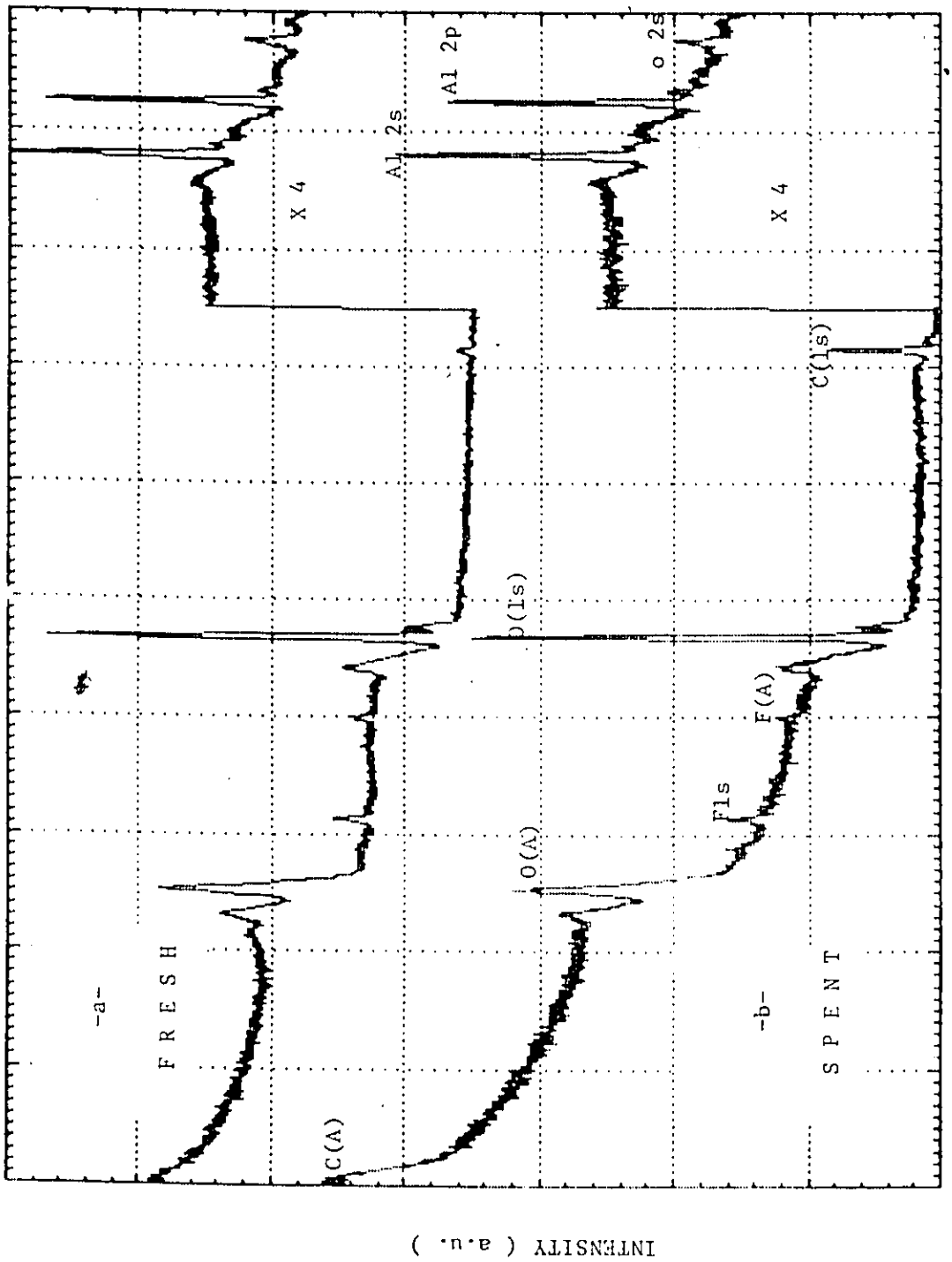

Fig. 8.13 A comparison of the XPS spectra for a fresh and used 1.5 wt % F on alumina catalyst for experiment 3.

Table 8.6

Comparison of used catalyst carbon content in various reactor bed layers[a]

Bed layer	Carbon content [mg/m^2]	Relative H/C ratio	Surface Area [m^2/g]
Inlet	0.120	0.48	261.4
Centre	0.100	0.41	260.5
Exit	0.065	1	243.8

[a] experimental conditions, temperature 375°C, catalyst 1.5 wt % F on alumina, weight-time 2.5 g.s/mL, initial concentration of C_2H_2 7 5 vol. %.

Measurements of surface (by XPS) and bulk (by elemental analysis) carbon contents of spent catalysts are listed in Table 8.7 along with the corresponding values of the deactivation parameter. The distribution of the carbon between the surface and bulk of the catalyst can be very different . The quantity of coke deposited in Experiment 4 was much greater than in Experiment 1 and was concentrated on the catalyst surface as compared to the approximately equal distribution found for Experiment 1. Despite the large amount of deposited coke, the value of k_d was significantly smaller for Experiment 4. These results imply that, although several layers of coke may be formed on the external surface of the catalyst without greatly altering catalyst activity, small amounts of coke deposited throughout the catalyst bulk deactivate it drastically. It is probable that the polymer which builds up on the external surface can continue to grow (no space restrictions) whereas the polymer which grows on internal surface is restricted by the size of the pores.

Coke has sometimes been found to act by blocking the catalyst pores in addition to covering the active sites. A number of workers have shown that coking is accompanied by a significant decrease in catalyst surface area and pore volume. However, according to Haldeman and Botty (40), the loss in surface area is negligible for coke in the range 0 to 10 weight percent observed in this study. The pore volume distribution of three spent catalyst samples removed from various positions in the tubular reactor and of the fresh catalyst (1.5 wt % F) are compared in Fig. 8.14. No measureable change in the pore distribution of the catalyst samples was detected. The corresponding surface areas of the layers were also similar (within experimental error) as seen in Table 8.6. The surface areas of the used catalysts were greater than for the fresh catalysts. This increase in the surface area is perhaps due to the increase in roughness of the coke deposit. The deactivation of these catalysts with time-on-stream could not be attributed to blocking of the catalyst pores or changing of the catalyst surface area.

Solvent extractions of spent catalyst samples were undertaken to identify the

Table 8.7

Comparison of bulk and surface carbon analyses

Experiment Number	F- content[a] [wt %]	Carbon content [wt %]		Surface to bulk ratio	k_d [10^{-3} min^{-1}]
		Surface[b]	Bulk[c]		
11	0	7.86	5.94	1.32	1.0
4	1.5	20.8	7.79	2.67	0.4
14	2.6	2.13	2.62	0.81	0.8
1	4.3	1.09	1.04	1.05	2.2

[a] determined by ion selective electrode
[b] determined by XPS, (+/- 10 %)
[c] determined by elemental analyzer.

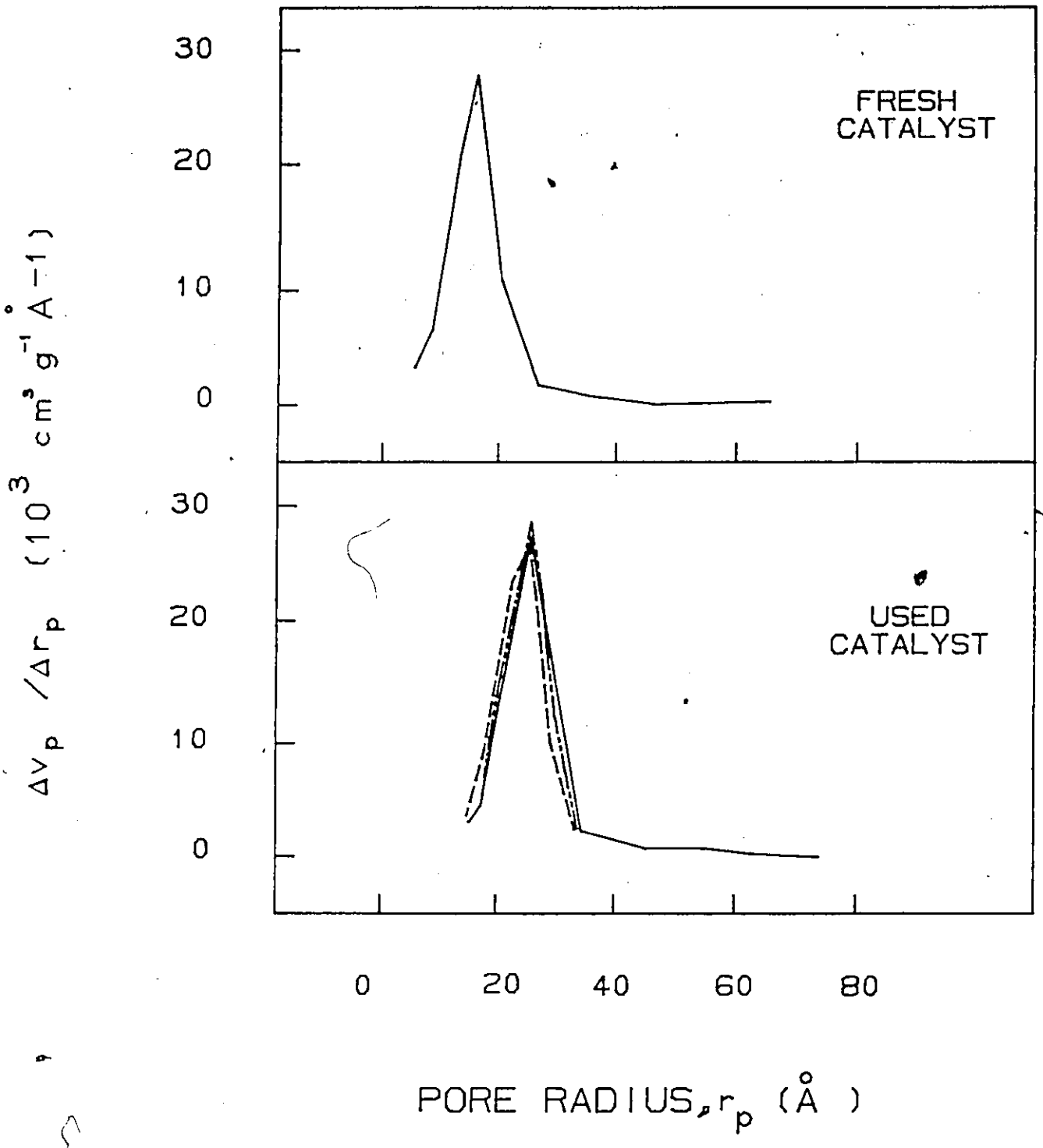

Fig. 8.14 Pore volume distribution of fresh and spent 1.5 wt % F on alumina catalysts for Exp't 3.

——— inlet

-·-·-· centre

----- outlet

differences in carbonaceous deposits. Samples were extracted with carbon disulphide, and trichloroethylene, both powerful solvents. Although the color of the extracts was darkened compared with the clear solvent, gas chromatograms of the concentrated extract showed only solvent peaks. No extracted components could be identified. These findings are consistent with the fact that high polymers from acetylene do not to dissolve in any known solvents (45). In fact, small particles could be detected in the solvent (CS_2) after sufficient sedimentation time. Over many catalysts which have been used, the polymer is synthesized in the form of powder rather than film (45).. This suggests very strongly that a linear polymer may form part of the coke deposits obtained in this study.

The nature of the coke deposits was also investigated by cross polarization magic angle spinning ^{13}C NMR spectrometry. NMR spectrometry has been used with increasing frequency in polymer characterization (55). Solid state NMR has been used to look at the structural features of coal, oil shales and coked catalysts (49, 55). A summary of the total NMR signal, the ratio of the aromatic/aliphatic carbon and the bulk carbon content is given in Table 8.8. There is excellent agreement between the bulk carbon measured via elemental analysis and the total carbon signal using NMR. These spectra reveal the presence of both aliphatic and aromatic structures in the coke deposits.

The variation in the nature of the products formed on the catalyst surface has been noted previously. For example, Léglise et al. (53) in studying the polymerization of C_2H_2 to alkylaromatics over CrY zeolites in a thermobalance in the temperature range 70 to 350°C found that all the residue deposited at a reaction temperature of 70°C was removed as benzene upon heating to 360°C. Similar treatment performed on the residue deposited at a reaction temperature of 200°C led to only 80% of deposit removal and the composition was C_3-C_6 (36%), benzene (10%), toluene (16%), C_8 aromatics (15%), C_9 aromatics (14%) and C_2H_2 (8%). Residues deposited at higher temperatures (300-360°C) were not removed upon heating to 360°C.

The deactivation parameter, k_d, has been linked in much of the previous

Table 8.8

Characterization of some used catalysts by NMR

Experiment Number	Carbon content [wt %]	Carbon content [mg]	^{13}C NMR Total signal	^{13}C NMR Ratio[a]	k_d [10^{-3} min^{-1}]
4	7.79	12.9	0.5147	0.587	0.3 0.6 [b]
2	2.53	4.3	0.2290	0.370	0.44 0.17
17	3.12	5.5	0.2286	0.818	0.8 1.3
11	5.18	8.4	0.4280	0.695	1.0
13	2.7	4.6	0.2120	0.724	0.9

[a] ^{13}C NMR ratio of signal corresponding to aliphatic and aromatic carbon
[b] repeated experiment

discussion to the coke content of the catalyst. It was pointed out however that only a fraction of the coke was probably responsible for the deactivation. A relationship between the deactivation parameter, k_d, and the ratio of the aliphatic/aromatic ^{13}C NMR signal is clearly visible in Fig. 8.15. This correlation implies that as the proportion of the aliphatic components of the coke increase, the deactivation becomes more severe. Aliphatic molecules with H/C of 1 or above are usually formed from the abstraction of hydrogen from highly condensed aromatic structures which are believed to be the coke precursors (33). In this reaction however, although this mechanism is not excluded, aliphatic molecules can be formed right from the start with the dimerization of acetylene and subsequent propagation of the polymer chain which will be discussed in Chapter 11. This accounts for the high rates of deactivation in this reaction.

8.5 CONCLUSION

Catalyst deactivation in acetylene polymerization over fluoridated alumina has been shown to be primarily due to coking. Empirical models, developed to describe the influence of the reaction temperature, the feed gas concentration and the weight-time on the parameters a_0 and k_d and on the catalyst coke content at 1h on stream showed that both the deactivation and the carbon content were lessened by using high temperatures (400°C), high weight-times (3 $g.s.mL^{-1}$) and low feed concentrations (5 vol %).

The degradation reaction(s) leading to coke have been associated with ion-pair sites which are responsible for acetylene adsorption. A decrease in the number of these sites, brought about by fluoridation, brings about a simultaneous decrease in the coke produced. The coking process appears to be complex; small amounts of coke dispersed throughout the catalyst bulk deactivate the catalyst more readily than coke built up on the external surface. Coking on the external surface would appear to increase with catalyst acidity. Furthermore, coke appears to be a primary product of acetylene conversion.

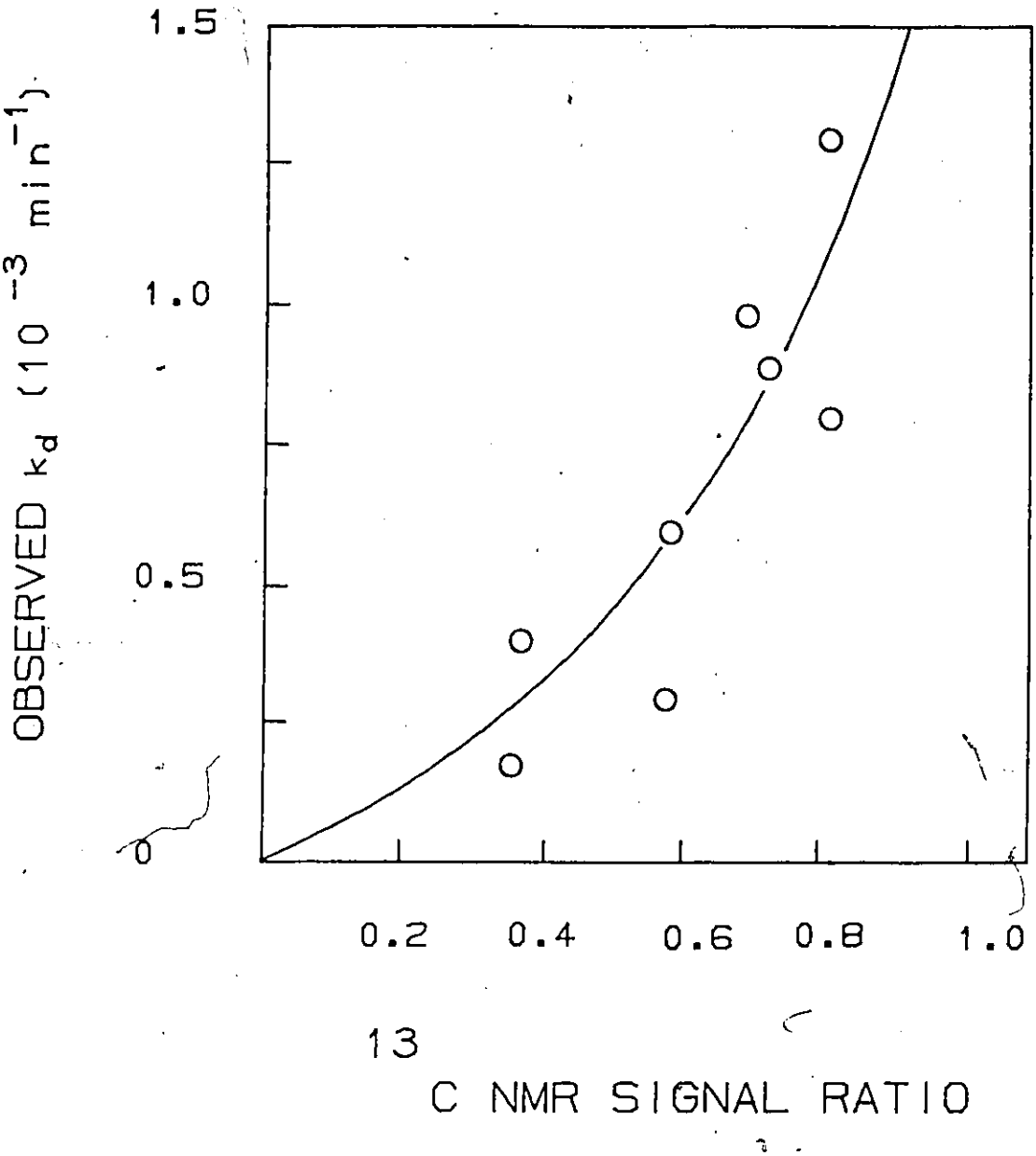

Fig. 8.15 Relationship between the observed deactivation parameter, k_d, and the ratio of the ^{13}C NMR signal associated with aliphatics and aromatics in the coke on the used catalysts.

The specific rate of deactivation in acetylene conversion has been correlated with the aliphatic structures in the deposited coke. This suggests that deactivation may be cause in part by the formation of aliphatic structures such as conjugated chains.

9. NATURE AND RATE OF COKE DEPOSITION

It was suggested in the previous chapter that part of the catalyst deposit was polymeric in nature. Considerable evidence was also gathered which pointed to the fact that this polymeric material was responsible for deactivating the catalyst. The data presented and discussed in Chapter 7 demonstrated that under conditions of low conversion only high molecular weight products were formed in the polymerization reaction. The polymerization reaction was studied in the microbalance where the rates of coke formation could be measured directly under conditions of low conversion. Furthermore, separation, identification and quantification of the deposited coke was achieved by temperature-programmed desorption in nitrogen which was carried out in situ. The microcomputer controlled microbalance system (Perkin-Elmer TGA 7) and ancillary equipment have been described in Chapter 4.

9.1 GENERAL FEATURES

Experiments performed in the microbalance without catalyst showed that at the highest operating temperature, 400^{o}C, there was a negligible weight uptake of the sample pan. Reproducibility in temperature-time history and in the weight-loss history of the fresh catalysts was excellent (Fig. 9.1). Fig. 9.2 shows a typical microbalance curve with no acetylene present (so no reaction could occur) for an alumina catalyst that was heated in nitrogen flowing at 65 mL/min. The solid line in Fig. 9.2b represents the weight-loss curve (the weight per cent of the original sample vs. time) while the line in Fig. 9.2c represents the rate of weight-loss curve as a function of time. The temperature-time history of the sample is shown in Fig. 9.2a. The major item of information one obtains from the weight-loss curve is the percentage weight-loss assignments (weight at the start and end of reaction). The decrease in weight in Fig. 9.2

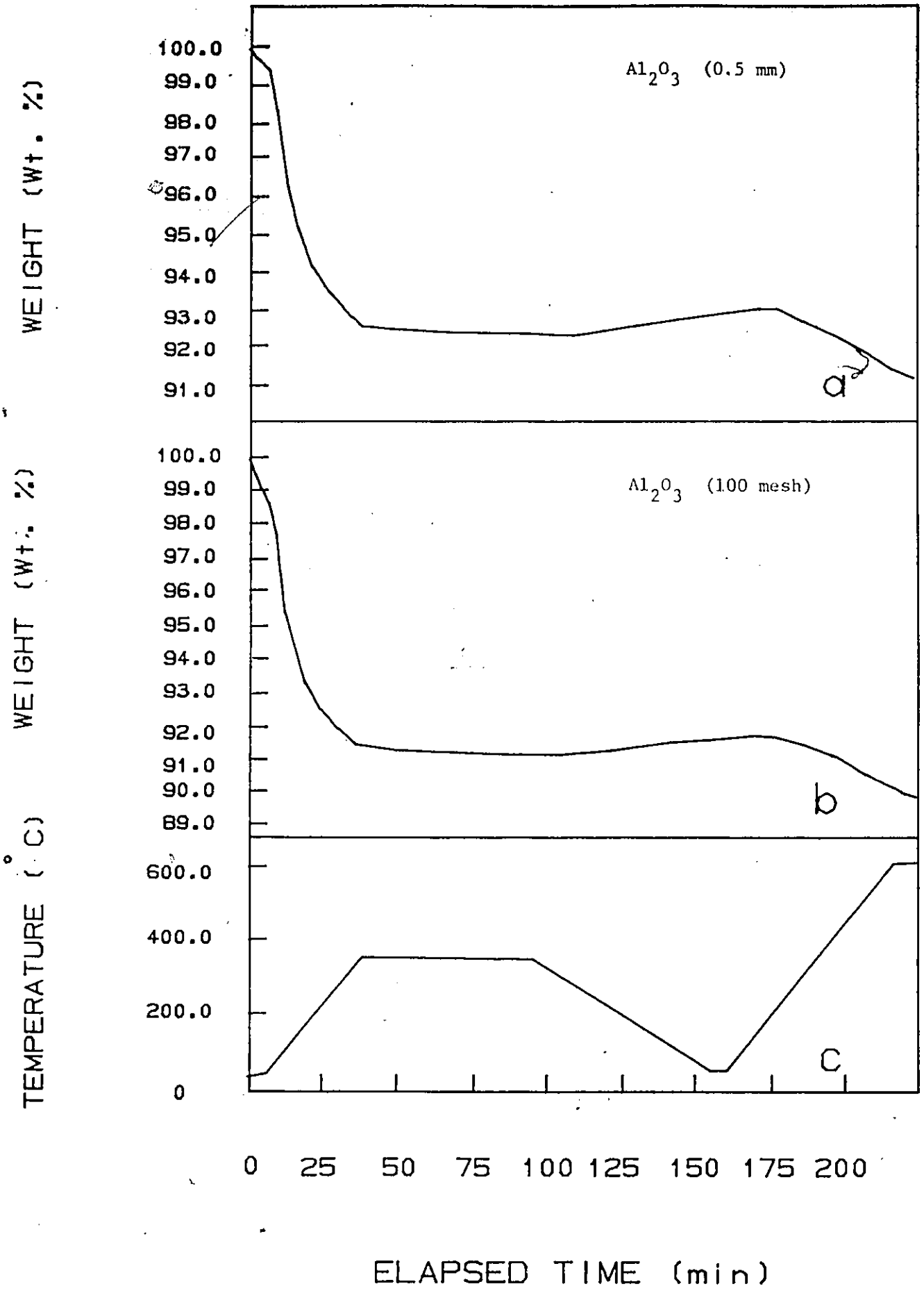

Fig. 9.1 A comparison of the temperature-time and weight-time history of two fresh Al_2O_3 catalysts.

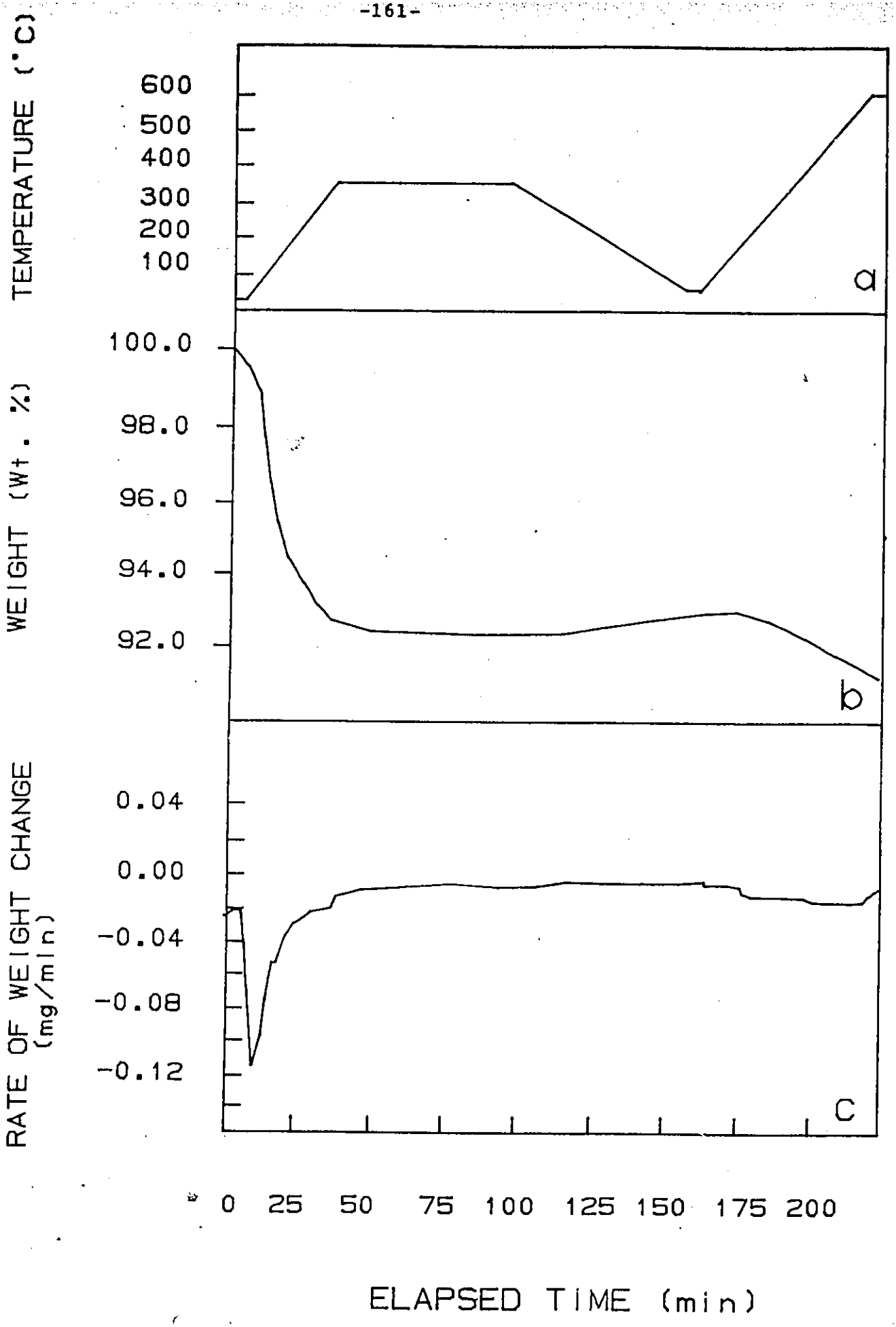

Fig. 9.2 Typical microbalance weight-loss and rate of weight-loss curves with no reactant present.

was attributed to the removal of moisture from the catalyst upon heating. Between 6 and 11 wt % moisture was lost by the alumina and fluoridated-alumina catalysts when they were heated to 350^{o}C (the average reaction temperature). The moisture loss during the constant-temperature period (corresponding to the reaction period of 1 h) was negligible, as inferred from the plateau region in Fig. 9.2. The increase in weight of the sample between 100 and 175 min was attributed to readsorption of moisture as the temperature was lowered to room temperature. In the temperature range between the reaction temperature and the final pyrolysis temperature of 900^{o}C, a significant weight-loss occurred probably accompanied by structural changes in the catalyst (34).

The reaction experiments were carried out at a pressure of 101 kPa, a reaction temperature between 300 and 400^{o}C, gas flow rates between 30 and 80 mL/min and gas-phase acetylene concentrations between 2.5 and 6.3 vol %. Results for a typical reaction experiment are shown in Fig. 9.3. The isothermal reaction step is the region between the points labelled A corresponding to a starting weight w_o and B corresponding to a final weight w_f. Two major items of information may be gleaned from the rate of weight loss/gain curve, these are the maximum rate of coke deposition together with the time at which it occurs) and the rate of coke deposition at the end of 1 h (steady state rate). The data handling shown in Fig. 9.3 and detailed in Appendix 9.1 describes the determination of these quantities. A summary of the results of the experiments conducted in the microbalance are listed in Table 9.1. The influence that the operating conditions and the type of catalyst have on the total amount of coke deposited and on the rate at which it is deposited will be described next.

9.2 INFLUENCE OF TEMPERATURE ON RATE OF COKE DEPOSITION

The amount of coke formed on alumina catalysts from acetylene at various temperatures, is plotted in Fig. 9.4 as a function of time. The curves show that temperature plays an important role in the formation of coke. The total amount of coke

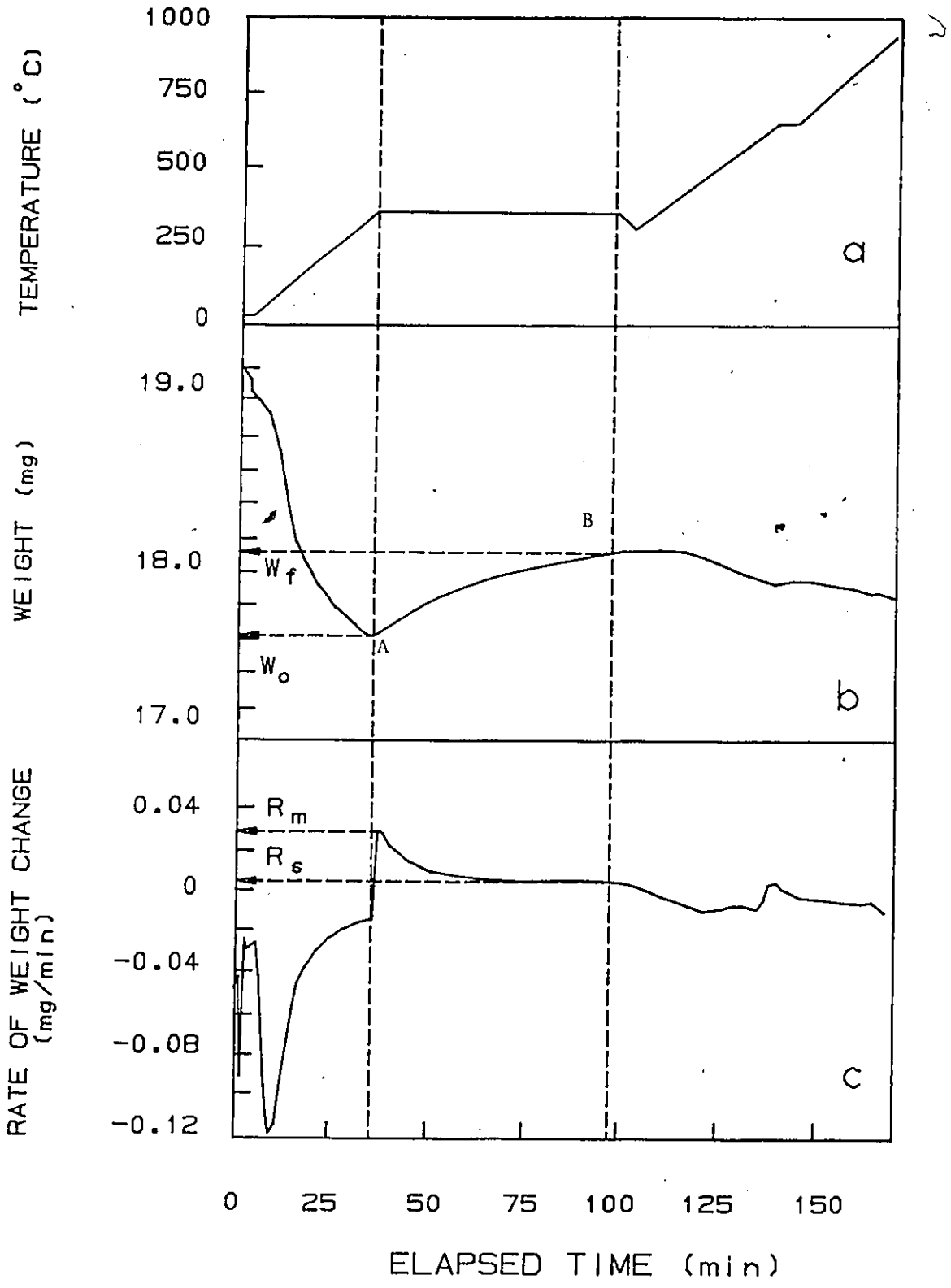

Fig. 9.3 Typical microbalance temperature-time (a), weight-time (b), and rate of weight change-time (c) curves with gas-phase acetylene concentration of 5.4 vol %.

Table 9.1

Rate of deposition as measured on the microbalance[a]

EXP'T NO	W_i [mg]	W_o [mg]	%	W_f [mg]	%	Rate of Deposition [mg/min] R_{max}	R_f	[min^{-1}] R'_{max}	R'_f	[$mg/m^2/min$] R^s_{max}	R^s_f
01	18.348	16.871	8.05	n.a.	n.a.	n.a.	n.a.	n.a.	n.a.	n.a.	n.a.
02	19.311	17.631	8.70	n.a.	n.a.	n.a.	n.a.	n.a.	n.a.	n.a.	n.a.
03	19.250	17.585	8.65	n.a.	n.a.	n.a.	n.a.	n.a.	n.a.	n.a.	n.a.
04	18.595	n.a.	n.a.	n.a.	n.a.	n.a.	n.a.	n.a.	n.a.	n.a.	n.a.
05	19.517	17.883	8.37	18.483	3.36	0.045	0.0043	0.25	0.24	1.32	0.13
06	19.067	17.411	8.69	19.089	9.64	0.153	0.0070	0.88	0.040	4.66	0.21
07[b]	19.285	17.733	8.05	18.044	1.75	0.009	0.0024	0.052	0.014	0.28	0.07
08[b]											
09	18.942	17.139	9.52	17.447	1.80	0.008	0.0035	0.040	0.020	0.20	0.103
10	19.186	17.111	10.8	17.326	1.26	0.001	0.0011	0.008	0.006	0.04	0.032
11	19.355	17.183	11.2	17.938	4.39	0.033	0.0056	0.189	0.033	0.95	0.163
12	19.792	18.120	8.4	18.680	3.09	0.029	0.0030	0.160	0.017	0.85	0.087
13	19.009	17.467	8.1	18.223	4.32	0.043	0.0041	0.243	0.023	1.29	0.124
14	19.442	18.050	7.1	n.a.	n.a.	n.a.	n.a.	n.a.	n.a.	n.a.	n.a.
15	18.915	17.660	6.6	18.362	3.97	0.033	0.0048	0.189	0.027	1.00	0.143
16	19.189	17.600	8.3	18.142	3.07	0.031	0.0033	0.171	0.019	0.91	0.099
17[b]	-	17.628	n.a.	18.225	3.38	0.037	0.0038	0.200	0.020	1.06	0.106
18[b]											
19	-	16.714	n.a.	16.940	1.35	0.008	0.0018	0.040	0.010	0.20	0.050
20	19.238	17.820	7.37	18.505	3.84	0.034	0.0038	0.190	0.021	1.00	0.111
21	18.666	16.892	9.50	17.150	1.53	0.007	0.0030	0.039	0.018	0.20	0.091
22	19.602	18.157	7.37	18.603	2.46	0.018	0.0038	0.101	0.021	0.53	0.111
23	18.493	16.975	8.21	17.124	0.88	0.003	0.0024	0.019	0.014	0.10	0.071
24	18.840	17.270	8.49	17.530	1.51	0.006	0.0034	0.036	0.020	0.16	0.089
25	18.938	17.987	5.02	18.026	0.22	0.001	0.0010	0.006	0.006	0.04	0.036
26	17.977	16.870	6.16	17.370	2.96	0.017	0.0045	0.100	0.027	0.53	0.141

[a] experimental conditions as in Table 8.2
[b] aborted

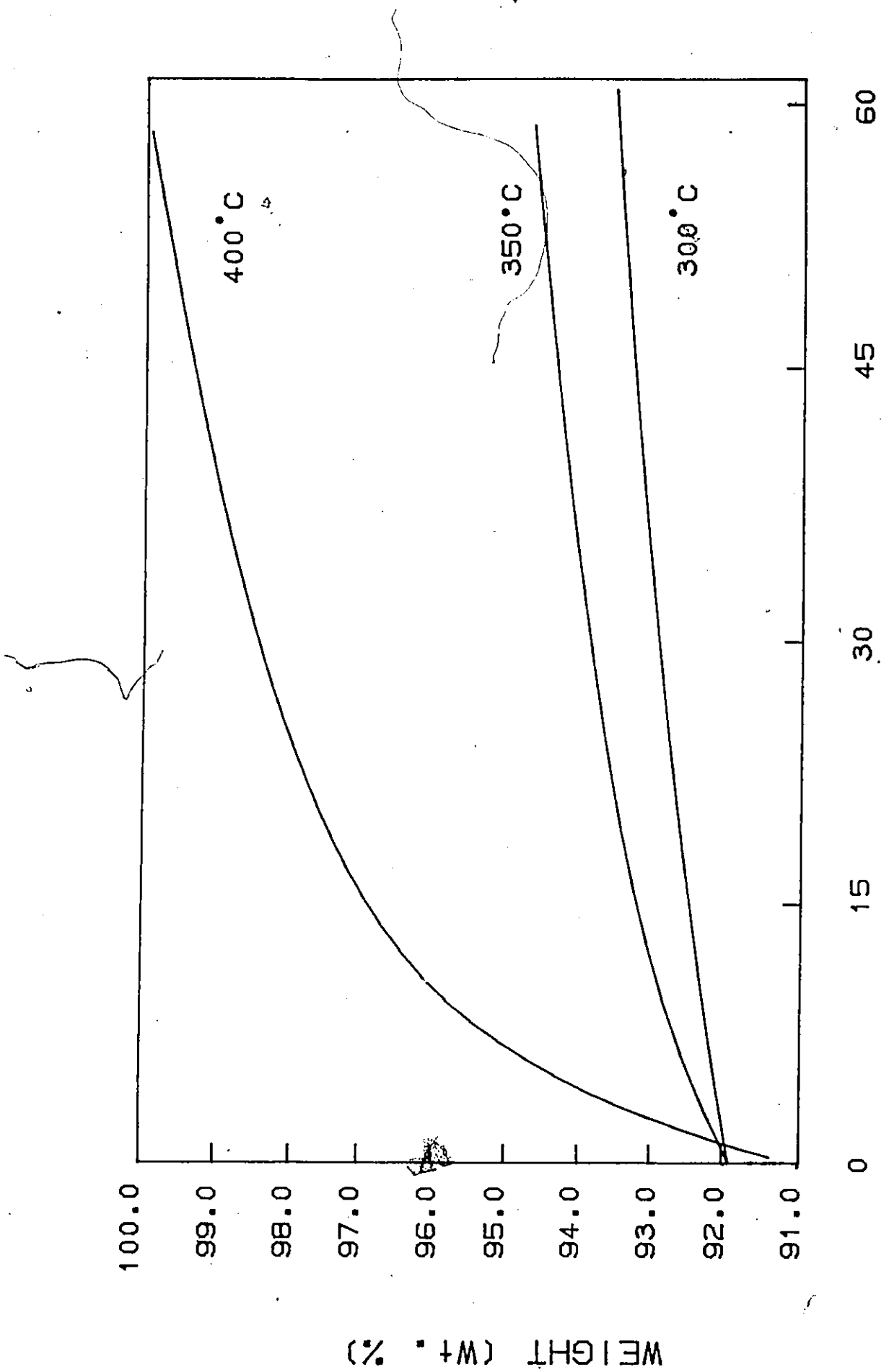

Fig. 9.4 Coke formation on alumina as a function of time at three temperature levels (64 mL/min, 5.15 vol % C_2H_2).

formed increases as the temperature is varied from 300 to 400°C at all times-on-stream. A similar temperature dependence is observed for the fluoridated alumina catalyst (2.6 wt% F) in Fig. 9.5. These findings are consistent with the model predictions for catalyst carbon content (Eq. 8.4) based on the data in the tubular reactor at 1 h on stream.

More information may be obtained from the rate of coke deposition shown in Fig. 9.6 and 9.7 for alumina and fluoridated alumina respectively, as a function of time. At low temperature, 300°C, there is a steady rate of deposition, R_f^s, albeit a rather low rate. Both the maximum and the steady-state rate of coke deposition increase with increasing temperature. The occurrence of steady rates of coke deposition at 1 h makes it possible to evaluate an Arrhenius type of activation energy from the data.

If the steady-state rate is expressed as the product of the reaction rate constant, k and the concentration of C_2H_2 in the gas-phase, c_f,

$$R_f^s = k \quad c_f \tag{9.1}$$

then the effect of temperature upon the experimentally observed reaction rate constants is given by :

$$k = A \exp (E_a/RT) \tag{9.2}$$

The overall activation energy can be calculated from a plot of $\ln(R_f^s)$ versus 1/T, for constant concentration, c_f, as indicated below:

$$R_f^s = A \exp (E_a/RT) \quad c_f$$

$$\ln(R_f^s) = \ln (A \; c_f) - E_a/RT \tag{9.3}$$

Arrhenius plots for the alumina and fluoridated alumina catalysts are given in Fig. 9.8. The values obtained for the activation energies, E_a, are based on a small number of data points and are used only to illustrate an order of magnitude. The activation energies are not very dependent on the catalyst used, 8 kcal/mol for alumina and 7 kcal/mol for the fluoridated alumina. These values are very low for chemical reactions. Diffusional limitations were considered, however, data given in Fig. 9.12 showed that the rates were independent of gas flowrate. Therefore the low values of E_a were not likely due to

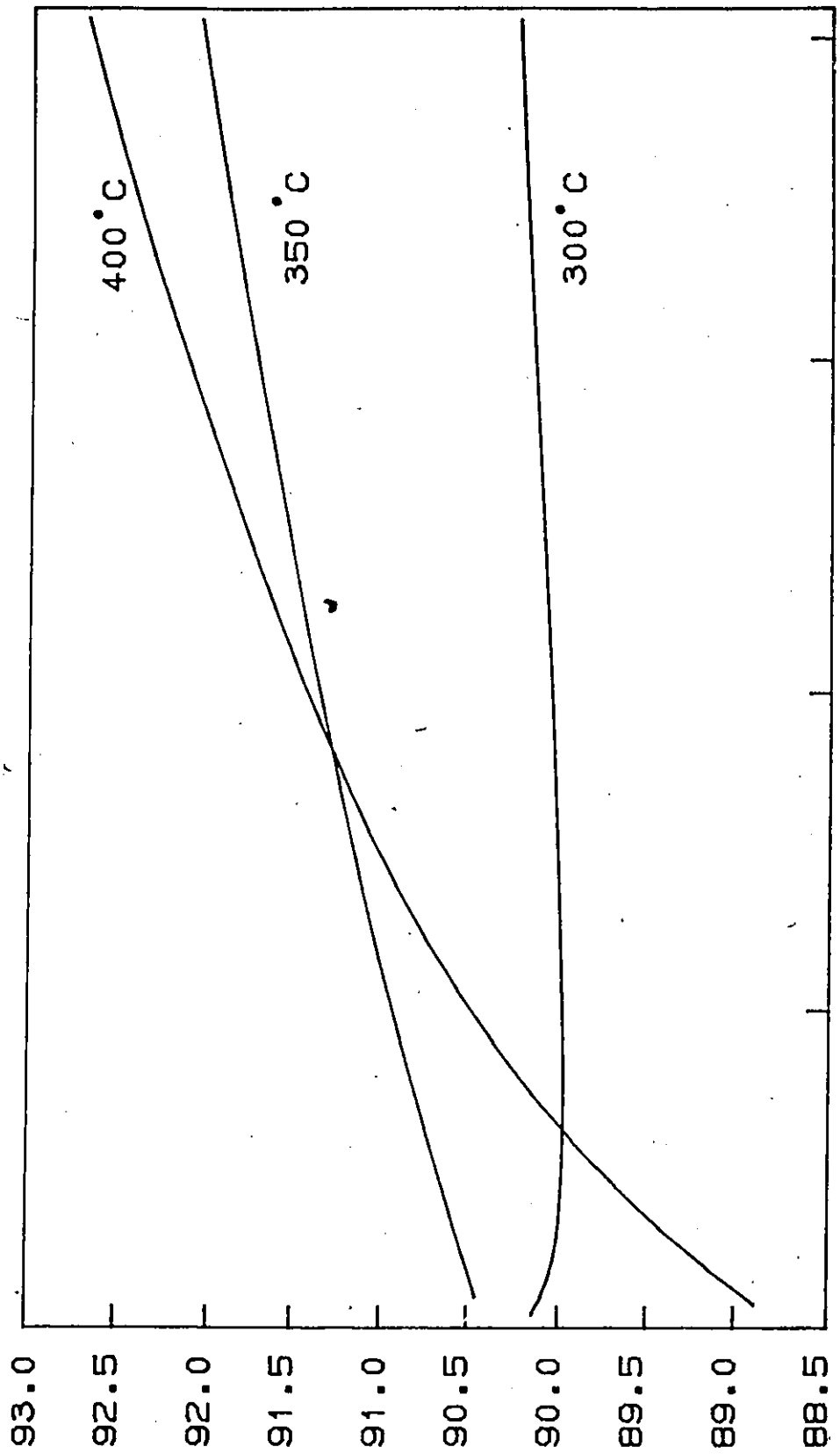

Fig. 9.5 Coke formation on fluorided alumina (2.6 wt %) as a function of time at three temperature levels. (64 mL/min, 5.15 vol % C_2H_2).

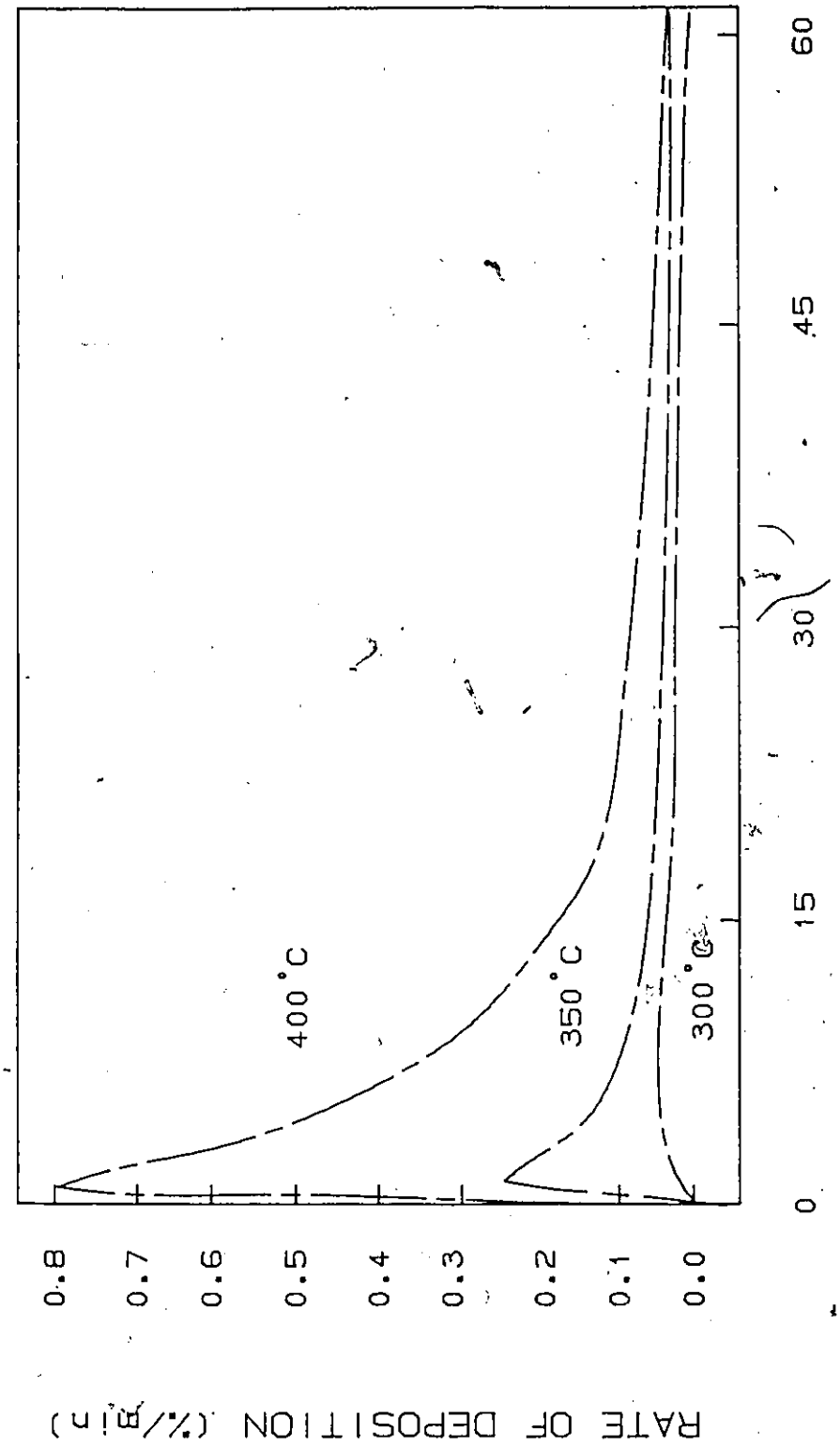

Fig. 9.6 Rate of coke deposition on alumina as a function of time-on-stream.

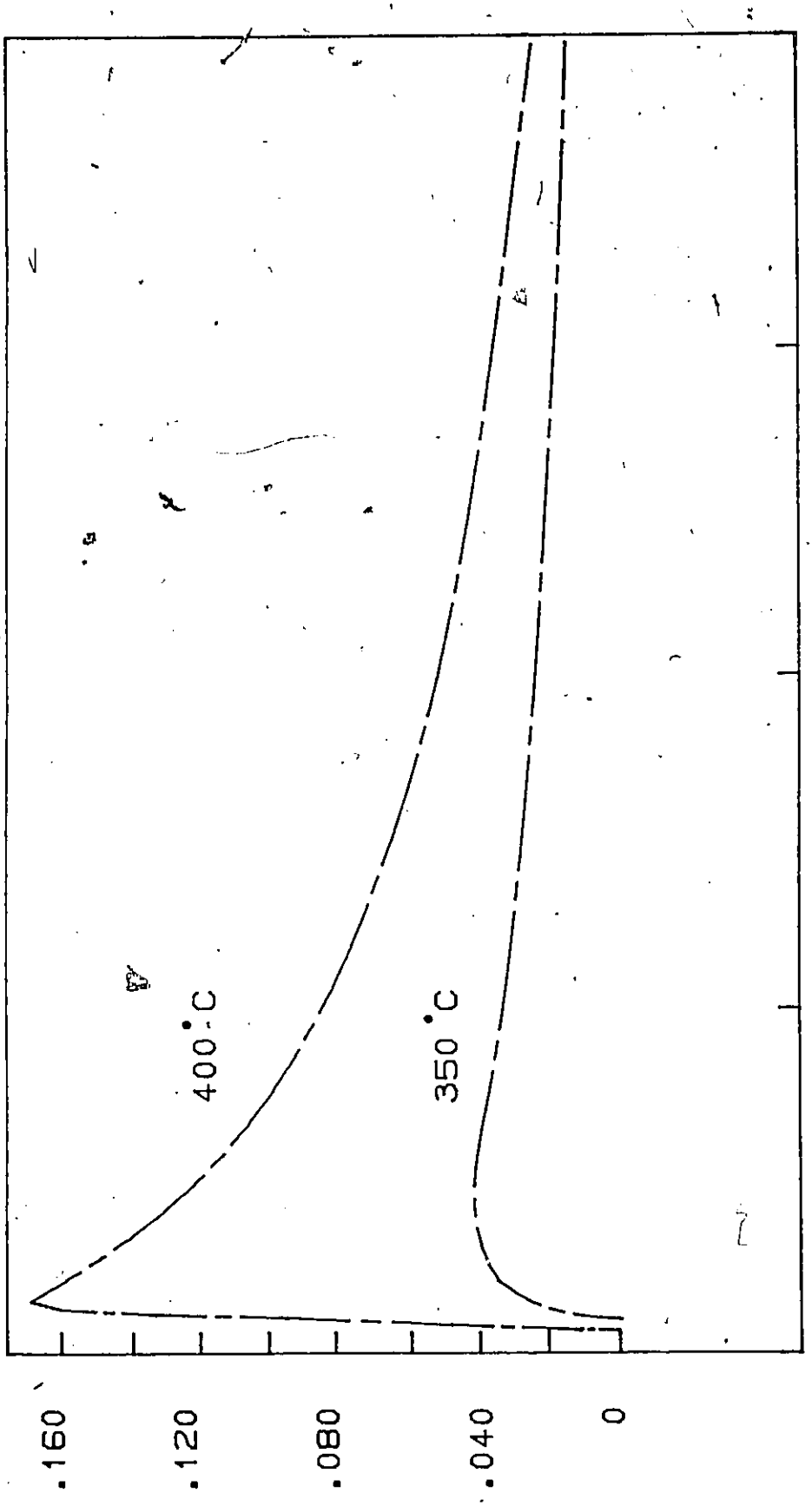

Fig. 9.7 Rate of coke deposition on fluorided alumina as a function of time-on-stream.

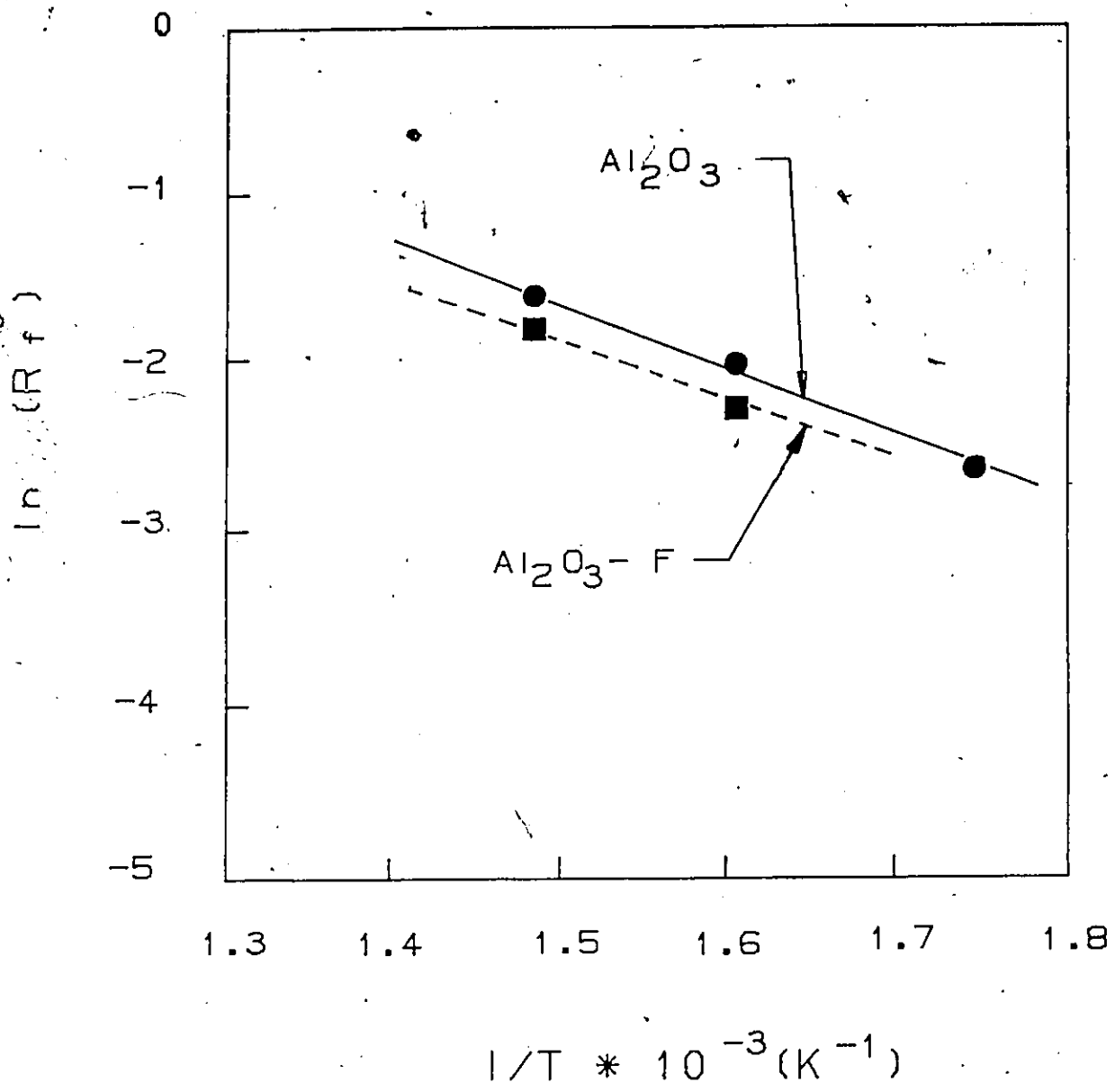

Fig. 9.8 Arrhenius plots of rates vs reciprocal temperature for alumina and 2.6 wt % F on alumina (64mL/min, 5.15 vol % C_2H_2).

diffusional limitations. The values are on the other hand consistent with the activation energy reported for "polymerization" on alumina-supported metals (15). In contrast, the activation energy obtained for the decomposition of acetylene to carbon on nickel, iron and cobalt is 33 kcal/mol (56, 81). Therefore on the basis of the activation energies, it would appear that the degradation reaction indeed yields polymeric species (CH-fragments) and not amorphous carbon.

The fact that both the amount of coke and the rate at which it is formed increase with temperature (the opposite trend observed with the specific rate of deactivation, k_d, in Fig. 8.10a) would imply that not all the species which make up the coke deactivate the catalyst. Lower rates of polymerization with increasing temperatures are common in polymerization reactions (70). One can postulate therefore that as the temperature is increased, less and less of the coke which forms is polymeric. This is confirmed when one examines the desorption patterns.

9.3 INFLUENCE OF TEMPERATURE ON DESORPTION PRODUCTS

The coked catalysts were subjected to a high-temperature pyrolysis in nitrogen at the end of the reaction time. The product desorption pattern of a fresh and spent alumina catalyst as a function of the programmed temperature are compared in Fig. 9.9. The desorption pattern for the fresh catalyst shows that water is removed steadily as the temperature is ramped. Clearly the biggest difference in the rate of weight loss observed in the desorption patterns of the fresh and spent catalysts occurs in the region between 450 and 600°C. A significant portion of the residues formed at a reaction temperature of 350°C, is removed in this temperature range. Many of the sharp peaks occurring with the fresh catalyst at high desorption temperatures are smoothed in the case of the spent catalyst. Analysis of the desorbed products of the fresh catalyst by mass spectrometry revealed only the presence of H_2 and H_2O. On the other hand, the analysis of the desorbed products of the coked catalysts revealed the presence of ions of all molecular weights from 2 to 200 amu, all at very low concentrations. No predominant species could be identified.

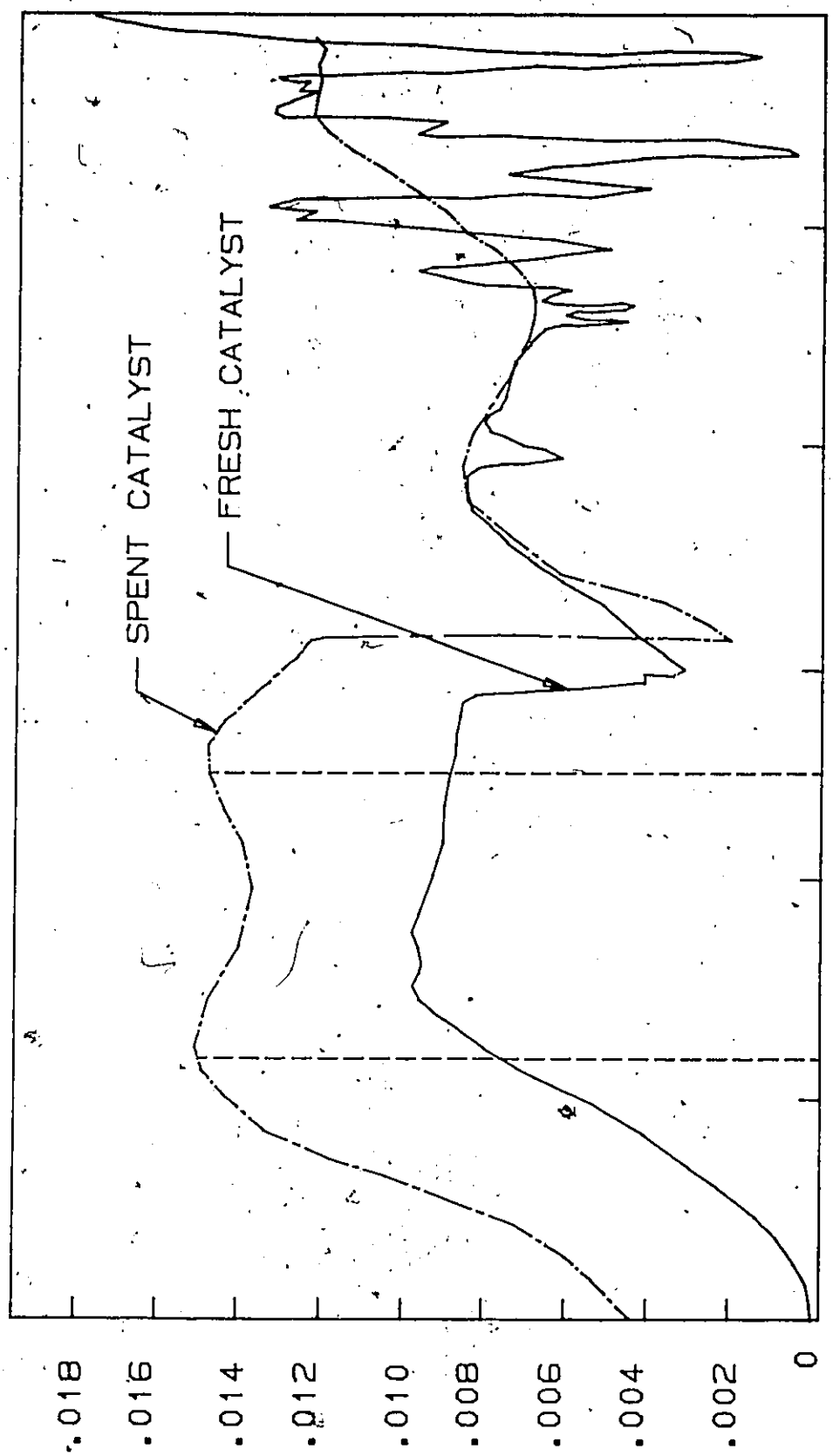

Fig. 9.9 A comparison of the product desorption patterns of a fresh and spent alumina catalyst as a function of the desorption temperature. ($350^{o}C$, 64 mL/min, 5.15 vol % C_2H_2)

The temperature-programmed desorption patterns for alumina catalysts reacted at 300, 350 and 400°C are compared in Fig. 9.10 a,b,c. Several important pieces of information emerge from a comparison of these desorption patterns. Distinct peaks at 450, 550 and 750°C are visible. At low reaction temperatures significant desorption occurs at 400°C and at 550°C. At 350°C, there appears to be a shoulder of the low temperature peak and the peak at 550°C is more pronounced. At a reaction temperature of 400°C, the low-temperature peak disappears and two strong peaks at 550°C and 750°C emerge. Similar observations may be made of the desorption patterns over fluoridated alumina as a function of temperature as seen in Fig. 9.11.

If it is assumed that the coke residue has many constituents, then one can postulate that the residues which are removed corresponding to desorption temperatures of 400, 550 and 750°C are somewhat different in nature. In general, the higher the pyrolysis temperature, the stronger the attraction is between the carbonaceous residues and the surface. The deposit removed at high temperatures (750°C) is very likely an amorphous carbon specie (low H content) while the deposit removed at low temperature (450°C) is very likely a highly polymeric specie (higher H content). In view of the fact that the deactivation is highest at the lowest reaction temperature, one can postulate that the existence of low temperature deposits contribute to this deactivation. In addition, since the deactivating species has been shown to be polymeric in nature, the species, which desorbs at a temperature of 450°C must correspond to the polymeric coke deposit.

9.3 INFLUENCE OF CONTACT TIME

The contact time between the catalyst and the reactant gas was alterred by varying the total gas flow rates in the microbalance between 30 and 80 mL/min. This range was limited by the operating requirements of the microbalance. The influence of the contact-time on the rate of coke deposition can be seen in Fig. 9.12 where both the steady-state rate, R_s, and the maximum rate, R_m, are plotted as a function of gas flow

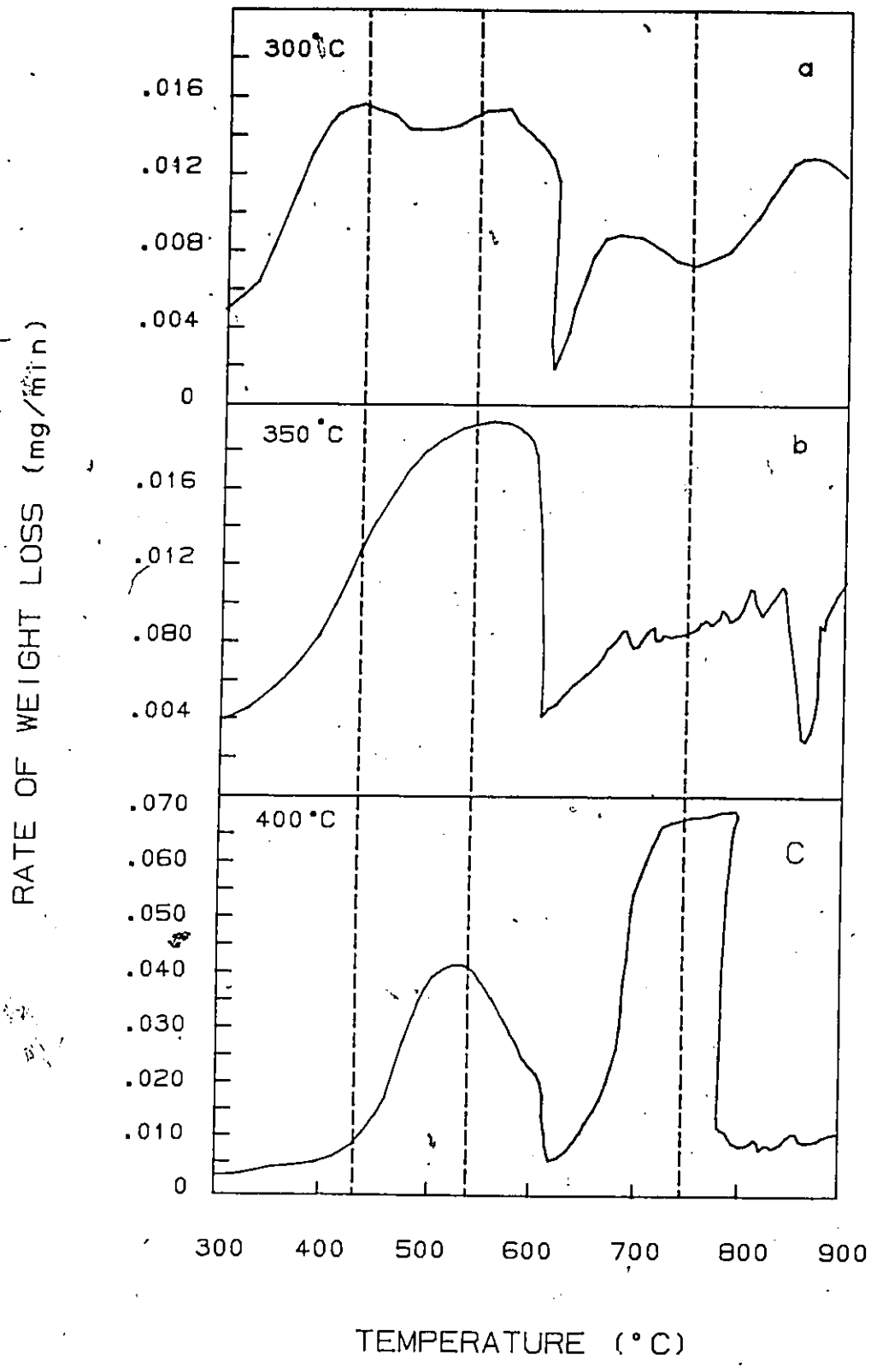

Fig. 9.10 Temperature-programmed desorption patterns for alumina catalyst reacted at three different temperature levels.

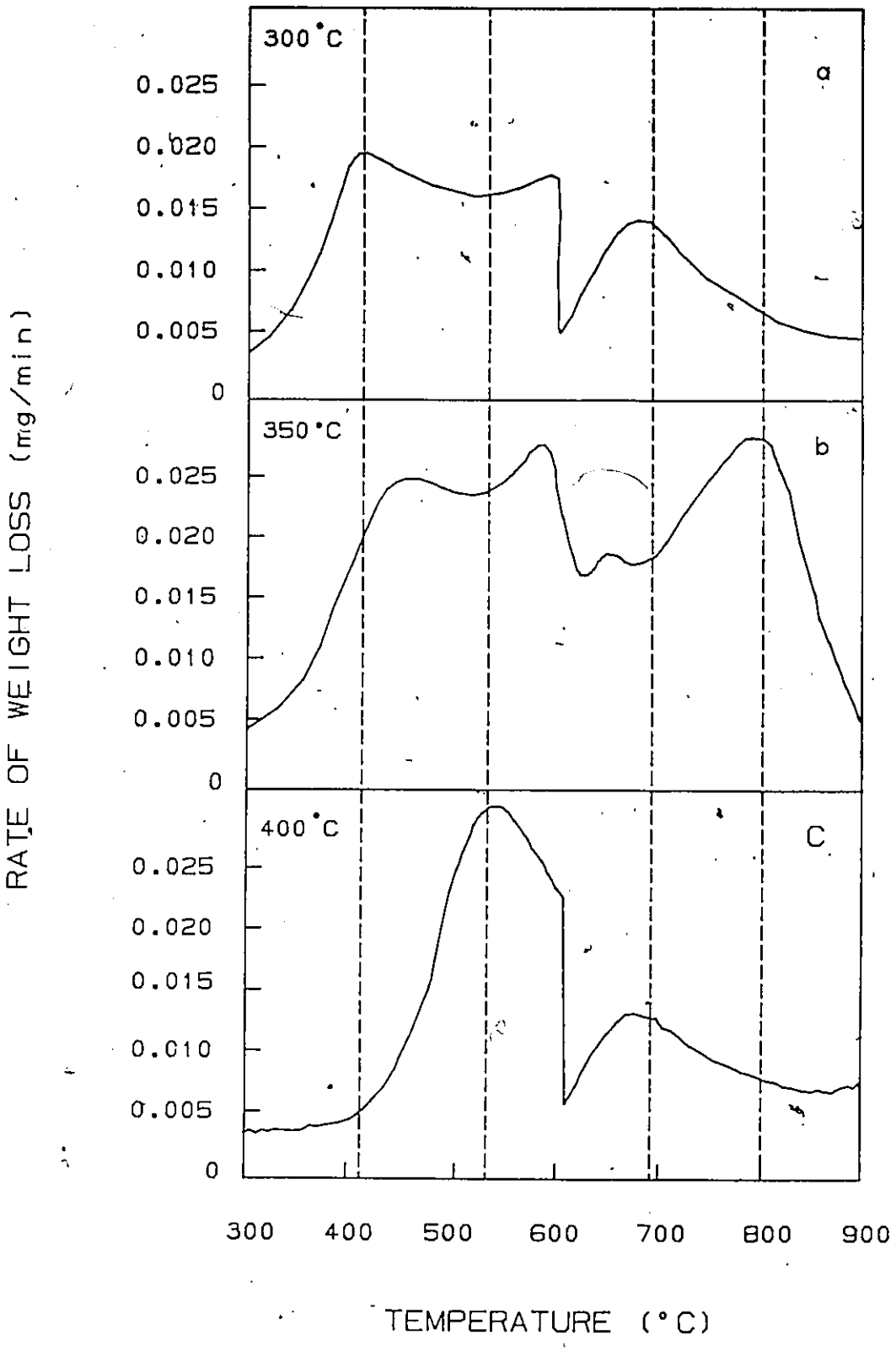

Fig. 9.11 Temperature-programmed desorption patterns for fluorided alumir catalyst (2.6 wt % F) reacted at three temperature levels.

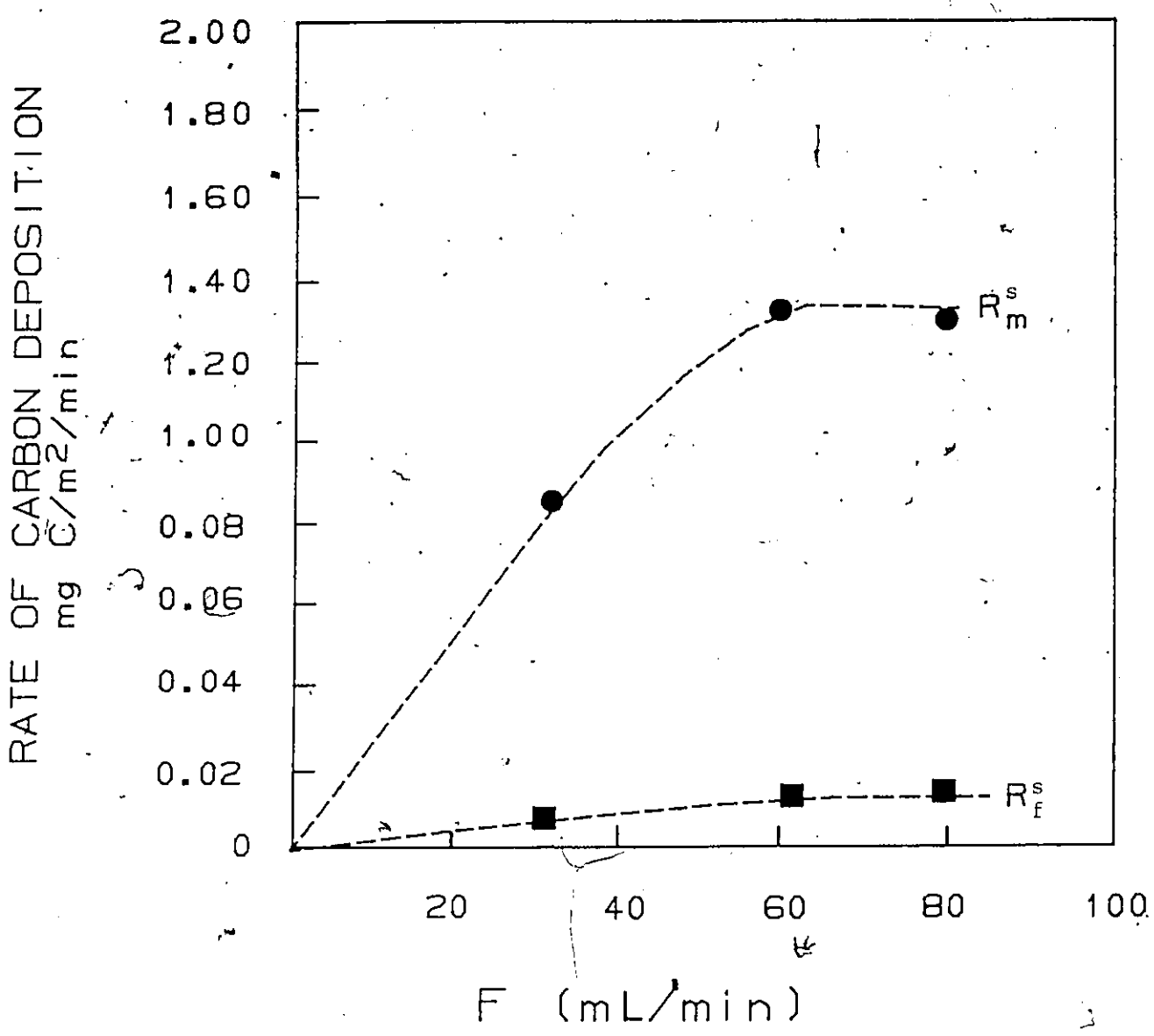

Fig. 9.12 The rate of carbon deposition versus total gas flowrate.

R_m^s = maximum rate of deposition

R_f^s = steady-state rate

rate. At high contact times (and low gas flow rates) the rate of the coking reaction is low. Presumably at low flow rates there is not enough acetylene present in the reactor (diffusion limited) to form coke rapidly. There is little difference in the rates observed at flows of 64 and 80 mL/min, therefore at high gas flow rates and corresponding low contact times the rate of coke deposition is independent of the contact time (not diffusion-limited). The rate of coke formation is proportional to the rate of acetylene entering the reactor until a certain flowrate produces the maximum rate of coke formation.

The product desorption patterns obtained at various gas flow rates are shown in Fig. 9.13 for a reaction temperature of 350°C. Two peaks at 450 and 550°C are visible under conditions of high gas flowrates and little differences are observed beyond this desorption temperature between the fresh catalyst and the spent catalysts.

The pattern changes significantly at the low flow rates and corresponding large contact times. The pattern shown in Fig. 9.13a has peaks which occur at a desorption temperature of 450°C and another above 750°C. The large peak at high temperature implies that at the low flowrates, the contact time is long enough to produce an amorphous carbonaceous product on the catalyst surface. Since a peak was not detected at 550°C it is possible that these species are the precursors of the deposits removed at desorption temperatures above 750°C. The only peak which is common to all three desorption patterns is at 450°C. It is the species which desorb at this temperature which have been associated with the loss in catalyst activity.

9.4 INFLUENCE OF INITIAL CONCENTRATION OF ACETYLENE

The concentration of acetylene in the microbalance was varied by changing the gas mixture being supplied to the sample arm of the balance. The nominal initial concentration was varied between 2.4 and 6.3 vol % C_2H_2 in nitrogen. It was observed in Chapter 6 that changes in activity brought about by altering the gas-phase concentration of acetylene are accompanied by similar although opposite changes in the rates of coke

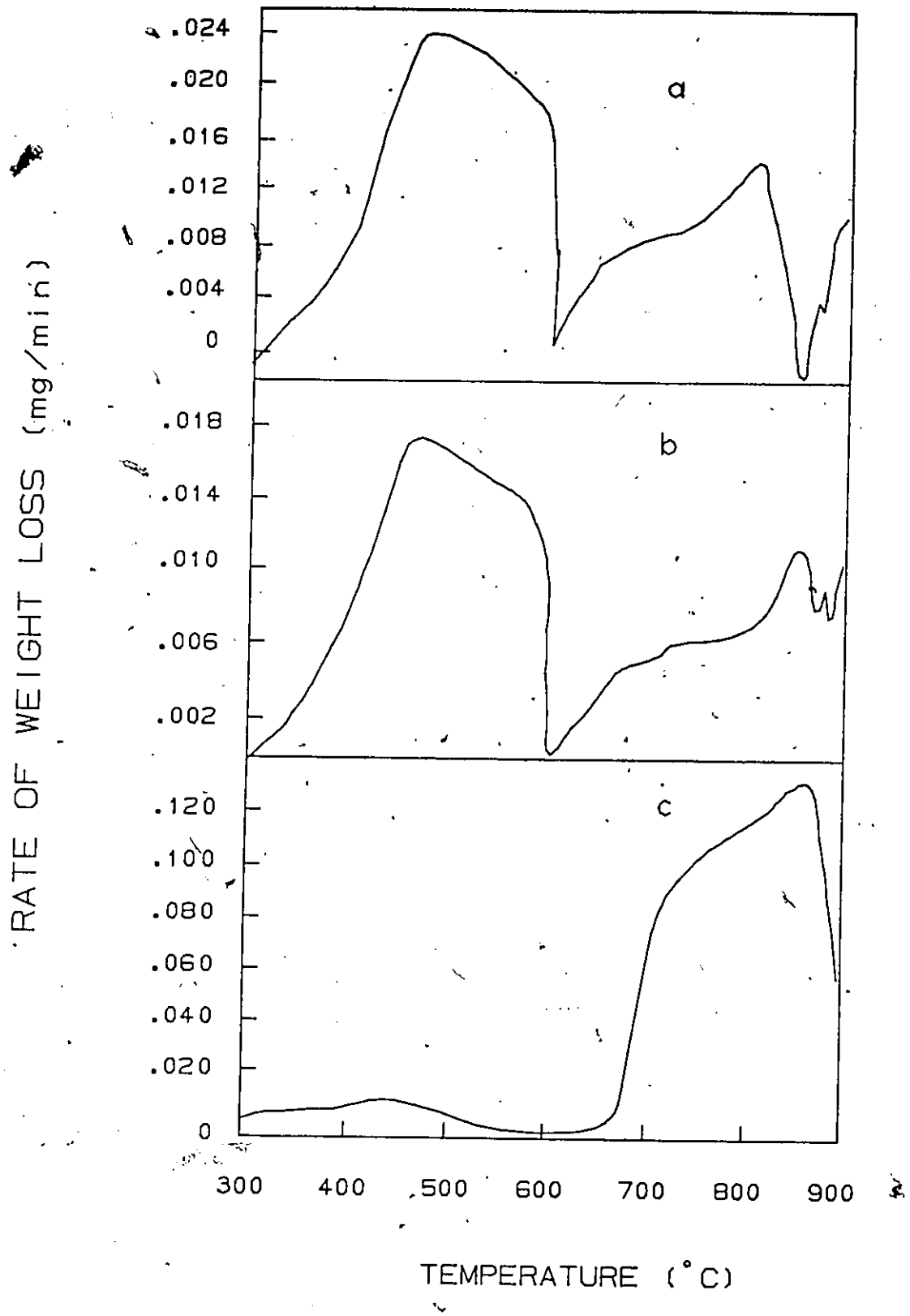

Fig. 9.13 The influence of contact time on the temperature-programmed desorption patterns of the spent catalysts. (350°C, 5.15 v % C_2H_2)

a) 80 mL/min b) 64 mL/min c) 30 mL/min

deposition (Fig. 6.12). As the initial concentration is increased from 2.5 to 4 % the rate of coke deposition increases greatly resulting in a large loss in activity over the same concentration range. On the other hand, as the initial concentration is increase beyond, 4 vol % the rate of coke deposition decreases moderately indicating less severe deactivation under these conditions.

The influence of the initial concentration of acetylene on the coke residues is demonsfrated in Fig. 9.14. At low gas-phase concentrations, a noticeable difference in the desorption patterns of the fresh and spent catalyst appears at 550°C. As the gas-phase concentration is increased to 5.3 vol % a second peak emerges at 450°C. It will be recalled that the species which are removed at this desorption temperature have been associated with the catalyst deactivation. The significant decline in activity observed in Fig. 6.9 at 5.3 vol. % C_2H_2 corroborates this postulate. At the highest gas phase concentrations used, a third peak emerges at a high desorption temperature, 750°C. Both peaks at the lower desorption temperature are reduced which means less of the species which are responsible for deactivation have been formed under these conditions. We would then expect the activity to be higher than at 5.3 vol % C_2H_2 which is indeed the case (Fig. 6.9).

9.5 THE INFLUENCE OF FLUORIDATION ON DESORPTION PRODUCTS

It was suggested in an earlier chapter, in discussing Fig. 8.9, that the total amount of coke depended upon the number of active sites available on the catalyst surface and that the nature and distribution of the coke varied with the catalytic properties. Studies in the microbalance confirmed this. The influence of fluoridation on the rate of coke deposition is shown in Fig. 9.15 at a reaction temperature of 350°C and an initial concentration of 2.5. Both the steady-state rate and the maximum rate decrease as the fluoride content increases. Although the rate of coke deposition decreases linearly with fluoride content, the conversion at these low concentrations of C_2H_2 goes through a

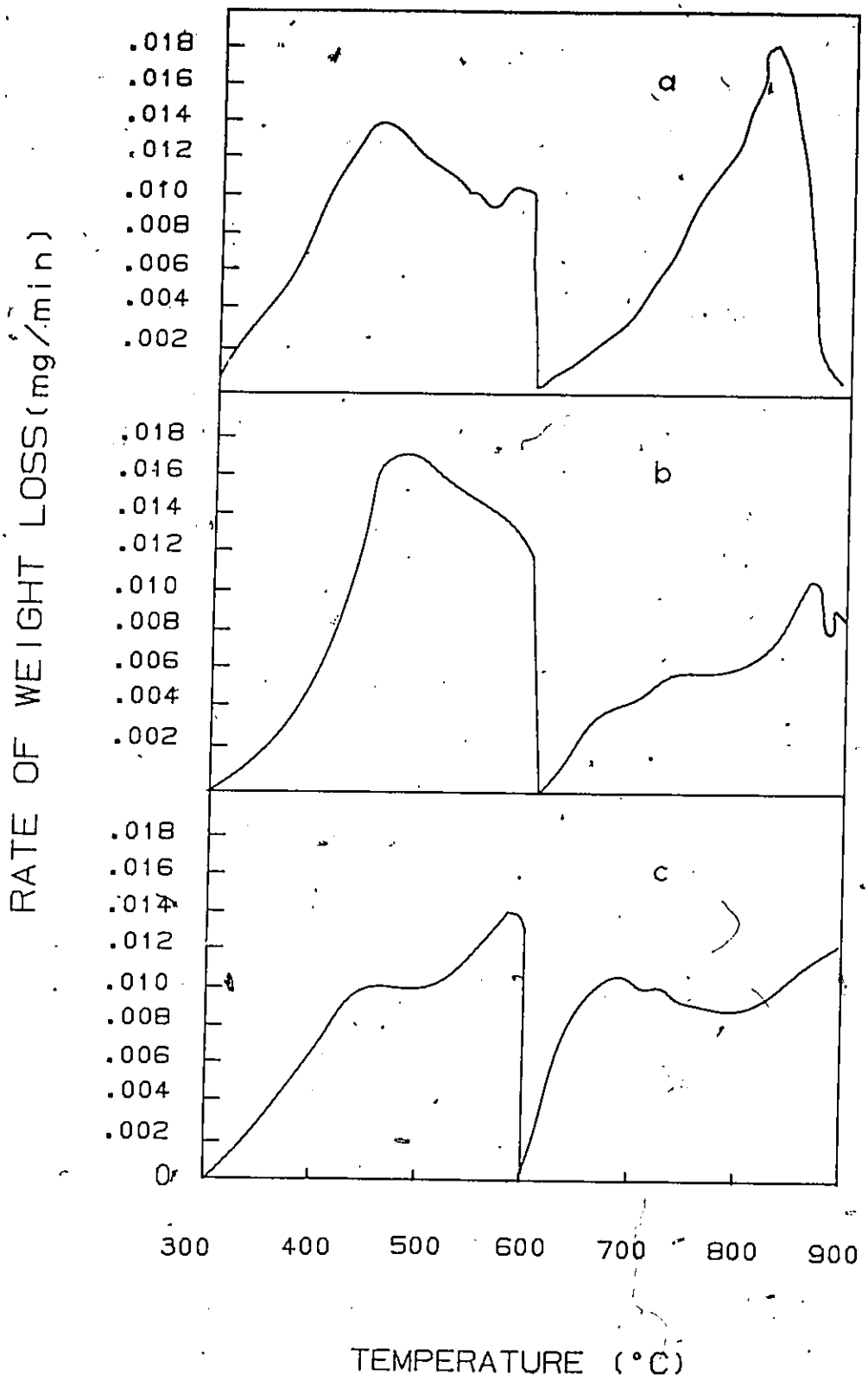

Fig. 9.14 Temperature-programmed desorption patterns for alumina catalysts reacted with different initial concentrations of acetylene in the feed. (350°C, 64 mL/min)

a) 6.3 vol % b) 5.2 vol % c) 2.5 vol %

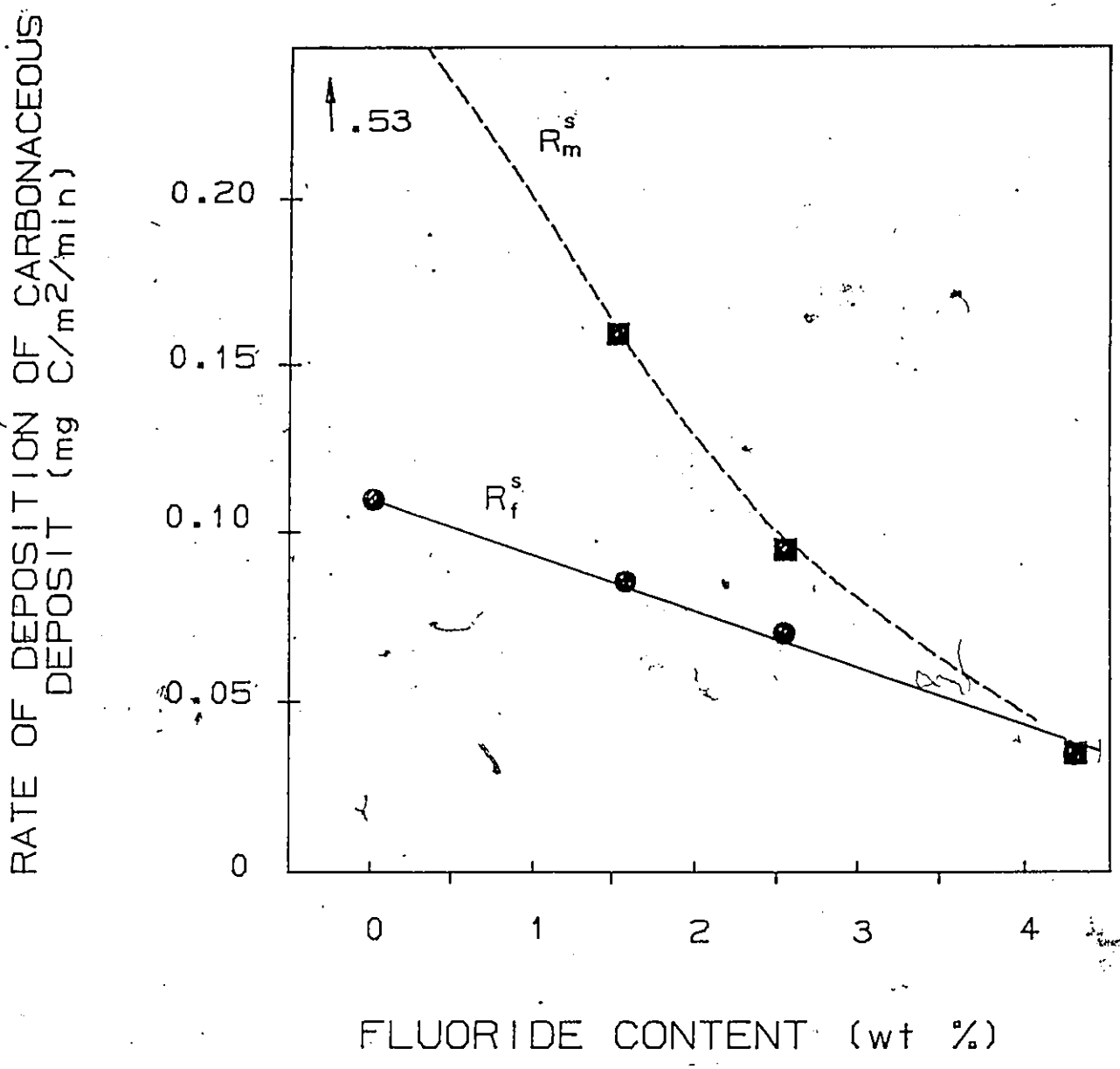

Fig. 9.15 Influence of fluoride content on the rate of coke deposition

R_m^s = maximum rate of deposition

R_f^s = steady-state rate of deposition

(350 °C, 64 mL/min, 5.15 vol %)

maximum (refer to Figs. 6.6 and 6.10) and the deactivation rate through a minimum (refer to Fig. 8.9c). This implies that the active sites of these catalysts are altered during fluoridation. The time at which the maximum rate of coke deposition was reached varied with the degree of fluoridation as observed in Fig. 9.16. Longer times would imply that more sites are available of the appropriate type. If the loss in activity depended only on the reduced number of active sites one would expect no change in this time factor. The dependence of this time factor on the fluoride content is another indication that the modified sites have a different attraction for the reactant. In fact a linear relationship exists between the time at which the maximum coke deposition-rate is reached and the catalyst acidity shown in Fig. 9.17. This suggests that there may be a link between the generation of gas-phase C_8 isomers and the deposition process occurring on the catalyst surface.

Examination of the product desorption patterns given in Fig. 9-18 a,b and c for alumina and fluoridated alumina sheds further insight into the manner in which changes in the active sites alter the coke products formed. At the reaction temperature of 300°C, one can already distinguish distinct differences in the coke products formed on alumina and fluoride-modified alumina. There are a greater quantity of species of the type which desorb at 450°C formed on the fluoridated surface. The difference at the desorption temperature of 450°C is considerably enchanced as the reaction temperature is raised to 350°C. At still higher reaction temperatures, the peak at a desorption temperature of 450°C disappears and is replaced by a large peak at a much higher desorption temperature for both catalysts. A larger number of the species identified by a desorption temperature of 450°C and associated with catalyst deactivation are formed on the fluoride-modified alumina. A minimum in the deactivation curve can now be explained more readily. Although the rate of coke deposition (and total coke formed) decreases with increasing fluoride content, the amount of the species which leads to deactivation (450°C) increases with fluoride content. The competition between these two phenomena results in a minimum in the

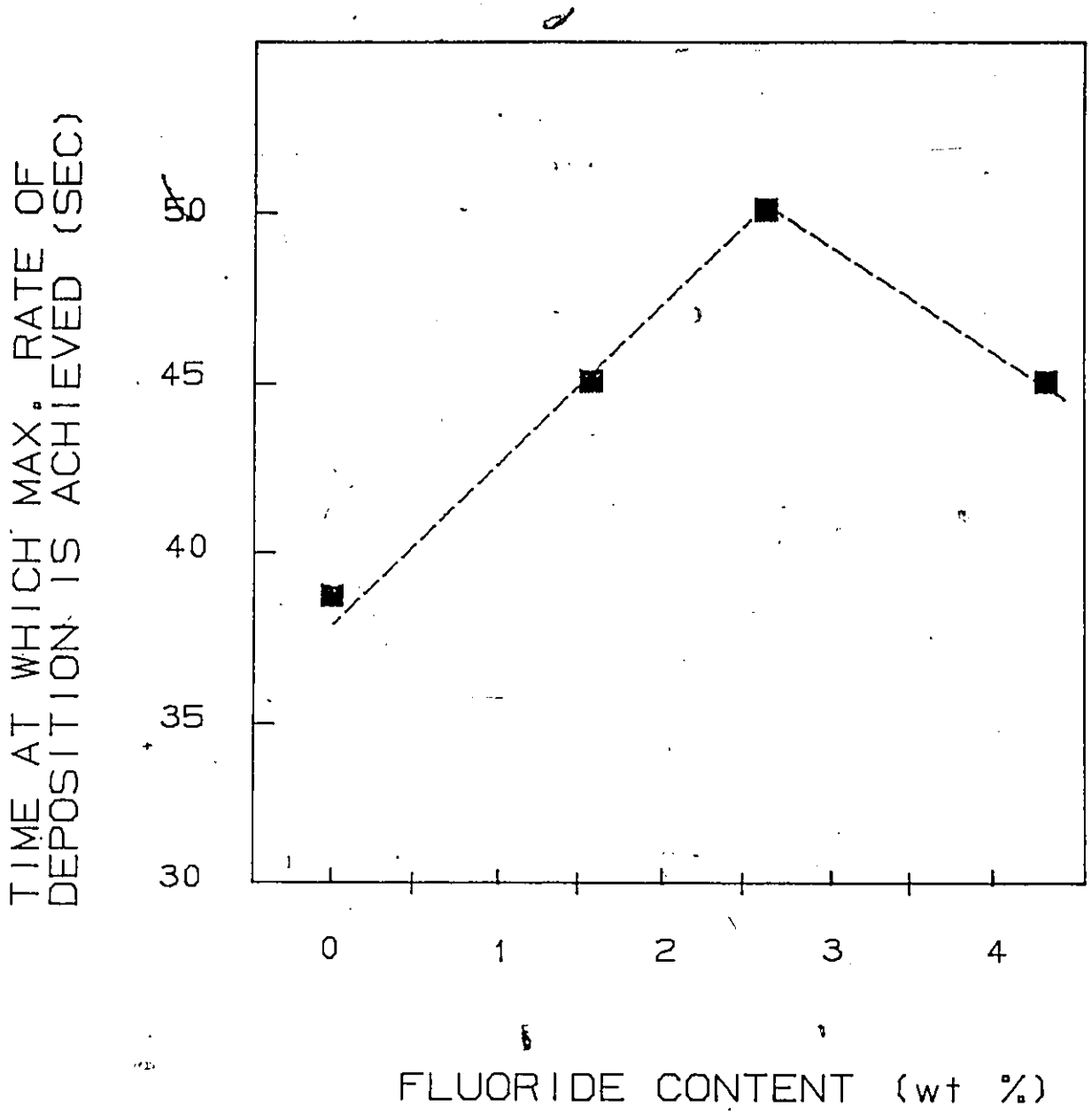

Fig. 9.16 Influence of fluoride content on the time at which the maximum rate of deposition is achieved.

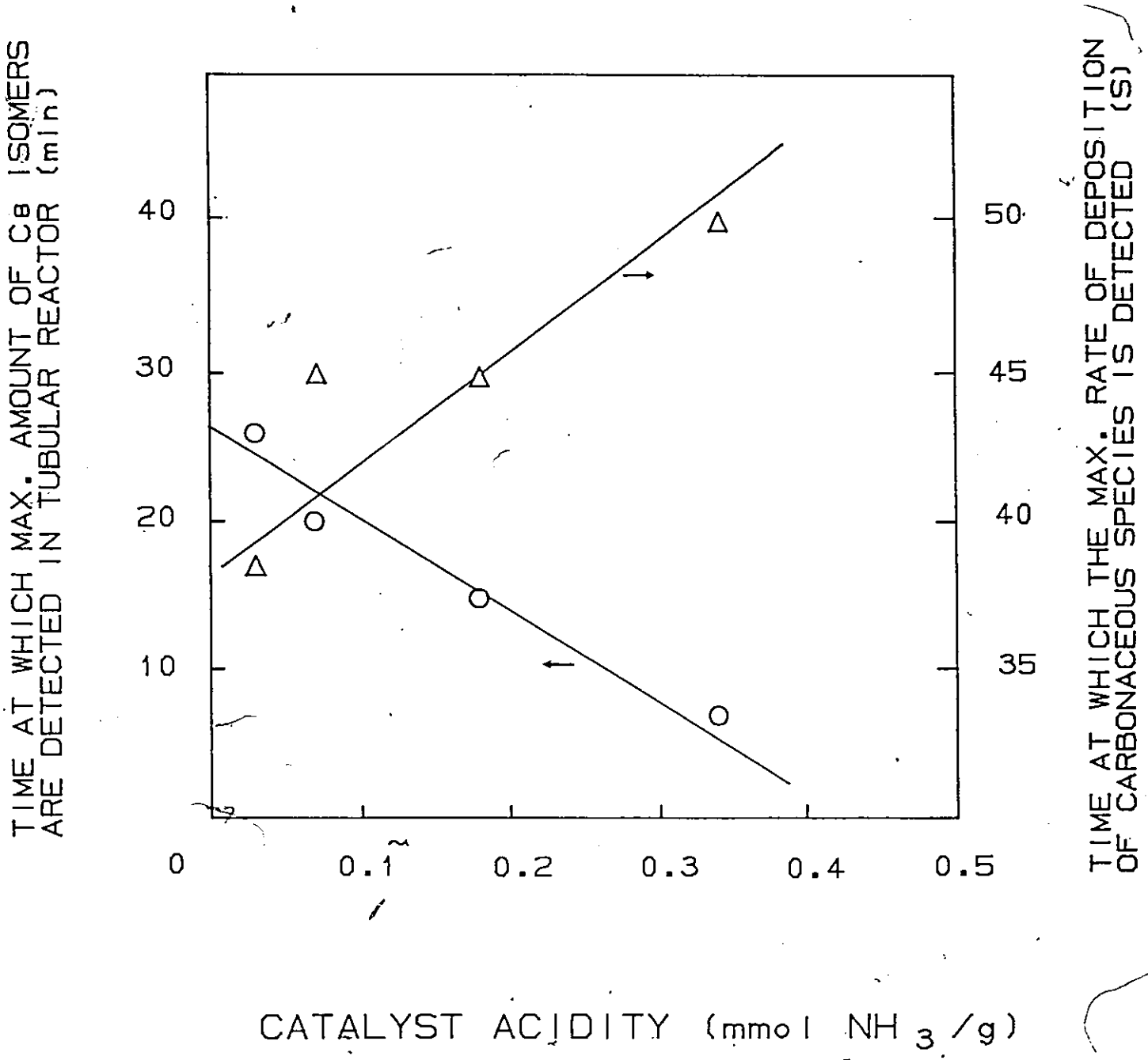

Fig. 9.17 Relationship between catalyst acidity and the time at which maximum amount of C_8 isomers are detected in the tubular flow reactor and the time at which the maximum coke deposition rate is observed.

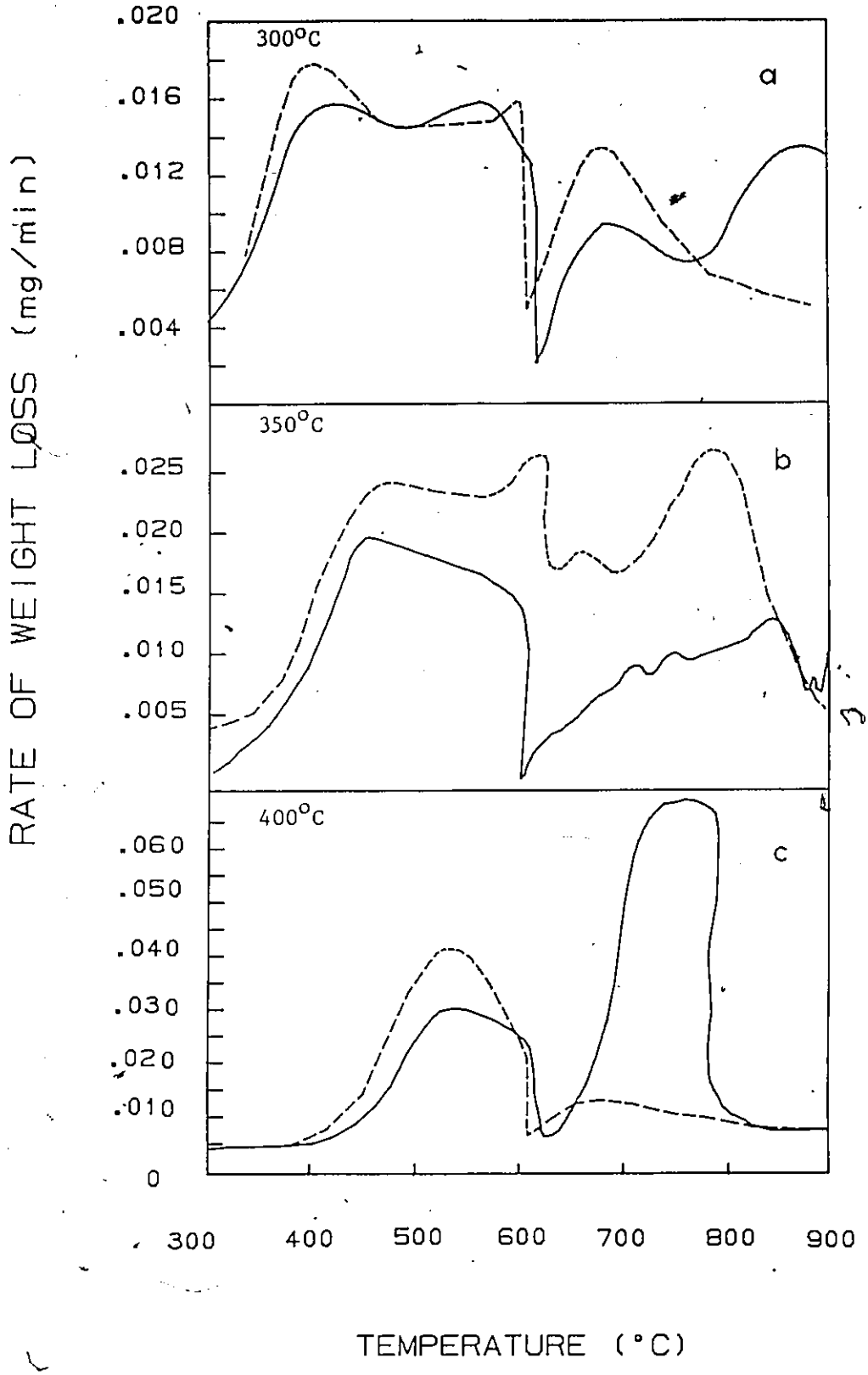

Fig. 9.18 Temperature-programmed desorption pattern as a function of fluoride content and temperature level. (5.15 v % C_2H_2, 64 mL/min)
---- 2.6 wt % F on alumina — alumina

deactivation (k_d) with respect to fluoridation.

The relationship obtained earlier between the specific rate of deactivation, k_d, and the ratio of the ^{13}C NMR signal for the aliphatic/aromatic carbon shown in Fig. 8.12 and now between k_d and the relative magnitude of the peak at a desorption temperature of 450°C both lead to the conclusion that the catalyst deactivation is a function of the nature of the active sites. The deactivation parameter, k_d, was found to increase with the aliphatic/aromatic carbon signal ratio and with the amount of coke species of the type which desorb at 450°C. It may be concluded from the above that these species must be aliphatic in nature, and more than likely unsaturated aliphatics. These compounds include linear polymers, alkenes, alkadienes.

The ionic polymerization of acetylene to high-molecular weight linear polymers has been studied to some extent in recent years (46) over Ziegler-Natta type catalysts. The polymerization occurs in the presence of large amounts of Lewis acids. It has been noted in these studies that the yield of polymer increased as the acidity of the medium increased, i.e., in the order polyphosphoric acid < sulfuric acid < antimony pentafluoride. It is highly likely therefore that the increased acidity introduced by the fluoridation process leads to an increase in linear polymer on the catalyst surface. These linear polymers of various chain lengths would then occupy the active sites and make them inaccessible for further reaction. Dehydrogenation of the linear polymer would occur quite easily at the higher reaction temperature and a carbonaceous residue would be left behind, which appears as the species which desorbs at pyrolysis temperatures above 700°C.

9.6 CONCLUSIONS

The data acquired with the microbalance and examined in this chapter confirm findings with the tubular reactor. Analysis of this data together with the models obtained using the tubular reactor proved very useful in understanding the deactivation phenomenon. The analysis suggests that the rate of coke deposition and the total coke

formed are a function of the number of active sites available for adsorption of acetylene. However, catalyst deactivation is mostly a function of the quantity of linear polymer formed in the coke and not of the total coke produced. The quantity of linear polymer formed is a function of the acidity of the catalyst and of the operating conditions. Operating conditions which minimize linear polymer formation, i.e., high temperature, high contact time, low gas phase concentration also minimize deactivation.

10. INFRARED RADIATION: ITS EFFECT ON CONVERSION AND CATALYST LIFE

It is well known that radiant energy can produce profound changes in organic material (70, 90). The exact effect produced depends on the substance irradiated and on the nature of the radiation (70). Infrared radiation provides enough energy to 'excite' molecules but not to ionize them. The amount of energy available can lead to breakage of a bond between atoms, but the atoms concerned will not, in general, lose or gain electrons and, as such will give rise to radicals. In this chapter, a comparison is made between experimental results obtained using an infrared furnace (source of infrared radiation) with those obtained using the resistance furnace described in Chapter 4.

10.1 ACTIVITY

Experimental data (4) for acetylene conversion as a function of reactor temperature, for both non-catalytic and catalytic experiments are shown in Fig. 10.1. A description of the infrared furnace may be found in Appendix 10.1. The catalytic experiments were performed with an alumina and a 2.6 wt % F on alumina catalyst. Axial temperature gradients of 5 to 10^{o}C were measured in the catalyst bed for both heating systems. In each case, greater conversions were obtained in the presence of infrared radiation.

The effect of the infrared radiation on the non-catalytic reaction shown in Fig. 10.1 can be explained in terms of two phenomena. First, the absorption of infrared radiation in the 2900-3400 cm^{-1} frequency range by gas-phase acetylene has been demonstrated by Sheppard and Simpson (90). When the energy for the thermal reaction is supplied by the infrared rays, vibrational excitation of the acetylene molecule occurs which weakens the C-H bonds. Second, the thermal conversion of acetylene which occurs only at temperatures exceeding 500^{o}C is believed to proceed via a free-radical mechanism, as proposed by Back (10). Presumably free radicals are generated from the excitation

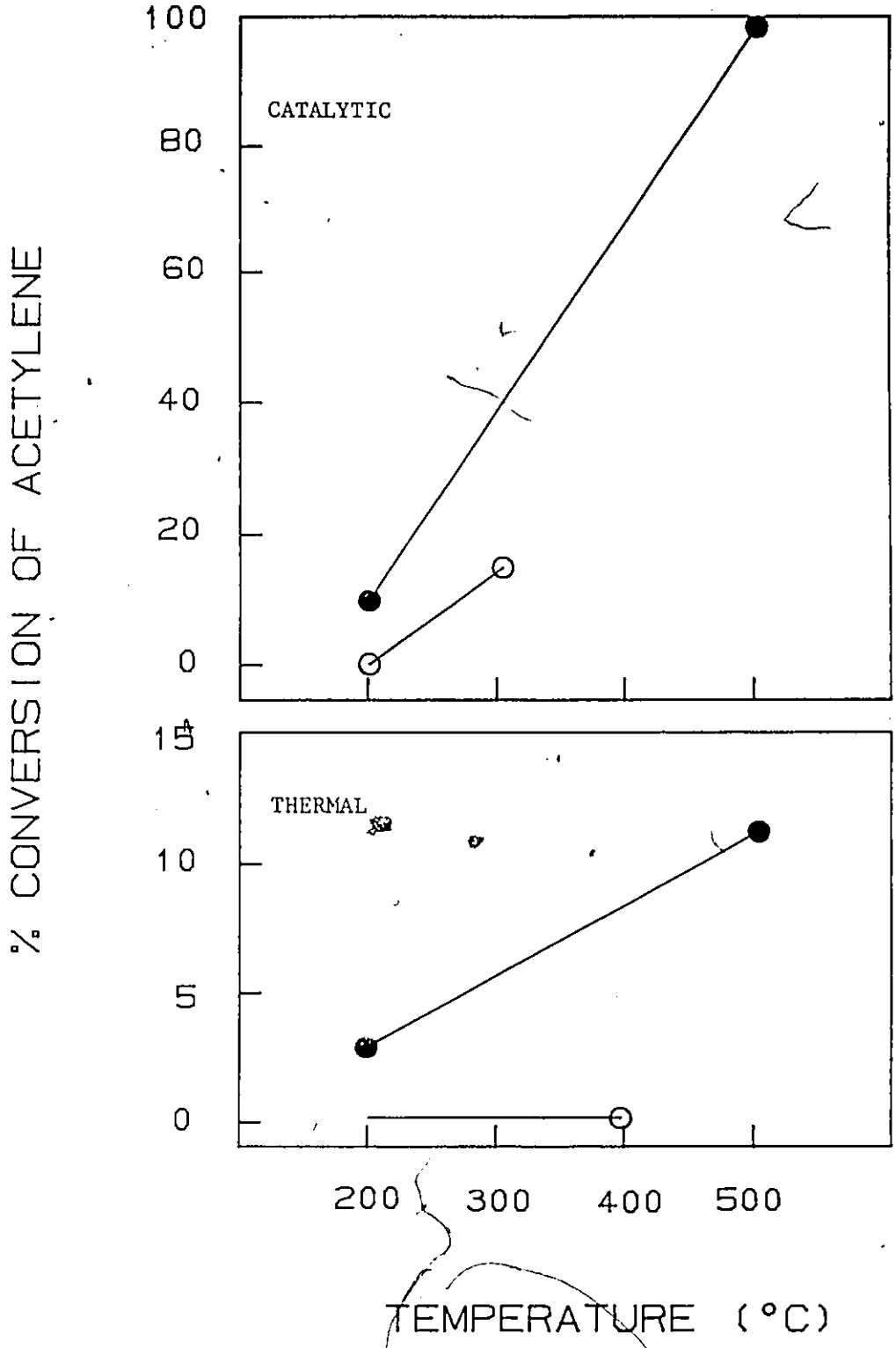

Fig. 10.1 Effect of infrared radiation on thermal and catalytic conversion of acetylene. Catalyst used had 2.6 wt % F.

● Infrared Furnace ○ Resistance Furnace

energy supplied by infrared radiation and these free radicals are responsible for the conversions observed in the non-catalytic experiments performed in the infrared furnace in the 200-500^{o}C temperature range. These findings are consistent with the fact that the rate of free-radical polymerization reactions increases as the number of free radicals increases (70).

The effect of the infrared radiation on the catalytic reaction shown in Fig. 10.1 can also be explained in terms of two phenomena. As in the thermal experiments, the gas phase acetylene absorption of infrared radiation contributes to the acetylene reactivity through vibrational excitation of the bonds in the acetylene molecule. In addition to this however, Yates and Lucchesi (100) have demonstrated that both strong and weak interactions occur when acetylene adsorbs on alumina. The strongly chemisorbed species from acetylene are held normal to the alumina surface (interaction through the C-H bond), while the weakly chemisorbed acetylene molecules are held flat on the alumina surface (interaction through C=C bond). A similar adsorption on the fluoridated alumina catalyst surface may be deduced from discussions in Chapter 7 and this adsorption may contribute to the high acetylene conversions. The greatest conversions were observed when infrared excitation of acetylene and adsorption of acetylene on the catalyst surface were combined. Induced vibrations of the bonds in the acetylene molecule may have facilitated the adsorption and subsequent transformation on the catalyst surface.

10.2 PRODUCT SPECTRUM

A significant difference was also observed in the products obtained from the catalytic experiments when carried out in the presence/absence of infrared radiation. In the former case, the product spectrum at 1 h time on stream over alumina and fluoridated alumina included H_2, C_2H_4, C_2H_6, CH_4 and a large fraction of condensable hydrocarbons (Table 10.1). In the latter case which was discussed in Chapter 7, the major product was in the condensable hydrocarbon range with ethylene, ethane, methane and light olefins

Table 10.1

Gas product distribution [mol %]

Component	No radiation[a]	Radiation[b]
C_2H_2	12.0 [c]	4
H_2	13.7	55
C_2H_4	45.8	16
C_2H_6	-	4
CH_4	28.6	6
C_6^+	-	15

[a] temperature 400 °C, 10 vol % C_2H_2 in N_2 feed, 2.6 wt % F on alumina.
[b] temperature 500 °C, 10 vol % C_2H_2 in N_2 feed, 2.6 wt % F on alumina.
[c] N_2 free basis

(C_4's) present only in traces. The presence of significant proportions of H_2 indicate a higher tendency for the decomposition reaction in the presence of infrared radiation perhaps caused by the induced weakening of the C-H bond. Nevertheless, 16 mol % of the product is light liquids (C_5 - C_8), a very high percentage after 1 h on stream. In fact, the product gas distribution changes very little with time-on-stream as observed in Fig. 10.2.

The molecular weight distribution of the condensed liquid product over both catalysts in the presence of infrared radiation is very similar and spans a wide range. An example of the simulated distillation boiling point curve is given in Fig. 10.3. Typical compounds which were identified by GC/MS include: naphthalene, indene, tetralin and substituted compounds of these. Many of these were also identified in the products of the transformation in the absence of infrared radiation.

10.3 CATALYST DEACTIVATION

The most dramatic effect of the infrared radiation was in extending catalyst life. The conversion of acetylene as a function of time-on-stream in the presence/absence of infrared radiation is shown in Figs. 10.4 and 10.5 for alumina and 2.6 wt % F on alumina catalysts respectively. It is evident with both catalysts that the use of infrared radiation significantly lengthens catalyst life. The mechanism outlined in Chapter 11 may be used to explain this finding. The energy provided by the radiation may be sufficient to overcome the activation energy barrier of the ring-chain reaction (Eq. 11.9) and lead to higher amounts of ring compounds, benzene, xylene. Less linear polymer will be formed and as a result less deactivation will be evidenced (see Chapter 8). In addition, a weakening of the interaction between the growing polymer chain and the catalyst surface will increase the ability of the chain to delocalize the positive charge of the active centre over itself (Eq. 11.9). More explicitly, the radical will be favored over the cation form. Less linear polymer is expected when this occurs. Despite the fact

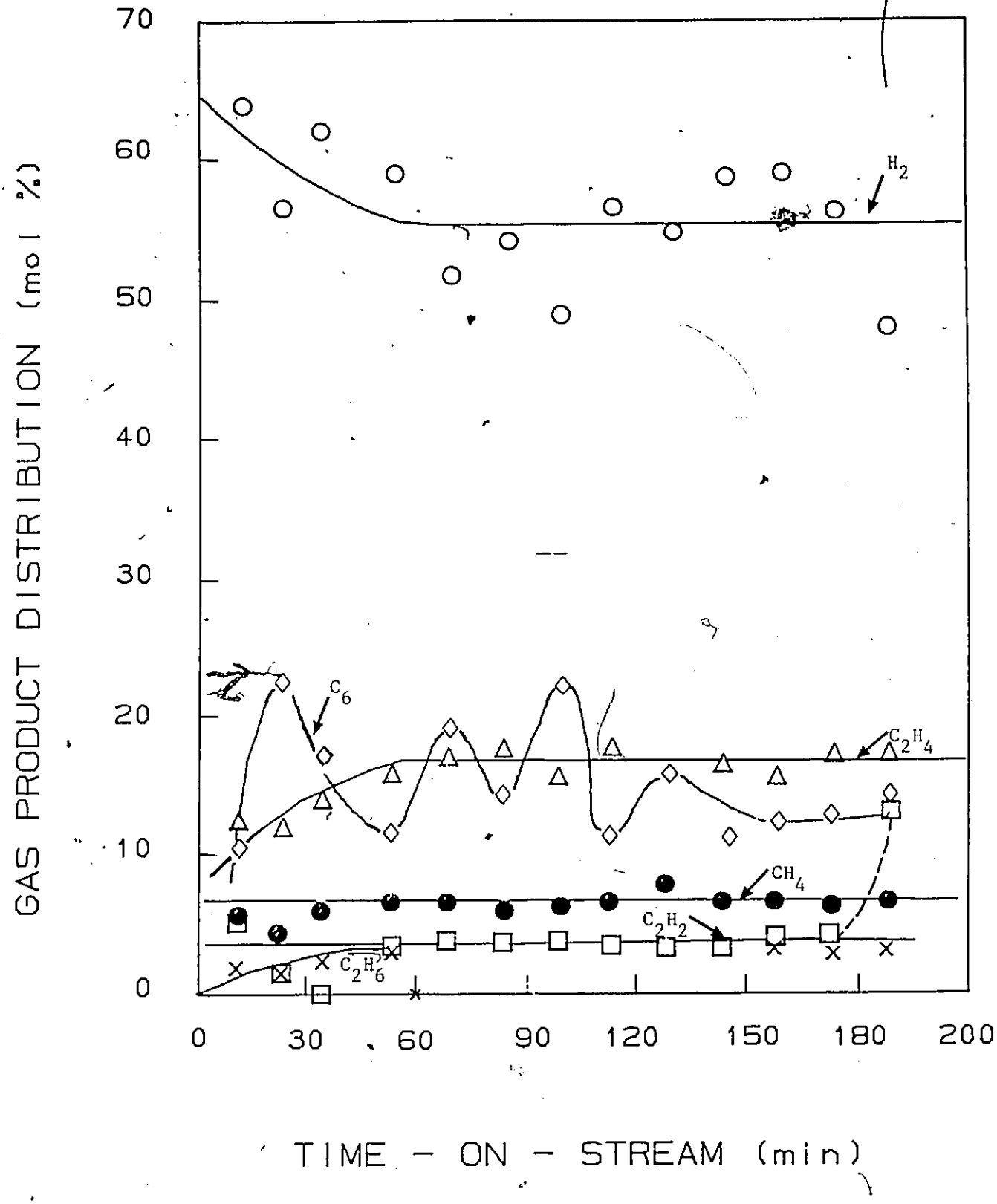

Fig. 10.2 Product gas distribution as a function of time in the presence of infrared radiation. (500°C, 250 mL/min, 10 vol % C_2H_2, 2.6 wt % F on alumina)

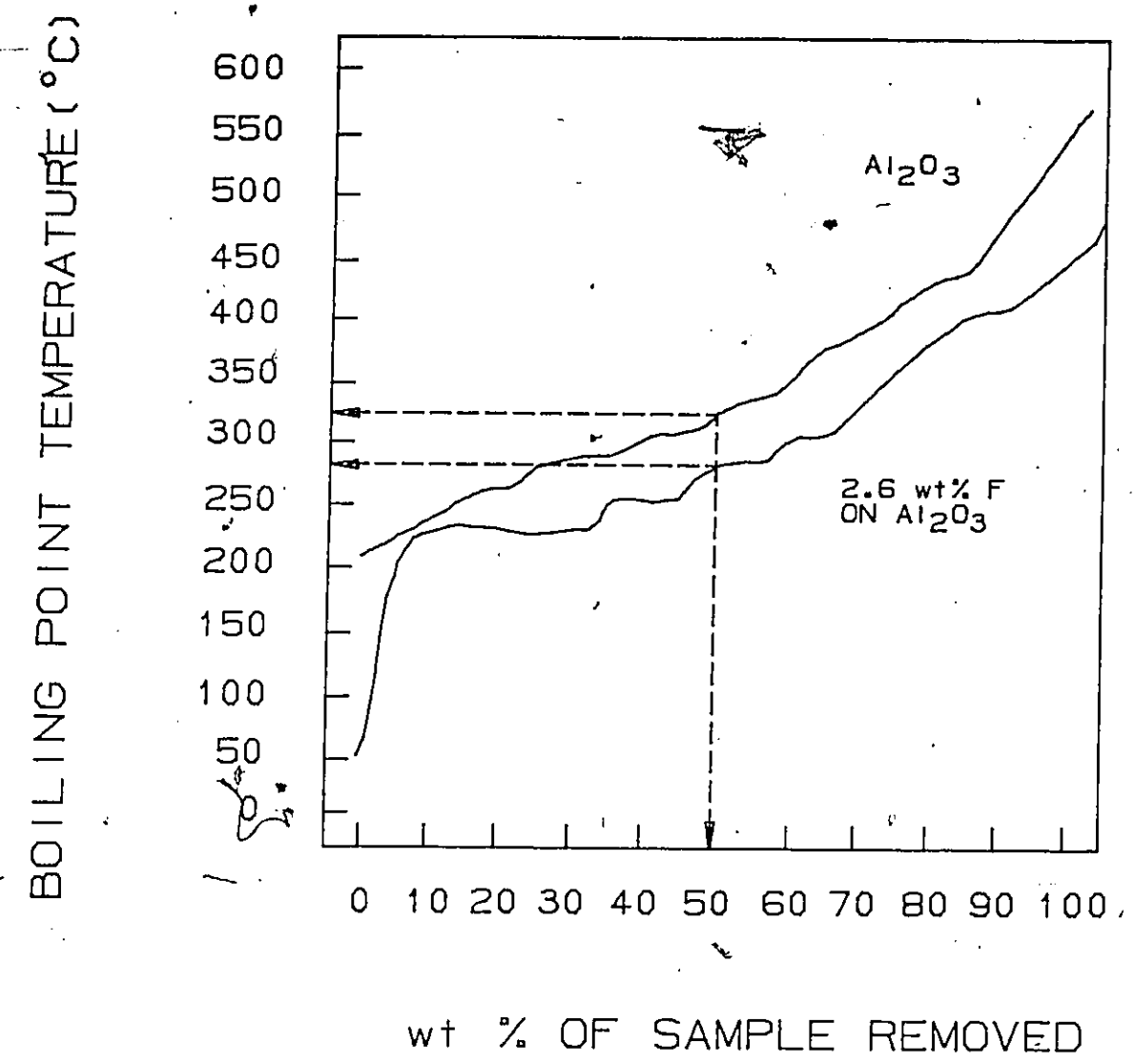

Fig. 10.3 Simulated distillation curve for condensable products of acetylene conversion in presence of infrared radiation.

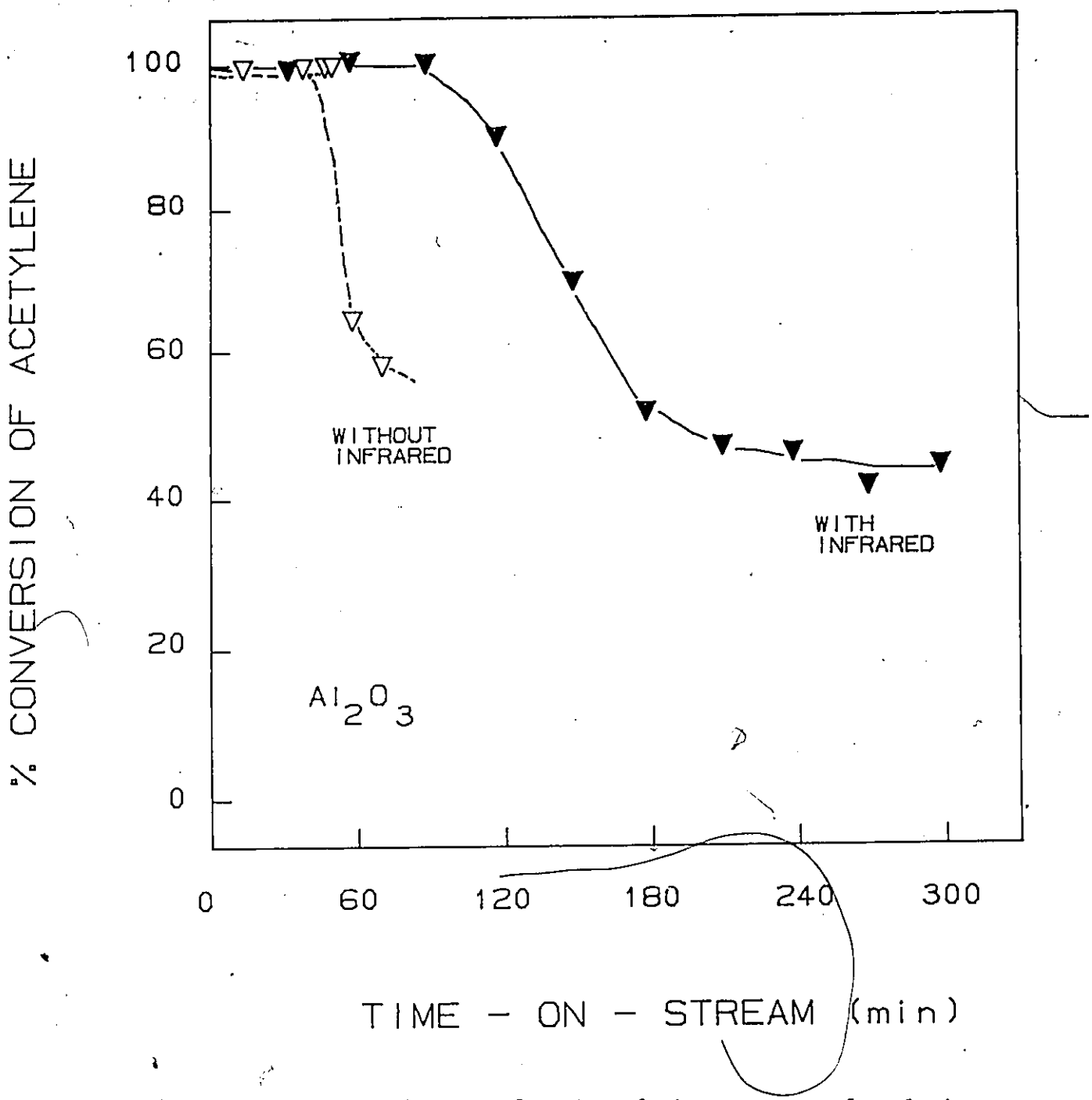

Fig. 10.4 Acetylene conversion as a function of time-on-stream for alumina in absence and presence of infrared radiation.

▼ 500°C, 2 g.s.mL^{-1}, 10 v % C_2H_2

▽ 350°C, 2 g.s.mL^{-1}, 10 v % C_2H_2

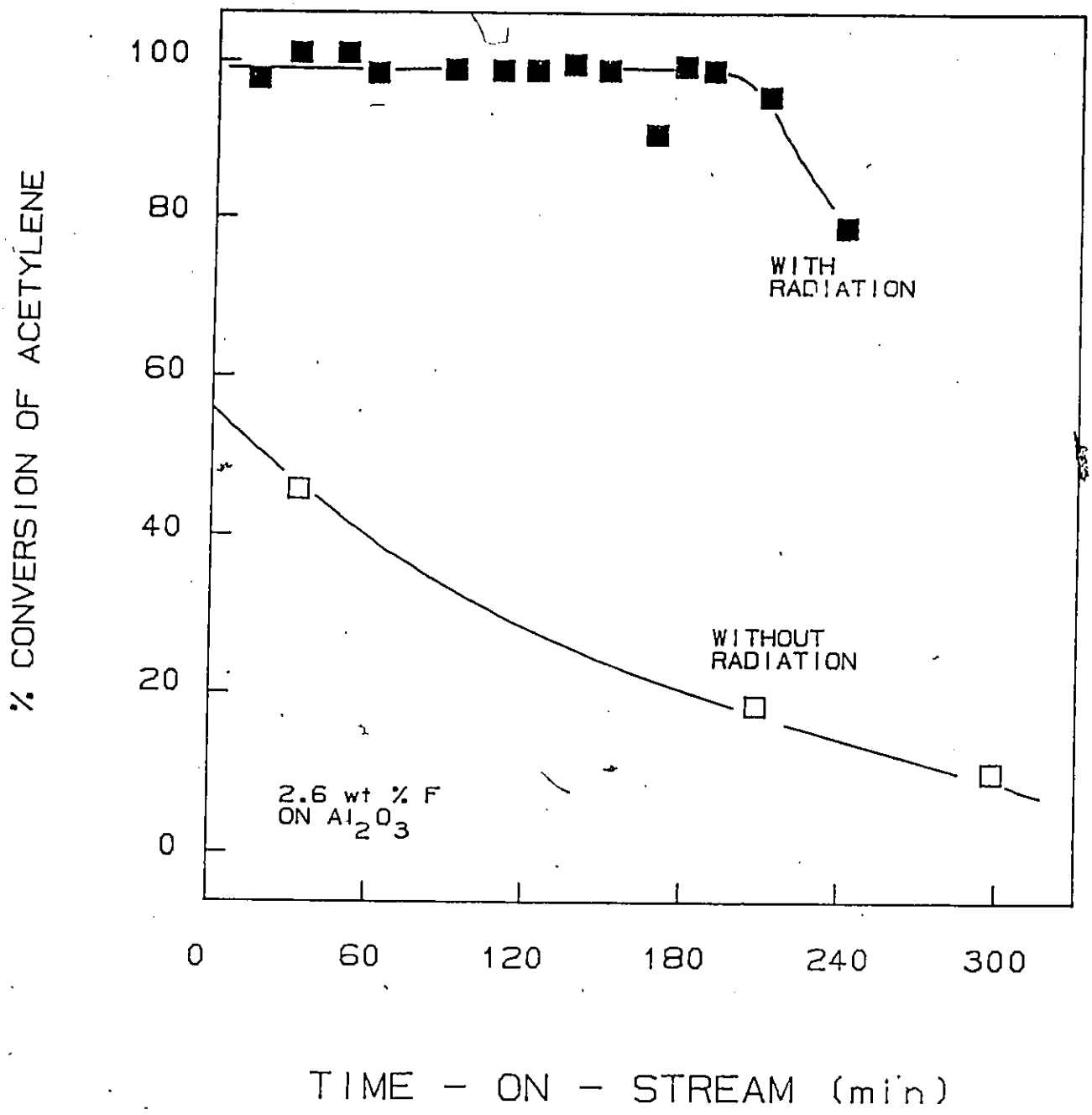

Fig. 10.5 Acetylene conversion as a function of time-on-stream for fluorided alumina in absence and presence of infrared radiation.

■ 500°C, 2 g.s.mL^{-1},10 v % C_2H_2

□ 350°C, 2 g.s.mL^{-1},10 v % C_2H_2

that limited linear polymer is formed, decomposition of acetylene to its elements is noticeable (high carbon content of the catalyst, 12 wt % carbon on Al_2O_3 and 21 wt % carbon on fluoridated Al_2O_3 after 5 h on stream). It is the accumulation of this "free carbon" which eventually begins to deactivate the catalyst sites.

10.4 CONCLUSIONS

The severe catalyst deactivation reported in earlier chapters was significantly reduced by external means. Alumina and fluoridated alumina lifetimes were doubled with the use of infrared radiation. These findings have been explained in terms of the following two phenomena. The excitation energy provided by the radiation was sufficient to overcome the energy barrier in the chain to ring reaction. The low-level energy was also sufficient to induce radical formation at the end of the growing polymer chain at the expense of active cations.

11. THE REACTION MECHANISM

The reaction of acetylene to produce hydrocarbons can be visualized as a polymerization process. Polymerization reactions may be written generally as:

$$x\text{-mer} + y\text{-mer} = (x + y)\text{-mer}$$

and are divided into two types based on the mechanism of the growth reaction, step growth and chain growth (48). In step growth, x and y may assume any value, i.e., chains of any size may react together as long as they are capped with the complementary functional end-groups. In step growth therefore, one type of reaction is involved in the reactions of either two monomer units with each other, a monomer with the end group on a polymer chain or two polymer chain end groups. Chain growth polymerization, on the other hand, generally consists of three different types of reactions, an initiation reaction which creates a highly active species; a propagation reaction in which the only reaction possible is the addition of monomer to active polymer chain end groups (i.e., y-mer is confined to monomer) and termination in which the activity of the end groups is destroyed and the polymer chain can no longer add new monomer units.

11.1 THE STEP GROWTH REACTION MECHANISM

A detailed and quantitative treatment of polymerization reactions which occur by the step-growth mechanism is given by Flory (31). In the development which follows, let

M = monomer

p = probability of finding a reacted M group
i.e., the conversion or extent of reaction

(1-p)= probability of finding an unreacted M group

N = the total number of molecules present in the reaction system

n_x = the number of molecules containing x M groups, both

reacted and unreacted

x = the number of monomer units in the chain

The probability of finding a molecule with x M groups (reacted and unreacted) is equal to the mole or number fraction of those molecules present in the reaction mass, n_x/N. This in turn is equal to the probability of finding a molecule with (x-1) reacted M groups and one unreacted M group, and since the total probability is the product of the individual probabilities,

$$\text{mole fraction } x\text{-mer} = n_x/N = p^{(x-1)}(1-p) \qquad (11.1)$$

This result gives the distribution of chain lengths in the reaction mass as a function of the conversion. The distribution results from the random nature of the reaction between chains of different lengths. In this number fraction distribution, the shorter chains are always more numerous, i.e.,the longer the chain length the fewer there are. Eq. 11.1 can be rearranged to

$$M_x = n_x/N = p^x (1-p)/p$$

where M_x is the mole fraction of a polymer with x monomers. After taking the logarithm of both sides, one arrives at the Flory equation for the number fraction.

$$\ln(M_x) = x \ln(p) + \ln((1-p)/p) \qquad (11.2)$$

A plot of $\ln(M_x)$ versus x would produce a straight line of slope, ln p, and intercept ln((1-p)/p). The Flory equation (Eq. 11.2) provides a macroscopic method to predict the molecular weight distribution of polymerization in a dynamic equilibrium state (31). This equation derived from a statistical treatment of the reaction system, is based on the assumption that all the functional groups involved in the polymerization process have the same reactivity. It has been applied successfully to predict molecular weight distributions of linear condensation polymers (31), to predict hydrocarbon distributions produced from the Fischer-Tropsch reaction (7) and to predict light olefin distributions in the synthesis of olefins from methanol (98).

The products from the polymerization of acetylene discussed in Chapter 7 were

not in thermodynamic equilibrium, therefore, the selectivity data contains valuable mechanistic information. With this in mind, a plot of the logarithm of the mole fraction of the product distribution found in thermal experiments carried out at 600°C in a flow reactor (20) is given in Fig. 11.1a starting with C_5. This plot shows a significant departure from linearity for the C_5 point. However, if benzene is chosen as the first product formed by the step growth process, the Flory plot starting from benzene produces a good straight line. Simple linear regression gives a correlation coefficient of 0.94 and an extent of polymerization, p, of 0.5 (Appendix 11.1). This p-value represents the probability of a stepwise reaction of the Flory-type. Although there is a high degree of correlation with the Flory equation observed for the products obtained from the thermal reaction of acetylene this does not prove that the reaction of acetylene with benzene and higher hydrocarbons, to give the next higher molecular weight homolog proceeds by a step growth mechanism.

For comparative purposes the liquid product distribution obtained over ZSM-5 (94) and over fluoridated alumina (data from this work) are also shown on the Flory plot (Fig. 11.1b). The lack of correlation of the product distribution obtained in the catalytic conversion of acetylene with the Flory equation would imply that the products are derived from a different mechanism than the step growth addition reaction. The underlying assumption of this mechanism, i.e., equal rates of formation of all the products is not likely in the case of the catalytic reaction.

Examination of the effects of reaction temperature, weight-time and concentration of acetylene on the total product yield and on the liquid product distribution which was presented in Chapter 7 reveals clues as to a possible reaction mechanism for the catalytic reaction.

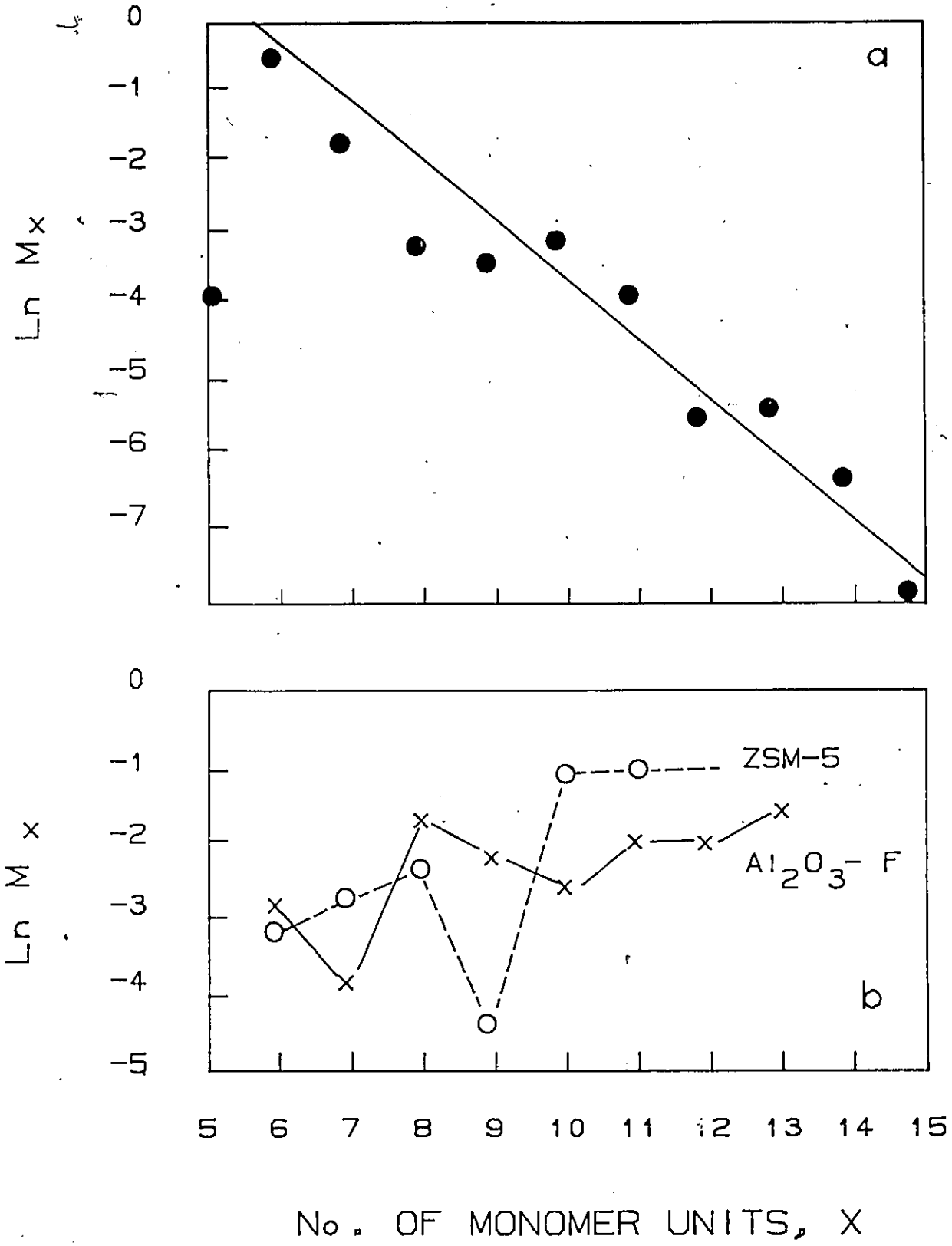

Fig.11.1 Flory plot of product distribution from the transformation of acetylene
a) thermal b) in presence of ZSM-5 and 2.6 wt % F on alumina.

11.2 THE CHAIN GROWTH REACTION MECHANISM

As stated earlier, in chain growth polymerization, three different types of reactions are believed to occur, initiation, propagation (growth) and termination. Chain growth polymerizations are divided into two categories, depending upon which type of chain carrier is involved, ionic or radical. Free-radical chain polymerization is initiated and continues by the action of free radicals, electrically neutral species with an unshared electron. Ionic chain polymerization may be either cationic or anionic depending upon whether the initiation and propagation steps occur through cations or anions respectively.

11.2.1 Free-Radical Reactions

Back (10) has suggested a homogeneous free-radical chain mechanism to describe the kinetics of the thermal polymerization of acetylene over a wide temperature range. In the development which follows, a dot will represent a single electron. The free-radical polymerization of acetylene can be described by the following reaction sequence:

INITIATION:

$$2\,C_2H_2 \longrightarrow {}^{\bullet}C_2H + {}^{\bullet}C_2H_3$$

PROPAGATION:

$${}^{\bullet}C_2H + C_2H_2 \longrightarrow {}^{\bullet}C_4H_3$$

$${}^{\bullet}C_2H_3 + C_2H_2 \longrightarrow {}^{\bullet}C_4H_5$$

TRANSFER: (a) intramolecular

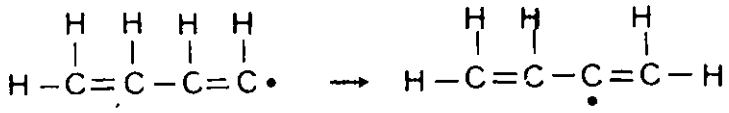

(b) intermolecular

$${}^{\bullet}C_4H_3 + C_4H_6 \longrightarrow C_4H_4 + {}^{\bullet}C_4H_5$$

TERMINATION: (a) by disproportionation

$${}^{\bullet}C_4H_5 + {}^{\bullet}C_4H_3 \longrightarrow C_4H_4 + C_4H_2$$

(b) by combination

$$2\,{}^{\bullet}C_4H_3 \longrightarrow C_8H_6$$

$$2\,{}^{\bullet}C_2H_3 \longrightarrow C_4H_6$$

The conditions under which the polymerization is carried out can influence the relative rates of these various reactions, and so the product distribution can be determined by control of reaction pressure, temperature, etc. In general, however, as in the step-growth mechanism described earlier, a distribution of chain lengths is obtained in free-radical reactions because of the inherently random nature of the termination reactions with regard to chain length. Theoretical calculation of the distribution is more complex in this case because of the number of reactions involved. Addition polymerization reactions can give the distribution obtained in Fig. 11.1a provided the termination stage does not involve the coupling of two chains (70). This implies therefore that at least in the case of the thermal reaction, termination does not occur by combination or disproportionation. Exactly what the other possible termination reactions might be in this process is not clear.

The increase in the thermal conversion observed in the presence of infrared radiation (Chapter 10) can be attributed to an increase in the initiation reaction (generation of radicals) due to the induced excited state of the acetylene molecules. Although all the reactions will be affected, the initiation reaction will be affected most because it is second order in the concentration of acetylene.

11.2.2 Ionic Chain Growth

A mechanism for the catalytic cyclization of acetylene to aromatic compounds, particularly benzene over solid oxides, has not yet been elucidated. The high reactivity of unsaturated acetylene make it susceptible to polymerization by anionic, cationic or free-radical processes. Both anionic and cationic initiation have been used to produce polymers from acetylene (59, 77). The ionic chain polymerization of acetylene leads to the formation of polymers with a degree of polymerization, x, equal to 10 (i.e., 10 repeated units in the polymeric chain) (59, 77). The solid product in the present studies consisted of at least 3 types of deposits (Chapter 9) and the molecular weights of the

individual deposits could not be determined. However, the highest molecular weight material which was observed in the liquid product was 275 corresponding roughly to 10 monomeric units of acetylene which is consistent with the ionic mechanism.

One plausible mechanism, first postulated by Tsai and Anderson (94) can be described by the general scheme,

$$\text{acetylene} \longrightarrow \text{n-polyene} \longrightarrow \text{aromatic} \qquad (11.3)$$

Polymerization of acetylene to polyene has been observed by Raman spectroscopy at the surfaces of alumina (42), zeolite KX (42) and TiO_2 (78). Although the extent of polymer formation was relatively small, its presence was beyond question. With these oxide catalysts, the polymerization mechanism is not known. Tsai and Anderson (94) proposed the vinyl cation route (cationic initiation) for conversion of acetylene over ZSM-5 to yield a 'C_6-polyene' intermediate which then cyclized to benzene (Chapter 2). Higher carbon number aromatic compounds, e.g., toluene and xylene are believed to be formed from a two carbon-atom precursor via cracking and isomerization reactions. The distribution pattern shown in Fig. 7.6 implies a much longer polyene chain is formed at the outset.

Analysis of the liquid product distribution obtained in the present study with alumina and fluorided alumina (Fig. 7.6) corroborates Eq. 11.3, however, the polyene chain formed at the outset appears to contain more than 3 monomeric units. As shown in Fig. 7.6, under conditions of low conversion the growing chain is not starved for monomer and the polyene will grow over the length of the catalyst bed. On the other hand, under conditions of high conversions, the growing chain is starved for monomer and the secondary reactions of the cyclic products which are desorbed can take place over the bulk of the catalyst bed since dealkylation and condensation reactions are also acid catalysed.

Evidence from Chapters 8 and 9 further supports the formation of a 'polyene'. The low activation energies observed (7-8 kcal/mol) are consistent with those reported for cationic chain polymerization (77). In addition, catalyst deactivation over these catalysts actually decreased as the temperature was increased (Fig. 8.10, k_d vs

temperature). The decrease in deactivation was linked to a decrease in the surface deposit which was associated with CH fragments (Chapter 9). Many polymerization reactions are favored by lower temperatures, therefore these findings also support the premise of the 'polyene'.

11.2.3 Proposed Reaction Mechanism

A modified mechanism is postulated in Fig. 11.2 involving cationic chain growth polymerization leading to both linear and cyclic products. The reactions of cationic chain polymerization specifically, initiation, propagation (growth), transfer and termination are presented and discussed below:

The Initiation Reaction

Cationic initiation may be expected with highly unsaturated monomers such as acetylene. On the other hand, strong Lewis acids behave as electron acceptors and are good initiators of cationic polymerization (45, 77). Little is known about heterogeneous cationic initiation of acetylene but some insight can be gained from homogeneous systems.

In homogeneous cationic polymerization, Lewis acids such as $AlCl_3$ and BF_3 are electrically neutral, but they are two electrons short of having a complete valence shell of eight electrons. These compounds require traces of co-catalyst, usually H_2O, to initiate polymerization, first by accepting a pair of electrons from the co-catalyst as illustrated below:

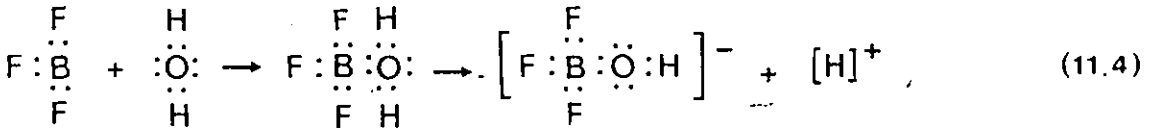

(11.4)

The leftover proton is believed to be the actual initiating species abstracting a pair of electrons from the monomer and leaving a cationic chain end which reacts with additional monomer molecules (80).

By analogy to this homogeneous chemistry, active sites must exist on the catalyst surface to generate the polymerization initiator. As discussed in Chapter 5,

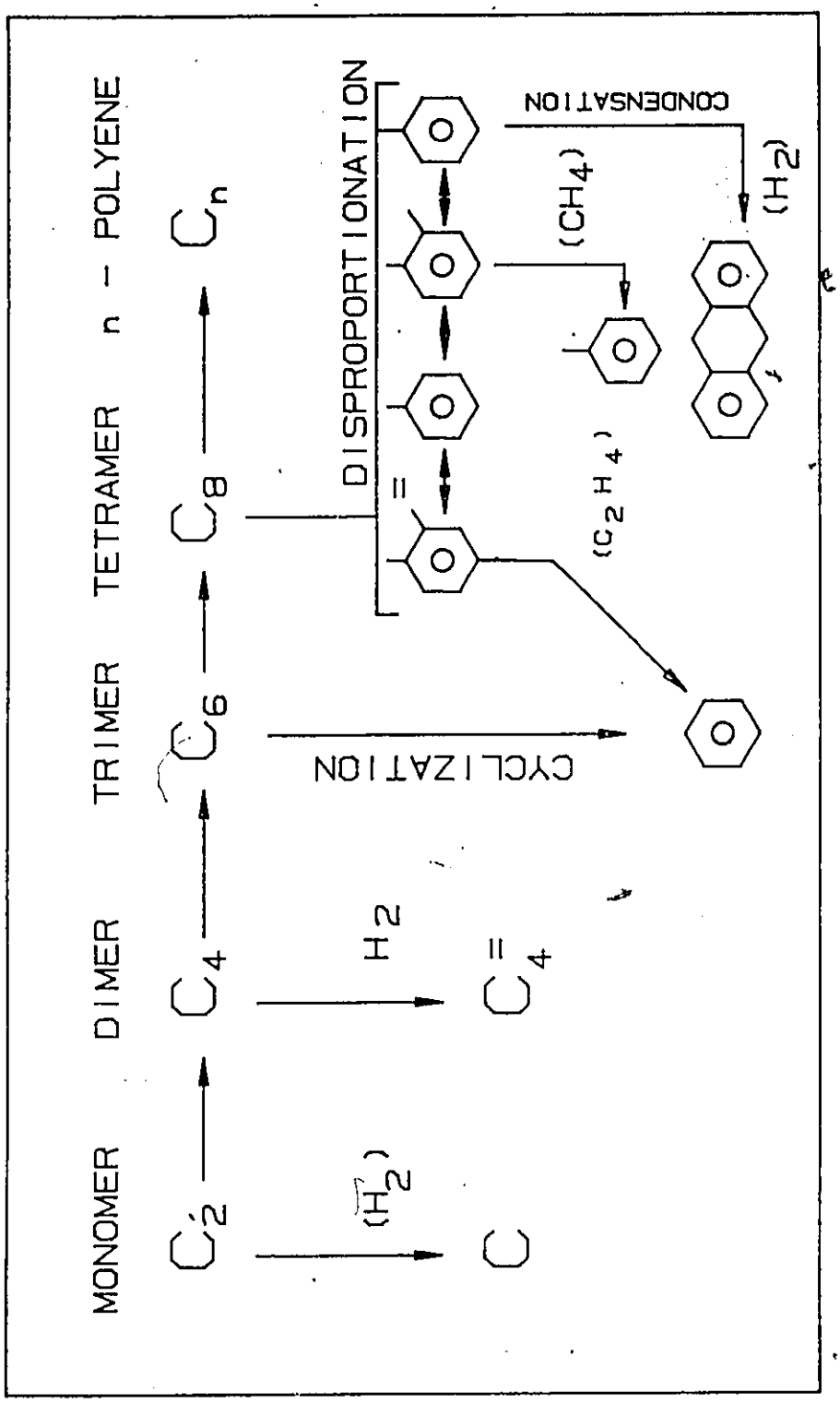

Fig.11.2 Postulated mechanism for acetylene conversion to reaction products observed over alumina and fluorided alumina.

alumina and fluorided alumina are believed to contain Lewis acid centres as well as a small number of Bronsted centres. This fact satisfies the above criterion, and favors the mechanism postulated.

Tsai and Anderson (94) proposed that in ZSM-5 the H^+ from the hydroxyl groups in the zeolite (Bronsted sites) served to generate a vinyl cation as the initiator:

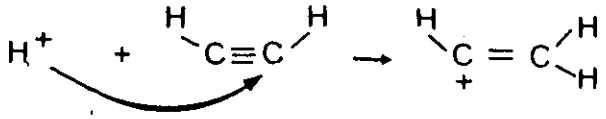

(11.5)

Acidic and basic sites on the surface of alumina can be pictured according to the following scheme (72). The Lewis acid site is visualized as an incompletely coordinated aluminum atom formed by dehydration and the Bronsted site as a Lewis site which has adsorbed moisture, while the basic site is considered to be a negatively charged oxygen atom.

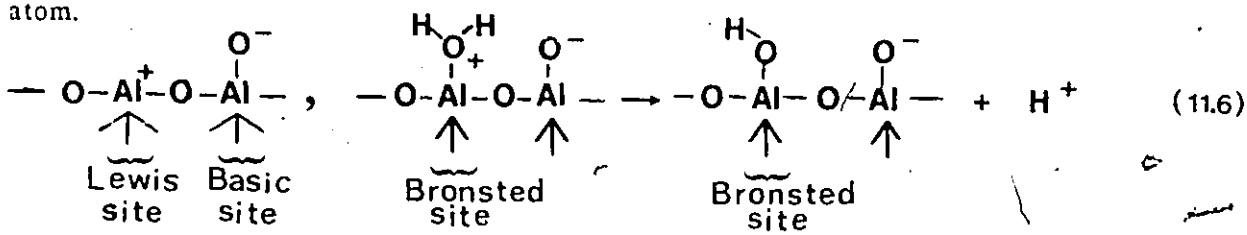

(11.6)

The Bronsted acid sites could possibly be the source of H^+ for the initiation reaction shown in Eq. 11.4. However, two facts make this route doubtful. First, alumina is a very reluctant Bronsted acid (Chapter 5). Second, the gas-phase vinyl cation has a high energy and is extremely reactive (ΔH_f^{298} = 266 kcal/mol). It seems more likely therefore that the initiating species is formed due to the presence of the Lewis sites.

Spectroscopic studies discussed in Chapters 2 and 10 have shown that acetylene adsorbs in two modes on alumina, head on (interaction through the C-H) and flat (interaction through C-C). The flat orientation was shown to be weakly adsorbed acetylene while the head-on orientation was strongly adsorbed acetylene. It is possible therefore that a polarized compound is formed upon chemisorption on the catalyst which then acts as the initiator:

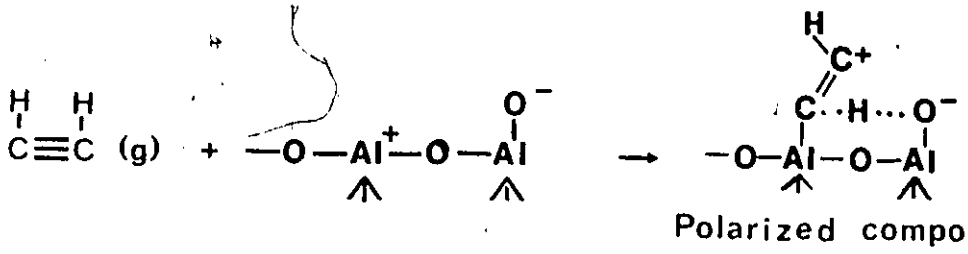

(11.7)

The rate of initiation and thereby the concentration of the initiator should increase as the number of acid sites increases. Adsorption and polarization will be a function of acid strength. Fluoridation, as discussed in Chapter 5, strengthens the Lewis acid sites and introduces some Bronsted acidity, both features would enhance this reaction. Since the rate of polymerization is a function of the concentration of the initiator, it is expected that the rate should increase as the total acidity is increased (Figs. 6.6 and 6.10).

The Propagation Reaction

Propagation or growth of the polymer consists of addition of monomer to the active centre of the growing chain (polarized compound or vinyl cation).

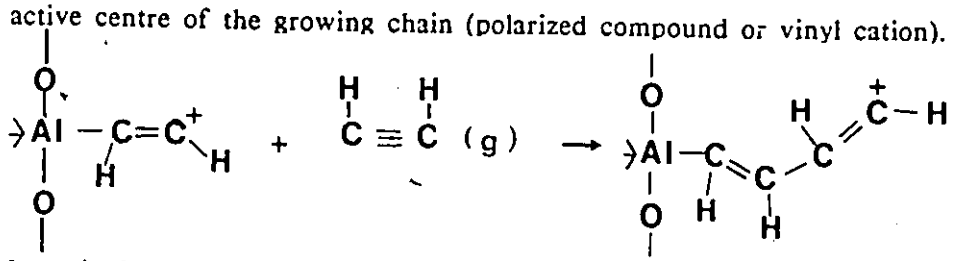

(11.8)

In cationic chain polymerization of acetylene, an electron is transferred from a polyene chain to an active centre with formation of a radical at the end of the chain and a radical-cation delocalized over the conjugation system (59).

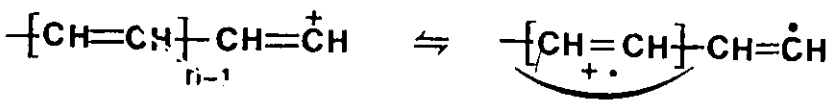

(11.9)

With acetylene, the isomerization of active centres (electron transfer) occurs in the first 2 or 3 units of the chain (77). Furthermore, formation of a ring stabilizes the ion at the end of the chain, for example, phenylacetylene. Cyclic products are obtained by

intramolecular ring closure and terminate the polymerization sequence. The chief factor determining whether rings or chains will be produced is the size of the rings which will be formed. Five-membered rings are the most stable. Six- and seven-membered rings are moderately stable and will usually compete with chain formation so that both products are formed. Both linear polymer and cyclic tri- and tetra-mers have been obtained in the conversion of acetylene using homogeneous catalysts (59). Moreover, benzene, toluene and ethylbenzene were obtained as cyclo-oligomerization products over Ziegler catalysts (77).

In order to have chain propagation, the catalyst must have powerful electron acceptor sites capable of forming stable donor-acceptor or radical-ion complexes with the polyene-chain. For linear growth to occur, the active site must be maintained, therefore the isomerization of the active centre by electron transfer must be minimized. When the polyene chain forms a complex with the catalyst the electron density cannot be displaced in the direction away from the polyene chain (to the right).

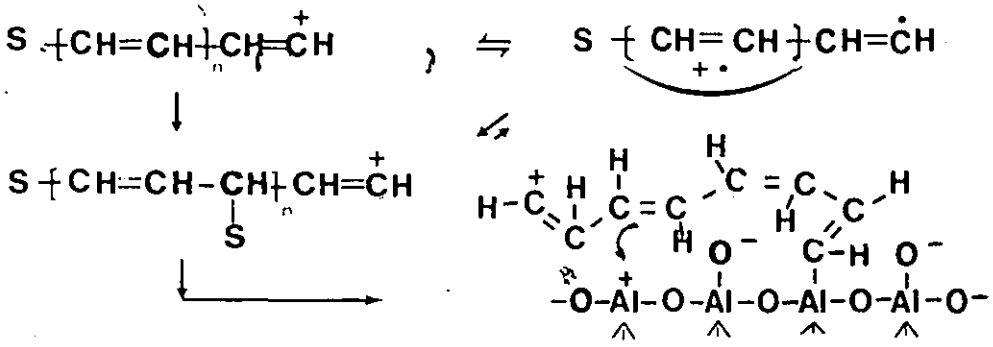

(11.10)

Chain propagation is therefore not prevented. In the presence of a sufficient number of electron acceptor sites (Lewis acid sites), the cationic polymerization without electron transfer will lead to high molecular-weight product. In fact, once a polymeric film deposits on alumina, the activity for chain growth drops drastically and an increase in the cyclic product is observed (Fig. 7.8). As the catalytic sites are covered with non-desorbable polymer the monomer could then react on this surface film and fewer contacts with the donor-acceptor sites occur. The chain length decreases due to an

increase in the electron transfer reaction which follows from the lack of complexing. Stabilization of the chain occurs through cyclization and produces a notable increase in benzene as a function of time-on-stream.

In the mechanism proposed, the number of donor-acceptor sites plays an important role in determining the chain length. Fewer sites would imply formation of less polymer and higher possibility of cyclization brought about by the transfer reaction. In support of this, one can see that as the degree of fluoridation increases, the maximum in the tetramers produced (Figs. 7.6 and 9.16) is achieved at earlier times-on-stream in response to the fewer sites. Catalysts containing the highest number of "ion-pair" sites show an increase in benzene levels with time-on-stream and simultaneously with the reduction of available surface sites by polyene formation (Fig. 7.8).

On the other hand, stronger sites would also be expected to promote the propagation and minimize the transfer reaction. When one compares the liquid product distribution over Al_2O_3 and fluoridated Al_2O_3 (2.6 wt %) in Fig. 7.7, it is evident that large levels of BTX are observed over the more acidic catalyst. No high molecular weight material appears probably because macromolecules are formed very quickly and do not leave the surface. As the polyene layer continues to form, the increase in the transfer reaction, due to the higher polyene-monomer interactions as compared with the surface monomer interactions, appears to offset the loss in intiator (due to covered sites) and benzene levels are maintained even after 1 h on stream (Fig. 7.8). At higher loadings of fluoride, both the acidity and the number of sites are greatly reduced. Therefore the compensation for loss of initiator (due to the loss in acidity and the number of sites) cannot be maintained by the low polyene transfer reaction (due to the low number of sites). As a result, the yield of benzene falls steadily with time-on-stream.

An increase in the conversion of acetylene over these catalysts in the presence of infrared radiation can probably be attributed to the ease with which the excited acetylene molecule can be converted into the polarized compound. Moreover, the fact that

t/

the catalyst lifetime has been increased significantly implies that isomerization of the active centres leading to cyclization products must be enhanced. This implies either a weakening of the growing chain surface interaction or an increase in the stabilization energy of the ring structures. A combination of these effects would certainly reduce the formation of long 'polyene' chains (C_9^+).

The Termination Reaction

Several termination mechanisms are possible. One type of chain termination occurs when macromolecules capable of giving up an electron to the active centre succeed in stabilizing the ions by cyclization as shown below:

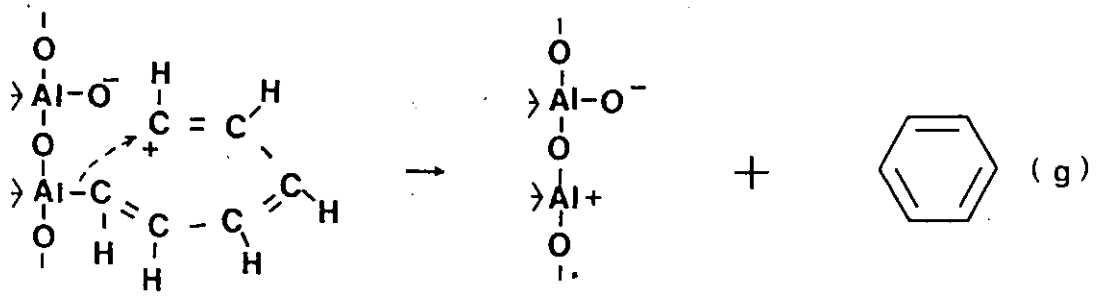

(g)

This type of termination regenerates the catalyst. Another possibility involves a disproportionation-like reaction:

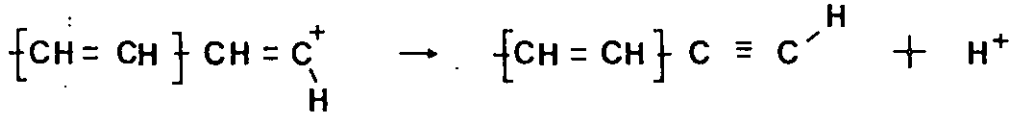

This type would generate new initiator molecules.

11.3 IMPLICATIONS AND CONCLUSIONS

The mechanism proposed in this section is consistent with all the experimental observations of this study. A summary of this evidence is given in Table 11.1. Implications of this mechanism can therefore be discussed. In the reactions of interest here, optimization of the chain growth to 4 monomeric units is desirable. Since chain propagation is prevented by the electron transfer reaction, it appears necessary to maximize the possibility for the isomerization of these active centres to take place. To

do so a catalyst should contain a minimum number of Lewis acid sites. On the other hand, Lewis acid sites are necessary for the initiation of the chain. Alumina and fluoridated alumina cannot be used therefore to achieve the desired result unless the two functions can be separated. The use of infrared radiation to weaken the C-Al bond and to enhance the transfer reaction was one approach to achieve this. Another approach would be to add a second component to the catalyst which would emphasize one of these functions without sacrificing the other.

Table 11.1

Evidence for cationic chain polymerization mechanism

	Item	Discussion
1.	Al_2O_3, Al_2O_3-F exhibit high Lewis acidity, a necessary prerequisite.	5, 6, 1
2.	Conversion is affected by catalyst acidity, typical of polymerization of other unsaturated monomers	6
3.	C_4^-, dimers such as butenes and butadiene detected in gas phase.	7.1
4.	Gaseous products, CH_4, C_2H_4 increase with temperature and with time-on-stream (attributed to condensation and dealkylation reactions)	7.3.1 7.4 11.2.3
5.	Overall distribution of liquid products shows a majority of high molecular weight product at low conversion	7.6
6.	Two rates in deactivation observed by several workers consistent with rapid polymeric film deposit and slow polycondensation of aromatic structures.	8
7.	Specific rate of deactivation decreases with temperature. Polymerization reactions are often favoured by lower temperatures which supports the premise that deactivation is linked to polymer formation.	8 [70][a]
8.	Activation energy of 7-8 kcal/mol is typical of cationic polymerization reactions.	9 [70]
9.	Three product desorption peaks consistent with three types of carbonaceous deposits on the catalyst surface	9, 11
10.	Lack of relationship between extent of conversion and length of chain typical of cationic mechanism.	11.1
11.	Ability of infrared radiation to influence one or more of the steps in the catalytic reaction is consistent with other chain polymerization reactions	10 [70]

[a] [ ] refers to reference number

12. CONCLUSIONS AND RECOMMENDATIONS

12.1 CONCLUSIONS

12.1.1 Processing Considerations

The conversion of acetylene to aromatic products proceeded relatively easily over alumina and fluoridated alumina catalysts. The following model was obtained which described the total per cent conversion of acetylene (X) over these catalysts at 15 min on stream within the operating region used in this study: reaction temperature (300-400°C), catalyst (0-5 wt% F), weight-time (1-3 $g.s.mL^{-1}$), and feed concentration of acetylene (5-15 vol %):

$$X = 60.63 + 13.82\ x_1 - 26.26\ x_2 + 13.36\ x_3 - 4.97\ x_2^2 + 7.83\ x_4^2 - 9.81\ x_2x_4$$

x_1 = (temperature [C] - 350) / 25

x_2 = -2 (0 wt % F), -1 (1.5 wt % F), 0 (2.5 wt % F), 1 (4.3 wt % F)

x_3 = (weight-time [$g.s.mL^{-1}$] - 2) / 0.5

x_4 = (concentration [vol %] - 10) / 2.5

Examination of the model revealed that the optimal processing conditions for testing catalysts in this family were at the upper boundary of the operating region with respect to both temperature and weight-time. A maximum in conversion was revealed with maximum catalyst acidity at low initial concentrations of acetylene.

The products of this reaction consisted of a broad spectrum of gases, liquids and solids. The total yield of gaseous products was low throughout the experimental region. On the other hand, the total yields of liquid and solid product varied considerably over the operating region. For the most part conditions which resulted in the highest yield of liquids (400°C, 3 $g.s.mL^{-1}$, 5 vol % C_2H_2) also corresponded to conditions in which larger proportions of BTX (benzene, toluene, xylene) were obtained.

Despite the high initial activity of these catalysts, the decline in activity

with time-on-stream was found to be a severe problem. Catalyst deactivation over fluoridated alumina was shown to be primarily due to coking. The decline in activity (conversion) with time-on-stream was found to be generally compatible with an exponential decay of the form $a(t) = a_0 \exp(-k_d t)$. Empirical models, developed to describe the influence of the reaction temperature, the feed gas concentration and the weight-time on the parameters a_0 (initial activity) and k_d (specific rate of deactivation) and on the catalyst coke content at 1 h on stream (C) are summarized below:

$$\hat{a}_0 = 70.2 + 7.9\ x_1 - 23.0\ x_2 + 14.7\ x_3 + 11.3\ x_4 + 13.4\ x_4^2$$

$$\hat{k}_d = 10^{-4}(10.2 - 5.3\ x_1 + 4.3\ x_2 + 2.4\ x_3 + 3.6\ x_4 + 2.8\ x_2^2 + 1.8\ x_4^2)$$

$$\hat{C} = 10^2\ (1.32 + 0.41\ x_1 - 0.50\ x_2 - 0.24\ x_3 + 0.18\ x_4 - 0.46\ x_1 x_3 - 0.18\ x_4^2)$$

Analysis of the models revealed that both the deactivation and the coke content were decreased by using high temperatures (400°C), high weight-times (3 $g.s.mL^{-1}$) and low feed concentrations (5 vol %). Operating conditions which minimized linear polymer formation, i.e., high temperature, high contact time, low gas phase concentration also minimized deactivation. Processing conditions which maximized activity yet minimized deactivation were 400°C, 3 $g.s.mL^{-1}$ and 10 vol % acetylene. Nevertheless, it should be pointed out that even under these conditions the catalyst life was short (a matter of hours).

12.1.2 Catalytic Considerations

Apart from the physical operating considerations noted above, the main factor influencing activity was the nature of the catalyst. The high activity of alumina and fluoride-modified alumina was attributed to acid-base properties of the catalyst. The alumina and fluorided alumina catalysts prepared in this study showed maximum total acidity in the 2 to 3 wt % F range (measured as mol NH_3 adsorbed per gram of catalyst at 350°C). At high initial concentrations of acetylene a decrease in total conversion was observed with increased fluoride content. At low initial concentrations of acetylene, however, the conversion was found to increase with total catalyst acidity.

An increase in catalyst fluoride content resulted in a simultaneous reduction in the coke produced. The coking process appears to be complex. Small amounts of coke dispersed throughout the catalyst bulk deactivated the catalyst more readily than coke built up on the external surface. Coking on the external surface increased with catalyst acidity. This was attributed to the higher concentration of fluoride on the surface of the catalyst. Coke was probably a primary product in acetylene conversion. The specific rate of deactivation in acetylene conversion increased with the quantity of aliphatic structures in the deposited coke.

The data obtained using the microbalance supported the data from the tubular reactor and proved very useful in understanding the deactivation phenomenon. The rate of coke deposition and the total coke formed were found to be functions of the number of active sites available for adsorption of acetylene. Catalyst deactivation, on the other hand, proved to be a function of the quantity of linear polymer formed in the coke and not of the total coke produced. The quantity of linear polymer formed increased with increased acidity of the catalyst. The chemical properties of the catalyst affected the time-dependent distribution of products. At early times-on-stream, the molecular weight distribution of the liquid products became considerably narrower as the acidity increased. This resulted from two events, the increase in average molecular weight of the solid product (increase in nondesorbable linear polymer), and the interaction among initiation, transfer and propagation process functions being achieved on the catalyst surface.

12.1.3 Mechanistic Considerations

The decrease in conversion observed with increasing catalyst fluoride content at high initial concentrations of acetylene (Fig. 6.6) supports the premise that ion-pair sites are responsible for adsorption of acetylene on the surface of the catalysts. The decrease in the catalyst carbon content with increasing catalyst fluoride content throughout the operating region (Fig. 8.8c) suggests that coke formation is also

associated with the ion-pair sites which are responsible for acetylene adsorption.

The product distribution in the thermal conversion of acetylene followed a chain-growth polymerization mechanism, which is consistent with the free-radical reactions proposed by Back (10). Infrared radiation was found to assist the thermal reaction and increased conversions (between 200 and 500^{o}C). The infrared radiation probably provided energy for the vibrational excitation of the acetylene molecule which weakened the C-H bonds. Presumably free radicals were generated from the energy provided by infrared radiation and these free-radicals were responsible for the non-catalytic conversions obtained at low temperatures.

A mechanism, based on cationic chain polymerization, has been proposed for the catalytic conversion of acetylene over alumina and fluorided alumina. This mechanism is consistent with the product distribution data generated in this work. Furthermore, the dependence of the activity on the concentration was typical of autocatalytic reactions where concentration of both reactant and product affect the rate of transformation. Enhancement in the catalytic conversion of acetylene in the presence of infrared radiation was ascribed to a shift to the left in both the transfer reaction, Eq. 11.9, (shorter chains) and the equilibrium between ring compounds and chain compounds. With infrared radiation, less linear polymer was present on the catalyst surface which resulted in an extended catalyst lifetime. Although mechanistic studies were not attempted in this thesis, the mechanism described in Fig. 11.2. is consistent with virtually all the experimental data on conversion, yields and deactivation which were obtained.

12.2 RECOMMENDATIONS

The following recommendations stem from the conclusions reached above:

12.2.1 Processing Considerations

Since the optimum conditions for obtaining high activity and low deactivation point to operating boundaries, it is worthwhile expanding the operating region in the direction indicated, temperature above 400°C and weight-times above 3 $g.s.mL^{-1}$. At much higher temperatures, one must keep in mind the possibility of thermal reactions becoming important.

12.2.2 Catalytic Considerations

Catalysts which shift the ring-chain equilibrium to the left are highly desirable. An increase in the transfer reaction would also improve the situation by decreasing the length of the chains. This requires a fine balance between the number of sites on the catalyst responsible for initiation and those responsible for the isomerization of the active centre on the growing chain. Cationic initiation implies that high Lewis acidity is needed to initiate a chain. Very litte interaction between the surface and the growing chain is needed for isomerization or electron transfer to take place. Both these functions must be achieved so there is a need for bifunctional catalysts in this reaction. In both homogeneous and heterogeneous applications to date, nickel and chromium have been used to facilitate cyclization, however the quantity of linear polymer formed is still unacceptably high. There is definitely a need for further work in this area.

12.2.3 Mechanistic Considerations

In most polymerization processes, the initiation, transfer and termination steps are controlled by external means, e.g., the addition of free-radical initiators. It was shown in this work that some of these reactions can be affected externally. For example infrared radiation appeared to affect the transfer reactions occuring. These possibilities should be explored further.

REFERENCES

1 Al-Ammar, A. and Webb, G., J. Chem. Soc. Faraday Trans. I, 74, 195, 1978. ibid., 74, 657, 1978.

2 Allenger, V. M., Brown, J. R., McLean, D. D. and Ternan, M., Proceedings of the 37th Canadian Chemical Eng. Conf., Montreal, May 18-22, 1987.

3 Allenger, V. M., Fairbridge, C., McLean, D. D. and Ternan, M., J. Catal., 105, 5, 71-80, 1987.

4 Allenger, V. M., McLean, D. D. and Ternan, M., Fuel, 66, 3, 1987.

5 Allenger, V. M., McLean, D. D. and Ternan, M., Proceedings of 34th Canadian Chemical Eng. Conf., Quebec, Sept. 30-Oct.3, 1984.

6 Allenger, V. M., McLean, D. D. and Ternan, M., J. Chrom. Sci., 24, 3, 95, 1986.

7 Anderson, R. B., J. Catal., 55, 114, 1978.

8 Anon., Chem. Eng., 75, 9 , 67, 1968.

9 Anon., Hydro. Proc. Petrol. Ref., 42, 11, 129-240, 1963.

10 Back, M., Can. J. Chem., 49, 2199-2204, 1971.

11 Back, M. H. and Back, R. A., in *Pyrolysis Theory and Industrial Practice*, Albright, Crynes and Corcoran (eds), Academic Press, 1983.

12 Bashin, M. M., Curran, C. and John, G. S., J. Phys. Chem., 74, 22, 3973-3980, 1970.

13 Berak, J. M., Kanik, B., Eysymontt, P., and Mejsner, J., React. Kinet. Catal. Lett., 25, 3, 4, 323-327, 1984.

14 Berl, E., and Hofmann, K. N., Z. Agnew Chem., 44, 259, 1931.

15 Bond, G. C., *Catalysis by Metals*, Academic Press, London, 1962.

16 Bond, G. C. and Wells, P. B., J. Catal., 4, 211-219, 1965. ibid., J. Catal., 5, 65-73 1965. ibid., J. Catal., 5, 419-427, 1966.

17 Boorman, P. M., Kydd, R. A., Sarbak, Z. and Somogyvari, A., J. Catal., 96, 115-121, 1985.

18 Breck, D. W., *Zeolite Molecular Sieves*, John Wiley, New York, 1974.

19 Cadariu, I., An. Acad. RSR Filiula Cluj., 3, 4, 77-94,1954.

20 Chang-Li, S., Chemistry (TAIPEI), 1, 1-14, 1963.

REFERENCES CONT'D

21 Choudhary, V. R., Ind. Eng. Chem. Proc. Res. & Dev., 16, 1, 12-22, 1977.

22 Cooke, N. E., Ashraf, F. A. and Fung, D. P. C., Proceedings of the 34th Canadian Chemical Engineering Conference, Quebec, Sept. 30 - Oct. 3, 1984.

23 Cullis, C. F., Minkoff, G. J. and Nettleton, M. A., Trans. Faraday Soc., 58, 1117-1127, 1962. ibid, 59, 361-368, 1963.

24 Deckwer, W. D., Oil & Gas J., Nov. 10, 198-213, 1980.

25 Derouane, E. G., in *Catalysis by Zeolites*, B. Imelik et al., eds., Elsevier Pub., Amsterdam, 1980.

26 Draper, N. R. and Smith, H., *Applied Regression Analysis*, 2nd ed., John Wiley, New York, 1981.

27 Egloff, G., J. Phys. Chem., 36, 1457, 1932.

28 Eisenlohr, K. H. and Gaensslen, H., Fuel Processing Technology, 4, 43-61, 1981.

29 Elev, I. V., Shelimov, B. N. and Kazanskii, V. B., Kinetics and Catalysis, 24, 4, 2, 797-799, 1983.

30 Fischer, F., Bangertund, F. and Picher, H., Brennstoff - Chem, 10, 279, 1929.

31 Flory, P. J., *Principles of Polymer Chemistry*, Cornell University Press, N.Y., 1967.

32 Fujio, C., J. Soc. Chem. Ind. Japan, 31, 78-86, 1928.

33 Gatz, B., in *Chemistry of Catalytic Processes*, McGraw-Hill, New York, 1975.

34 Gauguin, R., Gravlier, M. and Papee, D., *Adv. Chem. Ser. 143*, 147-160, 1975.

35 Gerberich, H. R., Lutinski, F. E. and Hall, W. K., J. Catal., 6, 209-219, 1966.

36 Ghosh, A. K., J. Catal., 96, 288-291, 1985.

37 Gladisch, H., Hydro. Proc. Petrol. Ref., 6, 6, 159-164, 1962.

38 Goldstein, M., in *Experimental Methods in Catalytic Research*, R. B. Anderson (ed.), Academic Press, New York, 1968.

39 Hague, E. N. and Wheeler, R. V., J. Chem. Soc., 391, 1929.

40 Haldeman, R. G. and Botty, M. C., J. Phys. Chem., 63, 489, 1959.

REFERENCES CONT'D

41 Hartley, F. R., *Supported Metal Complexes*, D. Reidel Publishing Co., Holland, 1985.

42 Heaviside, J., Hendra, J., Tsai, P. and Cooney, R. P., J. Chem. Soc., Faraday Trans. I, 74, 2542, 1978.

43 Himmelblau, D. M., *Process Analysis by Statistical Methods*, Wiley, N.Y., 1970.

44 Ika and Ogura, J. Soc. Chem. Ind. Japan, 31, 78-86, 1928.

45 Ikeda, S. and Tamaki, A., J. Polymer Sci., B, 4, 605, 1966.

46 Ito, T., Shirakawa, H., Ikeda, S., J. Polymer Sci., 12, 11-20, 1974.

47 Kesmodel, L. L., Dubois, L. H. and Somorjai, G. A., J. Chem. Phy., 70, 5, 2180-2188, 1979.

48 *Kirk-Othmer Encyclopedia of Chemical Technology*, 3rd ed., vol. 18, John Wiley, 1982.

49 Kotanigawa, T., Katsuyoshi, S. and Yoshida, T., J. Chem. Soc., Chem. Comm., 1184-1187, 1982.

50 Kovache, A. and Tricot, E., Chim. et Ind., 13, 361- 537, 1925.

51 Kranich, W. L., Weiss, A. H., Schay, Z. and Guczi, L., Applied Catalysis, 13, 257-267, 1985.

52 Leglise, J., Chevreau, T. and Cornet, D., Comptes Rendus des Seances Acad Sci. Ser C, 291, 2, 41-44, 1980.

53 Leglise, J. Chevreau, Th. and Cornet, D., Catalysis by Zeolites, 95-202, 1980.

54 Leutner, H. W. and Stokes, C. S., Ind. & Eng. Chem., 53, 5, 341-2,

55 Levy, G. C., Lichter, R. L. and Nelson, G. L., *Carbon 13 Nuclear Magnetic Resonance Spectroscopy*, 2nd ed., Wiley, N.Y., 1980.

56 Logan, M. A., Rucker, T. G., Gentle, T. M., Muetterties, E. L. and Somorjai, G. A., J. Phys., 90, 2709-2715, 1986.

57 Mardaleishvili, R. E. and Rappoport, Y. I., React. Kinetics Catal. Letters, 25, 1437-1444, 1984. ibid., J. Catal., 95, 447-454, 1985.

58 Massimiila, L., Sarcini, L. and Mastovita, E., Chim. e Ind., 44, 341, 1962.

59 Matnishyan, A. A. and Kobryanskii, V. M., Russian Chemical Reviews, 52, 8, 1983.

60 McGown, W. T., Kemball, C. and Whan, D. A., J. Catal., 51, 173-184, 1978.

REFERENCES CONT'D

61 McIntyre, N. S., Canadian Chemical News, 37, 5, 13-16, 1985.

62 McMillan, M., Brinen, J. S. and Haller, G. L., J. Catal., 97, 243-247, 1986.

63 Meyer, R., Ber., 45, 1609, 1912.

64 Mikulec, J., Beran, S., Wichterlova, B. and Jiro, P, Applied Catalysis, 16, 389-400, 1985.

65 Miller, S. A., *Acetylene, Its Properties, Manufacture and Uses*, Vol.1 & 2, Ernest Benn Ltd., London, 1965.

66 Moses, J. M., Weiss, A. H., Matusc, K. K. and Guczi, L., J. Catal., 86, 417-426, 1984.

67 Nelson, W. L., *Petroleum Refinery Engineering*, 3rd ed., McGraw-Hill, 1949.

68 Nie, N. H., Hull, C. H., Jenkins, J. G., Steinbrenner, K. and Bent, D. H., *SPSS, Statistical Package for the Social Sciences*, 2nd ed., McGraw-Hill, New York, 197

69 O'Reilly, D. E., in *Advances in Catalysis and Related Subjects*, Academic Press, New York, 1960.

70 Parker, D. B. V., *Polymer Chemistry*, App. Sci. Pub., 1974.

71 Paukshtis, E. A., Soltanov, P. I., Yurchenko, E. N., Jiratova, K., Collection Czechoslovak Chem. Commun., 47, 2044-2060, 1982.

72 Peri, J. B., J. Phys. Chem., 69, 211-220, 1965.

73 Pichat, P., Vedrine, J. C., Gallezot, P. and Imelik, B., J. Catal., 32, 190-203, 1974.

74 Pines, H., *The Chemistry of Catalytic Hydrocarbon Conversions*, Academic Press, 1981.

75 Pinto, A. and Rogerson, P. L., Chem. Eng., 84, 102-108, 1977.

76 Rabo, J. A., *Zeolite Chemistry and Catalysis ACS Monograph 171*, 1976.

77 Reikhsfel'd, V. O. and Makovetskii, K. L., Russian Chemical Reviews, 34, 7, 510-523, 1966.

78 Rives-Arnau, V. and Sheppard, N., J. Chem. Soc. Faraday I, 76, 394, 1980.

79 Roginskii, S. Z., in *Scientific Selection of Catalysts*, A. A. Baladin et al. (eds), Keter Pub. House, Kiryat Moshe, English translation, 1968.

80 Rosen, S. L., *Fundamental Principles of Polymer Materials*, Ryerson Press, 1971.

REFERENCES CONT'D

81 Rucker, T. G., Logan, M. A., Gentle, T. M., Muetterties, E. L., and Somorjai, G. A., J. Phys., 90, 2703-2708, 1986.

82 Sarkany, A., Weiss, A. H., Szilagyi, T., Sandor, P. and Guczi, L., Applied Catalysis, 12, 3, 373, 1984.

83 Sarkany, A. and Guczi, L., Applied Catalysis, 10,369-388, 1984.

84 Satterfield, C. N., *Heterogeneous Catalysis in Practice*, McGraw-Hill, New York, 1980.

85 Schlup, J. R. and Vaughan, R. W., J. Catal., 99, 304-315, 1986.

86 Schroder, G. *Cyclooctatetraene*, Verlag Chemie, Weinheim, 1965.

87 Schwarz, R. and Bessel, G., Ber., 77B, 512-515, 1984.

88 Scokart, P. O., Selim, S. A., Damon, J. P. and Rouxhet, P. G., J. Colloid Interface Sci., 70,2,209-222, 1979.

89 Seddon, D., B. H. P. Bulletin, 27, 1, 1983.

90 Sheppard, N. and Yates, D. J. C., Proc. Roy. Soc. A, 238, 69-88, 1957.

91 Sheridan, J., J. Chem. Soc., 133-142, 1945. ibid., J. Chem. Soc., 301-304, 1945. ibid., J. Chem. Soc., 305-311, 1945. ibid., J. Chem. Soc., 470-476, 1945. ibid., J. Chem. Soc., 2962-2966, 1952.

92 Tedeschi, R. J., *Acetylene Based Chemicals from Coal and other Natural Resources*, Marcel Dekker Inc., 1982.

93 The-Tam, N., Cooney, R. P. and Curthoys, G., J. Chem. Soc. Faraday Transactions I, 72, 2577-2597, 1976.

94 Tsai, P. and Anderson, J. R., J. Catal., 80, 207-214, 1983.

95 U.S. Patent 2,608,594 (Robinson).

96 U.S. Patent 3,176,045 (Jenny).

97 U.S. Patent 4,424,401 (White, N., Kagi, D., Creer, J. G., and Tsai, P., Jan.3, 1984)

98 Wu, M. H. and Kaeding, W. W., J. Catal., 88, 478-489, 1984 .

99 Wender, I. and Pino, P. (eds), *Organic Synthesis via Metal Carbonyls*, Vol. 1, Interscience Pub., 1975.

100 Yates, D. J. C. and Lucchesi, P. J., J. Chem. Phys., 35, 1, 243-255, 1961.

101 Zelinski, N. D., Ber., 57, 264, 1924.

APPENDIX 1.1

Calculation procedures for determination of free energy per carbon atom of some hydrocarbons

The temperature dependence of the Gibbs free energy was evaluated using a procedure outlined in Smith, J. M. and Van Ness, H. C., *Introduction to Chemical Engineering Thermodynamics*, 3rd ed., McGraw-Hill, New York, 1975, page 389. The standard Gibbs free energy of formation at 298 K data was obtained from Perry, J. H. and Chilton, C. H. , eds, *Chemical Engineer's Handbook*, 5th ed., McGraw-Hill, New York, 1973. A four parameter polynomial equation was used to determine the enthalpy as a function of temperature. The coefficients were also obtained from Perry's Handbook.

A comparison of various equations for predicting the heat capacity of hydrogen and carbon in the temperature range 300 and 1000K was carried out. A sample output of the computer program SY1:Heatcp:bas written for this purpose shows that the three equations used to predict the heat capacity of hydrogen give very similar heat capacities. On the other hand, only two of the equations used to predict the heat capacity of carbon agree up to about 1100K. The coefficients given in Perry's Handbook provided consistent results for both hydrogen and carbon and were used subsequently in free energy calculations.

SYI:HEATCP.BAS

```
5 OPEN 'LP' FOR OUTPUT AS FILE #6
10 REM Program to compare different equations for heat
20 REM capacity of hydrogen and carbon
30 REM cal gmol-1 C-1
40 REM hydrogen equations valid for 298-3000K
50 PRINT #6,'COMPARISON OF HYDROGEN HEAT CAPACITY EQUATIONS'
60 PRINT ' '
70 PRINT #6,' T(K)          CPH1          CPH2          CPH3'
80 T=300
90 FOR I=1 TO 12
100 H1=6.65+7.00000E-04*T
110 H2=6.52+7.80000E-04*T+12000/T^2
120 H3=6.62+8.10000E-04*T
130 PRINT #6,T,H1,H2,H3
131 T=T+200
132 NEXT I
140 REM carbon equations valid for 298-2500K
150 PRINT #6,'COMPARISON OF CARBON HEAT CAPACITY EQUATIONS'
160 PRINT #6,' T(K)          CPC1          CPC2          CPC3'
161 T=300
162 FOR J=1 TO 12
170 C1=4.03+1.14000E-03*T-204000/T^2
180 C2=2.673+2.61000E-03*T-116069/T^2
190 C3=1.1+2.40000E-03*T+4.00000E-07*T^2
200 PRINT #6,T,C1,C2,C3
210 T=T+200
220 NEXT J
300 END
```

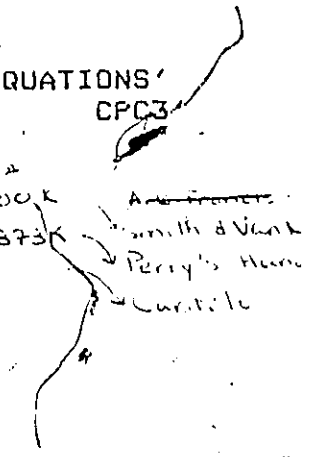

COMPARISON OF HYDROGEN HEAT CAPACITY EQUATIONS

T(K)	CPH1	CPH2	CPH3
300	6.86	6.88733	6.863
500	7	6.958	7.025
700	7.14	7.09049	7.187
900	7.28	7.23682	7.349
1100	7.42	7.38792	7.511
1300	7.56	7.5411	7.673
1500	7.7	7.69533	7.835
1700	7.84	7.85015	7.997
1900	7.98	8.00532	8.159
2100	8.12	8.16072	8.321
2300	8.26	8.31627	8.483
2500	8.4	8.47192	8.645

COMPARISON OF CARBON HEAT CAPACITY EQUATIONS

T(K)	CPC1	CPC2	CPC3
300	2.10533	2.16634	1.856
500	3.784	3.51372	2.4
700	4.41167	4.26312	2.976
900	4.80415	4.8787	3.584
1100	5.11541	5.44807	4.224
1300	5.39129	5.99732	4.896
1500	5.64933		5.6
1700	5.89741		6.336
1900	6.13949		7.104
2100	6.37774		7.904
2300	6.61344		8.736
2500	6.84736		9.6

Program calculates free energy of formation of hydrocarbons.

```
20 REM
30 REM Program calculates free energy of formation of hydrocarbons
40 REM
50 REM heat capacity of hydrocarbon gases expressed in the form
60 REM A + B T + C T**2 + D T**3
70 REM
80 REM heat capacity of hydrogen expressed in the form
90 REM A + B T
95 IF N$='**' GO TO 150
100 REM
110 REM heat capacity of carbon (Graphite)expressedintheform
120 REM A + B T + C /T**2 + D/T**3
130 REM
140 REM
150 READ R
160 DATA 1.987
170 READ C1,C2,C3,C4
180 DATA 5.32692,3.6954E-04,-7.35004E05,1.2954E08
190 READ H1,H2
200 DATA 6.62,8.1E-04
210 OPEN 'SY1:HEAT.DAT' FOR INPUT AS FILE #5
220 OPEN 'LP:' FOR OUTPUT AS FILE #6
240 INPUT #5,N$
245 IF N$='**' GO TO 9999
250 INPUT #5,P,H,C
260 INPUT #5,P1,P2,P3,P4
265 INPUT #5,H0,G0
280 PRINT #6,N$
290 PRINT #6,P1,P2,P3,P4
300 PRINT #6
310 PRINT #6,'  T                -LN K            K            DEL G'
320 REM
330 REM
340 REM
350 REM calculating the integration constants
360 REM
370 LET T2=298^2
380 LET T3=T2*298
390 LET L=LOG(298)
400 I1=P1*298+P2*T2/2+P3*T3/3+P4*T2*T2/4
410 I2=H1*298+H2*T2/2
420 I3=C1*298+C2*T2/2-C3/298-C4/2/T2
430 I4=-H0/298
440 I4=I4+P*(P1*L+P2*298/2+P3*T2/6+P4*T3/12-I1/298)
450 I4=I4-H*(H1*L+H2*298/2+I2/298)
460 I4=I4-C*(C1*L+C2*298/2+C3/T2/2+C4/T3/6+I3/298)
470 REM
480 REM
490 T=300
500 REM
510 REM
550 REM calculating the equilibrium constant
560 L1=LOG(T)
570 T5=T*T
580 T6=T5*T
590 T7=T/2
600 K1=-H0/T
610 K1=K1+P*(P1*L1+P2*T7+P3*T5/6+P4*T6/12+I1/T)
620 K1=K1-H*(H1*L1+H2*T7+I2/T)
630 K1=K1-C*(C1*L1+C2*T7+C3/T5/2+C4/T6/6+I3/T)
640 K1=K1-I4
650 REM
660 REM calculating the equilibrium constant
670 REM
680 K=EXP(K1/R-G0/R/298)
685 K2=-LOG(K)
690 REM
700 REM calculating the free energy of reaction
710 G=R*T*K2
720 IF T>2500 THEN  GO TO 9998
730 PRINT #6,T,K2,K,G
740 T=T+100
750 GO TO 560
760 REM
770 REM
780 REM
790 REM
9998 GO TO 240
```

INPUT FILE

C1H4

```
C1H4
1,2,1
4.59765,1.24471E-02,2.8597E-06,-2.7031E-09
-17889,-12140
C2H6
1,3,2
1.29285,4.25354E-02,-16.5699E-06,2.08148E-09
-20236,-7860
C3H8
1,4,3
-1.008568,7.31499E-02,-37.8885E-06,7.67782E-09
-24820,-5614
C2H4
1,2,2
0.985498,3.70262E-02,-19.4768E-06,4.05454E-09
12496,16282
C3H6
1,3,3
0.894648,5.58925E-02,-27.4978E-06,5.19139E-09
4879,14990
C2H2
1,1,2
7.331,2.622E-03,-3.889E-06,0
54194,50000
C6H6
1,3,6
-0.409,77.621E-03,-26.429E-06,0
19820,30989
C6H14
1,7,6
-3.4892,14.688E-02,-80.6345E-06,16.288E-09
-39960,-70
C7H16
1,8,7
-1.22928,16.1454E-02,-87.2008E-06,18.2892E-09
-44885,1920
C
0,0,1
0,0,0,0
0,0
**
```

C1H4

4.59765	.0124471	2.85970E-06	-2.70310E-09

T	-LN K	K	DEL G
300	-20.3009	6.55498E+08	-12101.4
400	-12.6565	313808	-10059.4
500	-7.89358	2680.02	-7842.27
600	-4.60912	100.396	-5494.99
700	-2.19304	8.96239	-3050.3
800	-.33527	1.39832	-532.945
900	1.13965	.31993	2038.04
1000	2.3392	.0964052	4647.98
1100	3.33333	.0356742	7285.66
1200	4.16983	.0154549	9942.55
1300	4.88266	7.57680E-03	12612.4
1400	5.49676	4.10004E-03	15290.9
1500	6.03096	2.40318E-03	17975.3
1600	6.49987	1.50364E-03	20664.4
1700	6.91499	9.92796E-04	23358.1
1800	7.28562	6.85326E-04	26057.7
1900	7.61937	4.90849E-04	28765.4
2000	7.9226	3.62459E-04	31484.4
2100	8.20064	2.74479E-04	34218.8
2200	8.45809	2.12178E-04	36973.7
2300	8.69889	1.66770E-04	39754.8
2400	8.92652	1.32819E-04	42568.8
2500	9.14405	1.06953E-04	45423.1

C2H6

1.29285	.0425354	-1.65699E-05	2.08148E-09

T	-LN K	K	DEL G
300	-13.0462	463348	-7776.86
400	-4.32801	75.7936	-3439.91
500	1.18003	.307271	1172.36
600	5.01494	6.63802E-03	5978.81
700	7.85371	3.88307E-04	10923.7
800	10.0447	4.34160E-05	15967
900	11.7874	7.59969E-06	21079.4
1000	13.2055	1.84046E-06	26239.3
1100	14.3803	5.68507E-07	31430.9
1200	15.3676	2.11801E-07	36642.6
1300	16.2076	9.14379E-08	41865.9
1400	16.9296	4.44173E-08	47094.9
1500	17.556	2.37436E-08	52325.5
1600	18.1037	1.37295E-08	57555.4
1700	18.5864	8.47327E-09	62782.8
1800	19.0146	5.52184E-09	68007.5
1900	19.397	3.76709E-09	73229.4
2000	19.7406	2.67160E-09	78449.1
2100	20.0512	1.95822E-09	83667.8
2200	20.3337	1.47634E-09	88886.7
2300	20.592	1.14030E-09	94107.4
2400	20.8294	8.99307E-10	99331.2
2500	21.0488	7.22128E-10	104560

C3H8 —

-1.00857	.0731499	-3.78985E-05	7.67782E-09

T	-LN K	K	DEL G
300	-9.20147	9911.7	-5485
400	1.50898	.221136	1199.34
500	8.2886	2.51365E-04	8234.73
600	13.0098	2.23824E-06	15510.3
700	16.5013	6.81646E-08	22951.7
800	19.1915	4.62622E-09	30506.8
900	21.3267	5.46924E-10	38138.6
1000	23.0601	9.66360E-11	45820.4
1100	24.4925	2.30699E-11	53533.2
1200	25.6935	6.94170E-12	61263.5
1300	26.7127	2.50515E-12	69001.5
1400	27.5865	1.04554E-12	76740.1
1500	28.3423	4.91016E-13	84474.2
1600	29.001	2.54109E-13	92200
1700	29.5788	1.42585E-13	99914.4
1800	30.0885	8.56482E-14	107615
1900	30.5401	5.45241E-14	115298
2000	30.9417	3.64920E-14	122962
2100	31.2996	2.55134E-14	130604
2200	31.6189	1.85383E-14	138219
2300	31.9039	1.39416E-14	145804
2400	32.1576	1.08172E-14	153353
2500	32.3828	8.63661E-15	160861

C2H4

.985498	.0370262	-1.94768E-05	4.05454E-09

T	-LN K	K	DEL G
300	27.3569	1.31535E-12	16307.5
400	22.2582	2.15473E-10	17690.8
500	19.3713	3.86500E-09	19245.4
600	17.5504	2.38752E-08	20923.6
700	16.3145	8.21642E-08	22691.9
800	15.4289	1.99219E-07	24525.7
900	14.7666	3.84324E-07	26407.1
1000	14.2541	6.44959E-07	28322.9
1100	13.8461	9.69902E-07	30263.4
1200	13.5135	1.35263E-06	32221.5
1300	13.2368	1.78368E-06	34192.1
1400	13.0028	2.25405E-06	36171.1
1500	12.8018	2.75585E-06	38155.7
1600	12.6269	3.28243E-06	40143.5
1700	12.473	3.82878E-06	42132.4
1800	12.3359	4.39109E-06	44120.7
1900	12.2127	4.96711E-06	46106.5
2000	12.1006	5.55600E-06	48087.9
2100	11.9977	6.15832E-06	50062.8
2200	11.9021	6.77601E-06	52028.9
2300	11.8123	7.41272E-06	53983.5
2400	11.7269	8.07379E-06	55923.2
2500	11.6446	8.76616E-06	57844.6

C3H6

.894648	.0558925	-2.74978E-05	5.19139E-09

T	-LN K	K	DEL G
300	25.2608	1.07002E-11	15057.9
400	23.4337	6.65076E-11	18625.1
500	22.6018	1.52811E-10	22454.9
600	22.2044	2.27385E-10	26472.1
700	22.017	2.74244E-10	30623.4
800	21.9365	2.97221E-10	34870.3
900	21.9115	3.04765E-10	39184.3
1000	21.9147	3.03777E-10	43544.6
1100	21.9317	2.98678E-10	47936
1200	21.9542	2.92017E-10	52347.6
1300	21.978	2.85145E-10	56771.4
1400	22.0007	2.78741E-10	61201.7
1500	22.0212	2.73089E-10	65634.3
1600	22.039	2.68285E-10	70066.3
1700	22.0538	2.64338E-10	74495.5
1800	22.0657	2.61210E-10	78920.2
1900	22.0749	2.58854E-10	83338.8
2000	22.081	2.57243E-10	87749.9
2100	22.0845	2.56347E-10	92151.9
2200	22.0852	2.56166E-10	96543.2
2300	22.083	2.56726E-10	100922
2400	22.0777	2.58082E-10	105284
2500	22.0692	2.60299E-10	109629

C2H2

7.331	.012622	-3.88900E-06	0

T	-LN K	K	DEL G	
300	83.8313	3.91312E-37	49971.8	
400	61.1114	2.88168E-27	48571.4	
500	47.5034	2.34168E-21	47194.6	23597
600	38.4572	1.98717E-17	45848.7	
700	32.0173	1.24474E-14	44532.8	
800	27.2039	1.53279E-12	43243.4	
900	23.4727	6.39637E-11	41976.2	
1000	20.4971	1.25382E-09	40727.7	20369
1100	18.0696	1.42064E-08	39494.7	
1200	16.0522	1.06812E-07	38274.9	
1300	14.3497	5.86153E-07	37066.7	
1400	12.8942	2.51261E-06	35869.1	
1500	11.6361	8.84082E-06	34681.5	17340
1600	10.5385	2.64959E-05	33504.1	
1700	9.57314	6.95729E-05	32337.1	OK
1800	8.71814	1.63591E-04	31181.3	
1900	7.9564	3.50413E-04	30037.8	
2000	7.27425	6.93163E-04	28907.9	14454
2100	6.66068	1.28028E-03	27793	
2200	6.10674	2.22780E-03	26695	
2300	5.60509	3.67910E-03	25615.8	
2400	5.1496	5.80170E-03	24557.4	
2500	4.7352	8.78070E-03	23522.1	

C6H6

-.409	.077621	-2.64290E-05	0

T	-LN K	K	DEL G
300	52.1121	2.33342E-23	31064
400	44.0414	7.46559E-20	35004.1
500	39.4998	7.00582E-18	39243
600	36.6563	1.20326E-16	43701.7
700	34.7376	8.19689E-16	48316.5
800	33.3654	3.23287E-15	53037.6
900	32.3363	9.04739E-15	57827
1000	31.5334	2.01942E-14	62656.8
1100	30.8861	3.85774E-14	67507.8
1200	30.3502	6.59258E-14	72367.1
1300	29.8973	1.03694E-13	77227.8
1400	29.5086	1.52963E-13	82087
1500	29.1715	2.14278E-13	86945.7
1600	28.8777	2.87455E-13	91808
1700	28.6215	3.71406E-13	96680.5
1800	28.399	4.63952E-13	101572
1900	28.2078	5.61733E-13	106493
2000	28.0461	6.60298E-13	111455
2100	27.913	7.54300E-13	116473
2200	27.808	8.37815E-13	121560
2300	27.7308	9.05049E-13	126732
2400	27.6814	9.50903E-13	132007
2500	27.6599	9.71496E-13	137401

C6H14

-3.4892	.14688	-8.06345E-05	1.62880E-08

T	-LN K	K	DEL G
300	.331974	.717506	197.89
400	17.592	2.29031E-08	13982.1
500	28.5278	4.07873E-13	28342.4
600	36.1411	2.01421E-16	43087.5
700	41.7642	7.27854E-19	58089.8
800	46.0879	9.64436E-21	73261.3
900	49.511	3.14519E-22	88540.5
1000	52.2822	1.96844E-23	103885
1100	54.566	2.00574E-24	119265
1200	56.476	2.97021E-25	134661
1300	58.0934	5.89321E-26	150061
1400	59.478	1.47581E-26	165456
1500	60.6746	4.46003E-27	180841
1600	61.7176	1.57169E-27	196213
1700	62.6334	6.29002E-28	211569
1800	63.4428	2.80002E-28	226909
1900	64.1619	1.36403E-28	242231
2000	64.8038	7.17876E-29	257530
2100	65.3786	4.04055E-29	272805
2200	65.8943	2.41250E-29	288050
2300	66.3572	1.51860E-29	303259
2400	66.772	1.00293E-29	318423
2500	67.1426	6.92339E-30	333531

C7H16

-1.22928	.161454	-8.72008E-05	1.82892E-08

T	-LN K	K	DEL G
300	3.74821	.02356	2234.3
400	23.1286	9.02323E-11	18382.6
500	35.4049	4.20584E-16	35174.8
600	43.9536	8.15079E-20	52401.5
700	50.2706	1.47146E-22	69921.4
800	55.1304	1.14074E-24	87635.2
900	58.9792	2.43029E-26	105473
1000	62.0953	1.07733E-27	123383
1100	64.6625	8.26832E-29	141333
1200	66.8076	9.67885E-30	159296
1300	68.6214	1.57803E-30	177256
1400	70.1703	3.35278E-31	195200
1500	71.5046	8.82931E-32	213120
1600	72.6625	2.77380E-32	231009
1700	73.6733	1.00942E-32	248861
1800	74.5603	4.15772E-33	266673
1900	75.3416	1.90353E-33	284437
2000	76.0315	9.54879E-34	302149
2100	76.6412	5.18972E-34	319801
2200	77.1798	3.02846E-34	337384
2300	77.6542	1.88449E-34	354888
2400	78.0697	1.24381E-34	372299
2500	78.4305	8.67098E-35	389604

C

0	0	0	0

T	-LN K	K	DEL G
300	2.11000E-05	.999979	.0125777
400	.0458109	.955223	36.4105
500	.145907	.864238	144.959
600	.272938	.76114	325.397
700	.412824	.661779	574.197
800	.557854	.572436	886.765
900	.703713	.494745	1258.45
1000	.847984	.428277	1684.94
1100	.989333	.371825	2162.39
1200	1.12705	.323988	2687.34
1300	1.26081	.283425	3256.79
1400	1.39048	.248956	3868.04
1500	1.51609	.219569	4518.71
1600	1.63774	.19442	5204.48

APPENDIX 1.2

Experimental work on the pyrolysis of methane

In the first phase of this project, the pyrolysis of methane was studied at high temperatures (900-1100°C). The pyrolysis was carried out in a 5 cm diameter high purity alumina ceramic tube (McDanel Refractory). Heating was provided by a high temperature Lindberg furnace. These studies confirmed the pioneering work in this area carried out in the early part of this century (Table A1.1). Liquid yields from direct pyrolysis of methane were found to be extremely low (< 5 %). The results of these studies were presented at the 34th Canadian Chemical Engineering Conference (A1).

The effect of temperature was significant, as seen in Fig.A1.1. Maximum combined tar and liquid yields were obtained at 1000°C, while the conversion of methane appears to increase steadily throughout the temperature range investigated (Fig. A1.2). The tar and liquid product covered a wide boiling range as demonstrated by a simulated distillation curve given in Fig. A1.3. The gas product was mostly hydrogen, however traces of ethylene, acetylene and propylene were also observed.

A1. Allenger, V.M., McLean, D.D. and Ternan, M., Proceedings 34th Canadian Chemical Engineering Conference, Quebec, 1984.

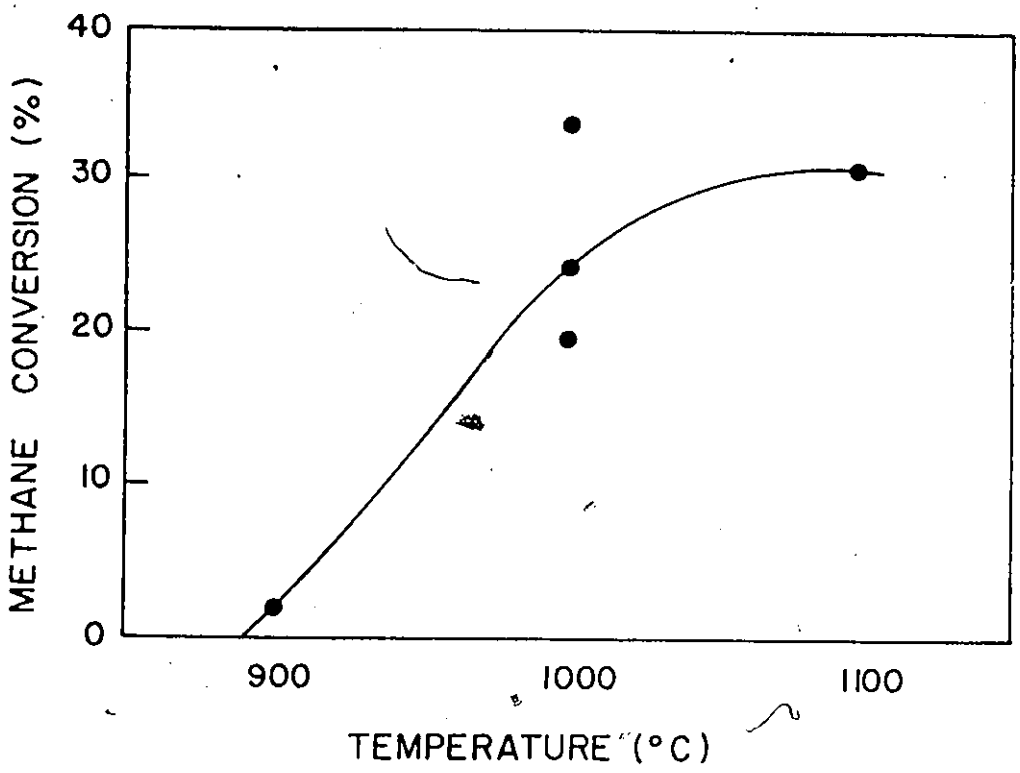

Fig. A1.1 The influence of temperature on the pyrolysis of methane, residence time 30s.

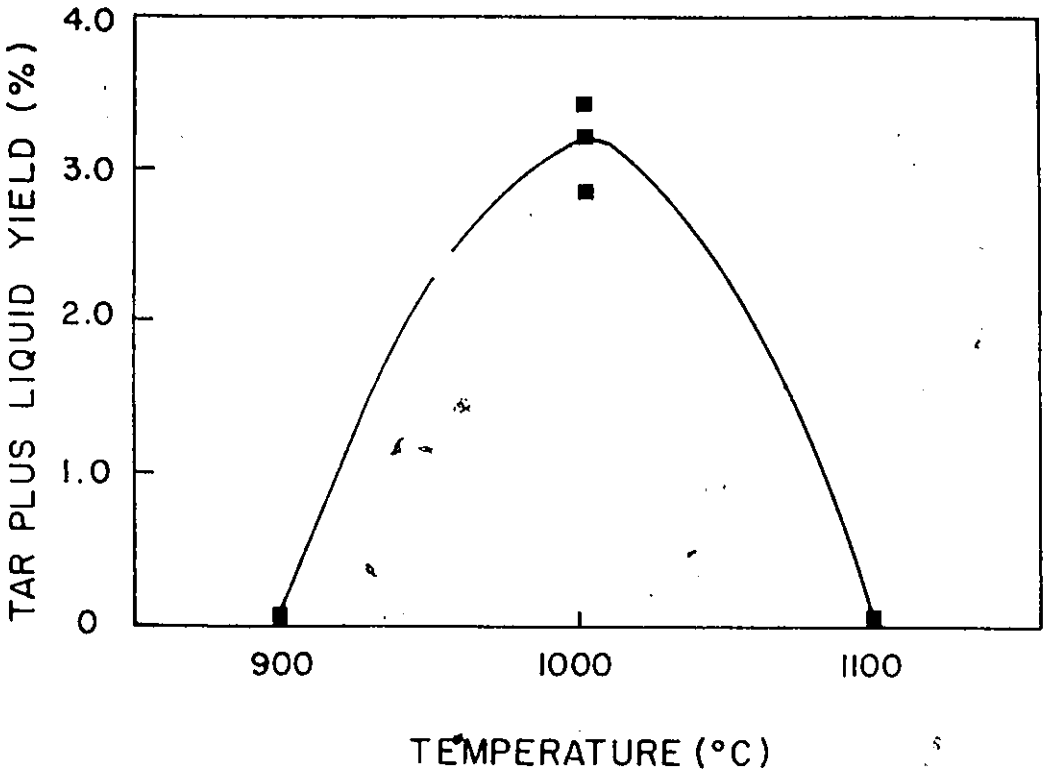

Fig. A1.2 The effect of temperature on the tar and liquid yield, residence time is 30 s.

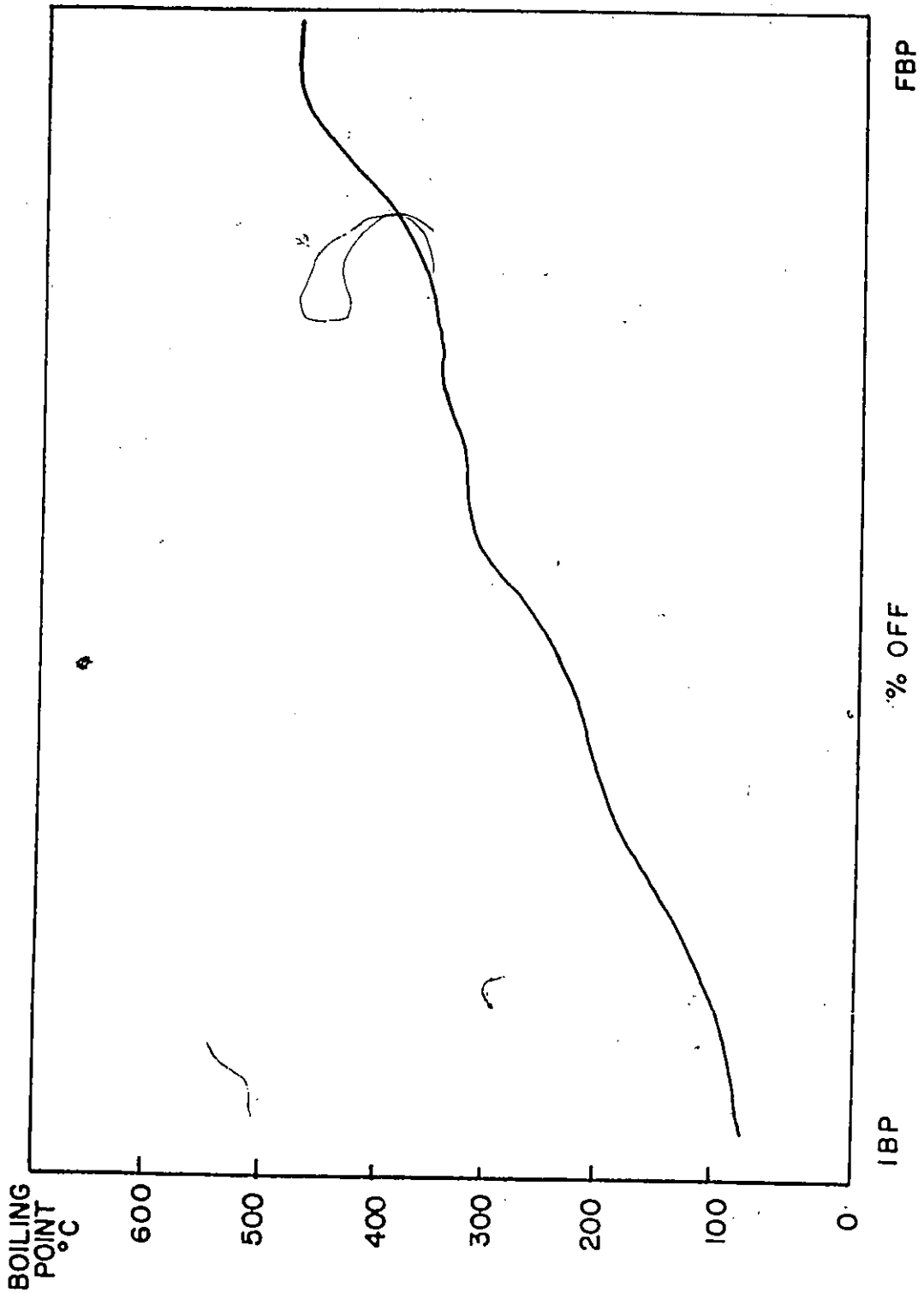

Fig, A1,3 Simulated distillation of methane pyrolysis products, temperature is 1000°C, 1 atm pressure, 30 s residence time.

TABLE A1.1

Maximum reported liquid yields from pyrolysis

YEAR	TEMPERATURE (°C)	PRODUCT YIELDS (WT %)		PRODUCT GAS COMPOSITION (MOL %)	
		LIQUID	TAR	C_2^+	H_2
1927	1150	4.28	5.35	3.7	32.8
1928	1000	3.21	-	3.0	42.6
1929	950	-	-	4.6	31.5
1929	1000	3.82	-	-	-
1930	1100	6.27	-	-	-
1931	1200	4.74	6.11	-	-
	1240	-	-	4.4	39.6
1932	1050	5.5	-	-	-
1934	-	5.5	-	-	-
THIS WORK	1000	3.06	1.53	1.0	32.3

APPENDIX 3.1

Analytical criteria for temperature gradients

Temperature gradient in a catalyst pellet:

The magnitude of the temperature difference inside a particle (without further complications of external mass and heat transfer resistances) was originally derived by Damkoehler. The derivation based on simultaneous solution of heat and mass balances for a particle of any geometry can be found in Levenspiel, O., *Chemical Reaction Engineering*, 2nd ed. The temperature difference, ΔT_p, is given by :

$$\Delta T_p = T_s^s - T_s = \frac{D_{eff} * (C_s^s - C_s) * (-\Delta H_r)}{k_{eff}}$$

where T_s - absolute temperature at the centre of the porous particle

T_s^s - absolute temperature at surface of porous particle

C_s - concentration of reactant at centre of porous particle

C_s^s - concentration of reactant at surface of porous particle

ΔT_p - temperature variation within catalyst pellet

D_{eff} - effective mass diffusivity

$-\Delta H_r$ - heat of reaction

k_{eff} - effective thermal conductivity

It can be seen that the maximum gradient, ΔT_{max}, occurs for complete reaction, $C_s = 0$, so that

$$\Delta T_p = T_s^s - T_s = \frac{(-\Delta H_r) * D_{eff} * C_s^s}{k_{eff}}$$

The result holds for a particle of any geometry under steady-state conditions. The temperature gradient is therefore dependent on the heat of reaction, the transport properties of the particle, and the surface concentration of reactant.

Assuming the reaction:

$$C_2H_2 \longrightarrow \text{Products}$$

is first order and that,

$$\Delta H_r = -50 \text{ kcal/mol } C_2H_2$$

$$C_s^s = \frac{y * P}{R * T} = \frac{100 \text{ kPa}}{R * (473 \text{ K})} = 3.6 \text{ E-03 mol } C_2H_2/L$$

$$D_{eff} = 29.3 \text{ E-03 } cm^2/s$$

$$k_{eff} = 5.24 \text{ E-04 cal/cm.s.K}$$

then a temperature gradient of 10 degrees across the pellet $\Delta T_p = 10$ K, is expected.

Temperature gradient in the film surrounding the pellet:

The temperature gradient in the film can be evaluated by equating the rate of of heat removal through the film with the rate of heat generation within the pellet. Thus,

$$\Delta T_f = \frac{L * (-r_a) * (-\Delta H_r)}{h}$$

where ΔT_f - temperature variation across the gas film

$L=R_p/3$ - effective length

$-r_a$ - reaction rate

h - heat transfer coefficient obtained from empirical correlations in the literature

For example,

$$R_p = 0.5 \text{ mm} = 0.05 \text{ cm}$$

For the steady state,

$$-r_a = 0.02 \text{ g C/g cat/min} = 1.77 \text{ E-05 mol C/ } cm^3/s$$

For the maximum rate, $-r_a$, is five times higher.

$$h = 40 \text{ kcal / h / } m^2 = 1.11 \text{ E-03 } cal.s^{-1}.cm^{-1}.K^{-1}$$

Then,

$$\Delta T_f = \frac{0.05 \ (1.77 \text{ E-05}) \ (-50000)}{3 \ (1.11 \text{ E-03})} = 13 \text{ K}$$

and for the maximum rate, $\Delta T_f = 50$ K. These estimates show that the largest particles are close to uniform in temperature and that the gas and solid temperature at steady state are close. However, at the max. rate of deposition, the solid may be 50°C higher than the surrounding gas.

APPENDIX 4.1

Calculation of nominal catalyst fluoride content

Molecular Weight NH_4F 37 g/mol

Molecular Weight Al_2O_3 102 g/mol

Molecular Weight $Al_2O_3*H_2O$ 120 g/mol

Although only 15 % weight loss is expected starting with the monohydrate, experience has shown that 25 % weight loss is usually the case with Catapal SB.

Basis: 500 g Catapal SB alumina monohydrate

Assuming a 25 % weight loss, 375 g Al_2O_3

g-atoms of Al = 375 g/ (51 g Al_2O_3/g atom Al) = 7.35 g-atoms Al

Desired atomic ratios of F/Al are 0.05, 0.10, 0.20

For a ratio of 0.05, the required amount of F- is

g-atoms F = atomic ratio * g-atoms of Al
= 0.05 * 7.35
= 0.36

Therefore the weight of NH_4F required is:

g NH_4F = g-atoms of F required * g NH_4F/ g-atom F
= 0.36 * 37
= 13.32

The weight percent fluoride present is given by:

$$\text{wt \% F} = \frac{\text{g-atoms F} * \text{atomic wt F}}{\text{g } Al_2O_3 + (\text{g-atoms F} * \text{atomic wt F})} * 100$$

$$= \frac{0.36 * 19}{375 + 0.36 * 19} * 100$$

$$= 1.83$$

Similar calculations were made for the other catalysts and are summarized in Table A4.1.

Table A4.1

Catalyst nominal composition

Designation	Atomic Ratio [F/Al]	Fluoride Content [wt %]
[-2]	0	0
[-1]	0.05	1.8
[0]	0.10	3.6
[1]	0.20	6.9
[2][a]	3	68

[a] starting material was $AlF_3.3H_2O$

APPENDIX 4.2

Calculation of adsorption capacity of the catalysts for ammonia

The experimental method consists of injecting pulses of ammonia into an inert carrier gas (Argon) which flows through a packed bed of catalyst (40 mg) and a thermal conductivity detector. The signal of the detector shows as a peak in the chromatogram, corresponding to the amount of ammonia which is not adsorbed on the catalyst surface for each pulse injected.

The number of moles of injected ammonia in one pulse, n, can be determined by using the ideal gas law:

$$n = \frac{P * V}{R * T} \qquad \ldots (A1)$$

where P=1 atm (101 kPa), V= 0.25 mL (size of the sample loop), R = 0.082 L-atm/K mol and T is the temperature of the sample loop (120°C, 393K).

The relationship between the sum of the differences in peak areas and the number of moles of ammonia adsorbed on the surface of the catalyst is given by the expression :

$$x = \frac{n * \sum_{i=1}^{k} (\bar{A}_{\infty} - A_i)}{\bar{A}_{\infty}} \qquad \ldots (A2)$$

where x number of moles of ammonia gas adsorbed

A_i response area of peak i

$\bar{A}_{\infty}$ average of p response areas, usually the average area of the last 5 constant peaks

n the number of moles of injected ammonia in a single pulse

k the total number of injections (k > 15)

To obtain a specific amount of ammonia adsorbed per unit weight of catalyst (C_{NH3}) one must divide by the weight of the catalyst loaded into the packed bed.

$$C_{NH3} = x / m$$

where m is the mass of the catalyst [g].

For example the peak areas and differences for 10 injections made with 40 mg of 1.56 wt % F on alumina catalyst are given in Table A4.2. The number of moles of injected ammonia in one pulse, n,

$$n = \frac{(1\ \text{atm})\ (2.5\ \text{E}\ -04\ \text{L})}{0.082\ \frac{\text{L atm}}{\text{mol K}}\ (393\ \text{K})}$$
$$= 7.76\ \text{E}\ -06\ \text{mol}$$

The number of moles of ammonia gas adsorbed, x,

$$x = \frac{7.76\ \text{E}\ -06\ (338,767 + 86,745)}{859,017}$$
$$= 3.84\ \text{E}\ -06\ \text{mol}$$

The specific amount of ammonia adsorbed per unit weight of catalyst, C_{NH3},

$$C_{NH3} = \frac{3.84\ \text{E}\ -06\ \text{mol}}{0.040\ \text{g}}$$
$$= 9.6\ \text{E}\ -05\ \text{mol/g}$$
$$= 0.096\ \text{mmol/g}$$

A summary of these calculations for all the catalysts is given in Table A4.3.

Table A4.2

Summary of peak areas and differences in ammonia adsorbed on 2.6 wt % F on alumina

Injection	Peak area	Average	Difference
1	520,250		338,767
2	772,272		86,745
3	879,803		-
4	888,659		-
5	829,026		-
6	834,681	859,017	-
7	857,925		-
8	861,741		-
9	858,601		-
10	861,700		-

Table A4.3

Summary of ammonia adsorption studies of catalysts

Catalyst Designation	Fluoride content [wt % F]	Ammonia adsorbed [mmol/g]
[-2]	0	0.142, 0.134[a]
[-1]	1.56	0.145, 0.215
[0]	2.6	0.325, 0.295
[1]	4.3	0.096
[2]	68 [b]	2.40[c]

[a] repeated experiments

[b] nominal composition

[c] some water may still have been present in the sample and would account for this high acidity.

APPENDIX 4.3

Pressure drop calculation for fixed bed reactor

Flowrate :	Nitrogen	250 mL/min @ NTP
	Acetylene	25 mL/min @ NTP
	Total	275 mL/min @ NTP

Reactor configuration:
- Length 55 cm
- Catalyst bed 12.5 cm
- Internal diameter 1 cm
- Thermowell O.D. 0.318 cm
- Catalyst particle size 0.05-0.1 cm

Reynolds number:

$$Re = \rho D_p U_m / \mu$$

where D_p particle diameter

U_m superficial velocity

μ viscosity

ρ gas density

At 500 C, 6 psig, the total volumetric flowrate (v_o) is given by:

$$v_o = 275 \text{ mL/min} * \frac{(273 + 500)}{298} * \frac{14.7}{(14.7 + 6)}$$

$$= 506.6 \text{ mL/min}$$

The superficial velocity , U_m, is given by v_o/A where A is the cross-sectional area of the annular catalyst bed:

$$U_m = \frac{4 v_o}{\pi (d_i^2 - d_t^2)} = \frac{4 * 506.6}{(1 - 0.318^2)3.1416}$$

$$= 717 \text{ cm/min} = 12 \text{ cm/s}$$

The density of nitrogen can be calculated from :

$$\rho (500 \text{ C}) = \frac{\frac{(14.7 + 6)}{14.7} (28)}{82.06 \quad (773)}$$

$$= 6.21 \text{ E -04 g/mL}$$

The viscosity of nitrogen at 500 ^{0}C, is 0.036 centipoise or 3.6 E-04 g/cm/s. (Perry's Handbook, 5th ed.)

The Reynold's number can now be calculated :

$$Re = \frac{(6.21\ E\text{-}04)\ (0.05)\ (12)}{3.6E\text{-}04}$$

$$= 1.04$$

The pressure drop parameter is 1500 at this Reynolds number. (Perry's handbook, 5th ed., page 5-52).

$$\frac{\Delta P \quad g_c \quad D_p^{\,2}}{\mu \quad L \quad U_m} = 1500$$

Rearrangement of this equation leads to an expression for ΔP, the pressure drop:

$$\Delta P = \frac{1500\ L\ U_m\ \mu}{g_c\ D_p^{\,2}}$$

$$= \frac{1500\ [55(1/2.54)\ (1/12)]\ [0.036(6.72E\text{-}04)]\ [12(1/2.54)(1/12)]}{32\ \frac{lbm\ ft}{lbf\ s^2}\quad \frac{0.05}{(2.54)(12)}\ cm^2}$$

$$= 298\ lbf/ft^2$$
$$= 2.1\ psi$$
$$= 14.5\ kPa$$

This is a fairly low pressure differential.

APPENDIX 4.4

Details of gas analysis with the thermal conductivity detector

Calculating response factors

$$RF(i) = \frac{CONC\ (i)\ *\ AREA\ (R)}{AREA\ (i)\ *\ CONC\ (R)}$$

where RF(i) - response factor for component i

CONC(i) - amount of component i in the calibration sample

AREA(i) - area of the component i peak

CONC(R) - amount in the calibration sample of component (identified as IP)

AREA(R) - area of the IP component peak

Calculating concentrations:

$$CONC(i) = \frac{RF(i) * AREA(i)}{\sum_{i=1}^{n} RF(i)\ AREA(i)} \qquad XF$$

where CONC(i) - percentage of component i present in the analysis sample

RF(i) - response factor for component i calculated in the calibration run

AREA(i) - the area of the component i peak measured in the analysis run

XF - total percentage of the analysis sample represented by the components integrated in the chromatogram, if other than 100

$\sum_{i=1}^{n} RF(i)AREA(i)$ - summation of all of the detector response connected areas in the chromatogram.

APPENDIX 4.5

Details of vapor analysis on flame ionization detector

Calibration for each component of interest i:

$$RF(i) = \frac{CONC(i)\ AREA(is)}{AREA(i)\ CONC(is)}$$

where RF(i) - response factor for component i
CONC(i) - amount of component i used in the calibration sample
AREA(i) - area of the component i peak
AREA(is) - area of the internal standard peak
CONC(is) - amount of the internal standard used in the calibratio sample

Analysis of each component of interest:

$$CONC(i) = \frac{IS\ RF(i)\ AREA(i)\ XF}{SA\ RF(is)\ AREA(is)}$$

where CONC(i) - amount of i present in the analysis sample (if this value is desired as a percentage, XF= 100)
IS - amount of internal standard added to the analysis samp
SA - amount of sample material measured
RF(i) - response factor of component i determined by calibrati
AREA(i) - area of the component i peak in the analysis run
RF(i) - response factor of the internal standard is 1, by definition
AREA(is) - area of the internal standard peak in the analysis run
XF - a scaling factor which may be used as a conversion fac If the CONC(i) is desired as a percentage, XF must equal 100, otherwise its use is optional.

To obtain quantitative results from the GC trace, it is necessary to use correction factors. The amount of the correction is a function of the response of a given compound to the detector. Relative sensitivity values for the FID detector are given by Dietz (A2). Each area is divided by the relative sensitivity to get the true area. Normalizing the results gives weight per cent of each component. For hydrocarbons with three exceptions, the values are all approximately 1.0. The three exceptions are benzene 1.12 and toluene 1.07 and acetylene 1.07. These however are not large variations.

A2. Dietz, J.H., J. Gas Chromatography, 5, 68, 1967.

APPENDIX 4.6

Comparison of the weight-time curve with and without reactant gas contacting the catalyst

Experiment vma08

The empty sample pan was taken through the temperature cycle in the presence of reacting gas. The change in weight of the pan is negligible and the thermal conversion was under 5 %.

Experiment vma02

An alumina catalyst weight-time curve with no reactant contacting the catalyst. The change in weight over a 1 h period was under 0.0005 g/min and assumed negligible compared with the rate of reaction.

Experiment vma05

An alumina catalyst weight-time curve with the reactant flowing over the catalyst. The change in weight over the 1 h period is substantial. The rate of weight change is two orders of magnitude higher than without the reactant gas.

TGA File Name: vma08
Sample Weight: 0.001 mg
Mon Oct 27 17:49:55 1986
Blank run, no catalyst

Sample pan taken through the temperature cycle in the presence of the reacting gas.

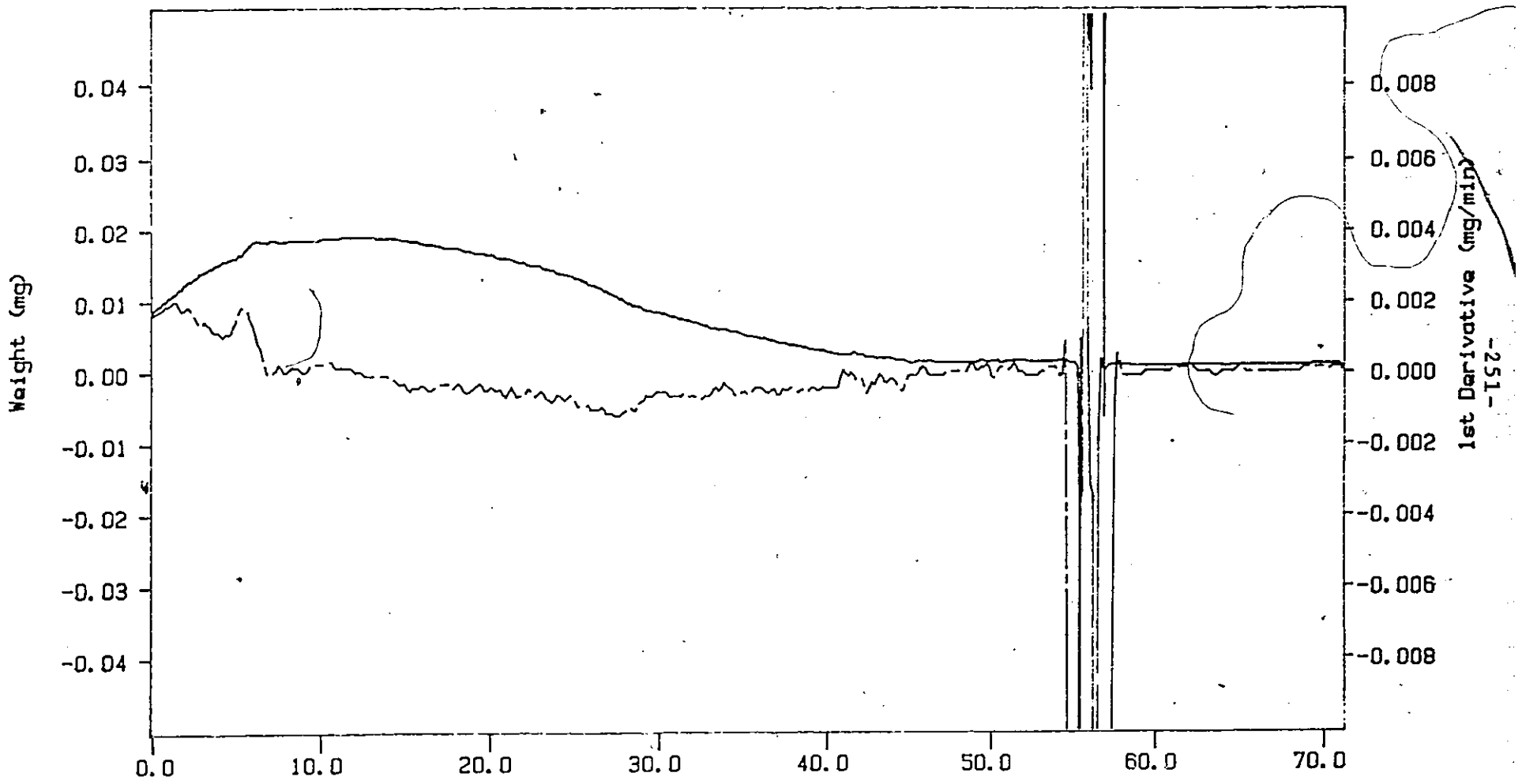

Reactant 11%, 350 C, 32/30ml/min

V.M. Allenger

TEMP 1:	40.0 C	TIME 1:	5.0 min	RATE 1:	10.0 C/min
TEMP 2:	400.0 C	TIME 2:	60.0 min	RATE 2:	5.0 C/min
TEMP 3:	50.0 C	TIME 3:	5.0 min	RATE 3:	10.0 C/min
TEMP 4:	800.0 C	TIME 4:	5.0 min	RATE 4:	10.0 C/min
TEMP 5:	800.0 C				

TGA 1st Derivative: vma02
Sample Weight: 19.311 mg
Wed Oct 22 13:22:41 1986
Al203, 0.5-1.0 mm

Example weight-time curve with no reactant contacting the catalyst.

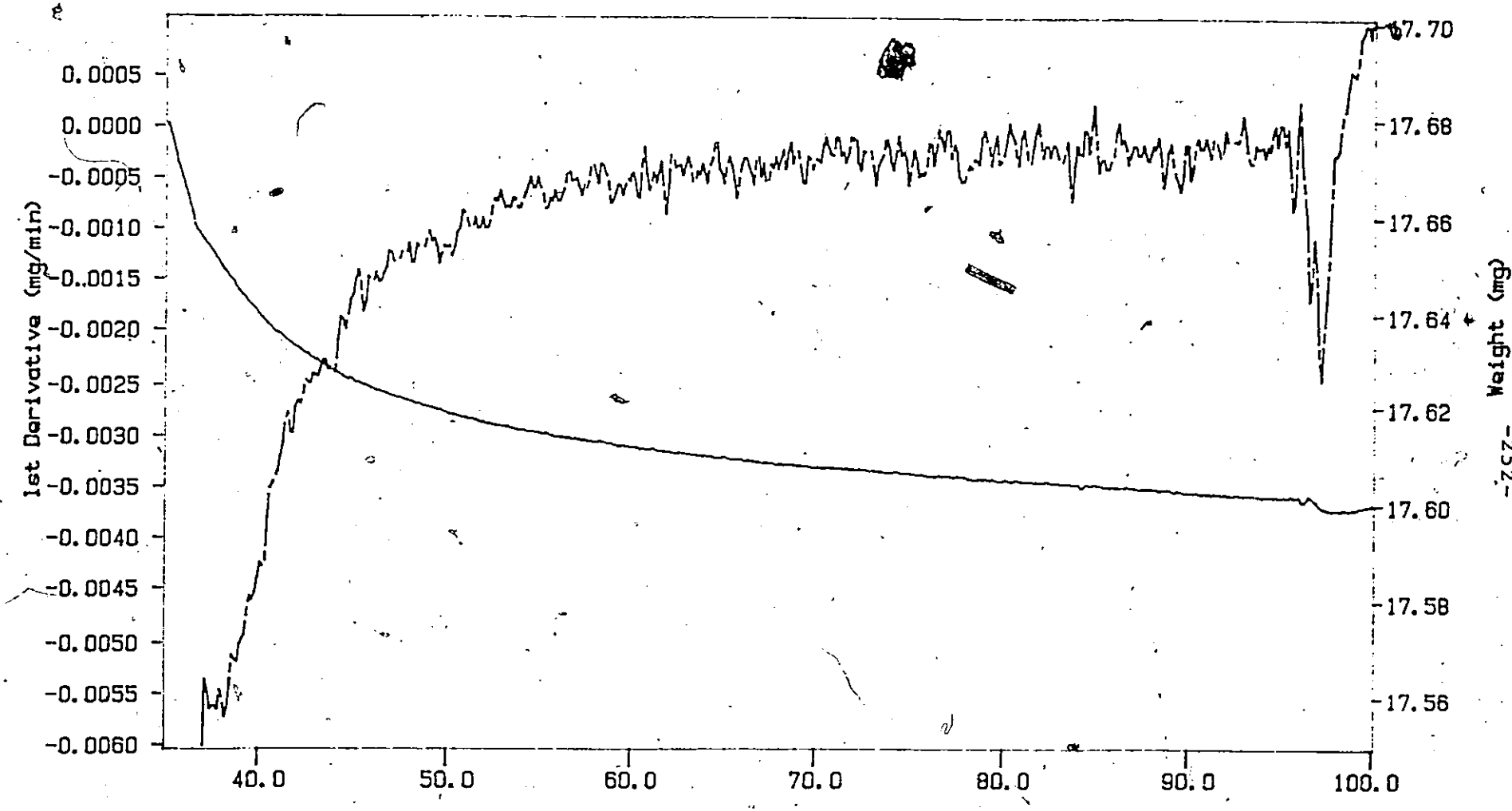

No reactant, blank, N2p=32, AIR=30ml/min

Time (minutes)

V. M. Allenger

TEMP 1: 40.0 C TIME 1: 5.0 min RATE 1: 10.0 C/min
TEMP 2: 950.0 C TIME 2: 60.0 min RATE 2: 5.0 C/min
TEMP 3: 950.0 C TIME 3: 5.0 min RATE 3: 10.0 C/min
TEMP 4: 600.0 C TIME 4: 5.0 min

TGA File Name: vma05
Sample Weight: 19.517 mg
Thu Oct 23 16:56:16 1986
Al203, 0.5-1 mm, repeat

Example weight-time curve with the reactant flowing over the catalyst.

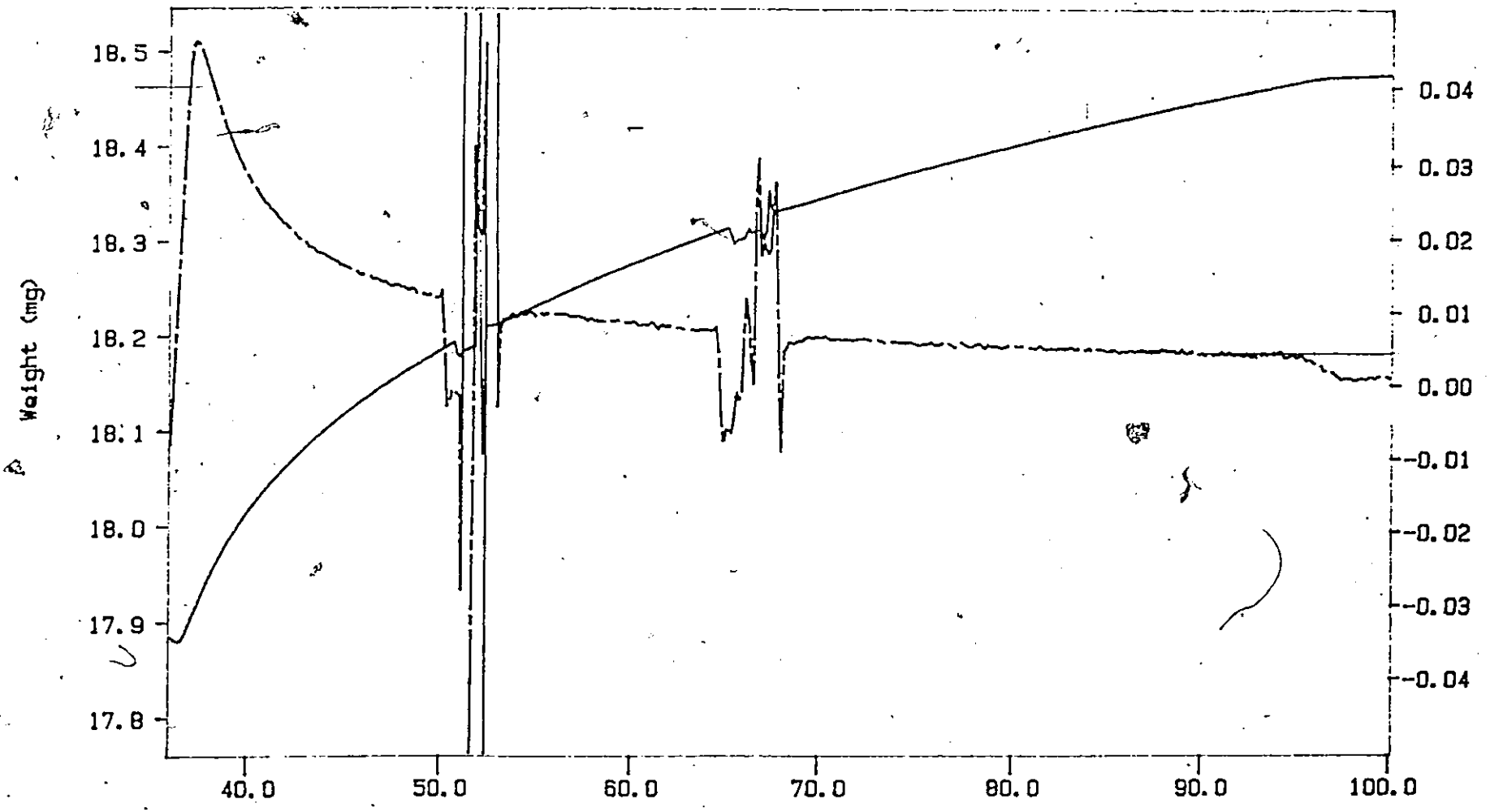

Bal Purge=32, Reactant 11% =30ml/min V. M. Allenger

TEMP 1:	40.0 C	TIME 1:	5.0 min	RATE 1:	10.0 C/min
TEMP 2:	350.0 C	TIME 2:	60.0 min	RATE 2:	5.0 C/min
TEMP 3:	50.0 C	TIME 3:	5.0 min	RATE 3:	10.0 C/min
TEMP 4:	600.0 C	TIME 4:	5.0 min		

APPENDIX 4.7

Calculation procedures for determining product yields

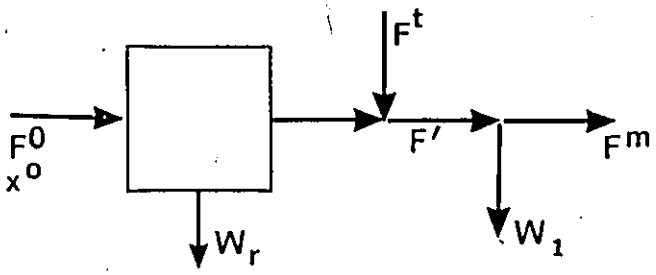

where W_1 - weight of the condensed liquid [g]

ρ - density of the condensed liquid [g]

t - length of the experimental run [min]

F^0 - feed flowrate [mL/min]

F^m - product gas flowrate without condensables [mL/min]

W_r - weight of the carbonaceous residue [g]

F^t - flowrate of the liquid tracer [mL/min]

x_o, x' - mole fraction of the components in the feed and product respectively

y' - mole fraction of the liquid vapor in the product stream

F' - product flowrate [mL/min]

Analysis

Tracer sample size: 1 mL loop

Tracer flowrate: F_t mL/min

Product flowrate: $F'' = F' \left(\frac{T + 273}{273}\right) \left(\frac{14.7}{14.7 + P}\right)$ at reaction conditions

Residence time in loop: $1/F'' = \tau$ min

In τ min, $(F^t \tau)$ mL of tracer will be in the loop, or
$(\rho_t F^t \tau)$ g of tracer will be in the loop.

Moles of tracer in sample loop IS $n_{is} = \frac{\rho_t F^t \tau}{M_t}$ where M_t - molecular weight of the tracer

Now to obtain SA, use the ideal gas law, $n = PV/RT$, where

$V/R = 1.219$ E-02

Moles of sample in sample loop SA $n_{sa} = \frac{1.219E\text{-}02\ P}{(273 + T)}$ abs -

and the CONC(i) - (n_{is}/n_{sa}) (AREA(i)/AREA(is)) mol %

Now the molar flowrate of a component is given by :

$$C(i) = \frac{CONC\ (i)}{22{,}400\ [mL/mol]}\ F'[mol/min] \qquad @\ STP$$

Reactant flowrate $F_{C2H2}^{o} = x_{C2H2}^{o}\ F^{o}$

Tie component balance $F^{m} = x_{N2}^{o}\ F^{o} / x'_{N2}$

Acetylene conversion $X = \dfrac{x^{o}_{C2H2}\ F^{o} - x'_{C2H2}\ F^{m}}{x^{0}_{C2H2}\ F^{0}}$

Total mass balance

moles/min of $N_2 = x'_{N2}\ F^{m}/\ 22400$

$H_2 = x'_{H2}\ F^{m}/\ 22400$

$C_2H_2 = x'_{C2H2}\ F^{m}/\ 22400$

. etc. for C_2H_4 and other gas components

moles/min of $C_6H_6 = y'_{C6H6}\ F'\ /22400$

$C_7H_8 = y'_{C7H8}\ F'\ /22400$

. etc. for other liquid components

Input $F^{0}\ (x_{N2}M_{N2} + x_{C2H2}M_{C2H2} + x_{H2}M_{H2})/22400 + F^{t}\ (x_{N2}^{t}\ 28 + x_{C7}^{t}\ 100)$

Output $F^{m}\ (x'_{N2}M_{N2} + x'_{C2H2}M_{C2H2} + x'_{H2}M_{H2} + \ldots)/22400$

$+ F'\ (y'_{C6H6}M_{C6H6} + y'_{C7H8}M_{C7H8} + \text{etc.})/\ 22400 + W_r$

where W_r is the carbonaceous deposit on the catalyst.

APPENDIX 6.1

ANOVA for model of catalyst activity

VOGELBACK COMPUTING CENTER
NORTHWESTERN UNIVERSITY

S P S S - - STATISTICAL PACKAGE FOR THE SOCIAL SCIENCES

VERSION 8.0 -- JUNE 18, 1979

```
FILE NAME              ACETYLENE CONVERSION REGRESSION AT 15 MIN
INPUT MEDIUM           DISK
VARIABLE LIST          X1,X2,X3,X4,X1S,X2S,X3S,X4S,X1X2,X1X3,X1X4,CONV15
INPUT FORMAT           FIXED(11(F2.0,1X),F5.0)
```

ACCORDING TO YOUR INPUT FORMAT, VARIABLES ARE TO BE READ AS FOLLOWS

VARIABLE	FORMAT	RECORD	COLUMNS
X1	F 2.0	1	1- 2
X2	F 2.0	1	4- 5
X3	F 2.0	1	7- 8
X4	F 2.0	1	10- 11
X1S	F 2.0	1	13- 14
X2S	F 2.0	1	16- 17
X3S	F 2.0	1	19- 20
X4S	F 2.0	1	22- 23
X1X2	F 2.0	1	25- 26
X1X3	F 2.0	1	28- 29
X1X4	F 2.0	1	31- 32
CONV15	F 5.0	1	34- 38

THE INPUT FORMAT PROVIDES FOR 12 VARIABLES. 12 WILL BE READ.
IT PROVIDES FOR 1 RECORDS (*CARDS*) PER CASE.
A MAXIMUM OF 38 *COLUMNS* ARE USED ON A RECORD.

```
REGRESSION             VARIABLES=X1 TO X4,X1S TO X4S,X1X2,X1X3,X1X4,CONV15
                       [illegible]
STATISTICS             ALL
OPTIONS                6
```

[illegible] OF NEEDED FOR REGRESSION

OPTION = 1
IGNORE MISSING VALUE INDICATORS
(NO MISSING VALUES DEFINED...OPTION 1 WAS FORCED)

OPTION = 6
SUPPRESS STEP-BY-STEP OUTPUT

END OF FILE OF FILE DATA
AFTER READING 21 CASES FROM SUBFILE ACETYLEN

FILE ACETYLEN (CREATION DATE = 03/04/86) CONVERSION REGRESSION AT 15 MIN

* MULTIPLE REGRESSION *

VARIABLE	MEAN	STANDARD DEV	CASES
X1	.3425	1.0342	21
X2	-.2381	.8651	21
X3	-.0476	1.0235	21
X4	.0476	1.0235	21
X1S	1.0000	1.0954	21
X2S	.8163	.8735	21
X3S	1.0000	1.0954	21
X4S	1.0000	1.0954	21
X1X2	.1429	.7928	21
X1X3	-.0476	.8647	21
X1X4	-.0476	.8647	21
CONVJS	71.2571	36.8414	21

CORRELATION COEFFICIENTS.

A VALUE OF 99.0000 IS PRINTED
IF A COEFFICIENT CANNOT BE COMPUTED.

	X1	X2	X3	X4	X1S	X2S	X3S	X4S	X1X2	X1X3	X1X4
X2	.2041										
X3	.0000	-.2041									
X4	-.0000	.2041	.1429								
X1S	.0000	.2041	.0000	.0000							
X2S	.0227	-.4479	-.0000	.0000	-.2917						
X3S	.0000	.2041	.0000	.0000	-.3333	-.2917					
X4S	.0000	.2041	.0000	.0000	-.3333	-.2917	-.3333				
X1X2	-.2132	.2947	.7642	-.7642	.0000	.4129	.0000	.0000			
X1X3	-.7500	.2947	.1429	-.1429	.0000	.4129	.0000	.0000	-.2956		
X1X4	.7500	-.2132	-.1429	.1429	.0000	.4129	.0000	.0000	-.0896	-.2329	
CONVJS	.3566	-.2032	.4766	.0244	-.1447	.3422	-.2743	.2319	-.2152	-.2567	.0052

FILE ACETYLENE [illegible] (CREATION DATE = 03/04/86) CONVERSION REGRESSION AT 15 MIN

* M U L T I P L E R E G R E S S I O N *

DEPENDENT VARIABLE.. CONV15

MEAN RESPONSE 71.55734 STD. DEV. 30.54141

FINAL STEP.

MULTIPLE R	.99393	ANALYSIS OF VARIANCE	DF	SUM OF SQUARES	MEAN SQUARE	F	SIGNIFICANCE
R SQUARE	.98748	REGRESSION	6.	18048.86937	3008.14485	69.41697	.000
ADJUSTED R SQUARE	.[illegible]	RESIDUAL	14.	606.66206	43.33443		
STD DEVIATION	6.[illegible]	COEFF OF VARIABILITY	9.2 PCT				

------------------- VARIABLES IN THE EQUATION -------------------

VARIABLE	B	STD ERROR B	F / SIGNIFICANCE	BETA / ELASTICITY
X1	13.[illegible]	1.[illegible]	83.[illegible] / .000	.45[illegible] / .[illegible]
X4S	7.[illegible]	1.3742157	32.43[illegible] / .000	.26[illegible] / .10[illegible]
X3	13.[illegible]	1.4787670	81.61[illegible] / .000	.4477150 / -.0[illegible]
X1X3	-9.[illegible]	1.[illegible]	27.0[illegible] / .000	-.25[illegible] / -.00[illegible]
X2S	-4.[illegible]	1.94[illegible]	6.50[illegible] / .023	-.142017[illegible] / -.05621
X2	-26.[illegible]	1.941[illegible]	182.98[illegible] / .000	-.765[illegible] / .0[illegible]
(CONSTANT)	60.[illegible]	2.[illegible]774[illegible]	543.0[illegible] / .000	

ALL VARIABLES ARE IN THE EQUATION.

COEFFICIENTS AND CONFIDENCE INTERVALS.

VARIABLE	B	STD ERROR B	T	95.0 PCT CONFIDENCE INTERVAL	
X1	13.[illegible]	1.[illegible]	9.1315971	10.[illegible]	17.067414
X4S	7.[illegible]	1.3742157	5.69[illegible]	4.6794422	10.774241
X3	13.[illegible]	1.4787670	9.0341907	10.[illegible]	16.531102
X1X3	-9.[illegible]	1.[illegible]	-5.[illegible]	-13.[illegible]	-5.[illegible]
X2S	-4.[illegible]	1.94[illegible]	-2.[illegible]	-9.[illegible]	-.79061222
X2	-26.[illegible]	1.941[illegible]	-13.[illegible]	-30.423319	-22.[illegible]
CONSTANT	60.[illegible]	2.[illegible]7746	23.303120	[illegible].049214	66.209717

VARIANCE/COVARIANCE MATRIX OF THE UNNORMALIZED REGRESSION COEFFICIENTS.

X1	2.29[illegible]					
X2	-.77[illegible]	3.7[illegible]				
X3	-.[illegible]	.[illegible]	2.1[illegible]			
X2S	-.4[illegible]	1.7[illegible]	.2[illegible]	3.79527		
X4S	-.[illegible]	-.[illegible]	.[illegible]	.48[illegible]	1.88647	
X1X3	.[illegible]	-.[illegible]	-.[illegible]	-.31228	-.00710	3.[illegible]
	X1	X2	X3	X2S	X4S	X1X3

FILE ACETYLEN (CREATION DATE = 01/04/86) CONVERSION REGRESSION AT 15 MIN

* MULTIPLE REGRESSION *

DEPENDENT VARIABLE.. CONV15

SUMMARY TABLE

STEP	VARIABLE ENTERED	VARIABLE REMOVED	F TO ENTER OR REMOVE	SIGNIFICANCE	MULTIPLE R	R SQUARE	R SQUARE CHANGE	SIMPLE R	OVERALL F	SIGNIFICANCE
1	X1		83.28667	.000	.33968	.11538	.11538	.33968	69.41697	.000
	X5		32.43849	.000	.41131	.16918	.05380	.23194		
	X3		21.61660	.000	.61756	.38138	.21220	.47866		
	X1X3		27.01028	.000	.76810	.58140	.12002	-.27597		
	X2S		6.21564	.023	.73651	.54244	.04104	-.14022		
	X2		162.55018	.000	.98361	.96748	.42504	-.03032		

FILE ACETYLEN (CREATION DATE = 01/04/86) CONVERSION REGRESSION AT 15 MIN

* MULTIPLE REGRESSION *

OBSERVATION #	Y VALUE	Y ESTIMATE	RESIDUAL	-2SD	0.0	+2SD
1.	41.00000	47.59360	-6.593596		I	
2.	99.20000	107.21156	-7.011568		I	
3.	98.91000	100.03233	-1.123271		I	
4.	C	.2324793	-.2324793		I	
5.	97.60000	99.05967	-1.459869		I	
6.	59.00000	52.75255	6.247445		I	
7.	58.10000	68.27179	9.828206		I	
8.	28.60000	32.96714	-4.367138		I	
9.	99.30000	93.27366	6.026338		I	
10.	87.20000	87.34835	-.1483913		I	
11.	29.20000	33.91044	-4.710544		I	
12.	99.60000	91.93683	7.663166		I	
13.	90.20000	91.93683	-1.736832		I	
14.	71.90000	60.62647	11.27353		I	
15.	57.80000	54.55373	3.226267		I	
16.	48.10000	47.50320	.596805		I	
17.	99.30000	107.11136	-7.811360		I	
18.	96.30000	100.02233	-3.723271		I	
19.	99.30000	99.19567	.2061310		I	
20.	90.00000	92.75255	-2.752555		I	
21.	51.50000	54.59373	-3.093733		I	

NOTE - (*) INDICATES ESTIMATE CALCULATED WITH MEANS SUBSTITUTED
R INDICATES POINT OUTSIDE RANGE OF PLOT

NUMBER OF CASES PLOTTED 21.
NUMBER OF 2 S.E. OUTLIERS 0 OR 0 PERCENT OF THE TOTAL

VON NEUMANN RATIO 1.84846 DURBIN-WATSON TEST = 1.76044

NUMBER OF POSITIVE RESIDUALS 8.
NUMBER OF NEGATIVE RESIDUALS 13.
NUMBER OF RUNS OF SIGNS 11.

NORMAL APPROXIMATION TO SIGN DISTRIBUTION IMPOSSIBLE.
USE A TABLE FOR EXPECTED VALUES.

APPENDIX 7.1

Sample material balance calculation

This calculation was performed for experiment no. 12 which had an alumina catalyst containing no fluoride.

1. Determining the quantity of tracer

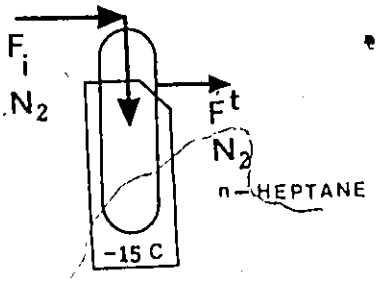

Vapor pressure of n-heptane at $-15^{o}C$ = 15 mm Hg

Material balance over bubbler

$$F_i = F^t\ (755/760)$$

$$F^t = 1.0066\ F_i$$

2. Overall balance assuming constant density

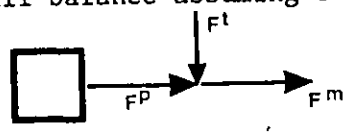

$$F^p + F^t = F^m$$

Tracer component balance:

$$x_{heptane} = \frac{F^t\ x^t_{heptane}}{F^m} \quad \frac{1.0066\ F_i\ x^t_{heptane}}{F^m}$$

3. Determining the number of moles of tracer using the ideal gas law:

1 mL / 22400 mL = 4.46 E-05 mol gas in sample loop at STP

N = 1 mL/ 47016 mL = 2.13 E-05 mol gas in sample loop at $350^{o}C$

Moles of n-heptane in sample loop = $x_{heptane}\ N$

$$n_{heptane} = (1.0066)(3.06)(6.6\text{ E-}03)(2.13\text{ E-}05) / 87$$

$$n_{heptane} = 5\text{ E-}09\text{ mol}$$

4. Obtaining distribution of the liquids [mol %]

$$\text{(Amount of Comp i)} = \frac{\text{(Response Area of Comp i)(Mol Tracer)}}{\text{(Response Area of Tracer Comp)}}$$

$$\text{mol of } C_6H_6 = \frac{44183\ (5\text{ E-}09)}{2660} = 8.31\text{ E-}08\text{ mol}$$

$$\text{mol of } C_7H_8 = \frac{7953\ (5\text{ E-}09)}{2660} = 1.49\text{ E-}08\text{ mol}$$

Similarly for other components.

5. Obtaining the cumulative weight of liquids.

$$\frac{F \text{ mL / min}}{22400} \sum \left\{ \frac{\text{mol comp i}}{\text{mol product}} \right\} (\text{M. W. comp i}) = \sum \text{mol fraction} * \text{M.W}$$

$$(F^m / 22400)(1/2.13 \text{ E-05}) \quad \sum (\text{mol. comp i})(\text{M.W. comp i})$$

$$(87 / 22400)(1/2.13 \text{ E-05}) \quad ((8.31 \text{ E-08} * 78) + (1.49 \text{ E-08} * 92) + \ldots)$$

Product = 388 (6.48 E-06 + 1.371 E-06 + ...)

Product = 5.75 E-03 g/min

6. Liquids : 5.75 E-03 g/min * 15 min (T.O.S.) = 0.0962 g

7. Gases: Composition at 15 min on stream:

		M.W.
0.1109	H_2	2
0.068	C_2H_2	26
0.0079	t-butene-2	56
0.1382	C_2H_2	24
0.0249	CH_4	16

Obtain wt % distribution.

(2 * 0.1109 + 26 * 0.068 + ...) = 6.145 E-02 g/mol total gas

(F/22400) (6.145 E-02) = 2.4 E-04 g/min

Total gases = 2.4 E-04 * 15 min T.O.S. = 3.59 E-03 g

8. Solid : 5.81 wt % C at 60 min.

By linear interpolation, 0.0581 g C / g cat * 4.5 g cat = 0.261 g of carbon at 60 min and 15/60 * 0.261 g = 0.0654 g at 15 min.

9. Feed: 9.12 vol % C_2H_2, F^o = 92.02 mL/min

0.0912 * 92.02 * 15 = 126 mL

126 mL / (22400 mL/mol) * 26 g/mol = 0.146 g C2H2

10. Material Balance

(IN - OUT) at 15 min on stream

0.146 - (0.0862 + 0.00359 + 0.0654)

-0.009

Therefore, 106.3 % closure.

APPENDIX 8.1

Summary of experimental results

Conversion of acetylene as a function of time-on-stream for experiments carried out in the tubular reactor for longer periods

TIME-ON-STREAM (MIN)	EXPERIMENT NUMBER 17 (C218)	1 (C220)	8 (C221)
5	91.4		
15		57.9	59.0
25	54.7		
30		36.1	41.5
45	42.3	24.2	33.7
60		23.2	31.0
66	40.9		
75		40.9	44.3
87	21.8		
90		17.3	22.1
105		20.6	25.4
120		14.4	17.4
135		12.0	14.6
147	26.9		
150		8.8	11.9
165		7.6	8.6
180	16.8	8.7	12.3
200	46.3		
220	14.6		
240	26.0	4.8	3.8
300		16.7	17.6

APPENDIX 8.2

ANOVA for model of initial activity, $\hat{a}_0$

VOGELBACK COMPUTING CENTER
NORTHWESTERN UNIVERSITY

S P S S -- STATISTICAL PACKAGE FOR THE SOCIAL SCIENCES

VERSION 8.0 -- JUNE 18, 1979

```
FILE NAME           REGRESSION FOR INITIAL ACTIVITY, AO
INPUT MEDIUM        DISK
VARIABLE LIST       X1,X2,X3,X4,X1S,X2S,X3S,X4S,X1X2,X1X3,X1X4,AO
INPUT FORMAT        FIXED(1(F2.0,1X),2X,F5.0)
```

ACCORDING TO YOUR INPUT FORMAT, VARIABLES ARE TO BE READ AS FOLLOWS

VARIABLE	FORMAT	RECORD	COLUMNS
X1	F 2.0	1	1- 2
X2	F 2.0	1	4- 5
X3	F 2.0	1	7- 8
X4	F 2.0	1	10- 11
X1S	F 2.0	1	13- 14
X2S	F 2.0	1	16- 17
X3S	F 2.0	1	19- 20
X4S	F 2.0	1	22- 23
X1X2	F 2.0	1	25- 26
X1X3	F 2.0	1	28- 29
X1X4	F 2.0	1	31- 32
AO	F 5.0	1	40- 44

THE INPUT-FORMAT PROVIDES FOR 12 VARIABLES. 12 WILL BE READ.
IT PROVIDES FOR 1 RECORDS (*CARDS*) PER CASE.
A MAXIMUM OF 44 *COLUMNS* ARE USED ON A RECORD.

```
REGRESSION          VARIABLES=X1 TO X4,X4S,AO
                    REGRESSION=AO WITH X1 TO X4,X4S/ RESIDUALS
STATISTICS           ALL
```

00055100 CM NEEDED FOR REGRESSION

OPTION - 1
IGNORE MISSING VALUE INDICATORS
(NO MISSING VALUES DEFINED...OPTION 1 WAS FORCED)

END OF FILE ON FILE TAPE2
AFTER READING 22 CASES FROM SUBFILE REGRESSI

FILE REGRESSI (CREATION DATE = 12/01/87) FOR INITIAL ACTIVITY, A0

* MULTIPLE REGRESSION *

VARIABLE	MEAN	STANDARD DEV	CASES
X1	.1364	.9902	22
X2	-.2273	.8691	22
X3	.0455	.9989	22
X4	-.0455	.9989	22
X4S	.9545	1.0901	22
A0	89.4645	33.1393	22

CORRELATION COEFFICIENTS.

A VALUE OF 99.00000 IS PRINTED
IF A COEFFICIENT CANNOT BE COMPUTED.

X2	.20372				
X3	-.05471	-.06731			
X4	.05471	-.06731	.14534		
X4S	.00602	.08910	.00199	-.00199	
A0	.11076	-.50980	.43997	.45891	.38831
	X1	X2	X3	X4	X4S

FILE REGRESSI (CREATION DATE = 12/01/87) FOR INITIAL ACTIVITY, AO

* MULTIPLE REGRESSION *

DEPENDENT VARIABLE.. AO

MEAN RESPONSE 89.46455 STD. DEV. 33.13934

VARIABLE(S) ENTERED ON STEP NUMBER 1.. x1, x4S, x3, x4, x2

MULTIPLE R	.92575	ANALYSIS OF VARIANCE	DF	SUM OF SQUARES	MEAN SQUARE	F SIGNIFICANCE
R SQUARE	.85701	REGRESSION	5.	19764.76822	3952.95764	19.17894 .000
ADJUSTED R SQUARE	.81232	RESIDUAL	16.	3297.74812	206.10926	
STD DEVIATION	14.35651	COEFF OF VARIABILITY	16.0 PCT			

VARIABLES IN THE EQUATION

VARIABLE	B	STD ERROR B	F SIGNIFICANCE	BETA ELASTICITY
x1	7.9219530	3.2506902	5.9390004 .027	.2367099 .01207
x4S	13.391659	2.8856967	21.536116 .000	.4405099 .14288
x3	14.697742	3.1903346	21.224074 .000	.4430331 .00747
x4	11.338925	3.1903346	12.631976 .003	.3417885 -.00576
x2	-23.032954	3.7250231	38.233261 .000	-.6040842 .05851
(CONSTANT)	70.213897	4.3135931	264.95236 .000	

VARIABLES NOT IN THE EQUATION

VARIABLE	PARTIAL	TOLERANCE	F SIGNIFICANCE

ALL VARIABLES ARE IN THE EQUATION.

COEFFICIENTS AND CONFIDENCE INTERVALS.

VARIABLE	B	STD ERROR B	T	95.0 PCT CONFIDENCE INTERVAL
x1	7.9219530	3.2506902	2.4370064	1.0307976 , 14.813108
x4S	13.391659	2.8856967	4.6407021	7.2742550 , 19.509062
x3	14.697742	3.1903346	4.6069593	7.9345346 , 21.460949
x4	11.338925	3.1903346	3.5541691	4.5757177 , 18.102132
x2	-23.032954	3.7250231	-6.1833051	-30.929650 , -15.136258
CONSTANT	70.213897	4.3135931	16.277357	61.069488 , 79.358305

VARIANCE/COVARIANCE MATRIX OF THE UNNORMALIZED REGRESSION COEFFICIENTS.

	x1	x2	x3	x4	x4S
x1	10.56699				
x2	-2.59757	13.87580			
x3	.84919	-1.11324	10.17823		
x4	-.94819	1.11324	-1.59035	10.17823	
x4S	.12369	-.96746	.05301	-.05301	8.32725

FILE REGRESSI (CREATION DATE = 12/01/87) FOR INITIAL ACTIVITY, AO

* MULTIPLE REGRESSION *

DEPENDENT VARIABLE.. AO

SUMMARY TABLE

STEP	VARIABLE ENTERED	VARIABLE REMOVED	F TO ENTER OR REMOVE	SIGNIFICANCE	MULTIPLE R	R SQUARE	R SQUARE CHANGE	SIMPLE R	OVERALL F	SIGNIFICANCE
1	X1		5.93900	.027	.11076	.01227	.01227	.11076	19.17894	.000
	X4S		21.53612	.000	.40317	.16254	.15028	.38631		
	X3		21.22407	.000	.60107	.36128	.19874	.43997		
	X4		12.63198	.003	.71786	.51532	.15404	.45891		
	X2		38.23326	.000	.92575	.85701	.34169	-.50980		

FILE REGRESSI (CREATION DATE = 12/01/87) FOR INITIAL ACTIVITY, AO

* MULTIPLE REGRESSION *

OBSERVATION	Y VALUE	Y ESTIMATE	RESIDUAL	-250	0.0	+250
1.	43.81000	42.45789	1.352112		I	
2.	109.0000	117.9193	-8.919279		I	
3.	110.6000	111.2016	-.6016452		I	
4.	77.10000	56.00947	21.09053		I	
5.	123.7000	124.7532	-1.053223		I	
6.	72.31000	72.67989	-.3698894		I	
7.	108.1000	86.05780	22.04220		I	
8.	31.50000	54.36999	-22.86999		I	
9.	124.8000	116.2798	8.520195		I	
10.	98.18000	99.60938	-1.429380		I	
11.	33.00000	40.81841	-7.818413		I	
12.	155.5000	146.4584	9.041620		I	
13.	98.00000	101.1027	-3.102681		I	
14.	78.50000	70.21390	8.286103		I	
15.	74.40000	94.53122	-20.13122		I	
16.	50.37000	42.45789	7.912112		I	
17.	103.0000	117.9193	-14.91928		I	
18.	103.3000	111.2016	-7.901645		I	
19.	81.30000	70.21390	11.08610		I	
20.	144.0000	124.7532	19.24678		I	
21.	66.80000	72.67989	-5.879889		I	
22.	80.95000	94.53122	-13.58122		I	

NOTE - (*) INDICATES ESTIMATE CALCULATED WITH MEANS SUBSTITUTED.
R INDICATES POINT OUT OF RANGE OF PLOT

NUMBER OF CASES PLOTTED 22.
NUMBER OF 2 S.D. OUTLIERS 0 OR 0 PERCENT OF THE TOTAL

VON NEUMANN RATIO 2.73976 DURBIN-WATSON TEST 2.61522

NUMBER OF POSITIVE RESIDUALS 9.
NUMBER OF NEGATIVE RESIDUALS 13.
NUMBER OF RUNS OF SIGNS 16.

NORMAL APPROXIMATION TO SIGN DISTRIBUTION IMPOSSIBLE.
USE A TABLE FOR EXPECTED VALUES.

APPENDIX 8.3

ANOVA for model of $\hat{k}_d$

```
VOGELBACK COMPUTING CENTER                                  12/01/87     14.23.18.     PAGE    1
NORTHWESTERN UNIVERSITY

S P S S  - -  STATISTICAL PACKAGE FOR THE SOCIAL SCIENCES

VERSION 8.0 -- JUNE 18, 1979


                FILE NAME           REGRESSION FOR DEACTIVATION PARAMETER,B  or KD
                INPUT MEDIUM        DISK
                VARIABLE LIST       X1,X2,X3,X4,X1S,X2S,X3S,X4S,X1X2,X1X3,X1X4,KD
                INPUT FORMAT        FIXED(11(F2.0,1X),12X,F5.0)

                ACCORDING TO YOUR INPUT FORMAT, VARIABLES ARE TO BE READ AS FOLLOWS

                VARIABLE   FORMAT  RECORD     COLUMNS
                X1         F 2. 0      1      1-   2
                X2         F 2. 0      1      4-   5
                X3         F 2. 0      1      7-   8
                X4         F 2. 0      1     10-  11
                X1S        F 2. 0      1     13-  14
                X2S        F 2. 0      1     16-  17
                X3S        F 2. 0      1     19-  20
                X4S        F 2. 0      1     22-  23
                X1X2       F 2. 0      1     25-  26
                X1X3       F 2. 0      1     28-  29
                X1X4       F 2. 0      1     31-  32
                KD         F 5. 0      1     46-  50

THE INPUT FORMAT PROVIDES FOR  12 VARIABLES.   12 WILL BE READ.
IT PROVIDES FOR   1 RECORDS (*CARDS*) PER CASE.
A MAXIMUM OF    50 *COLUMNS* ARE USED ON A RECORD.

                REGRESSION          VARIABLES=X1 TO X4,X2S,X4S,KD
                                    REGRESSION=KD WITH X1 TO X4,X2S,X4S/RESIDUALS
                STATISTICS           ALL

        00055100 BM NEEDED FOR REGRESSION


        OPTION  1
        IGNORE MISSING VALUE INDICATORS
        (NO MISSING VALUES DEFINED...OPTION 1 WAS FORCED)


END OF FILE ON FILE TAPE2
AFTER READING     22 CASES FROM SUBFILE REGRESSI
```

FILE REGRESSI (CREATION DATE = 12/01/87) FOR DEACTIVATION PARAMETER,B

* MULTIPLE REGRESSION *

VARIABLE	MEAN	STANDARD DEV	CASES
X1	.1364	.9902	22
X2	-.2273	.8691	22
X3	.0455	.9989	22
X4	-.0455	.9989	22
X2S	.7727	.8691	22
X4S	.9545	1.0901	22
KO	12.3057	8.5642	22

CORRELATION COEFFICIENTS.

A VALUE OF 99.00000 IS PRINTED
IF A COEFFICIENT CANNOT BE COMPUTED.

X2	.20372					
X3	-.05471	.06731				
X4	.05471	-.06731	.14534			
X2S	.03773	-.44986	.01247	-.01247		
X4S	.00602	.08910	.00199	-.00199	-.16220	
KO	-.50635	.19126	.40314	.39284	.02959	.21514
	X1	X2	X3	X4	X2S	X4S

FILE REGRESSI (CREATION DATE = 12/01/87) FOR DEACTIVATION PARAMETER,B

* MULTIPLE REGRESSION *

DEPENDENT VARIABLE.. XD

MEAN RESPONSE 12.30573 STD. DEV. 8.56420

VARIABLE(S) ENTERED ON STEP NUMBER 1.. X1, X4S, X3, X4, X2S, X2

MULTIPLE R	.85318	ANALYSIS OF VARIANCE	DF	SUM OF SQUARES	MEAN SQUARE	F	SIGNIFICANCE
R SQUARE	.72791	REGRESSION	6.	1121.16932	186.86155	6.68819	.001
ADJUSTED R SQUARE	.61908	RESIDUAL	15.	419.06531	27.93902		
STD DEVIATION	5.28574	COEFF OF VARIABILITY	43.0 PCT				

VARIABLES IN THE EQUATION

VARIABLE	B	STD ERROR B	F SIGNIFICANCE	BETA ELASTICITY
X1	-5.3203326	1.2118369	19.274770 .001	-.6151489 -.05896
X4S	1.7828323	1.0725375	2.7630963 .117	.2269285 .13829
X3	2.3589051	1.1774311	4.0137465 .064	.2751397 .00871
X4	3.5995116	1.1774311	9.3457930 .008	.4198425 -.01330
X2S	2.8302645	1.5230778	3.4531057 .083	.2872315 .17772
X2	4.2893707	1.5515394	7.6429598 .014	.4353101 -.07922
(CONSTANT)	10.173658	1.9426773	27.425399 .000	

VARIABLES NOT IN THE EQUATION

VARIABLE	PARTIAL	TOLERANCE	F SIGNIFICANCE

ALL VARIABLES ARE IN THE EQUATION.

COEFFICIENTS AND CONFIDENCE INTERVALS.

VARIABLE	B	STD ERROR B	T	95.0 PCT CONFIDENCE INTERVAL	
X1	-5.3203326	1.2118369	-4.3903041	-7.9033018	, -2.7373634
X4S	1.7828323	1.0725375	1.6622564	-.50322720	, 4.0688918
X3	2.3589051	1.1774311	2.0034337	-.15072980	, 4.8685400
X4	3.5995116	1.1774311	3.0570890	1.0899767	, 6.1091465
X2S	2.8302645	1.5230778	1.8582534	-.41609394	, 6.0766280
X2	4.2893707	1.5515394	2.7645904	.98234295	, 7.5963985
CINSTANT	10.173658	1.9426773	5.2369264	6.0329397	, 14.314377

VARIANCE/COVARIANCE MATRIX OF THE UNNORMALIZED REGRESSION COEFFICIENTS.

	X1	X2	X3	X4	X2S	X4S
X1	1.46855					
X2	-.49005	2.40727				
X3	.13047	-.21002	1.38634			
X4	-.13047	.21002	-.22222	1.38634		
X2S	-.28957	1.10499	-.12410	.12410	2.31977	
X4S	-.01114	-.07466	-.00477	.00477	.22354	1.15034

FILE REGRESSI (CREATION DATE = 12/01/87) FOR OFACTIVATION PARAMETER,B

* MULTIPLE REGRESSION *

DEPENDENT VARIABLE.. KD

SUMMARY TABLE

STEP	VARIABLE ENTERED	VARIABLE REMOVED	F TO ENTER OR REMOVE	SIGNIFICANCE	MULTIPLE R	R SQUARE	R SQUARE CHANGE	SIMPLE R	OVERALL F	SIGNIFICANCE
1	X1		19.27477	.001	.50635	.25639	.25639	-.50635	6.48819	.001
	X4S		2.76310	.117	.55136	.30400	.04760	-.21514		
	X3		4.01375	.064	.66708	.44500	.14100	.40314		
	X4		9.34579	.008	.76279	.58185	.13685	.39284		
	X2S		3.45311	.083	.76764	.58927	.00742	-.02959		
	X2		7.64296	.014	.85318	.72791	.13864	.19126		

FILE REGRESSI (CREATION DATE = 12/01/87) FOR DEACTIVATION PARAMETER,B

* MULTIPLE REGRESSION *

OBSERVATION	Y VALUE	Y ESTIMATE	RESIDUAL	-2SD	0.0	+2SD
1.	4.415000	7.797377	-3.382377			
2.	4.437000	3.936445	.5005547			
3.	6.340000	6.417658	-.7765831E-01			
4.	29.34000	23.15585	6.184148			
5.	20.21000	21.77613	-1.566134			
6.	15.95000	9.859300	6.090700			
7.	5.340000	-.4670068	5.807007			
8.	11.50000	20.81432	-9.314323			
9.	9.690000	12.91597	-3.225975			
10.	9.010000	14.89147	-5.881468			
11.	7.880000	5.455848	2.424152			
12.	22.75000	24.50401	-1.754011			
13.	8.634000	10.10596	-1.471964			
14.	8.000000	10.17366	-2.173658			
15.	21.46000	19.71421	1.745790			
16.	1.730000	7.797377	-6.067377			
17.	1.500000	3.936445	-2.436445			
18.	2.720000	6.417658	-3.697658			
19.	12.86000	10.17366	2.686342			
20.	27.36000	21.77613	5.583866			
21.	15.14000	9.859300	5.280700			
22.	24.46000	19.71421	4.745790			

NOTE = (*) INDICATES ESTIMATE CALCULATED WITH MEANS SUBSTITUTED
R INDICATES POINT OUT OF RANGE OF PLOT

NUMBER OF CASES PLOTTED 22.
NUMBER OF 2 S.D. OUTLIERS 0 OR 0 PERCENT OF THE TOTAL

VON NEUMANN RATIO 1.68458 . DURBIN-WATSON TEST 1.60801

NUMBER OF POSITIVE RESIDUALS 10.
NUMBER OF NEGATIVE RESIDUALS 12.
NUMBER OF RUNS OF SIGNS 12.

NORMAL APPROXIMATION TO SIGN DISTRIBUTION IMPOSSIBLE.
USE A TABLE FOR EXPECTED VALUES.

APPENDIX 8.4

Catalyst carbon and hydrogen content [wt %]

Elemental analysis of the spent catalysts was carried out on a LECO CHN analyzer and is given in Table A8.4. The precision of the measurements is +/- 0.05 %. Hydrogen content in some of these catalysts was high. This was attributed to hydroxyl groups on the catalyst surface which were removed at the elevated temperature of the analysis (1000K) and not to the hydrogen content of the solid product.. Studies with alumina in the microbalance indeed showed both H_2 and H_2O removal occurred up to 900°C.

It is also interesting to note that in design experiment 3, run C226, emptying of the reactor catalyst bed and subsequent physical mixing of the spent catalyst which was retrieved and analyzed showed roughly the same carbon content (2.01) as the average of three separate layers (1.45 + 2.24 + 2.62)/3 = 2.10.

TABLE A8.4

Spent catalyst carbon and hydrogen content [wt %]

EXPERIMENT DESIGN	NO.	DURATION OF RUN [min]	CARBON CONTENT [wt %]	HYDROGEN CONTENT [WT %]
	C243	65	1.04	0.50
1	C220	300	3.16	0.28
	C219	210	4.06	0.72
	C225	65	2.53	0.51
2	C245	60	1.33	0.51
	C246	65	2.32	0.40
3	C226	70	2.01	0.79
	C247	65	1.45 EXIT	0.81
			2.24 CENTRE	0.71
			2.62 INLET	0.87
	C228	70	6.5	1.20
4	C229	55	5.53	1.13
	C249	65	7.79	1.15
5	C223	70	0.37	0.40
6	C224	70	0.60	0.50
7	C227	90	1.62	0.96
	C248	65	1.31	0.44
8	C221	300	4.92	0.63
			4.31	
9	C244	65	1.15	0.57
10	C238	60	3.06	0.67
11	C239	65	1.11	0.71
12	C231	55	5.81	0.80
13	C232	65	0.19	0.41
14	C240	65	2.69	0.74
15	C234	65	2.69	0.62
16	C241	65	1.69	0.76
-	C242	65	1.09	0.58
	C218	245	2.97	0.55
17	C230	65	3.12	0.86
	C217	120	0.69	

APPENDIX 8.5

ANOVA for model of $\hat{C}$

VOGELBACK COMPUTING CENTER
NORTHWESTERN UNIVERSITY

S P S S - - STATISTICAL PACKAGE FOR THE SOCIAL SCIENCES

VERSION 8.0 -- JUNE 16, 1979

```
FILE NAME           REGRESSION FOR CARBON DATA
INPUT MEDIUM        DISK
VARIABLE LIST       X1,X2,X3,X4,X15,X25,X35,X45,X1X2,X1X3,X1X4,CARBON
INPUT FORMAT        FIXED(11(F2.0,1X),F5.0)
```

ACCORDING TO YOUR INPUT FORMAT, VARIABLES ARE TO BE READ AS FOLLOWS

VARIABLE	FORMAT	RECORD	COLUMNS
X1	F 2. 0	1	1- 2
X2	F 2. 0	1	4- 5
X3	F 2. 0	1	7- 8
X4	F 2. 0	1	10- 11
X15	F 2. 0	1	13- 14
X25	F 2. 0	1	16- 17
X35	F 2. 0	1	19- 20
X45	F 2. 0	1	22- 23
X1X2	F 2. 0	1	25- 26
X1X3	F 2. 0	1	28- 29
X1X4	F 2. 0	1	31- 32
CARBON	F 5. 0	1	34- 38

THE INPUT FORMAT PROVIDES FOR 12 VARIABLES. 12 WILL BE READ.
IT PROVIDES FOR 1 RECORDS (*CARDS*) PER CASE.
A MAXIMUM OF 80 *COLUMNS* ARE USED ON A RECORD.

```
REGRESSION          VARIABLES=X1 TO X4, X1X3, X4S, CARBON
                    REGRESSION=CARBON WITH X1 TO X4, X1X3, X4S/RESIDUALS
STATISTICS           ALL
```

00055100 CP NEEDED FOR REGRESSION

OPTION = 1
IGNORE MISSING VALUE INDICATORS
(NO MISSING VALUES DEFINED...OPTION 1 WAS FORCED)

END OF FILE ON FILE TAPE1
AFTER READING 20 CASES FROM SURFILE REGRESSI

FILE REGRESSI (CREATION DATE = 12/01/67) FOR CARBON DATA

* MULTIPLE REGRESSION *

VARIABLE	MEAN	STANDARD DEV	CASES
X1	.1500	.9681	20
X2	-.1500	.6751	20
X3	-.0500	.9987	20
X4	-.0500	.9987	20
X1X3	-.0500	.7592	20
X4S	.5500	1.1459	20
CARBON	15.0450	0.2101	20

CORRELATION COEFFICIENTS.

A VALUE OF 99.00000 IS PRINTED
IF A COEFFICIENT CANNOT BE COMPUTED.

	X1	X2	X3	X4	X1X3	X4S
X2	-.03346					
X3	-.04534	-.06926				
X4	-.04534	-.06926	-.05141			
X1X3	-.05964	-.05111	.20479	-.07269		
X4S	.00597	.09710	-.00230	-.00230	-.00303	
CARBON	.46212	-.47019	-.33425	.24734	-.42042	-.27145

FILE REGRESS1 (CREATION DATE = 12/01/67) FOR CARBON DATA

* MULTIPLE REGRESSION *

DEPENDENT VARIABLE.. CARBON

MEAN RESPONSE 13.04600 STD. DEV. 9.21006

VARIABLE(S) ENTERED ON STEP NUMBER 1.. X1
X4S
X3
X4
X2
X1X3

MULTIPLE R	.99113	ANALYSIS OF VARIANCE	DF	SUM OF SQUARES	MEAN SQUARE	F SIGNIFICANCE
R SQUARE	.98233	REGRESSION	6.	1279.64873	213.30812	8.35664 .001
ADJUSTED R SQUARE	.97554	RESIDUAL	13.	331.83175	25.52552	
STD DEVIATION	5.05220	COEFF OF VARIABILITY	38.7 PCT			

VARIABLES IN THE EQUATION

VARIABLE	B	STD ERROR B	F SIGNIFICANCE	BETA ELASTICITY
X1	4.1226749	1.1786484	12.234396 .004	.4422941 .64745
X4S	-1.8484609	1.0163686	3.3076367 .092	-.2299685 -.13460
X3	-2.3937196	1.1894623	4.0369749 .065	-.2592347 -.00916
X4	1.7724961	1.1701046	2.2946903 .154	.1621956 -.00579
X2	-4.9696802	1.3437938	13.677024 .003	-.4321940 .05714
X1X3	-4.5939313	1.5711755	8.5490645 .017	-.3766625 .01761
(CONSTANT)	13.177577	1.5256536	74.663951 .000	

VARIABLES NOT IN THE EQUATION

VARIABLE	PARTIAL	TOLERANCE	F SIGNIFICANCE

ALL VARIABLES ARE IN THE EQUATION.

COEFFICIENTS AND CONFIDENCE INTERVALS.

VARIABLE	B	STD ERROR B	T	95.0 PCT CONFIDENCE INTERVAL
X1	4.1226749	1.1786484	3.4977938	1.5763660 , 6.6689837
X4S	-1.8484609	1.0163686	-1.8189915	-4.0441917 , .34726984
X3	-2.3937196	1.1894623	-2.0059129	-4.9603916 , .17969129
X4	1.7724961	1.1701046	1.5146232	-.7553903 , 4.3003552
X2	-4.9696802	1.3437938	-3.6962460	-7.8727702 , -2.0665903
X1X3	-4.5939313	1.5711755	-2.9238815	-7.9882493 , -1.1996132
CONSTANT	13.177577	1.5256536	8.6362000	9.8811710 , 16.473983

VARIANCE/COVARIANCE MATRIX OF THE UNNORMALIZED REGRESSION COEFFICIENTS.

	X1	X2	X3	X4	X1X3	X4S
X1	1.38921					
X2	.07301	1.80578				
X3	.05407	-.09119	1.41482			
X4	.07576	-.11767	.06633	1.36914		
X1X3	-.10814	-.16236	-.86105	-.13267	2.46859	
X4S	-.01329	-.13353	-.00484	-.07878	-.00568	1.03301

FILE REGRESSI (CREATION DATE = 12/01/87) FOR CARBON DATA

* MULTIPLE REGRESSION *

DEPENDENT VARIABLE.. CARBON

SUMMARY TABLE

STEP	VARIABLE ENTERED	VARIABLE REMOVED	F TO ENTER OR REMOVE	SIGNIFICANCE	MULTIPLE R	R SQUARE	R SQUARE CHANGE	SIMPLE R	OVERALL F	SIGNIFICANCE
1	X1		12.23466	.004	.48812	.23844	.23844	.48212	8.35666	.001
	X45		3.30764	.082	.58455	.35707	.07553	-.27145		
	X3		4.03975	.066	.63736	.40610	.09813	-.23429		
	X4		2.29456	.154	.66102	.43692	.05814	-.24734		
	X2		15.67702	.003	.81161	.65871	.16945	-.47019		
	X1X3		8.54905	.017	.89113	.79411	.13540	-.42642		

FILE REGRESSI (CREATION DATE = 12/01/87) FOR CARBON DATA

* MULTIPLE REGRESSION *

OBSERVATION	Y VALUE	Y ESTIMATE	RESIDUAL	-2SD	0.0	+2SD
1.	16.150000	15.692428	.4957403			
2.	9.060000	11.666433	-2.606432			
3.	29.650000	29.178662	.1113836			
4.	2.370000	2.667479	-.2974787			
5.	3.840000	1.806044	2.033956			
6.	5.900000	16.15184	-10.25184	R		
7.	5.130000	8.200408	-3.020408			
8.	15.41600	21.42229	-6.012927			
9.	5.590000	4.932227	.6577725			
10.	30.74000	23.11694	7.623062			
11.	13.94000	8.396146	*.143854			
12.	15.54000	17.95901	-4.419004			
13.	6.511000	9.332730	-.8187297			
14.	2.490000	2.225737	3.251252			
15.	15.71000	13.17776	2.532423			
16.	6.590000	5.269068	1.320068			
17.	14.84000	15.69428	-.8042597			
18.	9.310000	11.68435	-2.454332			
19.	35.11000	34.17862	.9313944			
20.	14.95000	13.17758	1.772423			

NOTE - (*) INDICATES ESTIMATE CALCULATED WITH MEANS SUBSTITUTED
R INDICATES POINT OUT OF RANGE OF PLOT

NUMBER OF CASES PLOTTED 20.
NUMBER OF 2 S.D. OUTLIERS 1. OR 5.00 PERCENT OF THE TOTAL

VON NEUMANN RATIO 1.76374 DURBIN-WATSON TEST 1.67555

NUMBER OF POSITIVE RESIDUALS 11.
NUMBER OF NEGATIVE RESIDUALS 9.
NUMBER OF RUNS OF SIGNS 11.

NORMAL APPROXIMATION TO SIGN DISTRIBUTION IMPOSSIBLE.
USE A TABLE FOR EXPECTED VALUES.

APPENDIX 9.1

Calculation procedures for determining rate in microbalance

The calculation procedures based on the graphical output of the Perkin-Elmer system shown in Figs. A9.1 to A9.21 is given below and a summary appears in Table 9.1.

Let w_i - initial catalyst weight [mg]

w_o - catalyst weight prior to introduction of reactant [mg]

w_f - catalyst weight at the end of the reaction time [mg]

Then

$$\% \text{ loss} = 100 * (w_i - w_o)/w_i$$

$$\% \text{ gain} = 100 * (w_f - w_o)/w_o$$

and

R_m - maximum rate of carbon deposition [mg/min]

R_f - rate of carbon deposition at t= 60 min [mg/min]

R_m' - $100 * R_m/w_o$ $[min^{-1}]$

R_f' - $100 * R_f/w_o$ $[min^{-1}]$

R_m^s - rate of carbon deposition based on catalyst surface area, $10^3 * R_m' / S.A.$ - $[mg/m^2/min]$

R_f^s - $10^3 * R_f' / S.A.$ - $[mg/m^2/min]$

Bal Purge=32, Reactant 11% =30ml/min

TGA 1st Derivative: vma04
Sample Weight: 18.585 mg
Thu Oct 23 12:47:14 1986
A1203, 0.5-1 mm

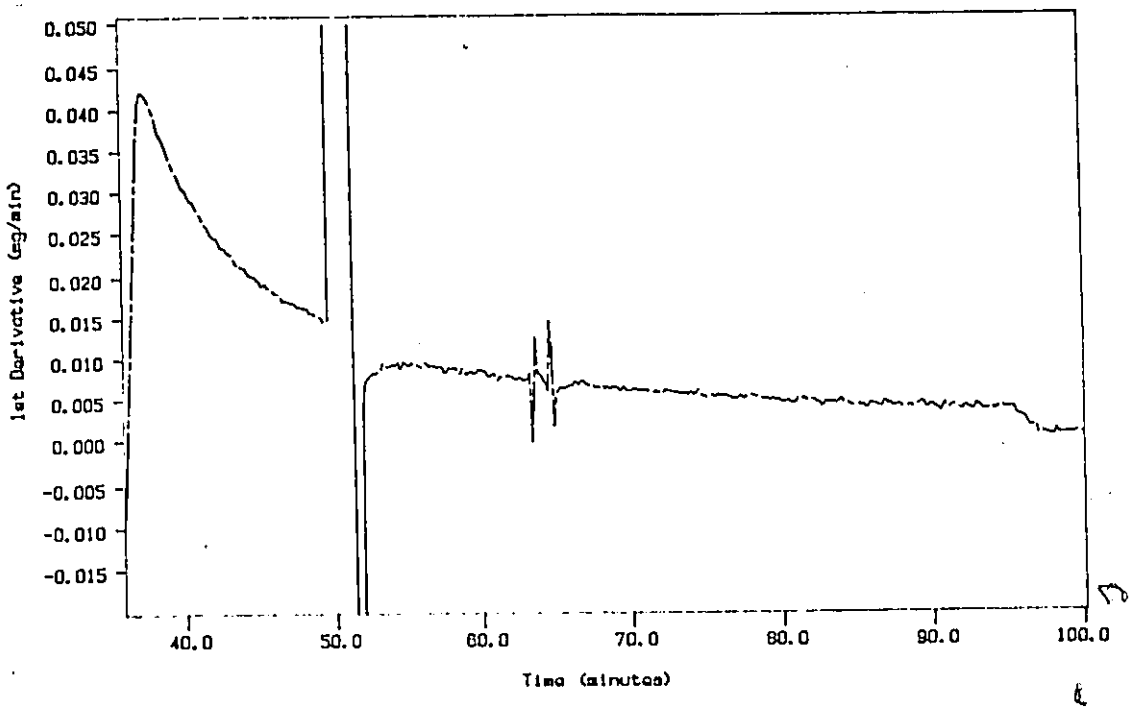

Bal Purge=32, Reactant 11% =30ml/min

TGA 1st Derivative: vma05
Sample Weight: 19.517 mg
Thu Oct 23 18:58:18 1986
A1203, 0.5-1 mm, repeat

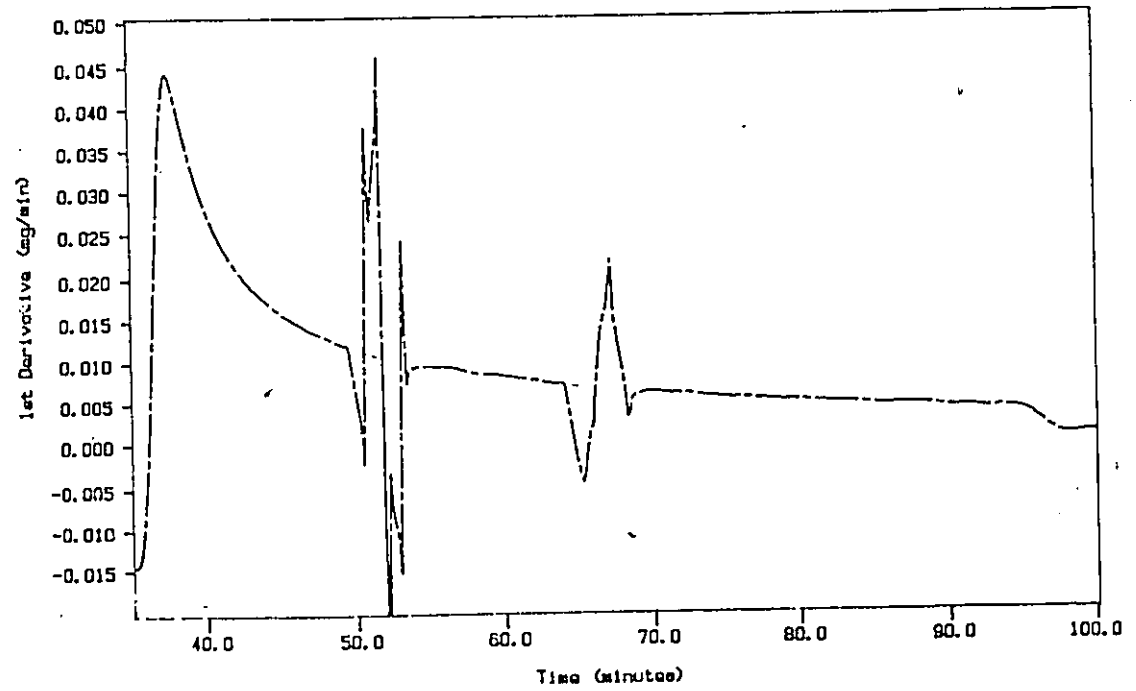

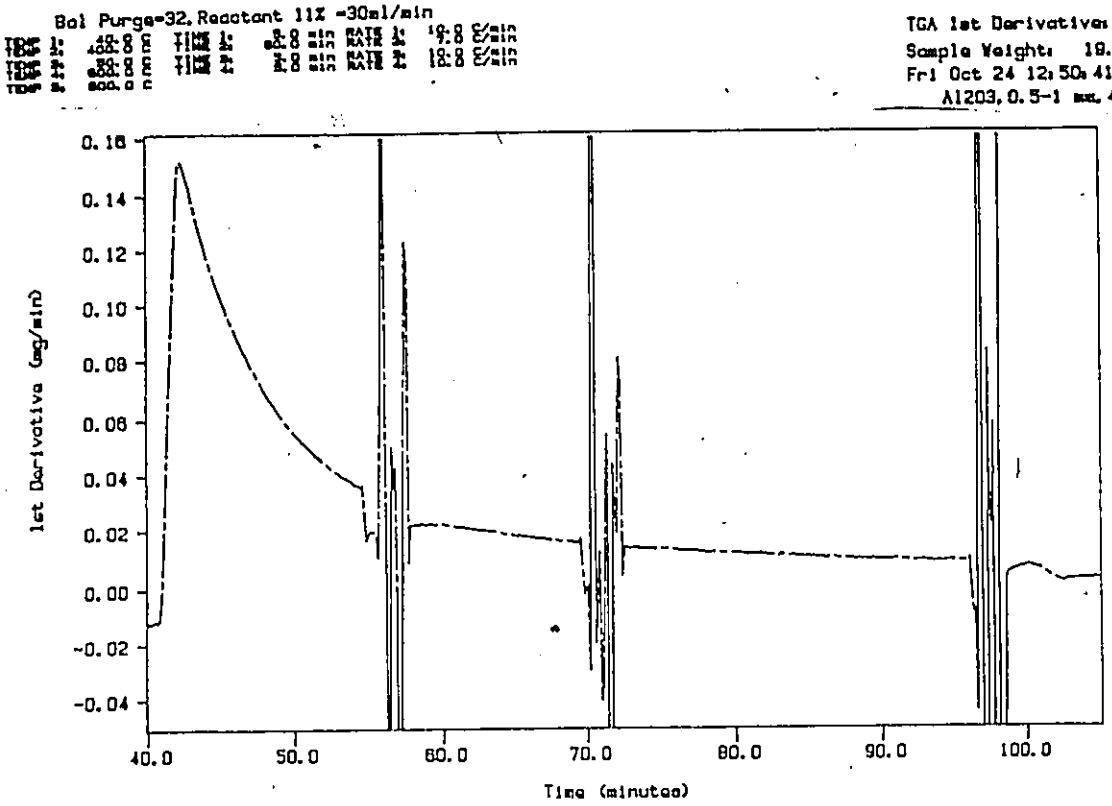
Bal Purge=32, Reactant 11% =30ml/min
TGA 1st Derivative: vma08
Sample Weight: 19.087 mg
Fri Oct 24 12:50:41 1988
A1203, 0.5-1 mm, 400
1st Derivative (mg/min)
0.16
0.14
0.12
0.10
0.08
0.06
0.04
0.02
0.00
-0.02
-0.04
40.0
50.0
60.0
70.0
80.0
90.0
100.0
Time (minutes)

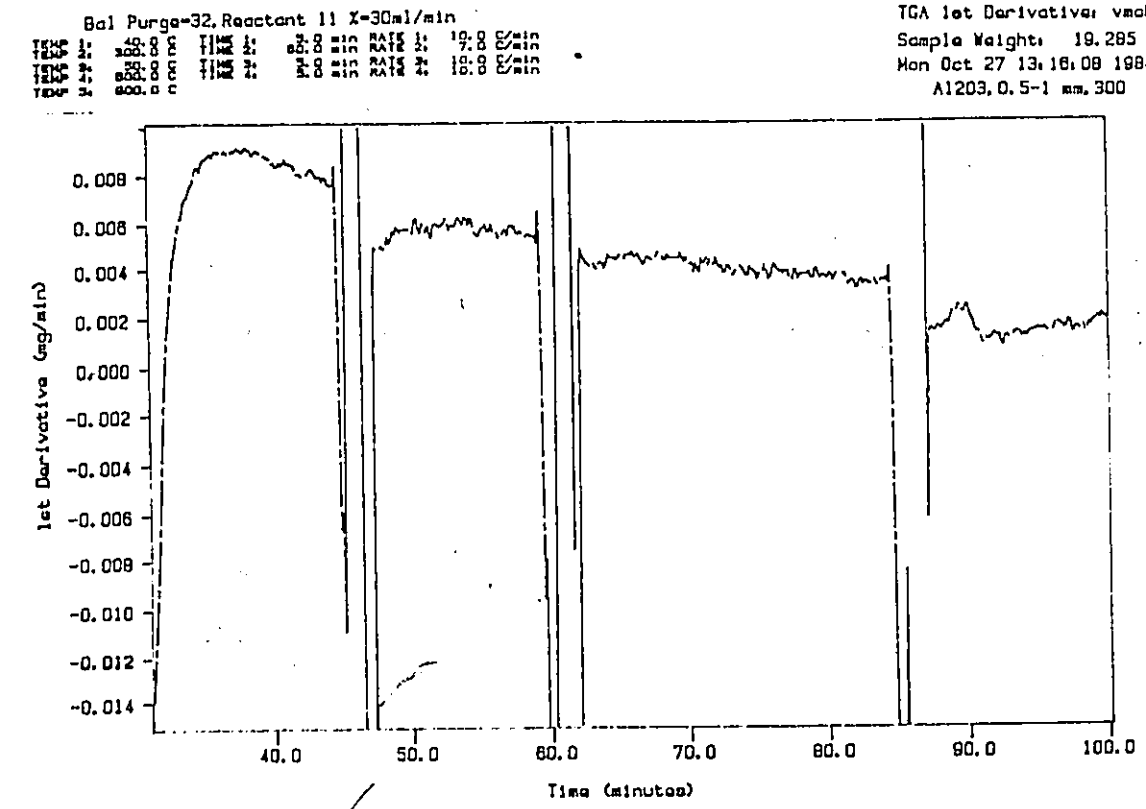
Bal Purge=32, Reactant 11 %=30ml/min
TGA 1st Derivative: vma07
Sample Weight: 19.285 mg
Mon Oct 27 13:16:08 1988
A1203, 0.5-1 mm, 300
1st Derivative (mg/min)
0.008
0.006
0.004
0.002
0.000
-0.002
-0.004
-0.006
-0.008
-0.010
-0.012
-0.014
40.0
50.0
60.0
70.0
80.0
90.0
100.0
Time (minutes)

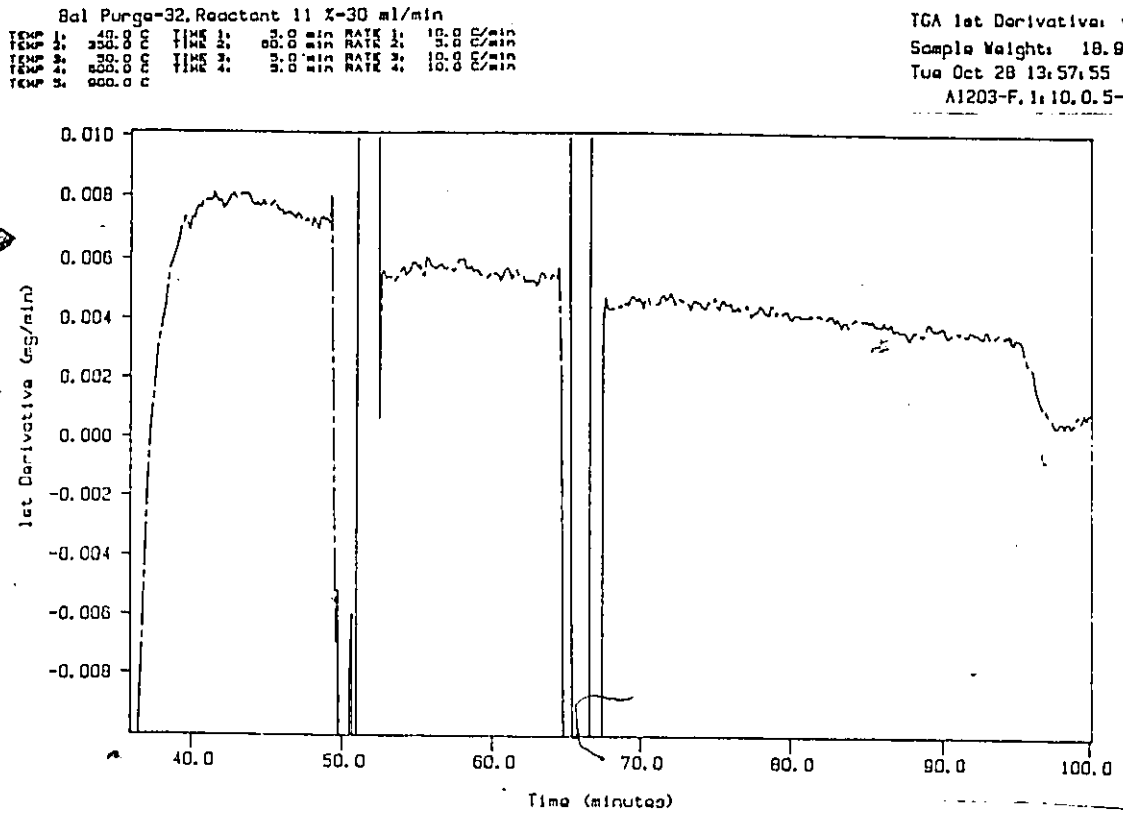
Bal Purge-32, Reactant 11 %-30 ml/min
TEMP 1: 40.0 C TIME 1: 3.0 min RATE 1: 10.0 C/min
TEMP 2: 350.0 C TIME 2: 60.0 min RATE 2: 5.0 C/min
TEMP 3: 350.0 C TIME 3: 5.0 min RATE 3: 10.0 C/min
TEMP 4: 600.0 C TIME 4: 5.0 min RATE 4: 10.0 C/min
TEMP 5: 600.0 C
TGA 1st Derivative: vma09
Sample Weight: 18.942 mg
Tue Oct 28 13:57:55 1986
A1203-F, 1:10, 0.5-1mm
0.010
0.008
0.006
0.004
0.002
0.000
-0.002
-0.004
-0.006
-0.008
1st Derivative (mg/min)
40.0
50.0
60.0
70.0
80.0
90.0
100.0
Time (minutes)

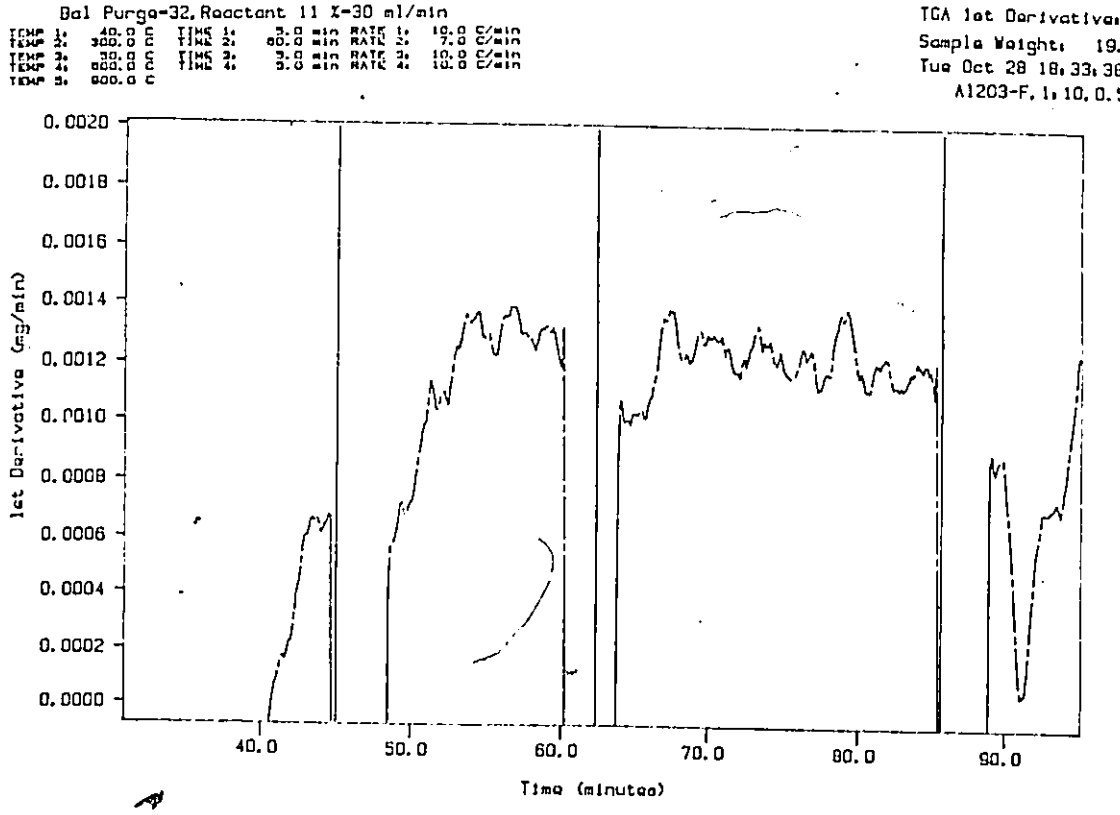
Bal Purge-32, Reactant 11 %-30 ml/min
TEMP 1: 40.0 C TIME 1: 3.0 min RATE 1: 10.0 C/min
TEMP 2: 350.0 C TIME 2: 60.0 min RATE 2: 7.0 C/min
TEMP 3: 350.0 C TIME 3: 5.0 min RATE 3: 10.0 C/min
TEMP 4: 600.0 C TIME 4: 5.0 min RATE 4: 10.0 C/min
TEMP 5: 600.0 C
TGA 1st Derivative: vma10
Sample Weight: 19.186 mg
Tue Oct 28 18:33:38 1986
A1203-F, 1:10, 0.5-1mm
0.0020
0.0018
0.0016
0.0014
0.0012
0.0010
0.0008
0.0006
0.0004
0.0002
0.0000
1st Derivative (mg/min)
40.0
50.0
60.0
70.0
80.0
90.0
Time (minutes)

Bal Purge 32, Reactant 11% 30 ml/min

V.H.Allenger

TGA 1st Derivative: vmal1
Sample Weight: 18.355 mg
Wed Oct 29 13:39:48 1986
A1203-F, 1:10, 0.5-1mm, 400C

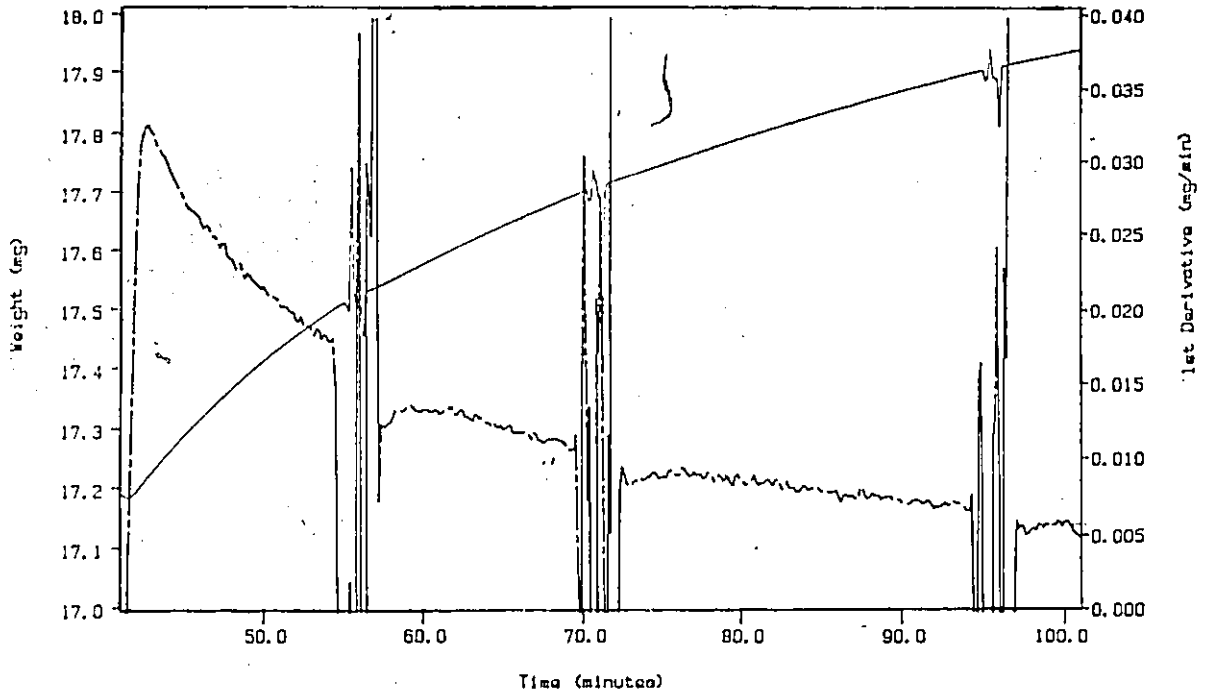

Bal Purge-24, Reactant 11%-22ml/min

V.H.Allenger

TGA 1st Derivative: vmal2
Sample Weight: 19.792 mg
Wed Oct 29 18:07:05 1986
A1203, 0.5-1mm, 350

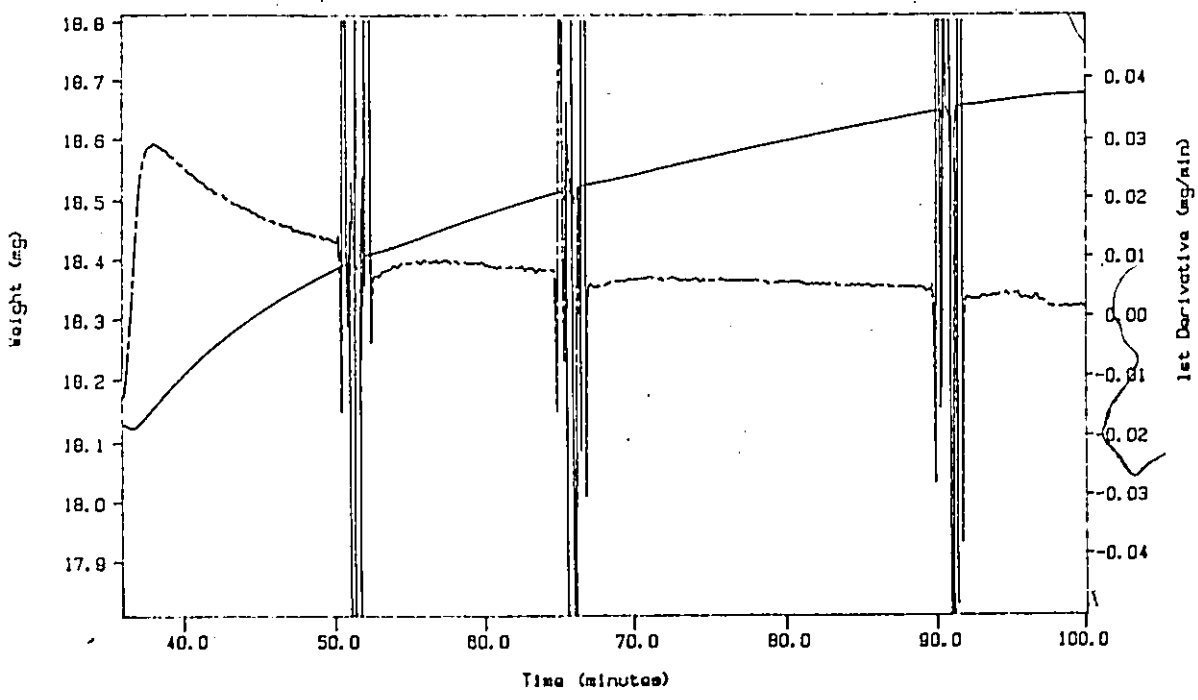

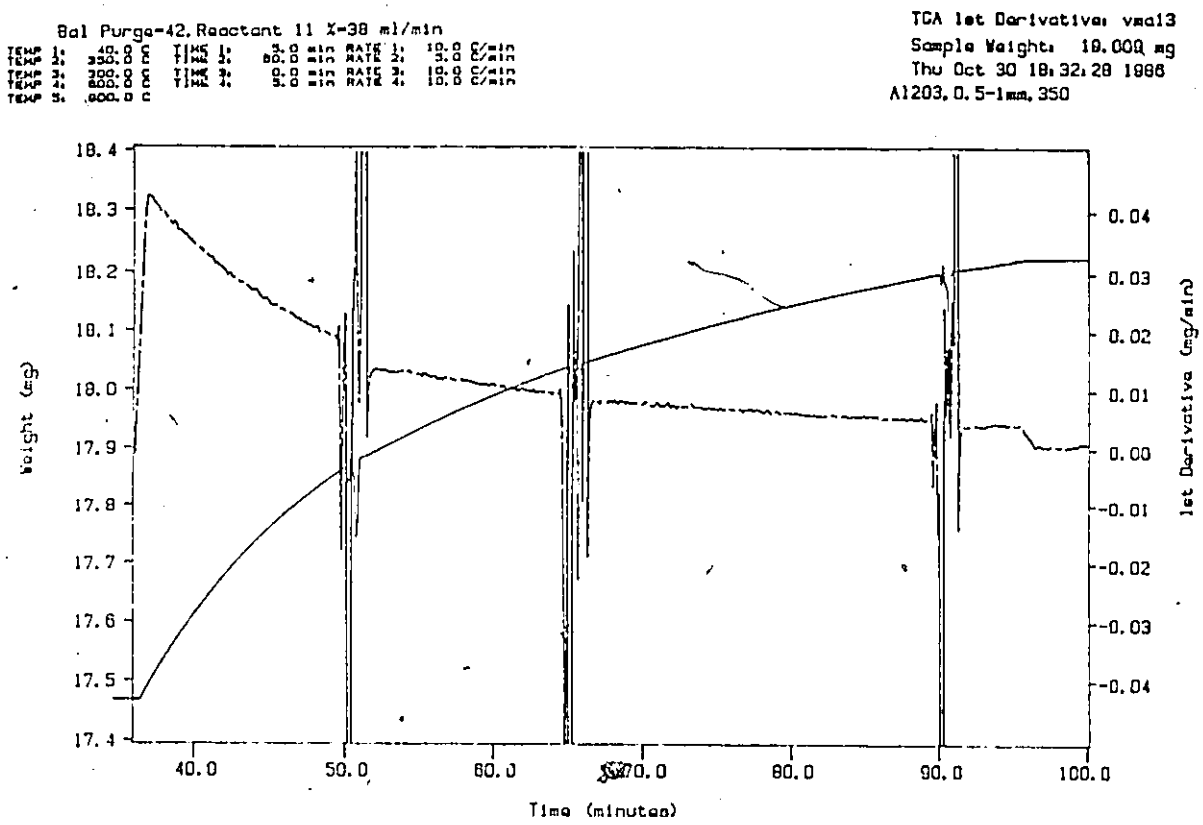
Bal Purge=42, Reactant 11 %=38 ml/min
TEMP 1: 40.0 C TIME 1: 3.0 min RATE 1: 10.0 C/min
TEMP 2: 350.0 C TIME 2: 60.0 min RATE 2: 3.0 C/min
TEMP 3: 300.0 C TIME 3: 0.0 min RATE 3: 10.0 C/min
TEMP 4: 600.0 C TIME 4: 3.0 min RATE 4: 10.0 C/min
TEMP 5: 900.0 C
TGA 1st Derivative: vma13
Sample Weight: 18.000 mg
Thu Oct 30 18:32:28 1998
A1203, 0.5-1mm, 350
Weight (mg)
1st Derivative (mg/min)
Time (minutes)

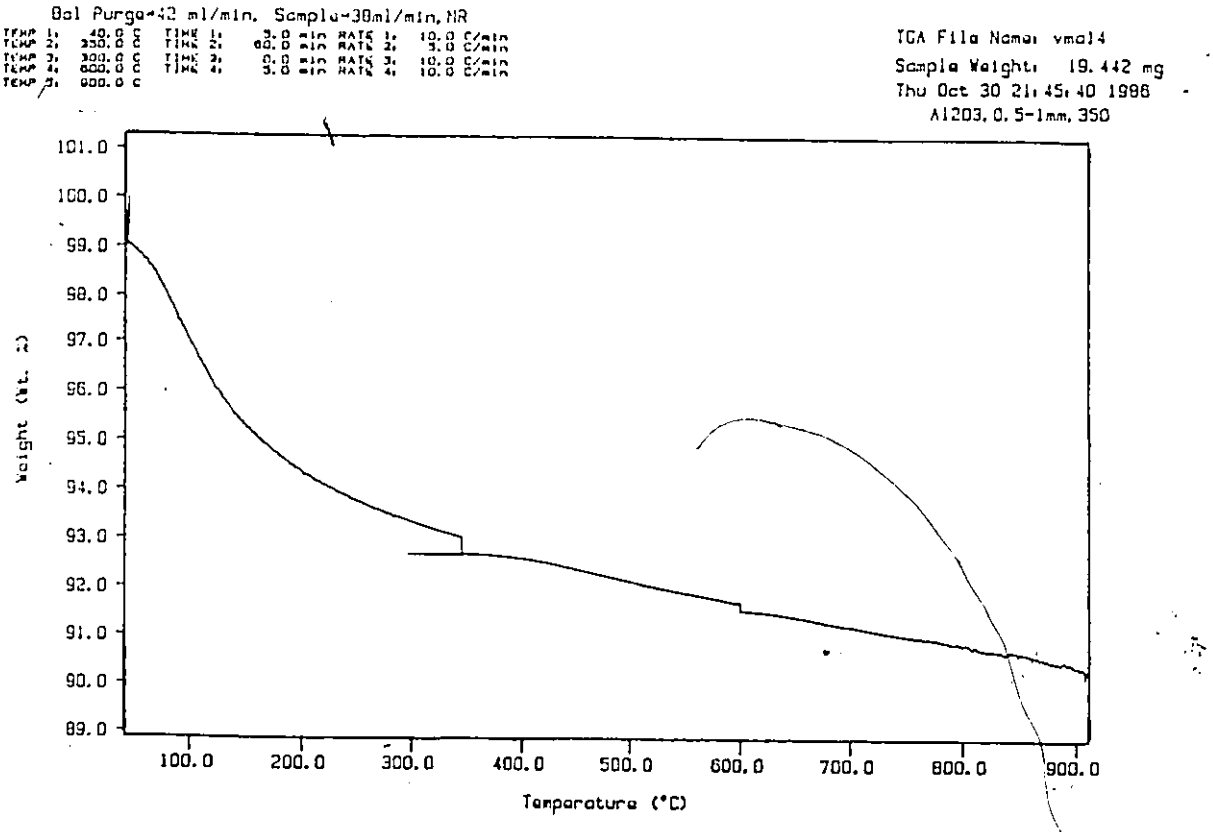
Bal Purge=42 ml/min, Sample=30ml/min, NR
TEMP 1: 40.0 C TIME 1: 3.0 min RATE 1: 10.0 C/min
TEMP 2: 350.0 C TIME 2: 60.0 min RATE 2: 3.0 C/min
TEMP 3: 300.0 C TIME 3: 0.0 min RATE 3: 10.0 C/min
TEMP 4: 600.0 C TIME 4: 3.0 min RATE 4: 10.0 C/min
TEMP 5: 900.0 C
TGA File Name: vma14
Sample Weight: 19.442 mg
Thu Oct 30 21:45:40 1998
A1203, 0.5-1mm, 350
Weight (Wt. %)
Temperature (°C)

Bal Purge=32, Reactant 11%=30 ml/min

TGA File Name: vma15
Sample Weight: 18.815 mg
Fri Oct 31 14:37:53 1986
A1203, 0.5-1mm, 350

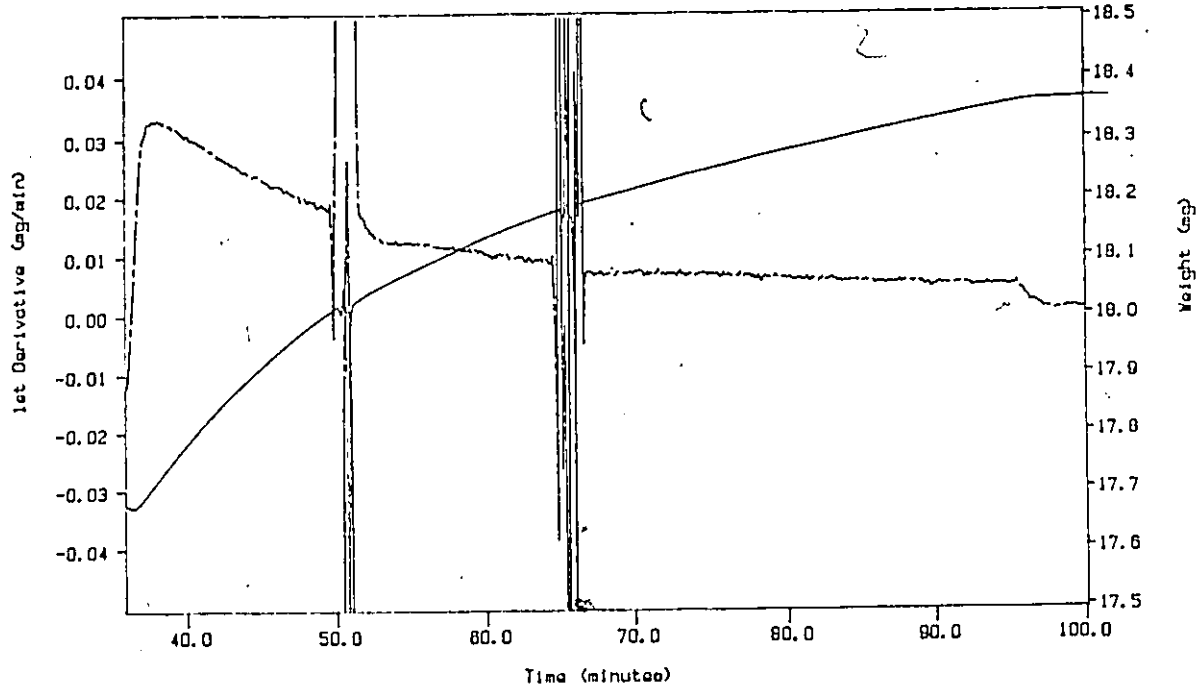

Bal Purge=32, Reactant 11%=30 ml/min

TGA File Name: vma16
Sample Weight: 19.189 mg
Mon Nov 03 13:54:36 1986
A1203, 100mesh, 350

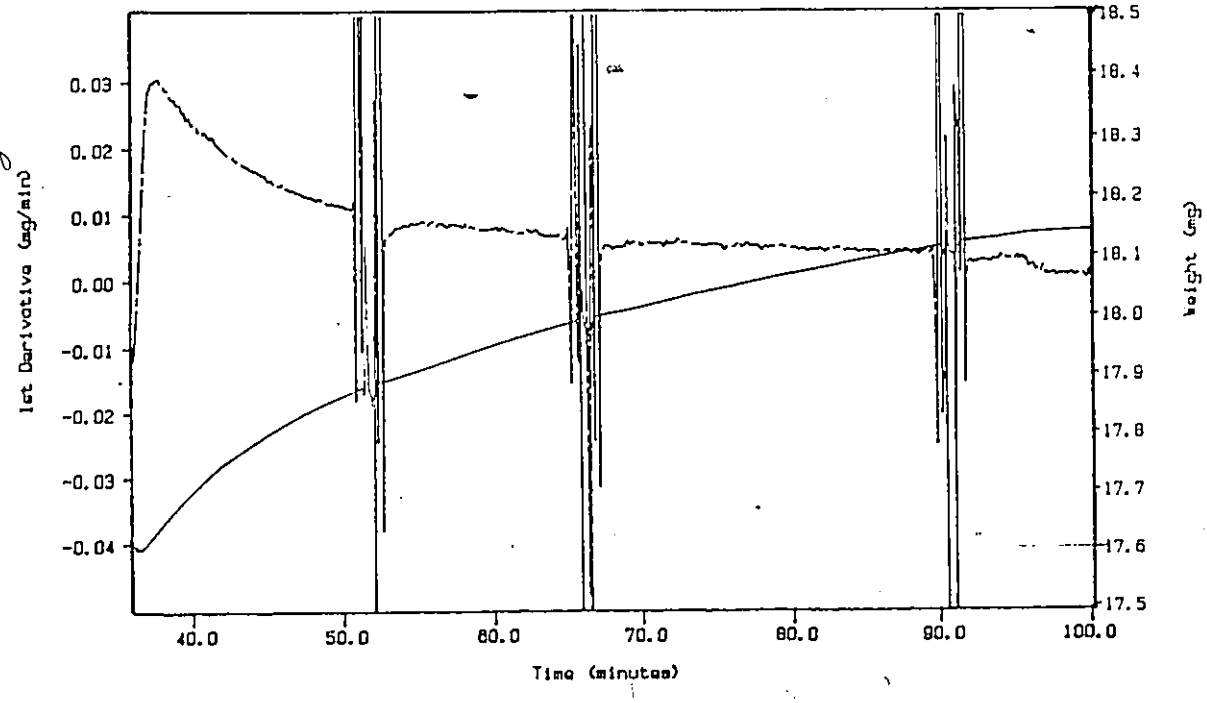

NH3 ads, Purge Bal=32, Reactant 11%-30

TEMP 1: 350.0 C TIME 1: 70.0 min RATE 1: 10.0 C/min
TEMP 2: 300.0 C TIME 2: 0.0 min RATE 2: 10.0 C/min
TEMP 3: 600.0 C TIME 3: 5.0 min RATE 3: 10.0 C/min
TEMP 4: 900.0 C

TGA 1st Derivative: vma17
Sample Weight: 17.628 mg
Wed Nov 05 18:14:19 1986
A1203, 0.5-1, 350, Part 2

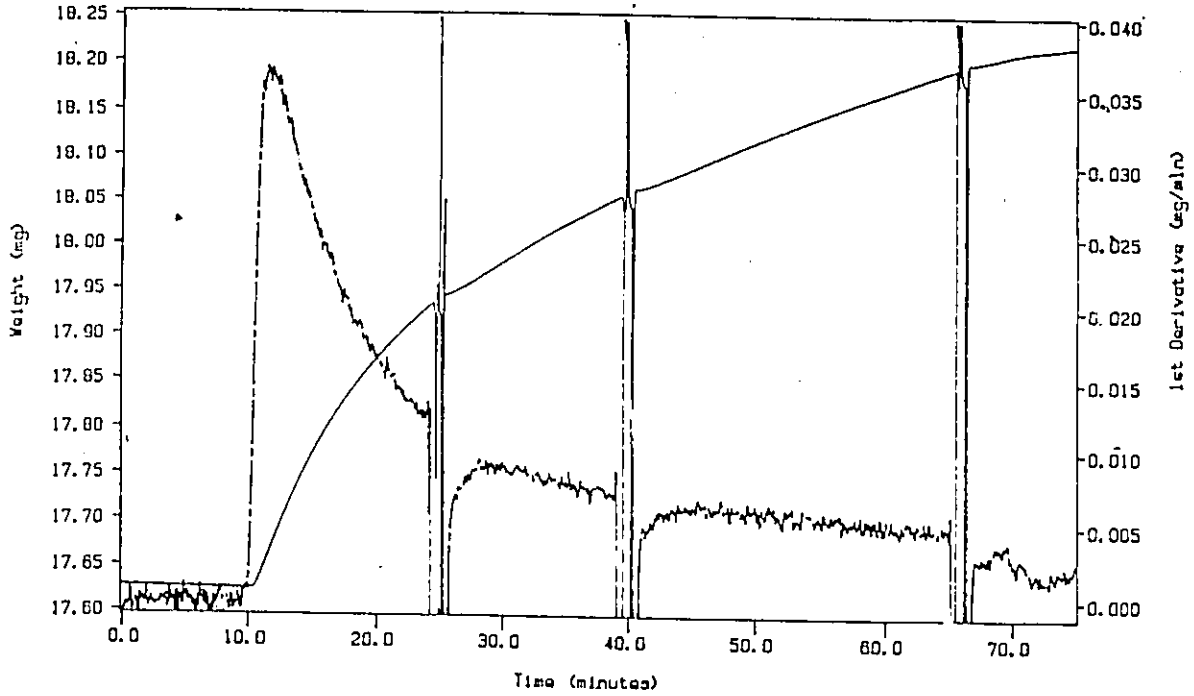

NH3 ads-des, Bal=32, Sample=20, Part 1

TEMP 1: 350.0 C TIME 1: 70.0 min RATE 1: 10.0 C/min
TEMP 2: 300.0 C TIME 2: 0.0 min RATE 2: 10.0 C/min
TEMP 3: 600.0 C TIME 3: 5.0 min RATE 3: 10.0 C/min
TEMP 4: 900.0 C

TGA 1st Derivative: vma18
Sample Weight: 16.714 mg
Fri Nov 07 13:38:40 1986
A1203-F, 1:10, 0.5-1, 350 C

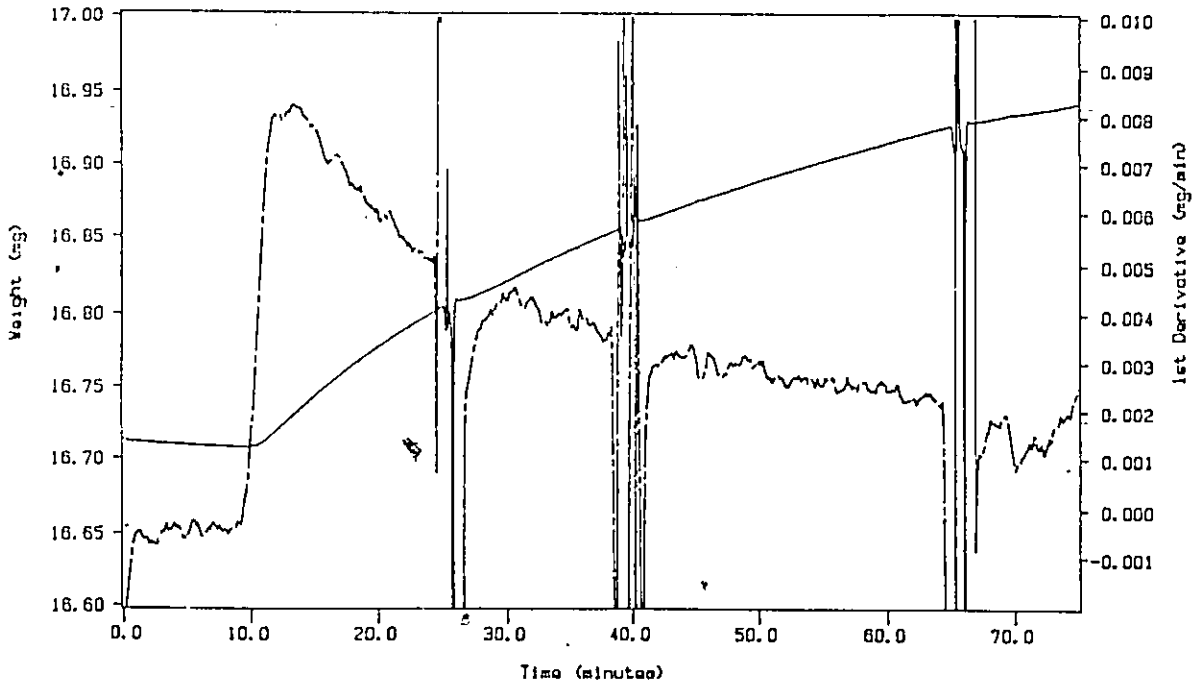

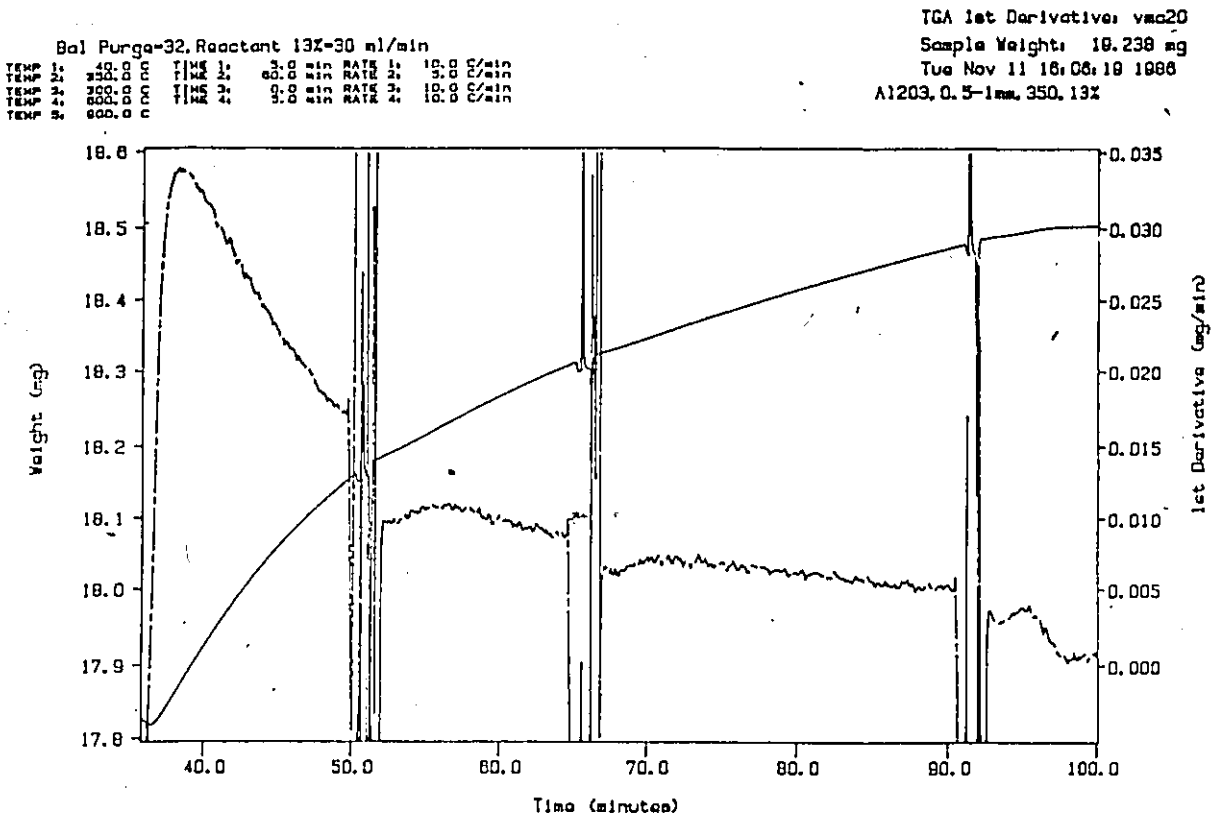
TGA 1st Derivative: vma20
Sample Weight: 18.238 mg
Tue Nov 11 16:06:19 1988
A1203, 0.5-1mm, 350, 13%
Bal Purge=32, Reactant 13%=30 ml/min
TEMP 1: 40.0 C TIME 1: 3.0 min RATE 1: 10.0 C/min
TEMP 2: 350.0 C TIME 2: 60.0 min RATE 2: 5.0 C/min
TEMP 3: 350.0 C TIME 3: 0.0 min RATE 3: 10.0 C/min
TEMP 4: 600.0 C TIME 4: 5.0 min RATE 4: 10.0 C/min
TEMP 5: 600.0 C
Weight (mg)
1st Derivative (mg/min)
Time (minutes)
18.6
18.5
18.4
18.3
18.2
18.1
18.0
17.9
17.8
0.035
0.030
0.025
0.020
0.015
0.010
0.005
0.000
40.0
50.0
60.0
70.0
80.0
90.0
100.0

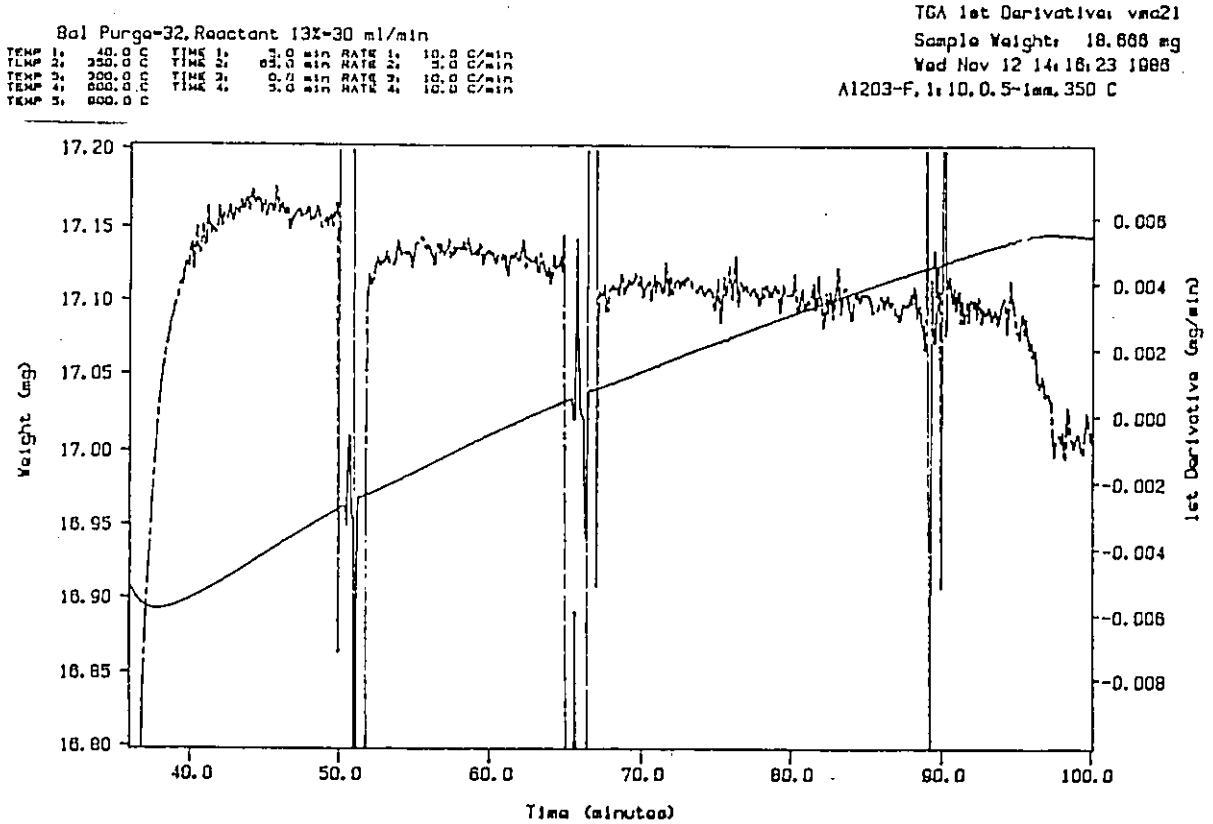
TGA 1st Derivative: vma21
Sample Weight: 18.668 mg
Wed Nov 12 14:16:23 1988
A1203-F, 1: 10, 0.5-1mm, 350 C
Bal Purge=32, Reactant 13%=30 ml/min
TEMP 1: 40.0 C TIME 1: 3.0 min RATE 1: 10.0 C/min
TEMP 2: 350.0 C TIME 2: 60.0 min RATE 2: 5.0 C/min
TEMP 3: 350.0 C TIME 3: 0.0 min RATE 3: 10.0 C/min
TEMP 4: 600.0 C TIME 4: 5.0 min RATE 4: 10.0 C/min
TEMP 5: 600.0 C
Weight (mg)
1st Derivative (mg/min)
Time (minutes)
17.20
17.15
17.10
17.05
17.00
16.95
16.90
16.85
16.80
0.006
0.004
0.002
0.000
-0.002
-0.004
-0.006
-0.008
40.0
50.0
60.0
70.0
80.0
90.0
100.0

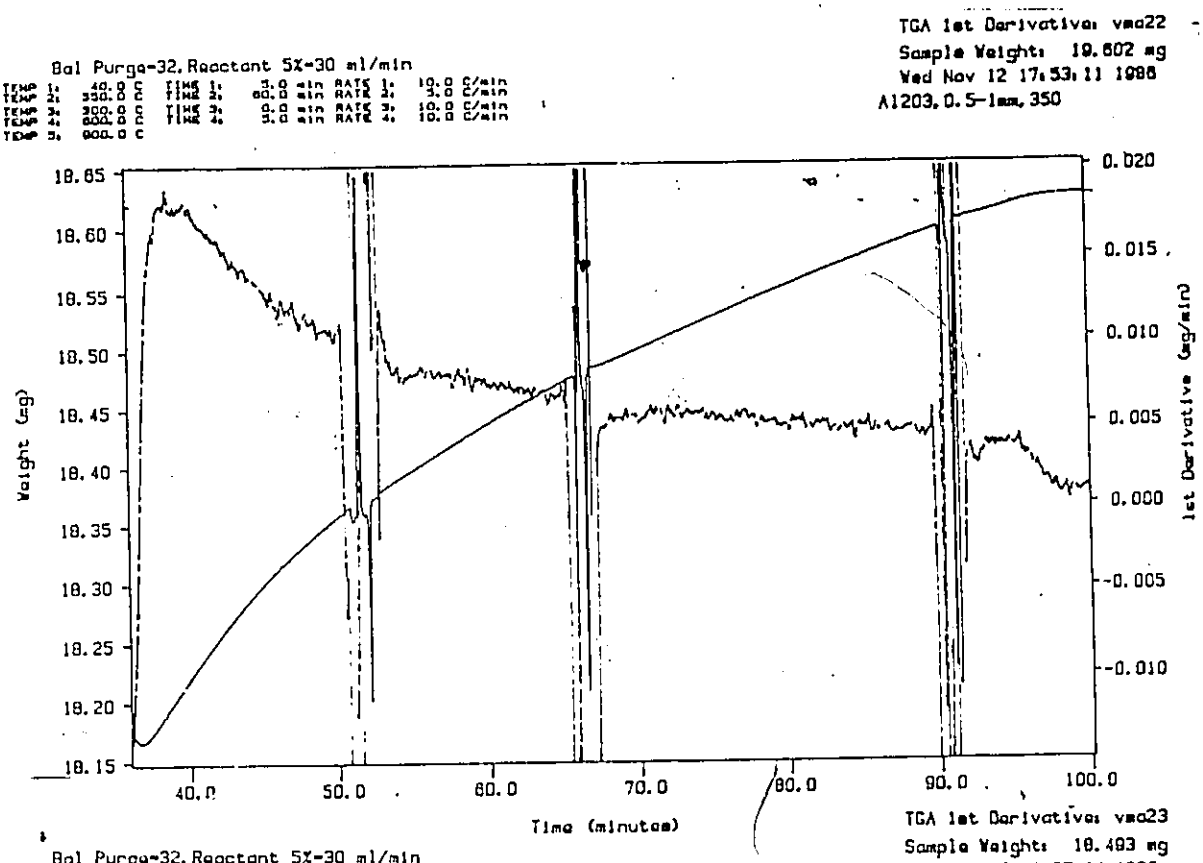
TGA 1st Derivative: vma22
Sample Weight: 19.602 mg
Wed Nov 12 17:53:11 1988
A1203, 0.5-1mm, 350
Bal Purge-32, Reactant 5%-30 ml/min
Weight (mg)
1st Derivative (mg/min)
Time (minutes)

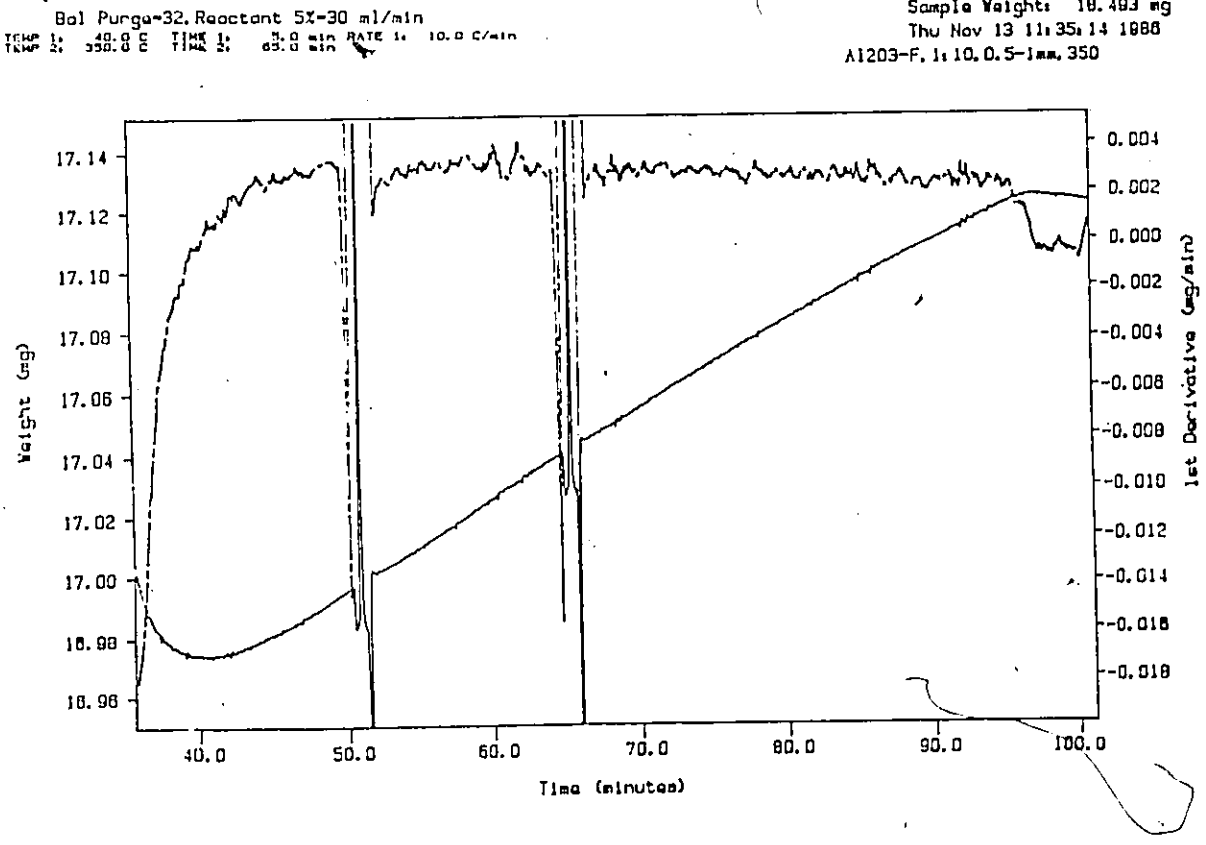
TGA 1st Derivative: vma23
Sample Weight: 18.493 mg
Thu Nov 13 11:35:14 1988
A1203-F, 1: 10, 0.5-1mm, 350
Bal Purge-32, Reactant 5%-30 ml/min
Weight (mg)
1st Derivative (mg/min)
Time (minutes)

TGA 1st Derivative: vma24
Sample Weight: 18.840 mg
Thu Nov 13 13:33:17 1986
Al203-F, 1:20, 0.25-0.5mm, 350

Bal Purge=32, Reactant 5%=30 ml/min
TEMP 1: 40.0 C TIME 1: 3.0 min RATE 1: 10.0 C/min
TEMP 2: 350.0 C TIME 2: 65.0 min

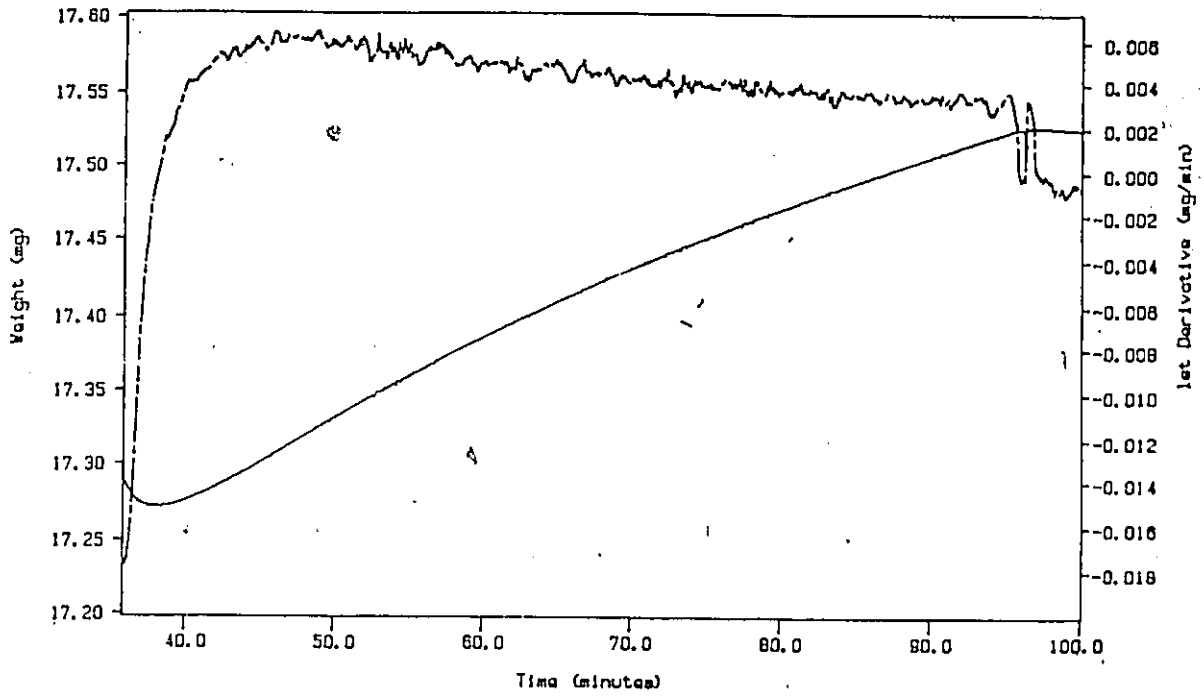

TGA 1st Derivative: vma25
Sample Weight: 18.938 mg
Thu Nov 13 15:32:28 1986
Al203-f, 1:5, 0.5-1mm, 350

Bal Purge=32, Reactant 5%=30 ml/min
TEMP 1: 40.0 C TIME 1: 3.0 min RATE 1: 10.0 C/min
TEMP 2: 350.0 C TIME 2: 65.0 min

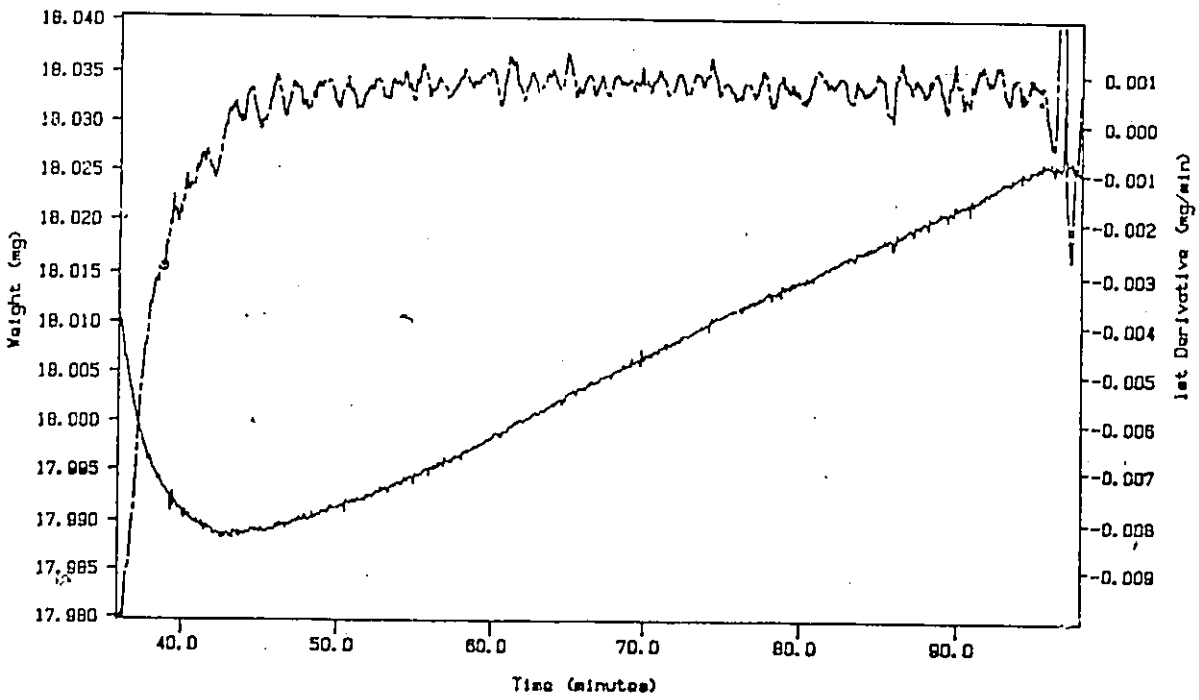

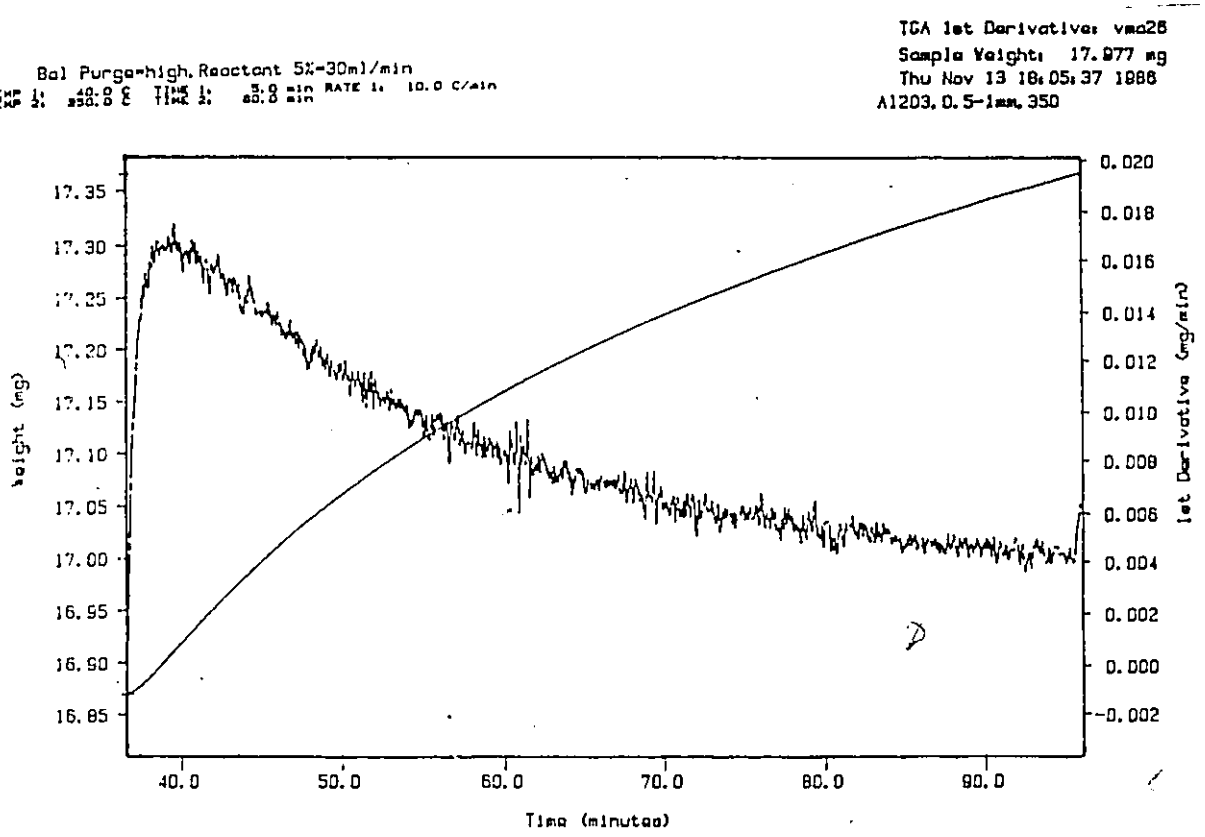
TGA 1st Derivative: vma26
Sample Weight: 17.977 mg
Thu Nov 13 18:05:37 1986
A1203, 0.5-1mm, 350
Bal Purge-high. Reactant 5%-30ml/min
TEMP 1: 40.0 C TIME 1: 5.0 min RATE 1: 10.0 C/min
TEMP 2: 350.0 C TIME 2: 60.0 min
Weight (mg)
17.35
17.30
17.25
17.20
17.15
17.10
17.05
17.00
16.95
16.90
16.85
1st Derivative (mg/min)
0.020
0.018
0.016
0.014
0.012
0.010
0.008
0.006
0.004
0.002
0.000
-0.002
40.0
50.0
60.0
70.0
80.0
90.0
Time (minutes)

APPENDIX 10.1

Description of infrared radiation furnace

Heat was provided to the reactor by means of an infrared gold image furnace (Sinku Riko RHL E 410) shown in Fig. A10.1. Temperature was controlled with a thermocouple inserted inside the catalyst bed and connected to a temperature controller (Sinku Riko Model 7103) shown in Fig. A10.1. This electric furnace is designed to heat the sample by reflecting infrared rays radiated by a tungsten lamp on an ellipsoidal polished plane (gold). Unlike the tubular furnace, the heat capacity is extremely small and the heating by radiation does not cause time delay. The furnace has rapid heating capability $100^{o}C\ s^{-1}$ compared with $20\text{-}35^{o}C\ min^{-1}$ for most resistance furnaces.

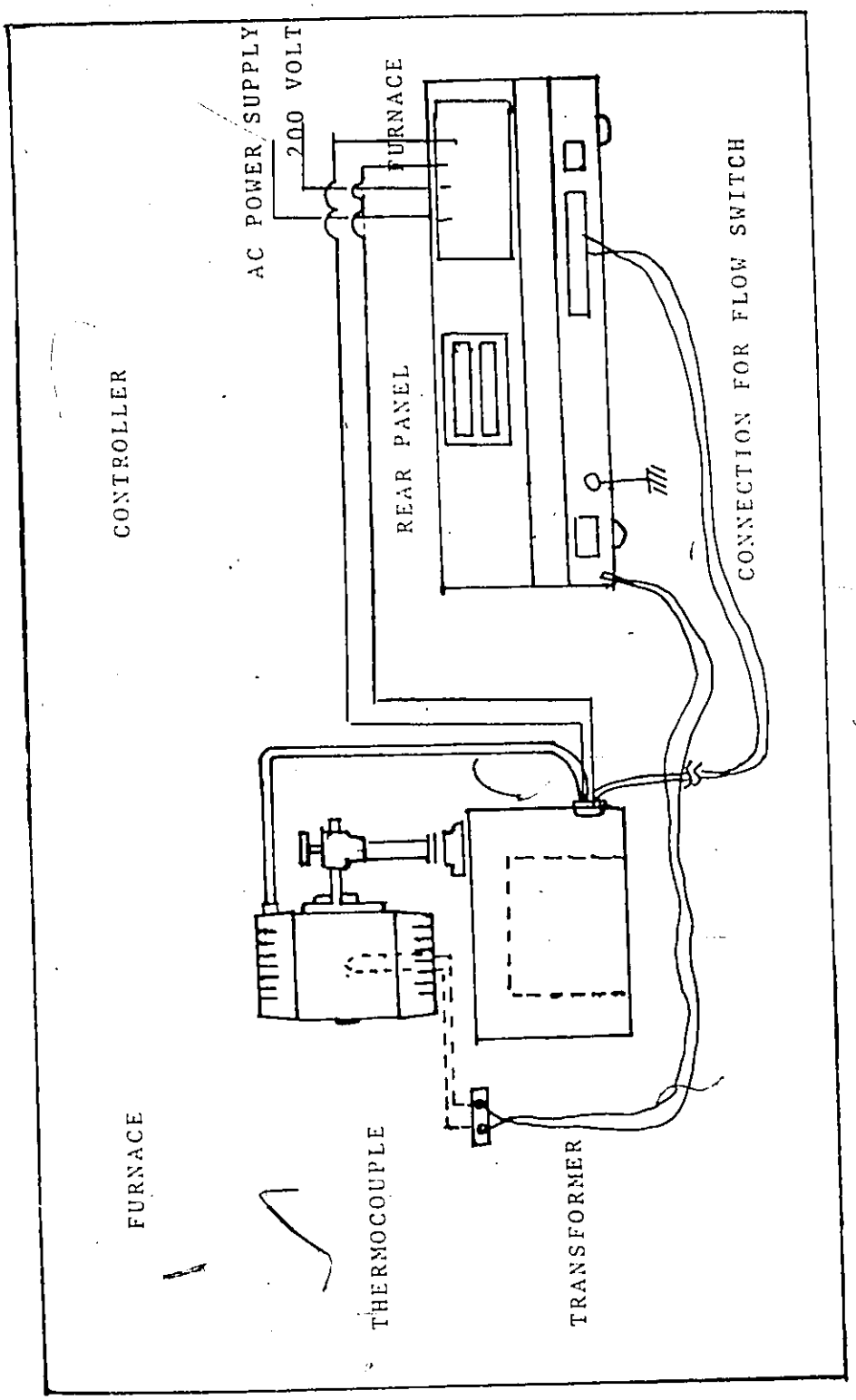

Fig. A10.1 Schematic of infrared furnace and temperature controller

APPENDIX 11.1

Calculation of probability for Flory distribution of thermal acetylene conversion data by Chang-Li.

The data reported by Chang-Li (20) was fitted to the Flory equation by linear least squares:

$$\ln(M_x) = x \ln(p) + \ln((1-p)/p) \qquad (11.2)$$

and the value of p was determined as shown in the next page:

$$p = \exp(\text{slope})$$

$$p = 0.5$$

```
** recap single
```

RUN #	Factor X	Characteristics MX	LNMX
1	6.000	0.6416	-0.444
2	7.000	0.1748	-1.744
3	8.000	0.0434	-3.137
4	9.000	0.0353	-3.344
5	10.000	0.0440	-3.124
6	11.000	0.0191	-3.958
7	12.000	0.0045	-5.404
8	13.000	0.0057	-5.167
9	14.000	0.0022	-6.119
10	15.000	0.0004	-7.824

```
** fit lnmx
LNMX:
  standard deviation about the regression = 0.5692
  explained variation about the mean (R-squared) = 93.85%
  condition of design matrix = 7.446
  model = LINEAR
** coefficients lnmx
```

Regression Coefficients for LNMX

Coefficient	Term	Standard Error	T-Value	Confidence Coef <> 0
3.242	1 (constant)	0.6822	4.752	99.7%
-0.6922	X	0.0627	11.05	99.9%

```
Confidence figures are based on 8 degrees of freedom
** plot lnmx.predicted vs x
```

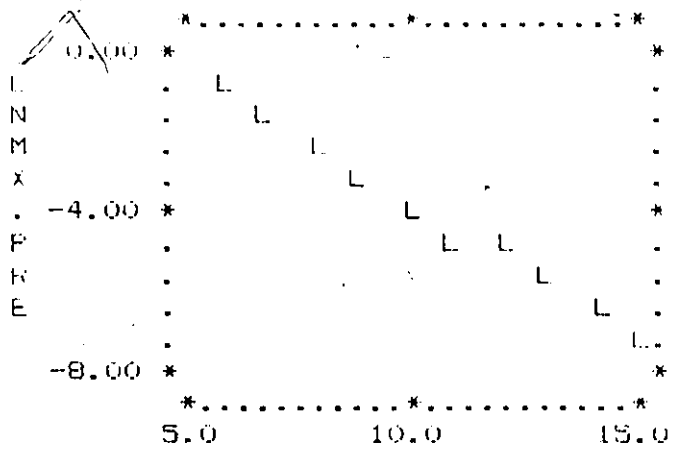


```
** display exp(-.6922)
    0.5005
** punt
```